UNIVERSITY OF SOUTHAMPTON

FACULTY OF ENGINEERING, SCIENCE AND MATHEMATICS

School of Civil Engineering and the Environment

The performance of diaphragm type cellular cofferdams

By

Qaiser IQBAL

Thesis for the degree of Doctor of Philosophy

June 2009

UNIVERSITY OF SOUTHAMPTON

ABSTRACT

FACULTY OF ENGINEERING SCIENCE AND MATHEMATICS SCHOOL OF CIVIL ENGINEERING AND THE ENVIRONMENT

Doctor of Philosophy

THE PERFORMANCE OF DIAPHRAGM TYPE CELLULAR COFFERDAMS

by Qaiser Iqbal

The construction of water management and navigation structures often requires temporary works to exclude water to facilitate construction in the dry or at least under a lower water level within the construction area. The use of cellular cofferdams for both temporary and permanent earth/water retaining works is very common. A number of theories are presented that describe the failure mechanisms involved. These failure mechanisms were identified from model studies on circular type cofferdams are applied independent of cofferdam geometry. It is common to use diaphragm type cofferdams. To asses the validity of common failure mechanisms associated with cellular cofferdams when applied to diaphragm type cofferdams, a series of numerical modelling analyses were conducted. These were validated using field monitoring results of a large scale diaphragm type cofferdam constructed at St. Germans, Norfolk, UK.

A series of plane strain analyses of a diaphragm type cofferdam were conducted using the geometry from a critical section of cofferdam. These analyses identified the lowest factor of safety based on the drained strength of the clay on which the cofferdam was constructed. The water level within the river was increased to accommodate flooding and soil strength was reduced to identify the general failure mechanism. The structural forces were calculated using both 2D and 3D models for a larger width section (13m wide) to allow comparison with wall bending moments and displacements measured in field. The 3D analyses used actual tie spacing and membrane effects whilst reducing the lateral stiffness of the wall to accommodate the stiffness reduction due to variation in the interlock forces.

To measure the bending moment in sheet piles, resistance type strain gauges were installed on a 13m wide section of cofferdam. The cell deflection, river and cell water levels were also monitored to identify tidal river effect and the influence of cell water level on performance. Comparison of field and numerical results highlighted a number of important design and construction detail related to diaphragm type cellular cofferdams.

Table of Contents

List of Figures

List of Tables

Declaration of Authorship

I, QAISER IQBAL, declare that the thesis entitled "***The performance of the diaphragm type cellular cofferdams***" and the work presented in the thesis are both my own, and have been generated by me as the result of my own original research. I confirm that:

- this work was done wholly or mainly while in candidature for a research degree at this University;
- where any part of this thesis has previously been submitted for a degree or any other qualification at this University or any other institution, this has been clearly stated;
- where I have consulted the published work of others, this is always clearly attributed;
- where I have quoted from the work of others, the source is always given. With the exception of such quotations, this thesis is entirely my own work;
- I have acknowledged all main sources of help;
- where the thesis is based on work done by myself jointly with others, I have made clear exactly what was done by others and what I have contributed myself;
- none of this work has been published before submission;

Signed: ……..

Date:…….

Acknowledgements

I feel very thankful and grateful of the support provided by the number of people, organisations and colleagues during the course of this project. I would like to take this opportunity and express my sincere thanks and wishes to the following individuals;

- My supervisor Prof. David Richards for his continuous support and guidance during my studies. He always remained there for providing moral, financial and technical support during the project.
- Prof. William Powrie for his active involvement in the project. I have always benefitted a lot from his useful suggestions and guidance throughout my PhD studies.
- Chris Pound from Mott MacDonald UK Ltd for his useful suggestions regarding FLAC programming.
- Dr. Tony Lock, for formatting and collecting the site data.
- NWFP, University of Engineering and Technology, Peshawar, Pakistan, for funding my PhD studies.
- COSTAIN Ltd, Mr Marten Ager, and the Staff working on St. Germans cofferdam for facilitating the collection of data and providing access to the site.
- All my friends and colleagues at University of Southampton for their emotional support and encouragement during my stay at Southampton.

Finally, I would like to pay my highest regards to my all brothers and sisters, my parents, my wife, and my cute little daughter Amna for being there and cheering me up during the times when I really needed them.

List of symbols

A_f	filter area
B	effective width of the cell
Ca	soil adhesion between soil/pile interfaces
D	embedment depth
D_f	embedment depth on unloaded side
d´	depth of plastic hinge below dredge line
d_c	depth of the flooded tension crack
E'	stiffness of the soil under effective stress conditions
$E-ratio$	ratio of horizontal to vertical stiffness of the wall
E_{steel}	stiffness of steel
E_{SH}	pile stiffness in lateral (in plane) direction
E_{SV}	pile stiffness in vertical direction
f	coefficient of internal friction between the interlocks of the sheet piles
F	piezometer shape factor
F	horizontal shear resistance force from the failure wedge
$FoS_{bearing}$	factor of safety against bearing capacity failure
$FoS_{seepage}$	factor of safety against seepage failure
$FoS_{sliding}$	factor of safety against sliding failure
FoS_{pen}	factor of safety against excessive penetration of the inboard sheeting

FoS_{hs}	factor of safety against horizontal shear failure
FoS_{int}	factor of safety against interlock failure
FoS_{vs}	factor of safety against shear failure on the vertical plane at the centreline
$FoS_{overturning}$	factor of safety against overturning failure
FoS_{pull}	factor of safety against pull out of outboard sheeting
FoS	factor of safety based on strength of the soil
G	shear modulus of elasticity
GF	gauge factor for resistance type strain gauge
h	free height of cofferdam cell
H	height of the cell
H'	height of the cell over which vertical shear resistance is applied
H_1	height of water table above dredge line
H_B	height of the berm
ϕ'_{inter}	intermediate effective angle of internal friction
k	hydraulic conductivity (permeability)
K	ratio of effective horizontal to vertical stress – earth pressure coefficient
Ka	active earth pressure coefficient
K_b	bulk modulus of elasticity
$K_{\text{h FLAC}}$	FLAC permeability (mobility coefficient) in horizontal direction
$K_{\text{v FLAC}}$	FLAC permeability (mobility coefficient) in vertical direction
K_n	normal stiffness of the interface

K_p	passive earth pressure coefficient
K_s	shear stiffness of the interface
k_v	permeability of soil in horizontal direction
k_v	permeability of soil in vertical direction
L	distance between centrelines of adjacent cells
M	net overturning moment
θ	angle between the joint and centreline of the cofferdam
ϕ'	angle of effective friction
$\phi'_{reduced}$	reduced soil strength
ϕ'_{design}	design effective angle of internal friction
ϕ'_{min}	minimum effective angle of internal friction
ϕ'_{peak}	peak effective angle of internal friction
ρ_w	density of water
y	distance between the neutral axis and the location of strain gauge
γ_e	effective unit weight of soil in contact with outboard pile
δ	friction (angle) between soil/pile interface
M_f	horizontal shear resistance (moment) from interlocks
M_o	net overturning moment
M_r	resisting moment
M_T	total resisting moment against horizontal shear failure
N_q	basic bearing capacity factor: for frictional soil strength analysis

N_c	basic bearing capacity factor: for undrained shear strength analysis
n	dimensionless rupture load
n_h	constant of horizontal subgrade reaction
N_γ	term to account for self weight effects
σ'_v	insite effective vertical stress
$\Delta Z_{\min}$	minimum width of the FLAC element neighbouring zone
I	moment of inertia
υ'	poisson ratio under effective stress conditions
τ_F	shear strength of soil at the failure surface
τ	shear stress developed at the failure surface
Q_T	total shear force at the base of the cell
γ_w	unit weight of water
W'	weight of soil block on unloaded side
p	constant average total stress
P	pressure difference of inboard sheeting
P_{max}	maximum inboard sheeting pressure
P_R	passive resistance offered by berm
P_s	fill pressure at centreline of the cell
P_T	interlock pressure
Q	rupture load (kN)
q_f	ultimate bearing capacity of soil

Q_u	ultimate pull out capacity
R	radius of the cell
r	radius of the cell (for circular cells)
S_F	shear resistance of interlocks
S_s	total vertical shear resistance due to fill
T	basic lag time from falling head test
t	maximum interlock pressure
U	uplift pressure on soil wedge on unloaded side
V_{CH}	measured signal voltage
V_{EX}	excitation voltage
V_r	voltage ratio
W_b	weight of the berm
γ_d	dry density of the soil
ε_y	yield strain for steel
ε	strain
ε_{ax}	axial strain

1 Introduction

The construction of water management and navigation structures often requires temporary works to exclude the water to facilitate construction in the dry or at least under a lower water level. Cellular cofferdam retaining structures are often used as both temporary and permanent earth/water retaining works. The first use of a cellular cofferdam was at Black Harbour, Buffalo USA, in 1908, followed by the construction of a second cofferdam at Havana Harbour, Cuba to raise the sunken battleship Maine. Overall, cellular cofferdams were found to be efficient and cost effective structures for these temporary works. The construction of Lock and Dam Number 26 (replacement) on the Mississippi river included a number of circular type cofferdams to facilitate the construction of the main Dam (Shannon and Wilson, 1982). These cofferdams were closely monitored by the US Army Corps of Engineers using both field monitoring and numerical modelling techniques. These studies provided the basis for the current design standards i.e. US Army Corps of Engineers (1989) and NAVFAC (1971) guidelines for the construction of cellular cofferdams.

Twin wall cofferdams are constructed by pushing two rows of sheet piles into the soil, excavating and then filling the middle part with fill material (usually granular fill). Cross walls can be provided to divide the structure in to a number of compartments to form a structure referred to as cellular cofferdam. Generally, cofferdams are used to exclude water to form a dry enclosure in which pumping stations, bridge piers, dock/marine, and river/canal management structures can be constructed. For this purpose the cells are usually arranged into a horse shoe or circular shape to resist thrust from the water and to provide easy access to the construction site from one side of the dam.

1.1 Types of cofferdams

Depending on the layout and the method of construction, cofferdams can be divided in three major types.

1.1.1 Diaphragm cells

In diaphragm type cell construction a number of cells are formed by connecting a series of straight walls (Figure 1-1 (a)), or circular arcs (Figure 1-1 (b)). In the latter case, the curved section has the same radius as the width of the cell to maintain equal tension in the sheet pile joints. The curved section is connected to the cross wall at an angle of 120º. The cells in this case cannot be filled and excavated independently sequentially as the differential level (during excavation and filling) should not exceed 1.5m during construction in order to avoid excessive deflection of the sheet piles (USACE, 1989). Also the cells are dependent on adjacent cells once the dam is constructed, and failure of one cell may lead to failure of the entire cofferdam. This type of temporary works structure is usually used for modest retained heights and where the width of cofferdam is comparatively small (height to width ratio ≤ 1).

1.1.2 Circular cells

Circular cofferdams comprise of a number of semicircular (Figure 1-1 (c)), or complete circular cells connected by curved sections as shown in Figure 1-1 (d). The curved sections are connected at an angle between 30 to 45 degrees to the axis of the cofferdam in the case of completely circular cells. The cells can be constructed, excavated and filled independently, as the cells work independently and failure of one cell will not affect adjacent cells. This type of construction is frequently used for moderate width and retained height of cofferdam (height to width ratio between 1 and 1.5).

1.1.3 Cloverleaf cells

In this type of configuration, each cell is divided in four compartments using two straight wall sections connected by four curved walls intersecting central diaphragms at an angle of 120 degrees (Figure 1-1 (e)). Cells are connected to each other using arcs making an angle of 30 to 45 degrees with the longitudinal axis of the cofferdam. The differential level between adjacent cells during construction is limited to approximately 1.5m between compartments within the cell, but the cells can be constructed independently. Also, the cells react independently and failure of one cell will not affect the other cells, hence this type of construction has lower interlock tension in comparison to the circular cell construction. This configuration is used when the width and retained height of the cells is large. However, it is comparatively difficult to construct.

1.2 Difference between diaphragm and circular type cellular cofferdams

Although there are number of cofferdams types configurations (for detail see section 1.1) based on the geometry and construction of cofferdams. The design stability checks required in current design guidelines are applied to all types of cofferdams without considering the shape, type and size of cofferdam. The circular type cofferdam was used in a number of important cofferdam studies (Lock and Dam number 26 replacement cofferdam, Havana Harbour cofferdam etc) and their performance forms the basis of existing guidelines (USACE, 1989: NAVFAC, 1971). However, there are fundamental differences in behaviour between circular and the diaphragm type cofferdams due to construction and geometrical effects that must be addressed in their design. Steel ties are provided in the case of diaphragm type cofferdams (Figure 1-1) at two or more levels to tie the sheet piles together. These ties are usually provided in both the lateral and parallel direction to the axis of the cofferdam to tie the inboard/outboard and cross walls together (Figure 5-2). The use of steel ties will affect the bending moment distribution in the sheet piles, the overall stiffness of the structure, and the movement of the inner pile towards the excavated area depending on the installation depth and spacing between the ties. However, in the case of circular type cofferdams, the circular geometry provides the support and no such steel tie arrangement is required.

1.3 Components of a cofferdam

Depending upon the type of cofferdam and retained height the cellular cofferdam may have number of components. The typical cross section of a diaphragm type cellular cofferdam is shown in Figure 1-2. The detail of these components is provided in the following;

1.3.1 Pile/structure elements

Cast iron flat web sections were developed and used as an early (around 1820) type of sheet piles section (Figure 1-3). They were efficient in comparison to timber piles but the brittleness of the cast iron was a problem (Cornfield 1968). Rolled steel sections replaced cast iron during early 19th century (Figure 1-4) but the low joint strength was a limiting

factor with these piles. The piles were either riveted or loosely jointed together. With the introduction of modern rolling/milling methods, interlocking joints were developed which possessed high interlock strength. These modern sections are shown in Figure 1-5. These include Z, and U sections or the combination of Z/U and H sections. Combining these elements considerably enhances flexural rigidity allowing even greater retained heights to be attained and where a high flexural capacity is desired. To further enhance structural rigidity, two rows of sheet piles may be tied together using one of more levels of ties and the material between the sheet pile walls replaced with engineered fill. By creating a cellular structure as depicted in Figure 1-1a, tying the sheet piles together at a number of elevations and enhancing the backfill, a stiff structure can be constructed.

1.3.2 Fill material for cells

Granular fill with a high permeability and density is commonly used as fill material within cofferdam cells. A gravel drainage bed is often provided at the base of the fill, a low water level to increase the cell stability. Drainage pumps are usually used in combination with the drainage layer at the bottom of the fill. If no pumping is provided, then weep holes are often provided on dry side, while sealing the joints to prevent water ingress from the water side, to allow the phreatic line to drop to a minimum level. The fill is usually compacted to achieve a high density to increase cell stability. A Vibro-compaction technique, with placement of the fill in layers is usually adopted for this purpose.

1.3.3 Flooding structure

Cofferdams are designed to safely resist a load which is generally a water pressure. If, during the construction or within the service life of the cofferdam the water level rise is predicted to above the design level or there is a danger of overtopping of the structure and subsequent failure, the dry side of the cofferdam may be flooded to provide a resisting force to prevent failure of the cofferdam. The flooding structure comprises of pipes and valves designed according to river flow and the size of the cofferdam. When the outside water level rise is predicted to be above the design level, the gates of the flooding pipes are opened to allow the water level to rise up to certain level within the dam to counter the rising water level within the river.

1.3.4 Berm

An earth berm may be provided on the dry side if additional sliding/overturning capacity is required. The berm is usually constructed by placing a free draining material on the excavated side of the cofferdam. A berm was used to facilitate dewatering of cofferdam used to raise the battleship Maine in 1910. The other advantages of the berm are that it will lengthen seepage flow paths under the cofferdam to avoid boiling/uplift pressure by the water on the dry side. It can be also be used to increase site accesses. The berm is generally placed prior to dewatering and shaped once the cofferdam is dewatered (Mosher, 1992). However there is no formal guidance/specification for sizing berm used for cofferdam support, therefore the berm size should be fixed with great care as the oversize berm will not only increase the construction cost and time but it considerably reduces the workable space within the cofferdam.

1.4 Typical construction sequence

The cofferdam construction may vary depending upon the scale and type of cofferdam but general constructions steps can be outlined as follows;

i. The sheet piles are driven into the ground to their design depth

ii. Once the cell is complete, the excavation within the cell is made. The cell should be excavated under balanced water to avoid the pile movement towards the inside of the cell, and by using a temporary bracing system at appropriate levels.

iii. Once the excavation is complete engineered fill is placed in layers and compacted. Ties are installed at appropriate levels during cell filling.

iv. Once the cofferdam structure is complete i.e. all the cells are compacted and filled, the water may be removed to form a dry excavation on the unloaded side. If the retained water height is high excavation within the cofferdam may be undertaken under balanced water to avoid excessive structural movement during the excavation

v. The berm (if required) is usually placed underwater or in the dry once the soft deposits are removed, depending upon the undrained behaviour of the underlying

soil. Care should be exercised at this stage to take advantage of the undrained strength of the soil (if construction sequence is designed as undrained case).

vi. The water can be removed to form a dry working area once the excavation is completed on the inside of the cofferdam.

1.5 Research objectives

The objective of this research was to study the behaviour of the St. Germans diaphragm type cellular cofferdam during both construction and in service. The construction of St. Germans cofferdam used to facilitate the construction of second largest pumping station in Europe at Norfolk United Kingdom provided an opportunity to use field instrumentation to study the behaviour of diaphragm type cellular cofferdams. It was also necessary to analyse the cofferdam to derive a factor of safety under working conditions (i.e. normal tidal levels) and for a highest flood level using numerical modelling techniques for the critical cofferdam section. Further objectives include measurement of bending moments, wall deflections and their comparison with the numerical results in order to verify these analyses and to identify the important load changes affecting the structural response due to seasonal variations and also construction effects.

1.6 Methodology

The objectives of this research were achieved using numerical analyses combined with field observations. The methodologies adopted to achieve these goals were achieved by;

- An extensive literature review to help understand the available design guidelines for the construction of cellular type cofferdams;
- Evaluation of geotechnical properties and site geology from field and laboratory study on the high quality samples from various boreholes;
- An extensive plane strain (two dimensional) numerical study to calculate the factor of safety for a critical section (10.5m wide cell N4/S3) using ‘Class A’ analyses;

- Two and three dimensional numerical modelling of the cofferdam were used to calculate the structural forces and deflection from a representative section based on observations from the instrumented cell (13m wide cell C3);

- Analysis and interpretation of the field data related to the major construction stages and tidal fluctuations during construction and once the cofferdam was commissioned i.e. in service;

- Comparison of measured response from field instrumentation with numerical calculated results to provide the basis for the calculation of the structural forces and wall deflections using two and three dimensional numerical analyses of the diaphragm type cellular cofferdams.

1.7 Organisation of the thesis

The work presented in this thesis is divided into nine chapters

Chapter 1: This chapter provides the general introduction to the cofferdams, research objectives and methodology adopted to achieve these objectives.

Chapter 2: This chapter contains the review of the available literature on cofferdam performance with detail of previous numerical, laboratory and field studies. Failure case studies based on the documented failures of cofferdams are provided to help identify the most critical failure modes.

Chapter 3: Overview of existing design guidelines is presented. The analytical methods used to calculate the performance of the cofferdam structure against previously identified failure mechanisms are discussed in detail. Gaps in the current design guidelines specific to the diaphragm type cellular cofferdams are identified.

Chapter 4: The detail of St. Germans cofferdam case study and soil properties for various soil layers at site are provided in this chapter.

Chapter 5: This chapter presents the two dimensional plane strain analyses of critical section (10.5m wide) to calculate the factor of safety for the design of the St Germans cofferdam. The 13m wide cell which was also instrumented was used to calculate the structural forces and wall deflections.

Chapter 6: This chapter includes a comprehensive three dimensional analysis of the 13m wide cell cross section to calculate the structural forces and cell deflection. The reduction in lateral stiffness of the wall to incorporate flexibility due to the presence of the clutches in lateral direction of the sheet piled cell walls was used to asses interlock effects on wall performance.

Chapter 7: The measured bending moments and wall deflection (inboard and outboard) together with the tidal fluctuations are presented. Major load changes are identified using both the site diary and the monitored response.

Chapter 8: A comparison of the bending moments and wall deflections from the two/three dimensional analyses compared to the measured response.

Chapter 9: Conclusions arising from the study and recommendations for future work are presented.

The borehole logs, displacement and velocity vectors to show soil/structural movement are presented in the appendices.

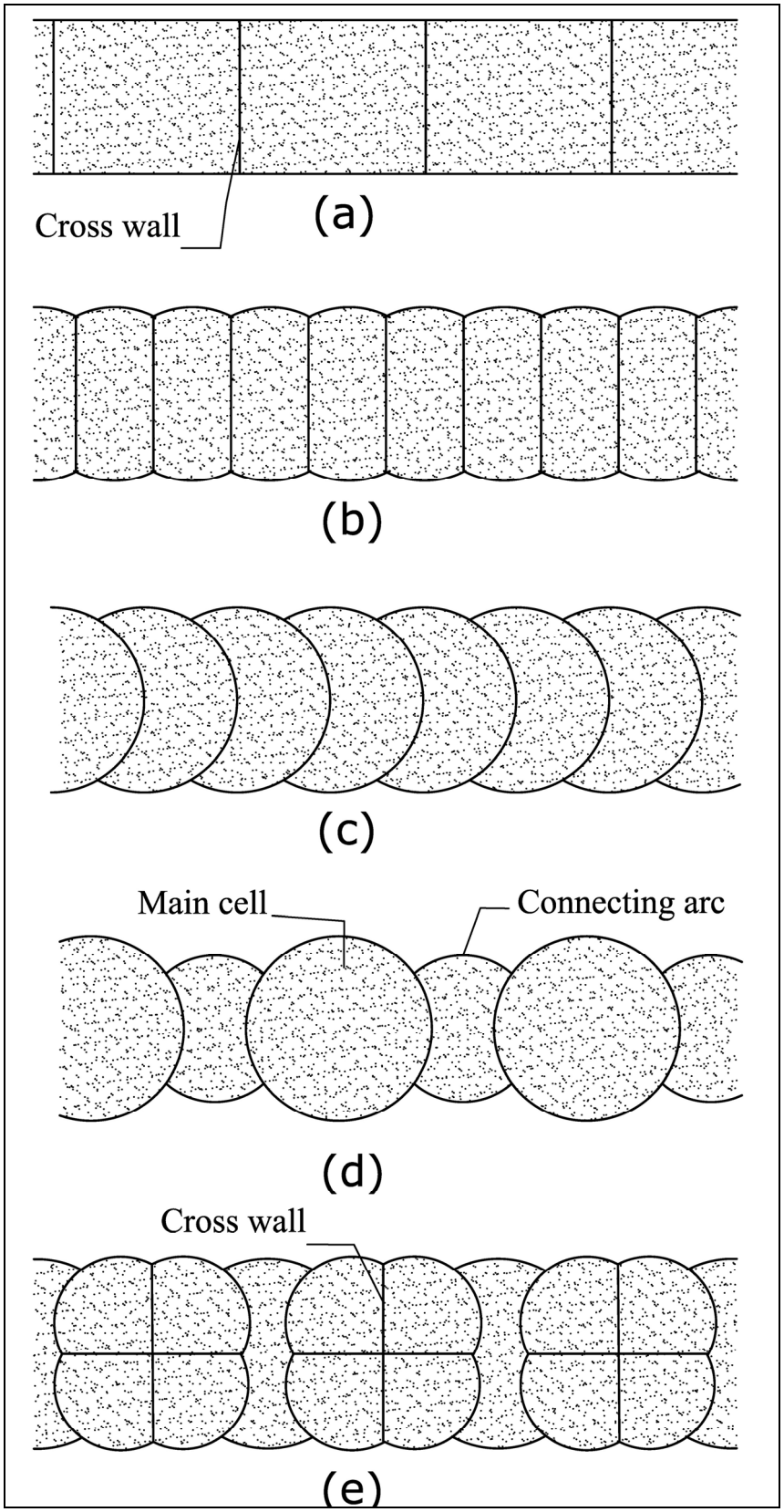

Figure 1-1: Types of cellular cofferdams

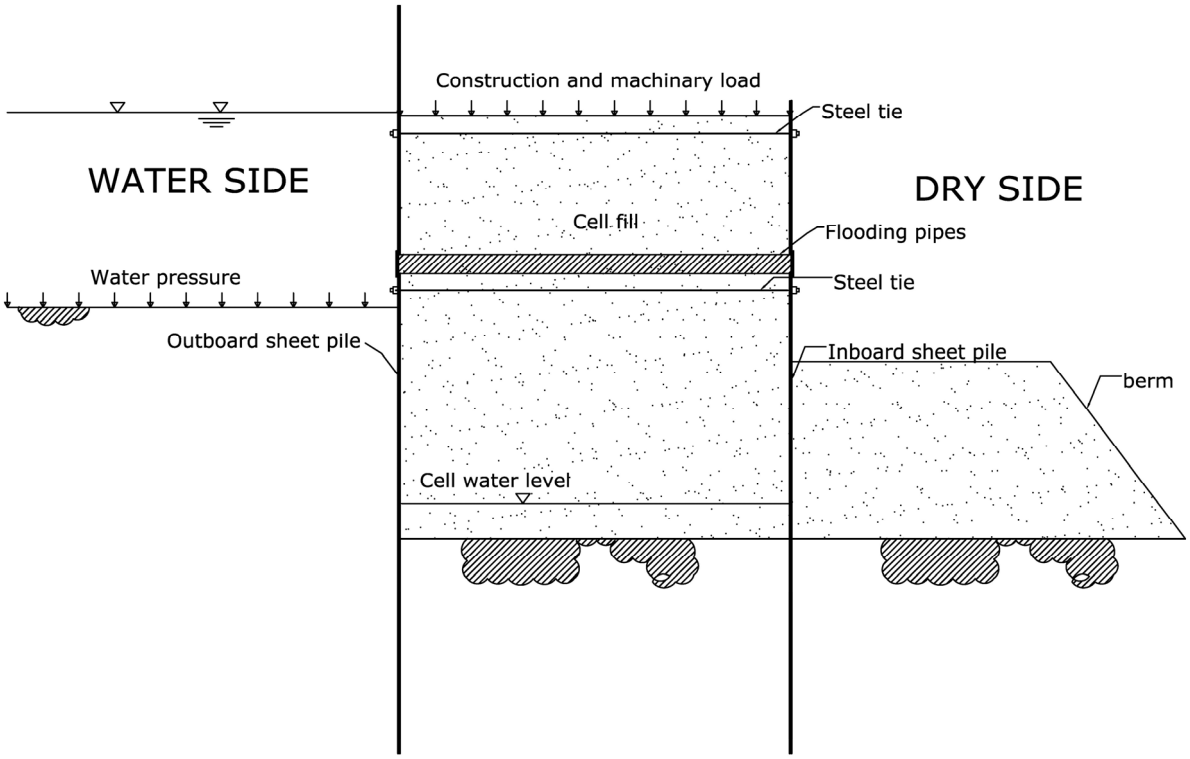

Figure 1-2: Typical cross section of diaphragm type cellular cofferdam

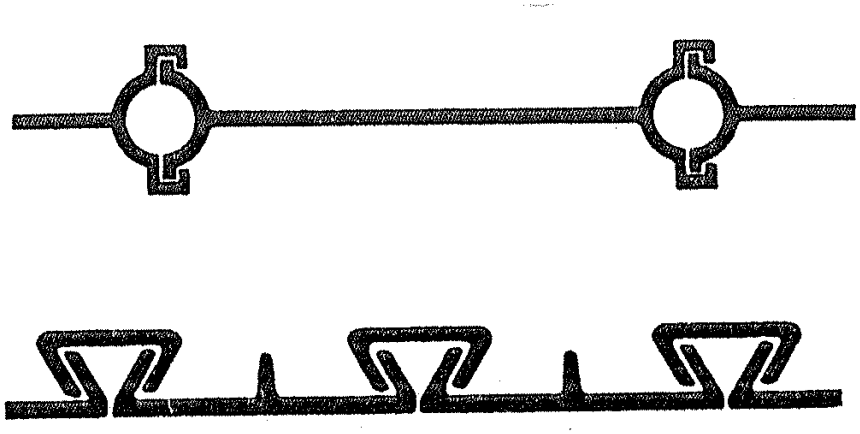

Figure 1-3: Early cast iron sections used for piling – Pre 1820 (after Cornfield, 1968)

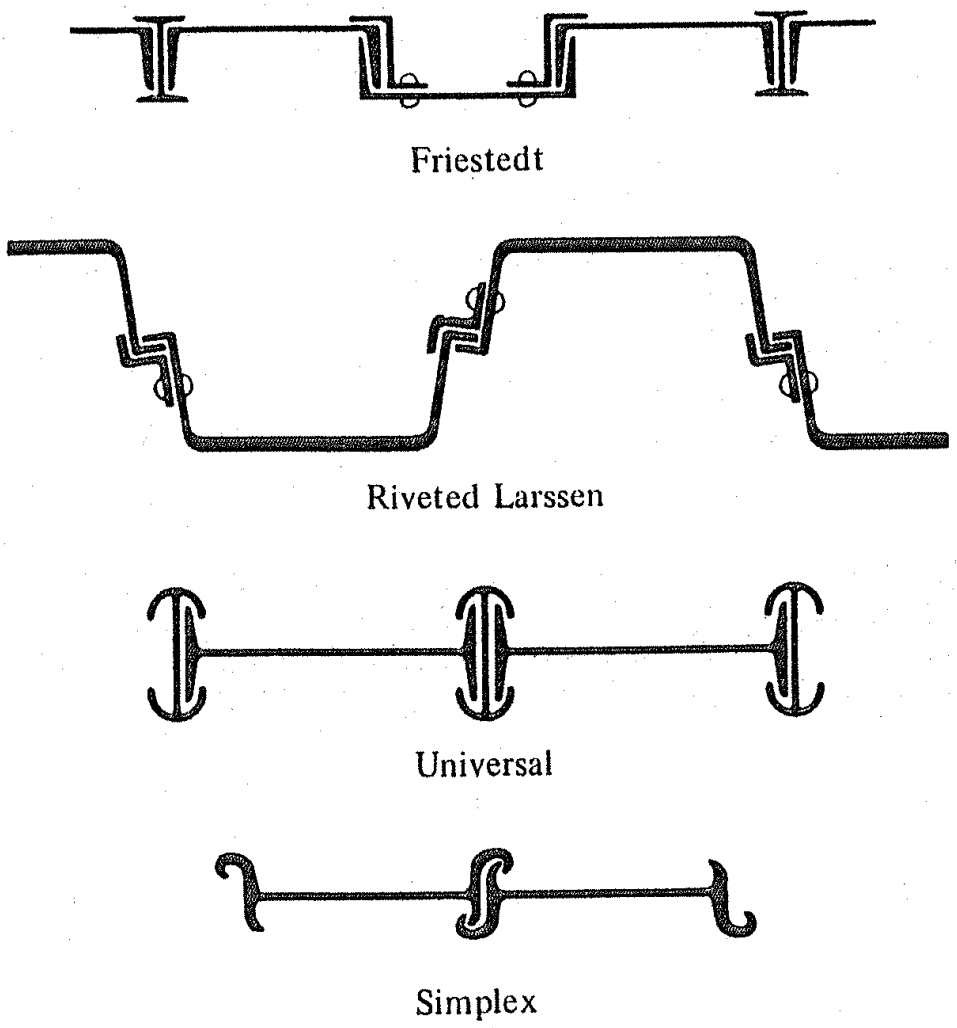

Figure 1-4: Obsolete sections of steel sheet piling – used in early 19th century (Cornfield, 1968)

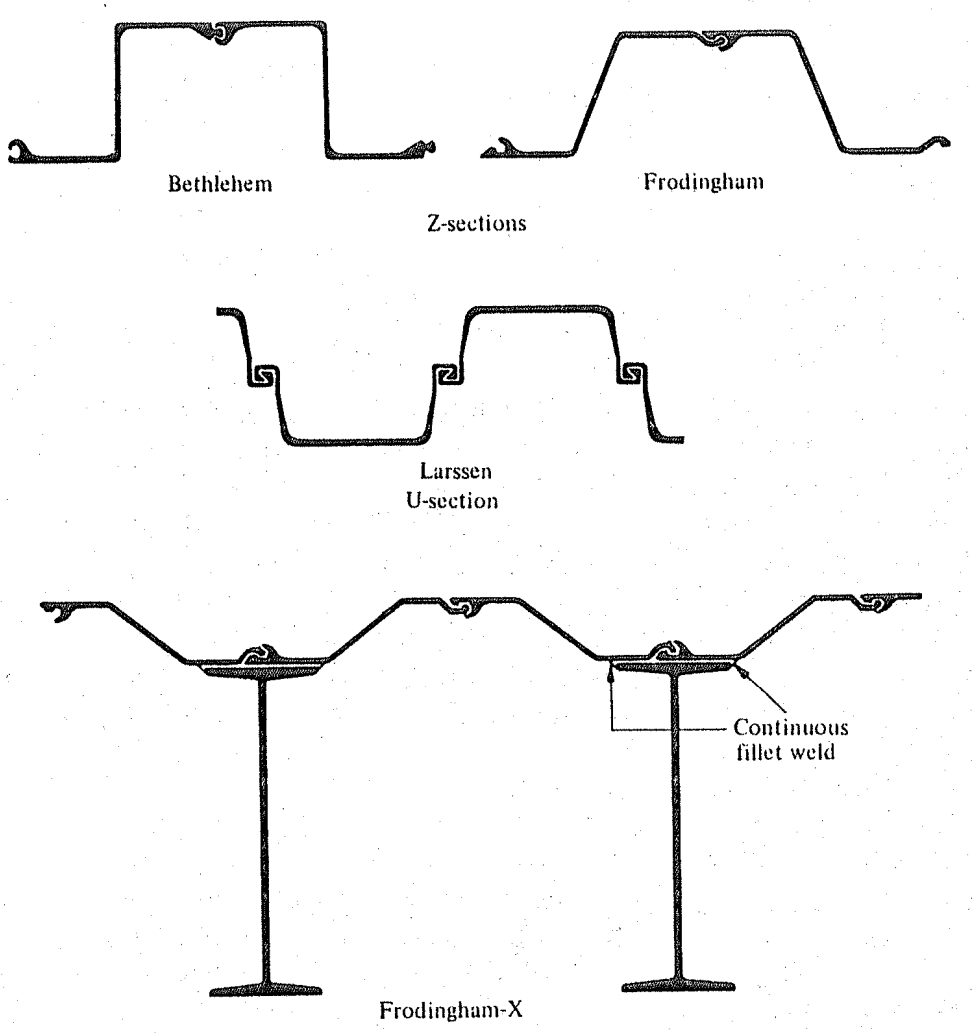

Figure 1-5: Modern steel sheet piling sections (Cornfield, 1968)

2 Literature review

2.1 History of Cofferdams

The first known cofferdam was constructed at Black Harbour, Buffalo, New York, in USA during 1908-09. This consisted of 77 square cells of 9.15 × 9.15m dimensions, constructed using flat web pile sections with an average inner height of 30 feet (Boardman, 1917). This inspired Major General Harley B. Ferguson of the US Army, to use a cofferdam structure to recover the sunken battle ship Maine in Havana Harbour, Cuba. This cofferdam was constructed using 20 circular cells, each of 15.2m in diameter. The cells were connected by circular arcs to make them self supportive. Since this time cofferdams have been widely used for temporary works for retaining both soil and water. The design of cofferdams has not evolved greatly and some of these structures have failed due to errors in their design and construction; however they are a popular option within the construction industry because of their durability and economy as a structure (Mosher, 1992).

2.2 Design of cofferdams

Several attempts have been made to define the internal and external stability requirements of these structures and to develop design guidelines to asses the long and short term stability of the cellular cofferdams. Various failure mechanisms have been suggested over the last century since the first use of cellular cofferdams in 1908. Relatively few of the failure mechanisms e.g. log spiral and interlock failure are verified by the field/lab studies, while the rest are idealised mechanisms based on theoretical calculations.

Pennoyer (1934) suggested the first theoretical solution to asses safety against sliding and overturning (Figure 2-1). He considered the cofferdam cell as a rigid box which can rotate about its inner edge, and considered as a centre of rotation. The forces acting on the cell were considered as the load of the cell and applied pressure due to retained soil/water. The internal stability was assessed by calculating the interlock tension in the

sheet piles to avoid bursting of the cells. This method was further developed by Jacoby and Davies (1941).

Vertical shear failure at the centre of the cell was identified as a critical failure mechanism by Terzaghi (1944). He stated that the cofferdam would fail by shear failure at the centreline of the cell before sliding or overturning failure occurred (Figure 2-2). He found reasonable agreement between theoretical and field results for cells with fill earth pressure factors ranging from 0.4 to 0.5. The cofferdam constructed to recover the battle ship Maine was back analysed and indicated that this cofferdam showed no sign of distress until the overturning moment became equal to the resisting moment. However the cofferdam starts to deflect excessively as the overturning moment becomes equal to 0.75 times the resisting moments. It was also concluded that considering the cofferdam cell as a gravity wall may lead to erroneous calculation of soil pressure below the base of the cofferdam.

Terzaghi's (Terzaghi, 1945) theoretical method was a significant step forward in comparison to previous design methods and further improvements were suggested by Hansen (1953). There were two major objections raised to challenge Terzaghi's vertical shear failure theory. Firstly, Terzaghi's equations were applicable to the fill material having earth pressure coefficient of 0.4 to 0.5, while Hansen found that the earth pressure factor for a material with ϕ' = 30º was 0.75 and for ϕ' =35º was 0.67, when the earth pressure factor is equal to $\cos^2\phi'$. It is well known that the ϕ' of granular fill generally used to backfill the cells range between 30º and 35º. Terzaghi (1945) found that only lower values of earth pressure coefficient are sufficient to provide stability, which shows that the equation cannot be used to check the stability of cell with higher earth pressure factor. The second objection was that the vertical slip mechanism is dependent on the development of a full plasticity zone within the cell in order to calculate the corresponding active and passive pressures. This might only be possible if the cofferdam cell width is very large (to develop fully plastic soil movement within the cell), but is not generally true for the more usual size cofferdams. Therefore the vertical slip mechanism cannot be considered as critical in all cases.

Hansen (1953) suggested a curved rupture line at the base of the cell, which is statically and kinematically admissible (Figure 2-3). Two methods for the analyses of stability were

presented, termed as the extreme and equilibrium methods. The shape of the rupture line was taken as log spiral for the extreme (Figure 3-6) and a circular (Figure 3-5) in the case of the equilibrium method. In the case of a cofferdam founded on soil a rupture was considered to be concave for a cofferdam with shallow pile depth, while a convex rupture was assumed for cells with more deeply embedded sheet piles. However, no limits were provided for the classification of a deep or shallow cofferdam. The overall assumption is reasonable as sheet piles with a greater depth will have a centre of rotation located above the foot of the wall, however in the case of deep sheet piles the development of plastic hinge should also be checked.

The limitations regarding the insitu stress ratio and shortcomings in the vertical failure mechanism were identified by Cummings (1957). He introduced a base shear failure, also known as horizontal shear failure (Figure 2-4). This method suggests that the failure wedge within the cell is responsible for the development of horizontal shear resistance and the fill on the unloaded side can be reduced if require (for details see section 3.3.2.2). However this practice is not recommended by many designers as the method suggests that the fill load on unloaded side can be reduced which is considered to be unsafe side when considering the overturning stability of the cell (Dismuke, 1970)

The method of analyses suggested by Hansen (1953), was also identified by Zaczek (1952), Cattin (1955) and Schneebeli and Cavaillé-Coll (1957), but none of these researchers were able to validate their methods with results from model or field tests until Ovesen (1962). This work compared the analytical methods suggested by Hansen (1953) with results from scaled physical model tests on cofferdams. Two different model sizes (termed large and small scale) were considered for this purpose. The models comprised circular cells attached together using circular arcs intersecting the circular cells at 120 degrees with reference to the axis of the cofferdam (see Figure 1-1d). The large scale model consisted of three cells with individual cell diameter of 72cm and total length of 224cm. The small scale model comprised of four cells with individual cell diameter of 20cm and total length of 83cm. The small scale model was adopted as it was easier and quicker to perform a large number of tests in a limited time. The cells were either founded on a bed rock surface or embedded in sand. The tests were performed using various depths to height and width to height ratio for a cofferdam founded on the sand to

asses the effect of changing the size of the cells. It was found that the rupture line identified by Hansen (1953) is a true mechanism from his model tests (Figure 2-8; Figure 2-9). It was also shown that the load does not act at the lower third point of the cell under ordinary working conditions; therefore it is not possible to determine deflections under working conditions from these model tests. The logarithmic dimensionless rupture load 'log *n*' was calculated at from number of small scale models tested in the laboratory and plotted against the angle of internal friction of soil in which the sheet piles were embedded for each model test. Where,

$$n = \frac{Q}{\frac{1}{2}\gamma_w h^2}$$ **Equation 2.1**

Q = Rupture load (kN)

γ_w = Unit weight of water

h = Free height of cofferdam cell

These results were compared with other theories such as Pennoyer (1934), Terzaghi (1944), and Hansen (1953) and are shown in Figure 2-10, where PEN. TUR (Pennoyer overturning), PEN. SLI (Pennoyer sliding), TERZ (Terzaghi method), BR. HA (Brinch Hansen method) .Overall, a good agreement was found with the analytical methods suggested by Terzaghi (1944 and 1945) and Hansen (1953). However the calculation based on results from cofferdams with greater driving depths were 10 - 20% on the unsafe side in comparison to model tests.

Other failure mechanisms identified include interlock separation (Figure 2-5), shear failure at the sheet-pile/fill interface (Figure 2-6), bearing capacity failure at the base of the cell (Figure 2-7). The interlock failure mechanism is considered to be very important, while the other two mechanisms are only suggested checks by NAVFAC (1971), and generally considered to be less important for the design/analysis.

A number of studies were made by various other researchers including, Fröhlich (1940), Blum (1944), Lee (1945), Verdeyen (1948), Descans (1952-1954 and 1958), Dismuke

(1970), Swatek (1970), and Mosher (1992). However, this work has not led to any fundamentally different mechanism of behaviour being identified.

2.3 Numerical and physical modelling studies

Early attempts on numerical analyses of cofferdam performance which include construction stages often include gross simplifications and assumptions due to the difficulty in modelling soil structure interaction. As the interlock tension was one of the major causes of cofferdam failure most of these studies were aimed at calculating the interlock forces during cell filling and cell deflection under working conditions. An axisymmetric analysis of the single circular cell by Kittisatra (1976) is considered to be the first attempt to model the influence of the cofferdam cell filling process. This analysis used isotropic shell elements to model the pile with no slippage (i.e. interface elements) between the cell walls and soil. These analyses predicted a maximum deflection of 0.5 inch (12mm) in the sheet piles during cell filling which is well below the values that would be expect in reality.

The first detailed and comprehensive numerical modelling study can be regarded as the numerical modelling of Lock and Dam No. 26 (R), constructed on Mississippi river in United States. A computer program SOILSTRUCT developed by G.W. Clough and his co-workers was used for modelling the response of the cofferdam. This program allowed for the introduction of interface elements for the modelling of slippage between the soil and sheet piles. Clough and Hansen (1977) modelled a single vertical slice taken through the cofferdam using plain strain analyses technique. The two sheet piles were connected together by a series of springs to model the three dimensional effect from the cross walls. The deformations predicted were in reasonable agreement with the actual values measured during construction of the cofferdam, but in common with Kittisatra (1976) the predicted deformations during cell filling were very small. Stevens (1980) further refined the Clough and Hansen (1977) vertical slice model by reducing the spring stiffness used to connect the two sheet piles to account for the gaps between interlock using back analyses technique (Figure 2-11). Although the results were comparable with the observed deflections this work was unable to provide a general guideline for spring stiffness reduction that would account for a lack of fit between the sheet piles.

Further finite element analyses were conducted for Lock and Dam No. 26 (Replacement) to verify the results from instrumentation used to monitor the first and second stage of construction by the US Army corps of engineers (reported by Mosher 1992). It was acknowledged at the time that the cofferdam analyses problem is in reality a three dimensional problem but as the results were required before the completion of the first stage of cofferdam, vertical slice, axisymmetric, and generalised plain strain horizontal slice analyses were conducted to cover any three dimensional issues. The vertical slice model used was the same as that employed by Clough and Hansen (1977). The axisymmetric model let the cell filling process of a single isolated cell to be analysed (Figure 2-12). The E-ratio concept was introduced to model the orthotropic response of the sheet piles to model the reduced stiffness in the lateral direction due to the lack of fit within the interlocks. This allowed modelling of the accurate interlock behaviour which led to reasonable predictions of cell deformation during cell filling process in comparison to the vertical slice model. However, it was suggested not to reduce the lateral stiffness once the dry side is unloaded and the cofferdam is commissioned.

The generalised horizontal slice analyses (Clough and Kuppusamy, 1985) represented an analysis of a single main cell and interconnecting arc cell (Figure 2-13). This allowed the analysis of the interaction between the main cell and the arc cell under uniform cell filling conditions to be considered. The interlock stresses and deformations of the main and arc cells were calculated using a horizontal slice model (Figure 2-13). However this model was unable to include the support from the foundation. Therefore it was considered to be applicable to the upper two thirds of the cell to limit the foundation effect. Also, the main cell and arc cell were supposed to be filled simultaneously which generally is not the case in reality.

The results from two dimensional analyses by Clough and his associates suggest the need for three dimensional analysis of the problem. For this purpose a full three dimensional analyses for a single circular cell along with arc cell (Figure 2-14) were undertaken by Mosher (1992). The analyses of single isolated main cell showed the development of an arching effect within the cell fill which was attributed to the friction between fill and sheet piles as they moved. This resulted in lateral earth pressure above the active limit above the cell's mid height and less than the active limit below mid height of the cell.

Arching also resulted in reduced vertical stress from gravity conditions within the cell. The interlock forces were significantly reduced by these arching forces in the arc cell during cell filling due to the small size of arc cell. This arching effect highlighted by the three dimensional analyses provided improved results in comparison to the generalised plane strain model which was unable to model the overall response of the main cell and arc cell and their interaction. The inboard wall on the construction side of the cofferdam was computed to exhibit greater movement towards the unloaded side in comparison to the outboard wall. This was believed to be a result of increasing effective stresses within cell during cell dewatering, and the lateral spread from the vertical settlement of the fill which pushed the unrestrained inboard pile towards the unloaded side.

Centrifuge model tests were conducted on the cofferdams founded on the sand (Khan *et al.,* 2001) and clay (Khan *et al.,* 2006) foundations on a twin wall cofferdam model tested under 70g acceleration (Figure 2-15). The tests on the cofferdam founded on the sand revealed that the cofferdam has failed due to the high pore water pressure resulting in shear deformation of material within the cofferdam fill. The bending moments from the downstream (inboard) wall was found to be larger in comparison to the upstream (outboard) wall in case of cofferdam founded on the sand foundation (Figure 2-16), while for the cofferdam founded on the clay, the difference in the bending moment profile was observed for outboard and inboard wall (Figure 2-17); however, the amount of maximum bending moment was found to be similar for both the inboard and outboard walls. The cell wall deflection from the cofferdam founded on the clay foundation was markedly less (Figure 2-18) in comparison to the cofferdam with similar dimensions and embedment depth but founded on a clay foundations (Figure 2-19), suggesting that the cofferdam founded on the sand foundation will perform better when compared to the one founded on the clay foundation. Increase in the overall stability of the cofferdam was found to be directly related to the increase in the cell width for both the cofferdams founded on sand and clay. The increase in embedment depth was found to have no role in increasing the cofferdam stability in case of the cofferdam founded on the sand foundation, whereas in case of clay foundation a reduction in stability was observed when increasing embedment depth of the cofferdam.

2.4 Performance and monitoring studies

Assessing the performance of structures during their construction through the use of appropriate instrumentation can provide important insights into behaviour (Richards *et al.,* 1999; Batten et al 1999; Batten and Powrie, 2000). Field instrumentation is very important in assessing the behaviour of cellular cofferdams particularly during construction and working of cofferdams. Modern instrumentation techniques can provide real time monitoring to record the changes on a daily and seasonal basis using sophisticated electronic data transfer techniques (Richards *et al.,* 2003; CIRIA 2002). The field instrumentation involves the use of inclinometers, piezometers, strain gauges and manual surveying instrumentation. However, there are few field case studies related to cellular cofferdams and none where an instrumented section has failed that provide the data relating to the reasons behind the failure.

The interlock forces are typically recorded during cell filling operations while wall deflections are considered critical during in service loading of the cofferdam cell. Marten and Clough (1988) presented results from an instrumented cofferdam during cell filling and differential loading stage of five large cofferdams constructed in the US. During cell filling, interlock forces were observed to increase as a result of vibro-compaction but the basic deflection profile remained the unchanged. The interlock forces recorded during the field study were compared with various analytical methods (TVA Engineers guidelines 1957; Maitland and Schroeder, 1979), and similar profiles were observed from field and analytical results (Figure 2-20). The embedment depth was observed to influence the location of the maximum interlock force which was seen to increase and more higher up the piles with increasing embedment depth.

The instrumentation employed to monitor the performance of a cofferdam cell under differential loading conditions includes recording cell deflections using manual survey techniques and deflection profiles from inclinometers. Swatek (1967) reported that the typical cofferdam moves about 1 percent of its free height. While the study by Martin and Clough (1988) showed that recorded deflections during normal loading are less than 0.6 percent of the free height of cofferdam (Figure 2-21). It can be clearly observed that the minimum cofferdam deflections were recorded at Willow island cofferdam; the reasons for the small deflection were its large diameter to height ratio, strong foundation support

and the presence of a berm. The Trident cofferdam deflected uniformly, while the cofferdam used to construct Lock and Dam No 26 (Replacement) showed a non-uniform deflection with reduced deflection observed in the embedded portion (Figure 2-22), as they were non-embedded and embedded respectively. Martin and Clough (1988) showed that the deflection profile of 1 percent of free height may only be applied to a cell with the highest flood level and no berm support.

2.5 Failure case studies

The cofferdam is a popular method of providing both short/long term retaining structures although some notable cofferdams have failed. The first failed cofferdam to be extensively reported failed due to excessive bulging (~1m between its cross walls) (Terzaghi, 1945). He proposed that these structures usually fail by bursting during or immediately after cell filling, and that there are no reported cases of bursting failure during the application of differential loading. It was further reported that only two cases of failure due to overturning were recorded, attributed to boiling/piping on the dry side at the Mississippi River and Grand Coulee, USA, and that the failure is generally triggered by structural failure or imperfect interlock connections rather than the global failure of the structure. Most of the failures occurred due to a breach in one portion followed by progressive failure of the whole cofferdam.

Grayman (1970) reported a structural failure following saturation of the fill within a cell either due to waves overtopping the outboard wall or leakage through the interlock connections. The common location of structural failure is connecting tees between the two cells. The riveted tees used in this case were found to have greater resistance against failure in comparison to welded connections due to the presence of a greater amount of metal in the section. Splices in sheet piles were also found to be a common location of stress concentrations and subsequent failure of the section. There was only one sliding failure reported by Grayman (1970), in which the cells slid approximately 2.36 meters towards the excavation on the weak stratum below the bottom of the cells.

The US Army Corps of Engineers report (Department of Army, US Army Corps of Engineers, Technical Report, 1974) has summarised 35 circular type cofferdam failures at 21 different sites, constructed between 1956 and 1971. Structural failure was the most

frequent cause of failure with 24 recorded cases, and included interlock separation or failure of the connection wye[1] piles joining the cells together. Four failures were reported due to scouring under high velocity flow and two due to foundation instability. The remaining five failures were attributed to careless construction including overloading the cell and overtopping.

Cofferdam failure due to faulting in the underlying bedrock was reported at the Uniontown Locks and Dam on the Ohio River whilst under construction (Thomas *et al.,* 1975). The failure occurred during rising water just after the cofferdam was dewatered. The cells on the upstream side moved towards the upstream side resting on coal underclay, with the overlaying shale and limestone moved as an intact unit with the cells until it encountered a fault in the middle of the cofferdam. The fault acted as a baffle forcing the cofferdam to fail along the fault. The failure was devastating and 5 of the cells collapsed within 10 minutes of the initial cell movement being observed.

A more recent and devastating failure was recorded during hurricane Katrina at New Orleans, USA. The sheet piled levees failed (Raymond & Robert, 2006) due to the development of a flooded tension crack (Bolton and Powrie, 1987) on the water side of the structure. A rise in water level increased the load on the water side which led to separation at the sheet-pile/soil interface. This allowed the intrusion of water into the crack resulting in the hydrostatic pressure acting on the loaded face of the wall and eventually a failure of the whole flood support structure (ASCE, 2007). This mechanism was first identified by Bolton and Powrie (1987) and subsequently incorporated in British codes of Practice (BS 6349, 1988; BS 8002, 1994). The recent USACE (USACE, 1989) guidelines recognise the flooded tension crack as an important factor in their design, but the levees were designed using old guidelines, which did not take the flooded tension crack into consideration.

[1] Wye piles are used to connect two circular cells together making and angle of 120º at connection between two cells.

2.6 Summary of literature review

The review of the literature shows that a lot of work has been done on the design of circular type cellular cofferdams. The key mechanisms involving the local/global failure mechanisms were identified as horizontal/ shear failure, interlock separation, bearing, structural and log spiral failure mechanisms. However, it is evident that current guidelines for cellular cofferdams are at best unclear and no single design guidance exists that covers all possible mechanisms. Many of the failure mechanisms are only applicable under certain circumstances, but still applicable to any type of cofferdam according to certain design guidelines such as the USACE (1989) and NAVFAC (1971). This design guideline was developed on the basis of studies conducted on cofferdams consisting of circular type cells but it is still generally applied all other types of cofferdams, i.e. cloverleaf and diaphragm type cellular cofferdams.

It is accepted that cofferdam structures are challenging three dimensional design problem but there have been only one case where the full three dimensional analysis of cofferdams (Mosher, 1992) was undertaken. Such analyses should include cell interactions and construction stages which were not routinely modelled due to limited computing resources. Also, the Mosher (1992) analyses used a circular cell configuration for analyses therefore it may be inappropriate if applied to other types, i.e. Cloverleaf and diaphragm type cells. The circular type cells did not include any ties which are integral part of diaphragm type cells.

The field studies available in the literature were conducted to record cell deflections and interlock forces. No studies attempt to measure bending moment of piles, pore pressure changes and seasonal variation in cofferdam cells. The sheet piles are designed using ultimate limit state bending moments and full plastic zone development within the cell which cannot realistically develop within the limited width of a typical cofferdam cell. Therefore there is a need to record the bending moments within the sheet piles based on correct cell pressure to reduce the construction costs. The bending moments and pore pressure changes can also help to identify the soil condition i.e. drained/undrained.

The results from previous studies include gross simplifications in design and ignore important contributions from recent developments e.g. flooded tension cracks and the

ability of numerical analyses to capture the complex construction sequence. Therefore there is a need for detailed numerical-modelling/back-analyses of field monitoring to identify short comings in current design guidance and to improve the current design methods.

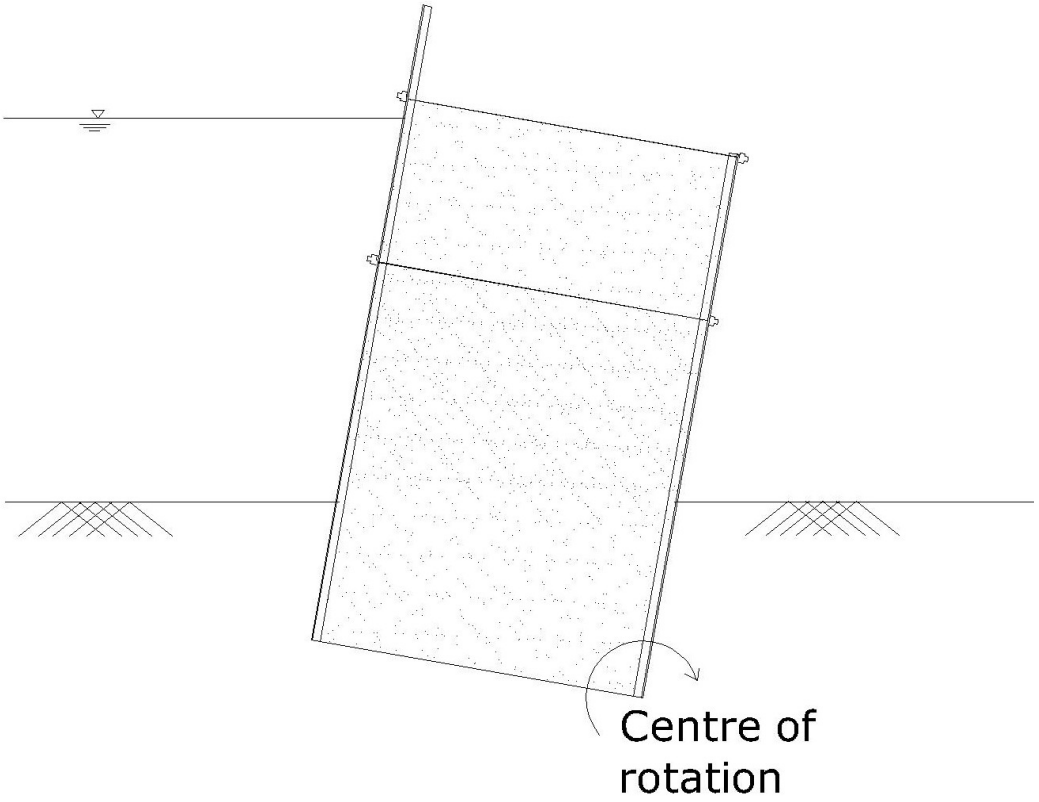

Figure 2-1: Rotational failure suggested by Pennoyer, 1934

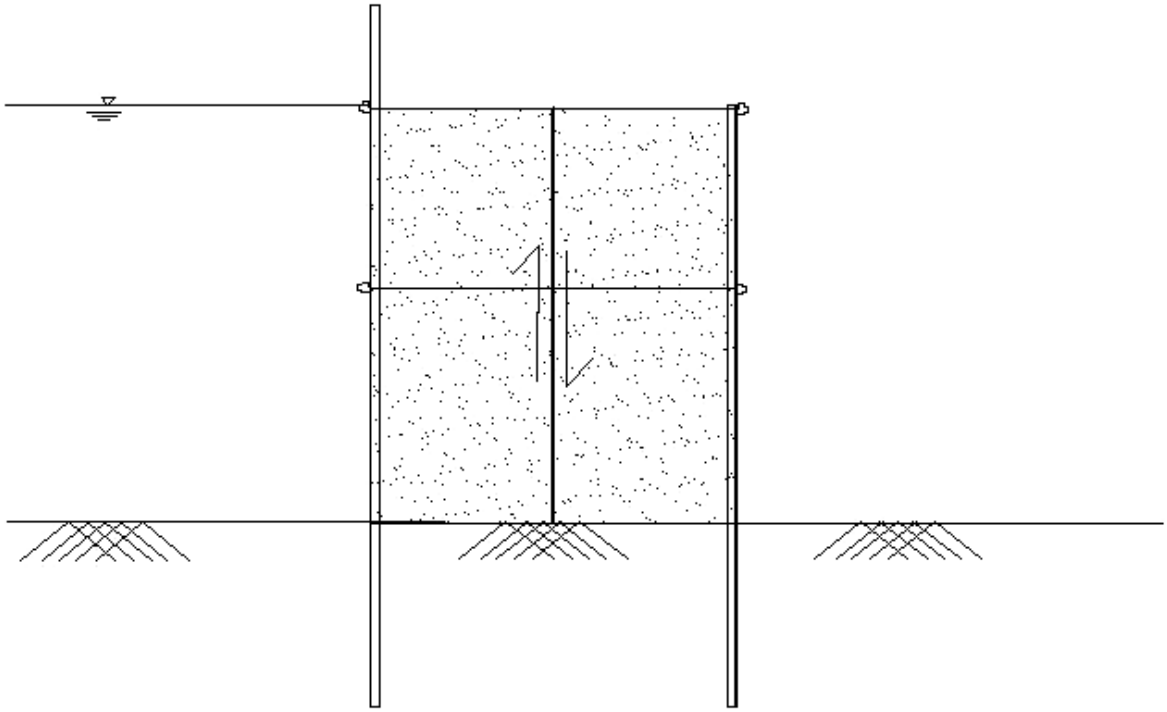

Figure 2-2: Vertical shear failure at the centreline of the cell (Terzaghi, 1944)

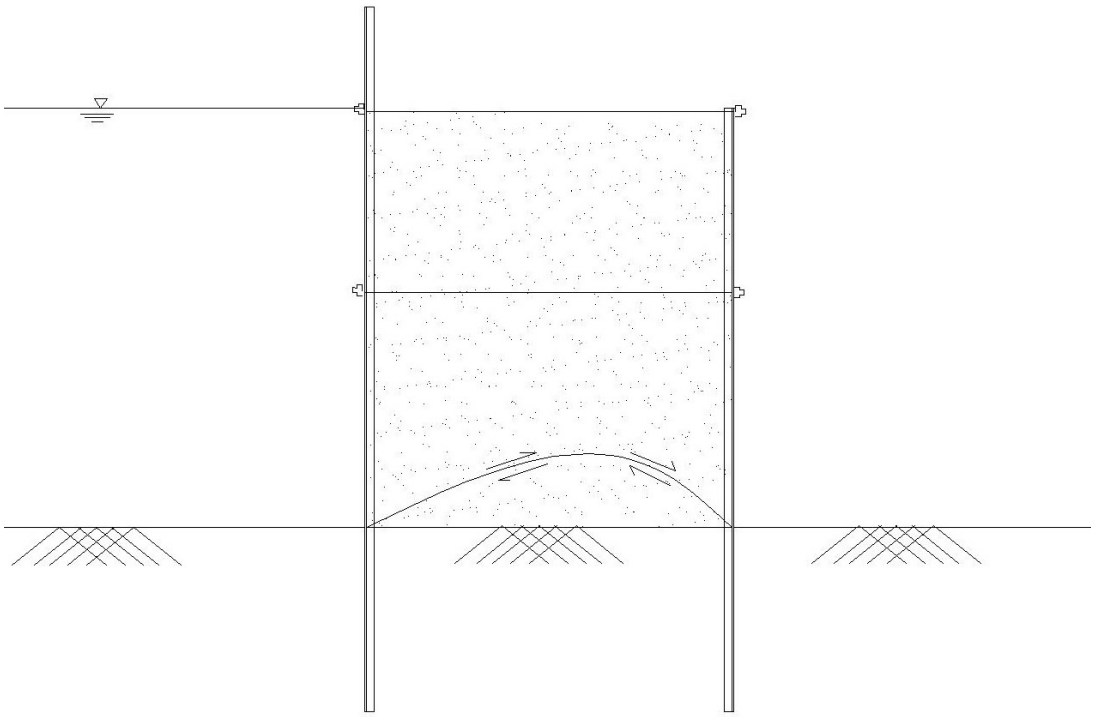

Figure 2-3: Log spiral failure mechanism (Hansen, 1953)

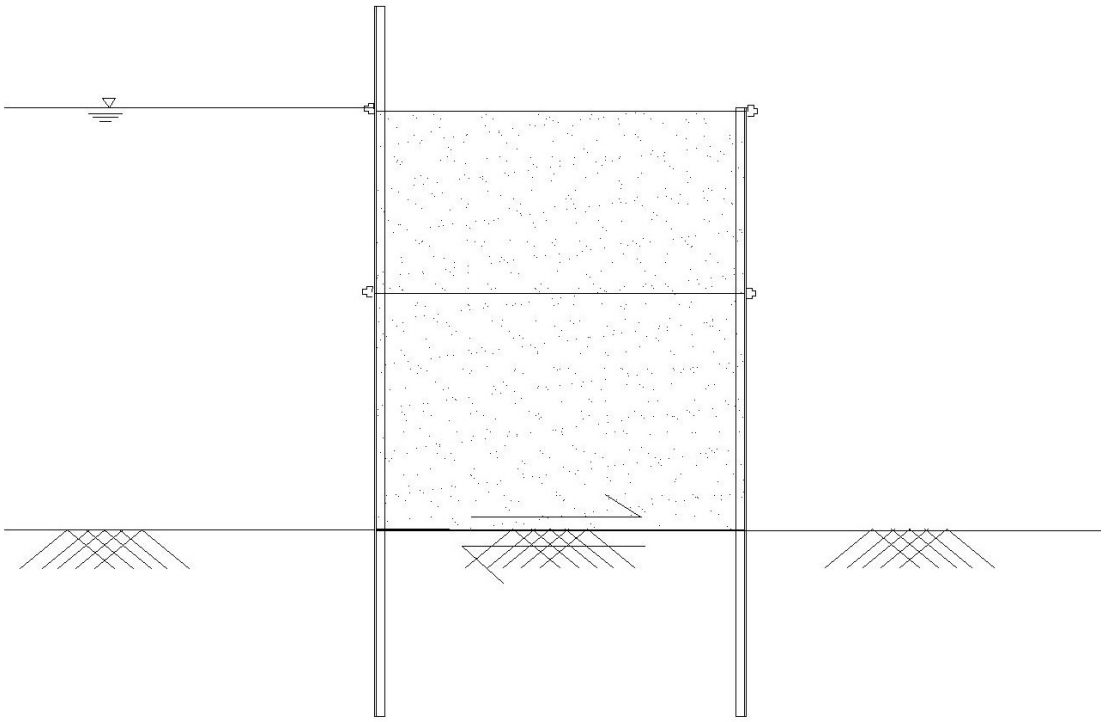

Figure 2-4: Base shear failure (Cummings, 1957)

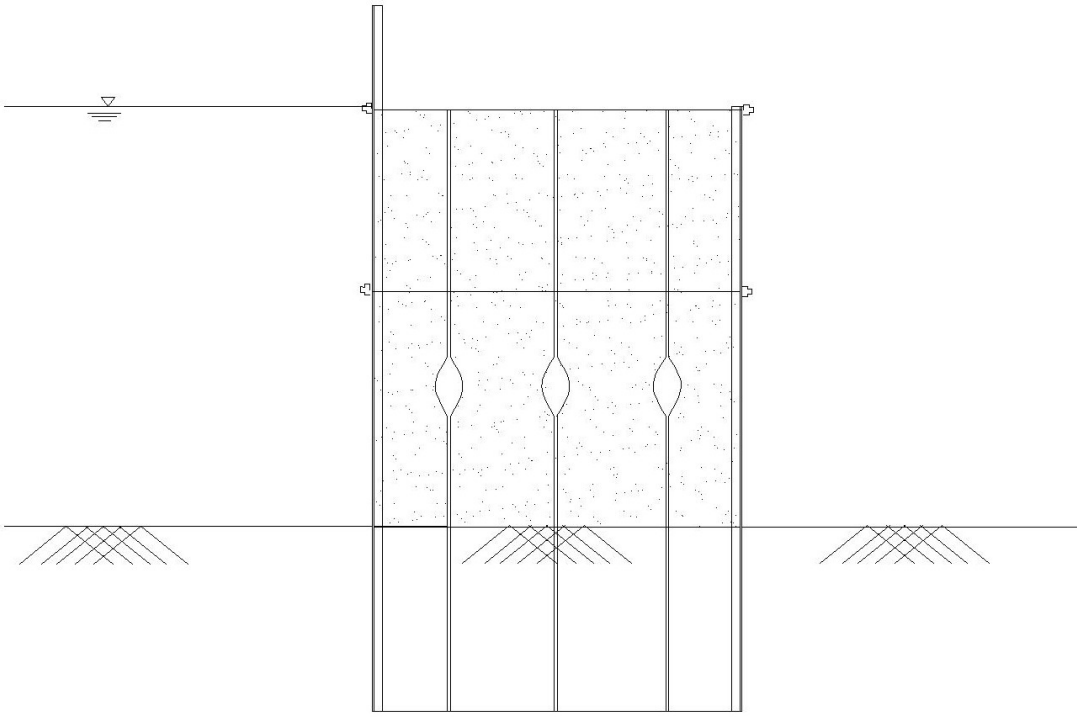

Figure 2-5: Interlock failure (NAVFAC, 1971)

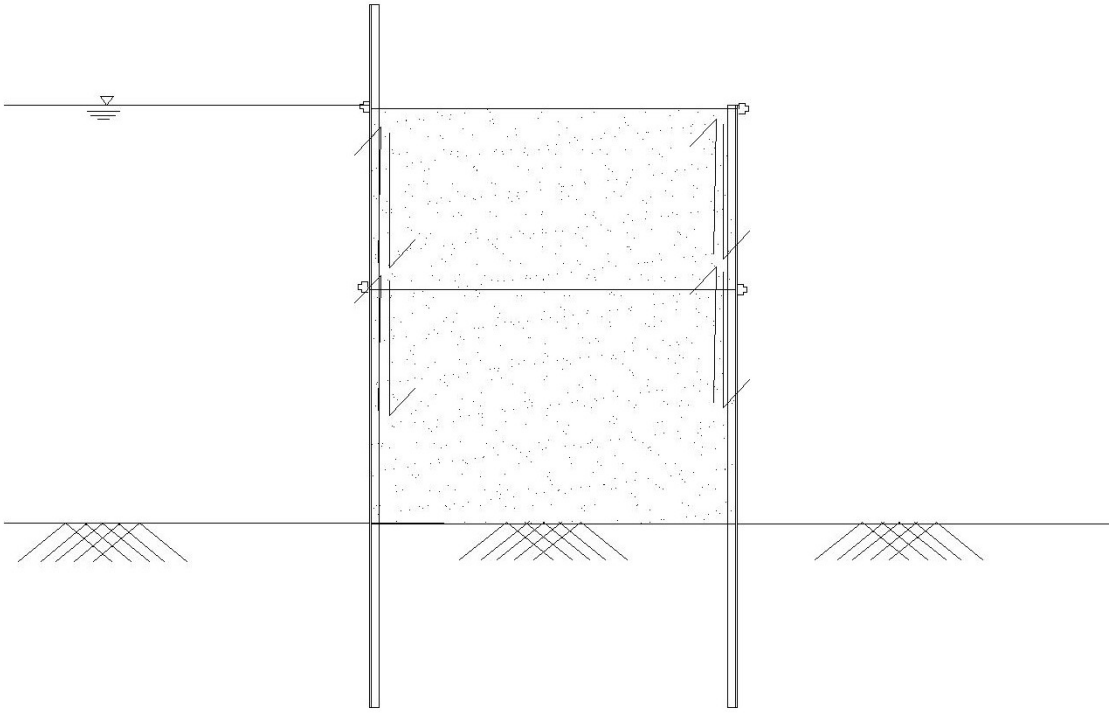

Figure 2-6: Shear Failure at the pile/fill interface (NAVFAC, 1971)

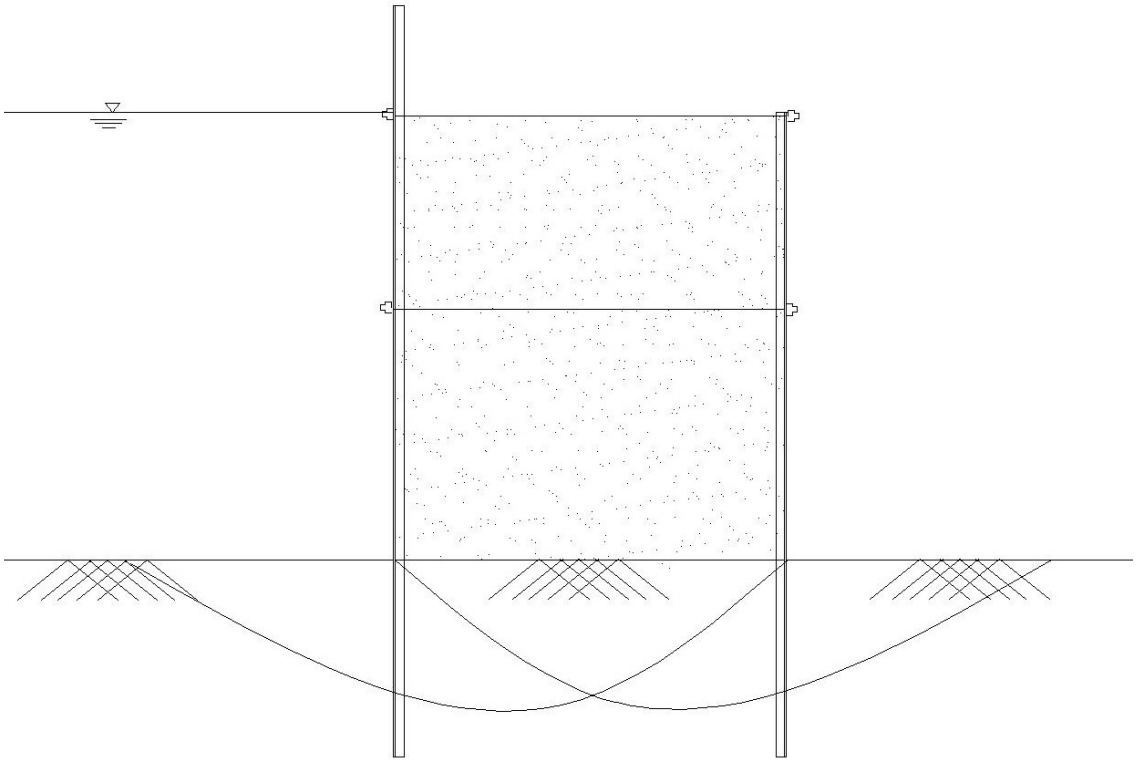

Figure 2-7: Bearing capacity failure at the base of the cell

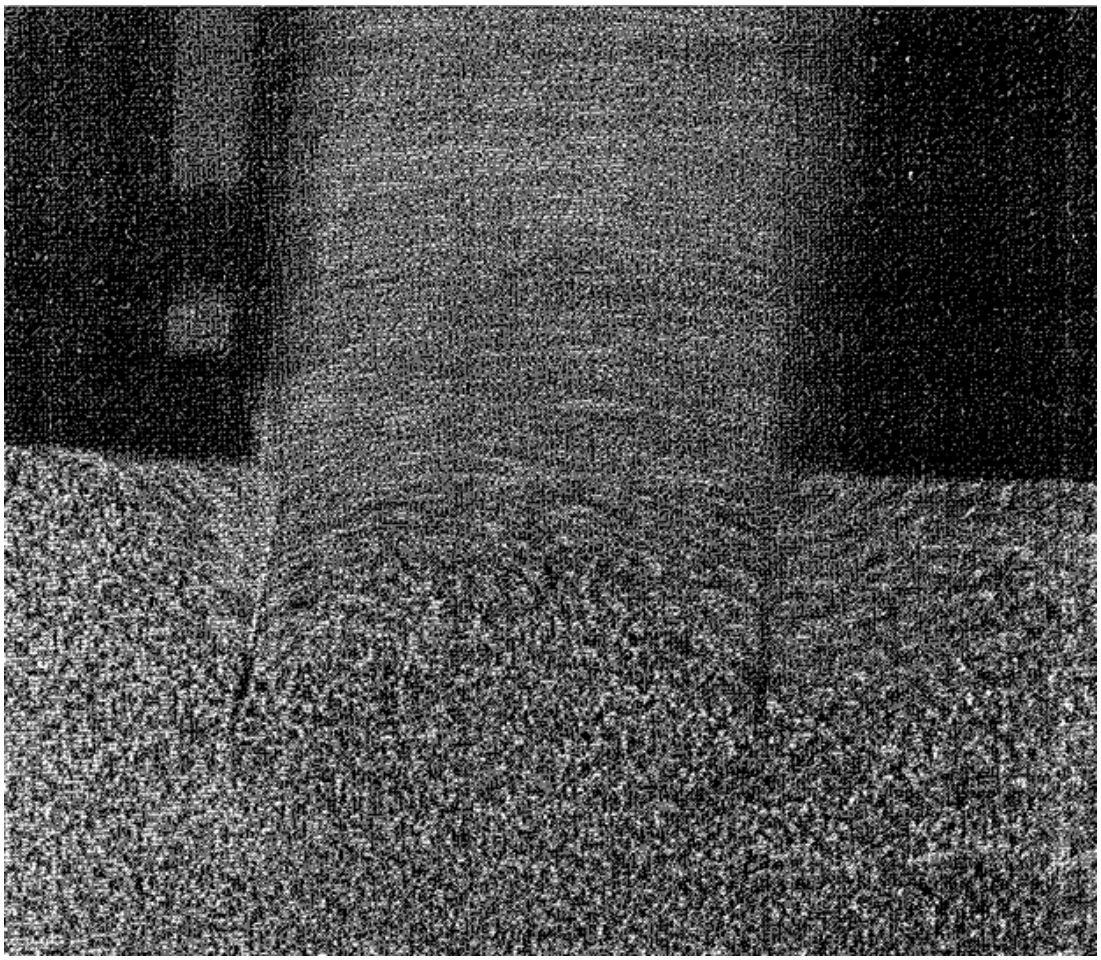

Figure 2-8: Convex failure mechanism from physical test (Ovesen, 1962)

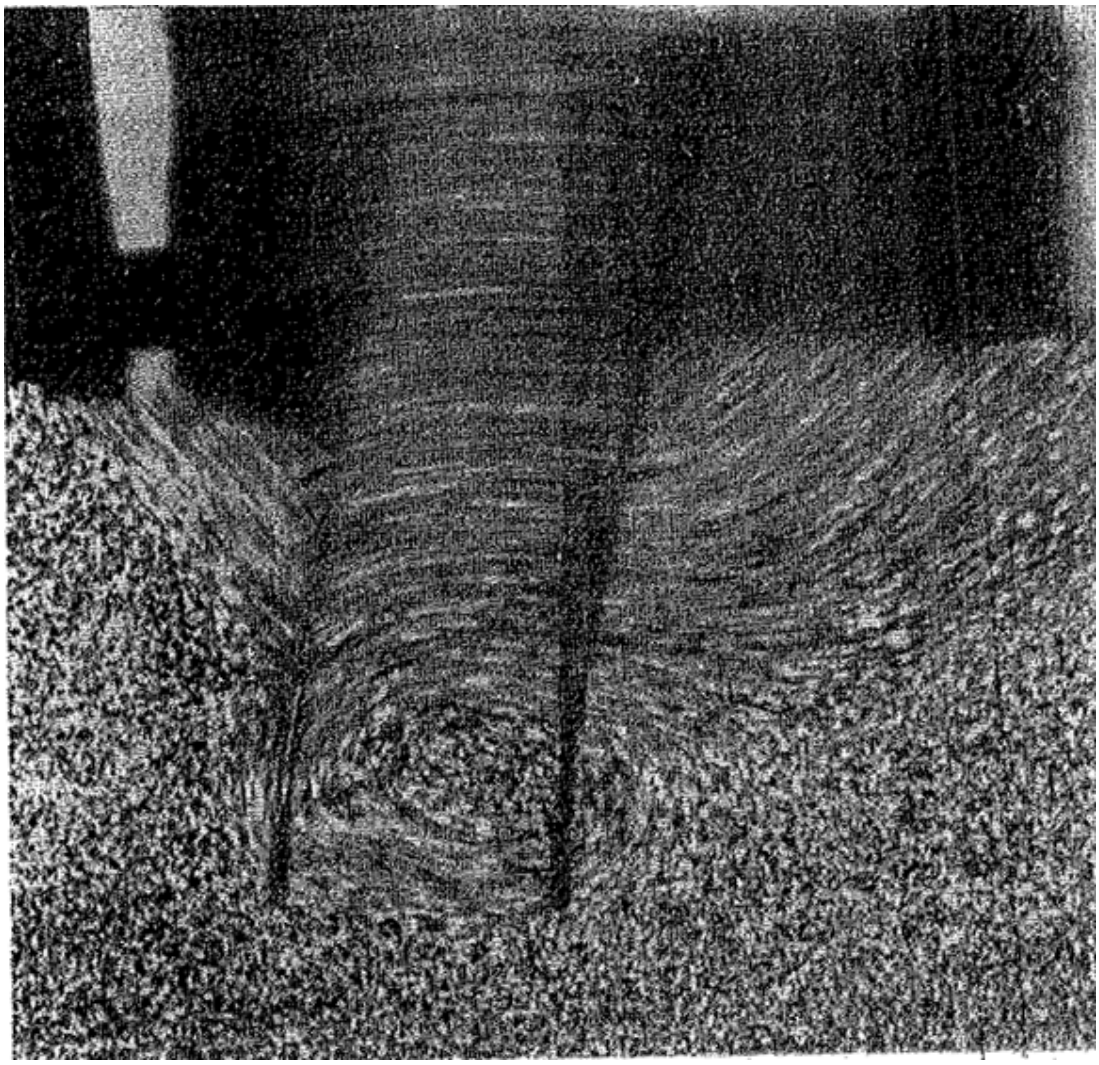

Figure 2-9: Concave failure mechanism from physical test (Ovesen, 1962)

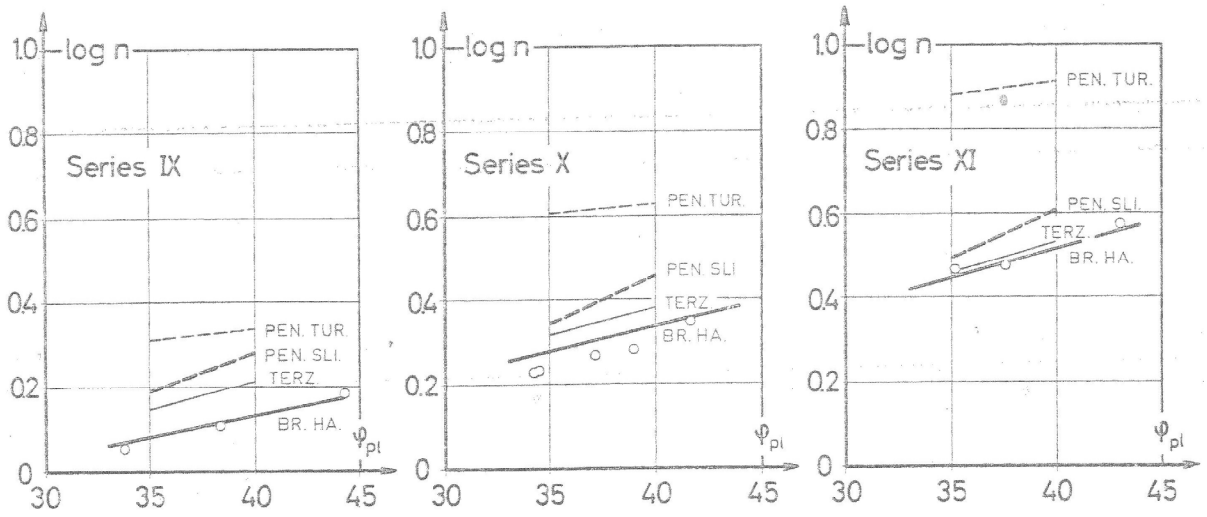

Figure 2-10: Comparison of Ovesen lab test results with Pennoyer (1934), Terzaghi (1944) and Hansen (1953) theories (Ovesen, 1962)

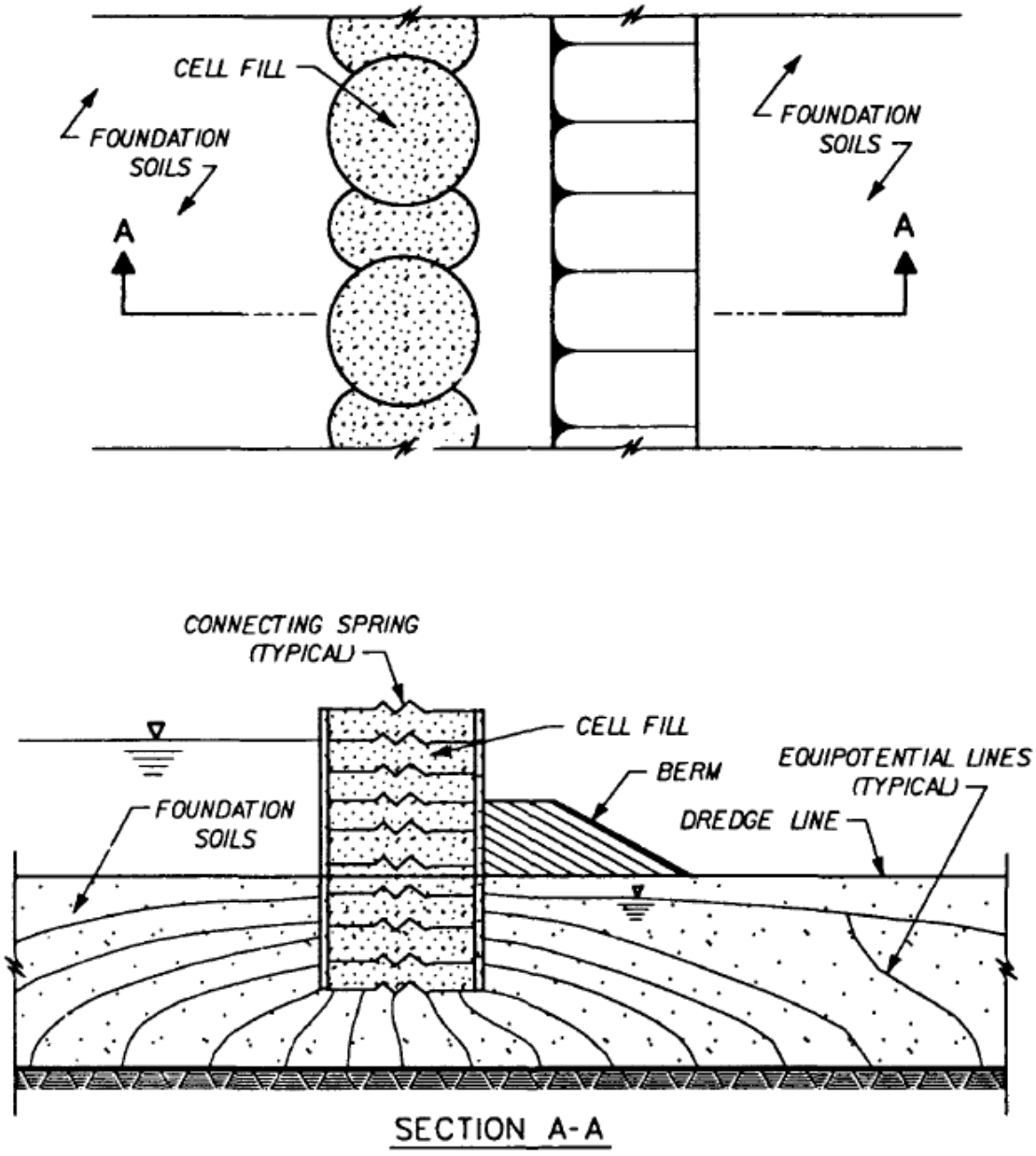

Figure 2-11: Vertical slice model (Clough and Hansen, 1977)

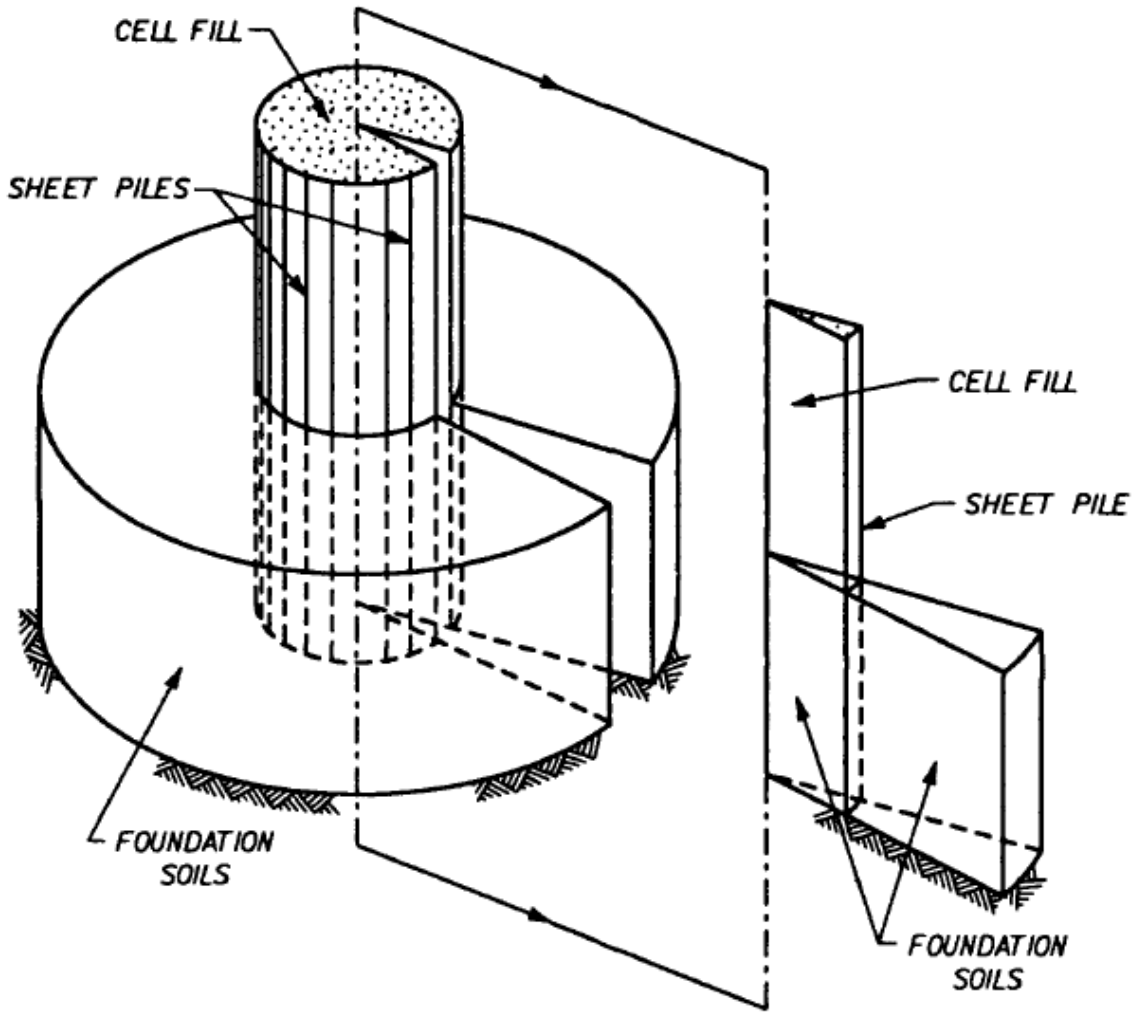

Figure 2-12: Axisymmetric model for single isolated main cell (Shannon and Wilson, 1982)

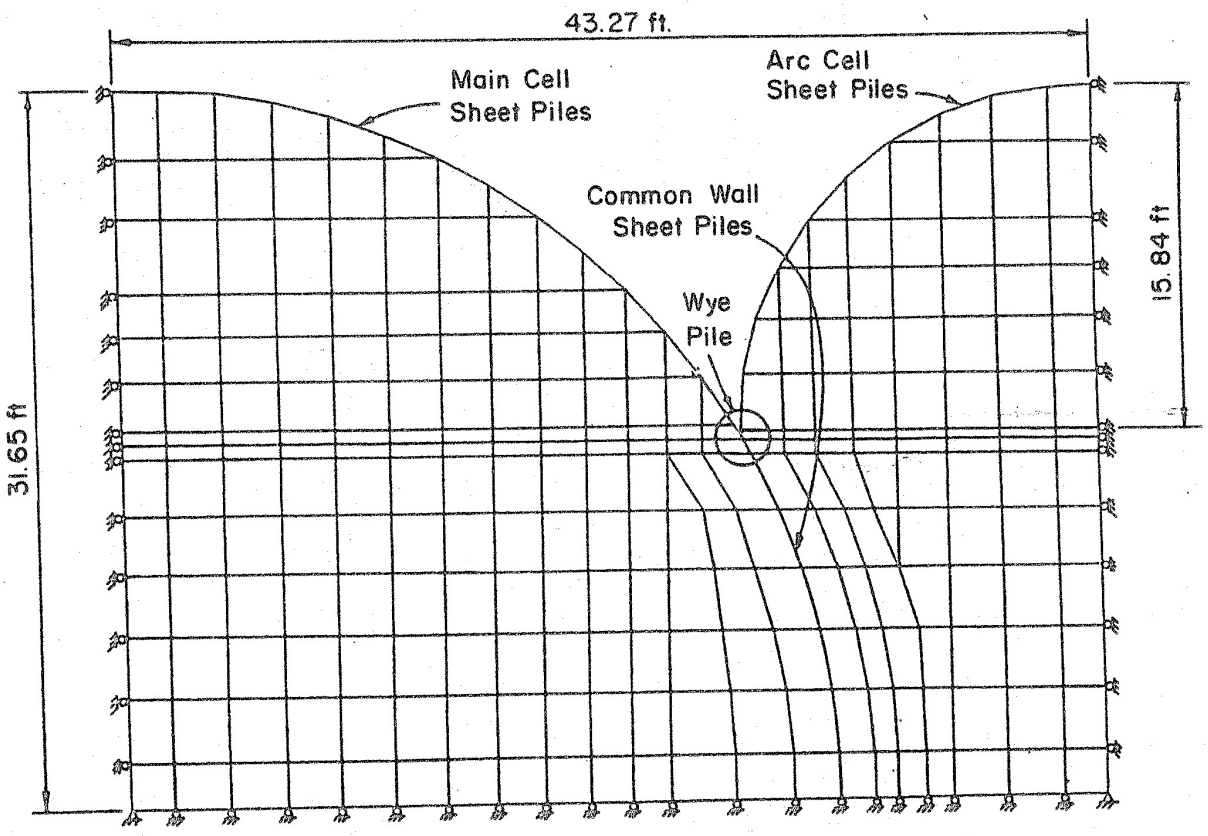

Figure 2-13: Horizontal slice model for main cell along with arc cell (Clough and Kuppusamy, 1984)

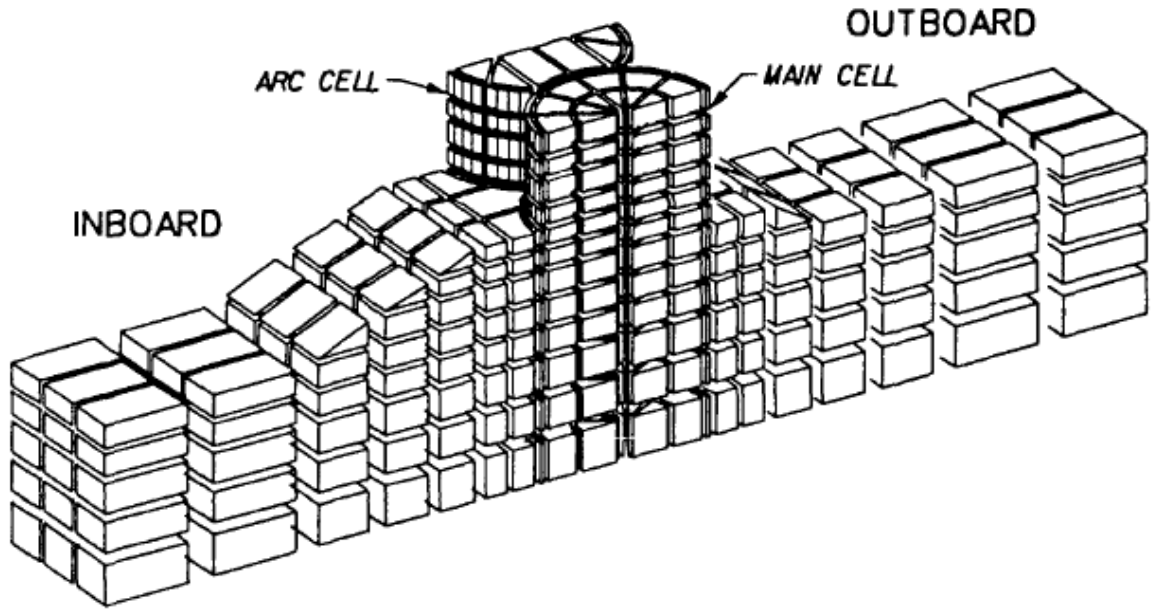

Figure 2-14: Three dimensional finite element mesh for three dimensional analyses (Mosher, 1992)

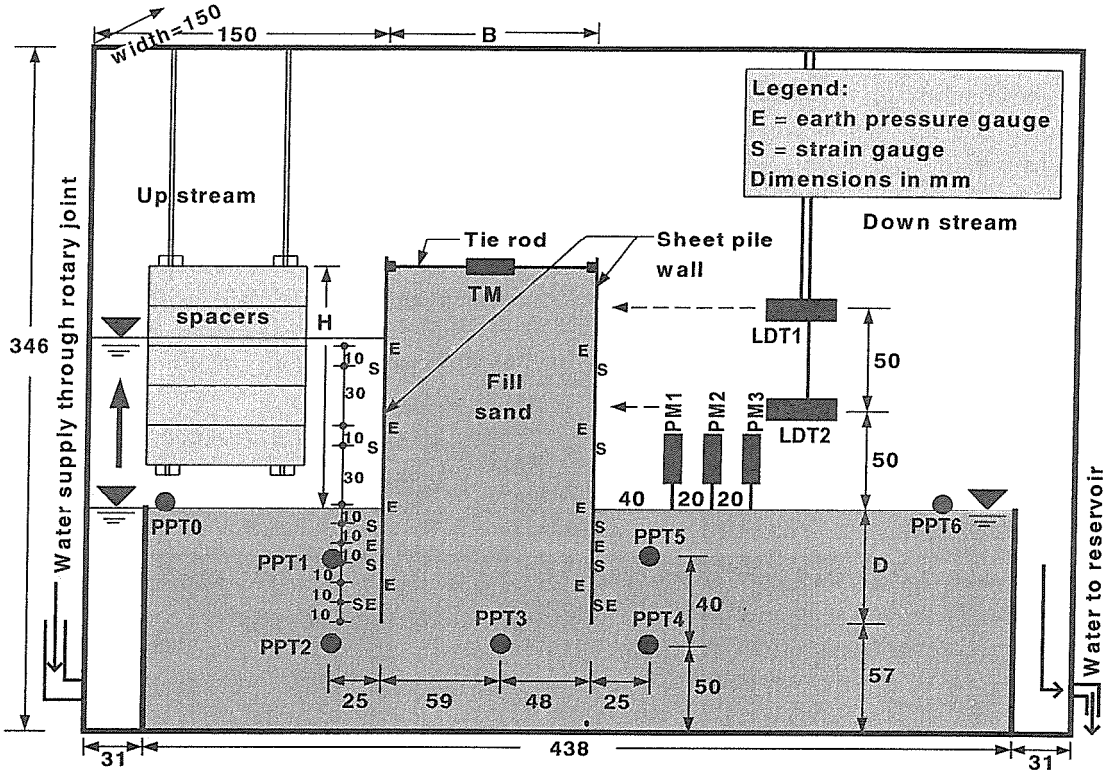

Figure 2-15: Centrifuge model test set up for cofferdam founded on sand foundation (Khan et al., 2001)

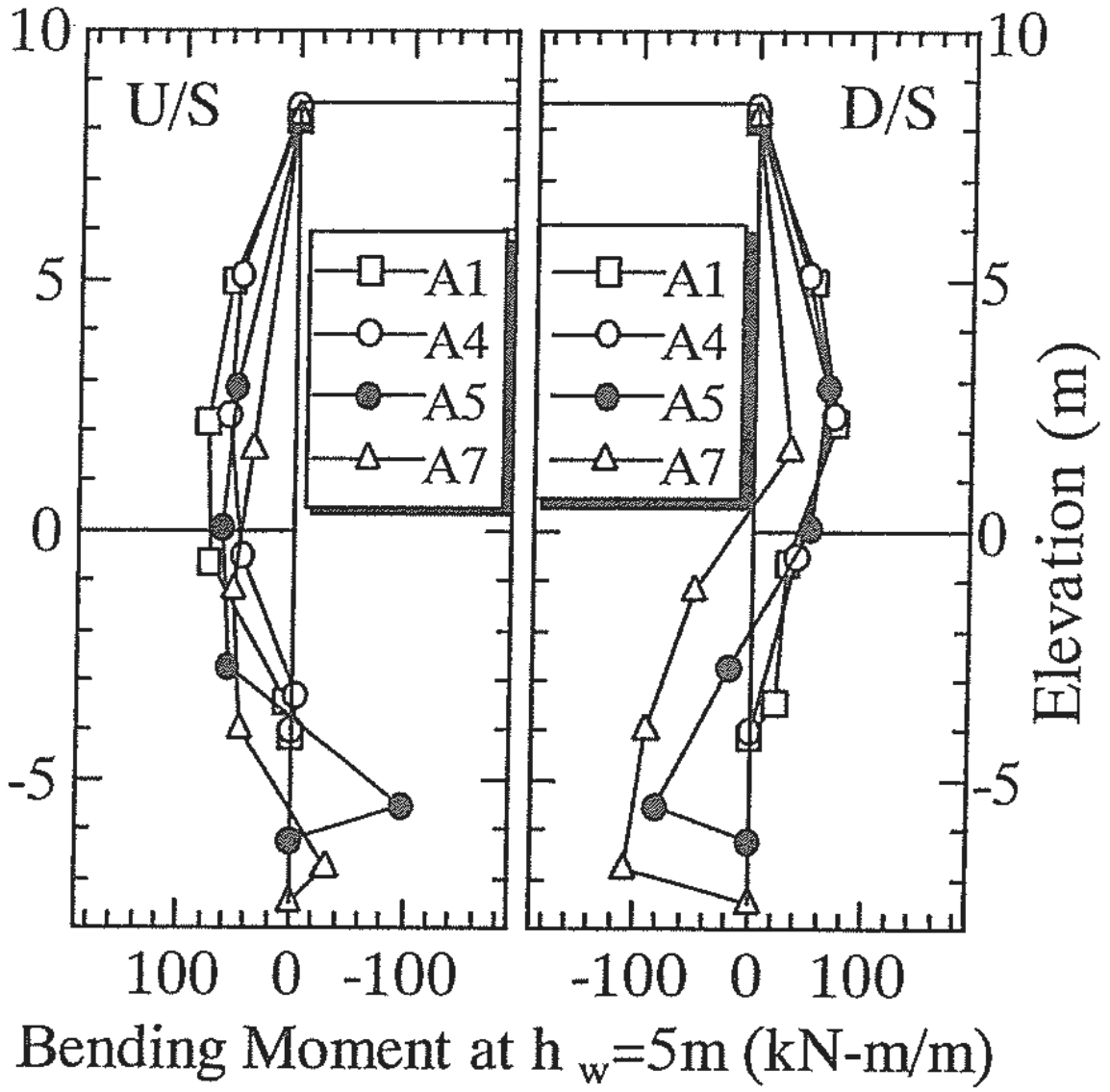

Figure 2-16: Bending moments in inboard (D/S) and outboard (U/S) wall from centrifuge tests on cofferdam founded on sand foundation (Khan et al., 2001)

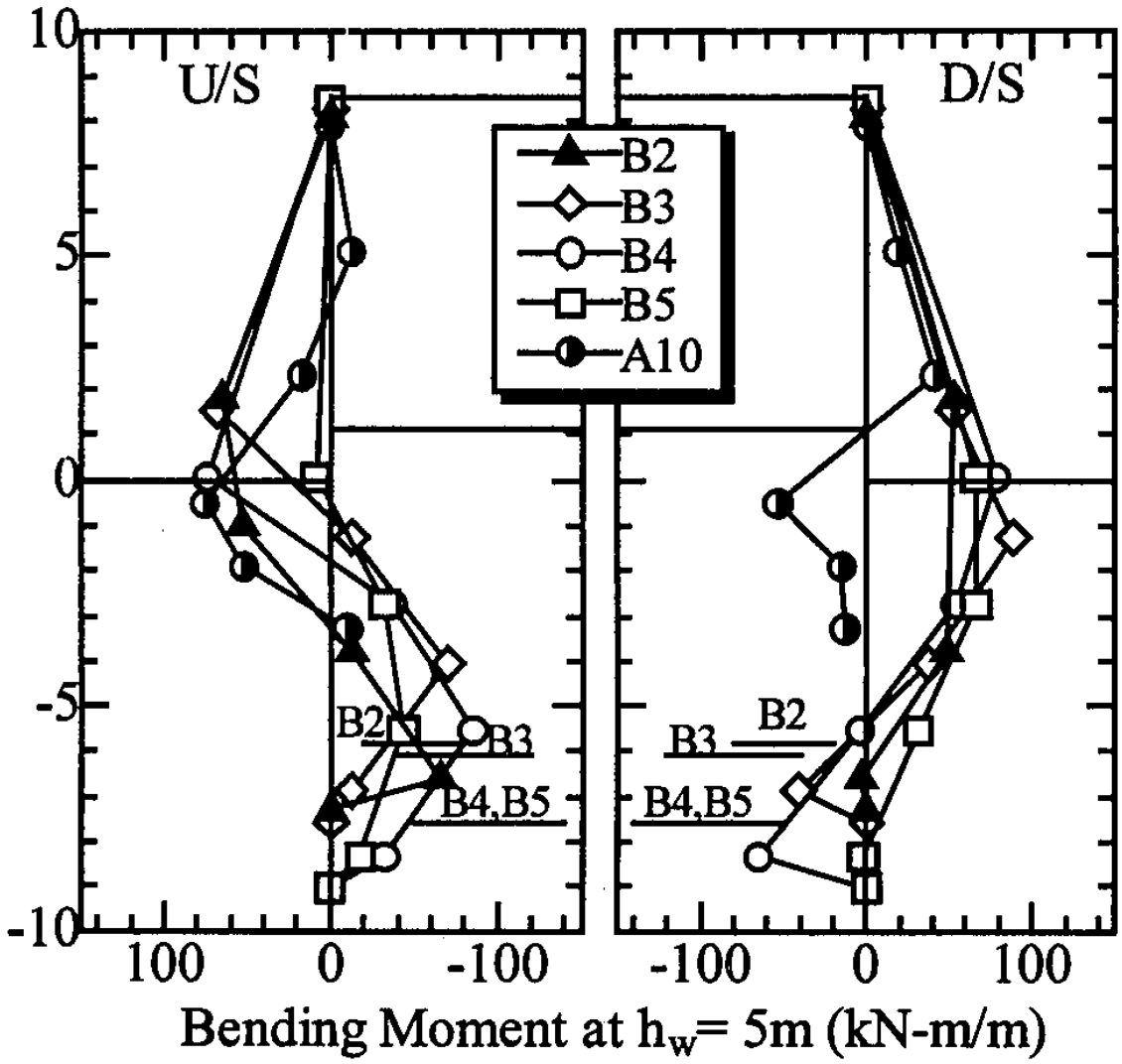

Figure 2-17: Bending moments in inboard (D/S) and outboard (U/S) wall from centrifuge tests on cofferdam founded on clay foundation (Khan et al., 2006)

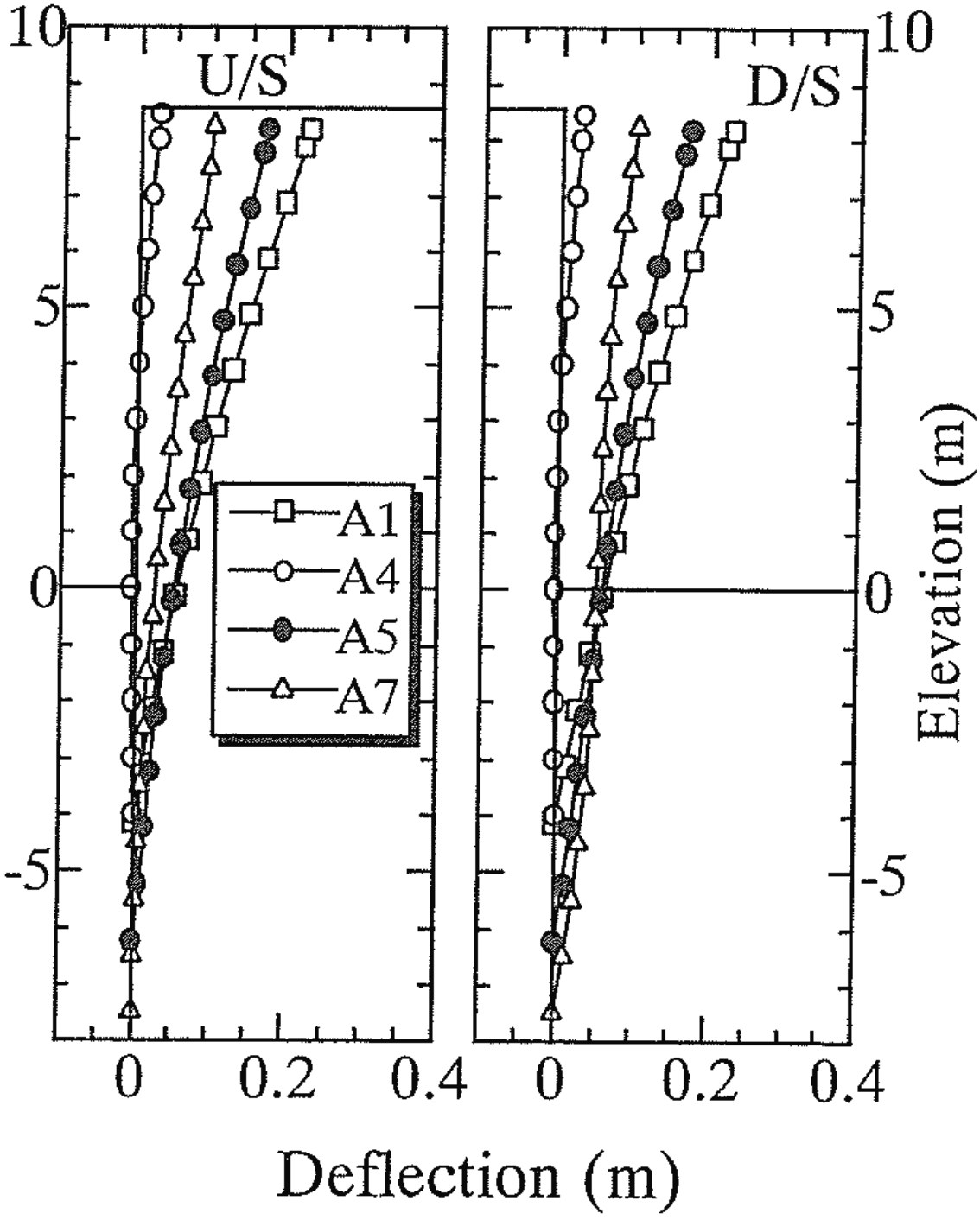

Figure 2-18: Cell wall deflection for the inboard (D/S) and outboard (U/S) wall from centrifuge tests on cofferdam founded on sand foundation (Khan et al., 2001)

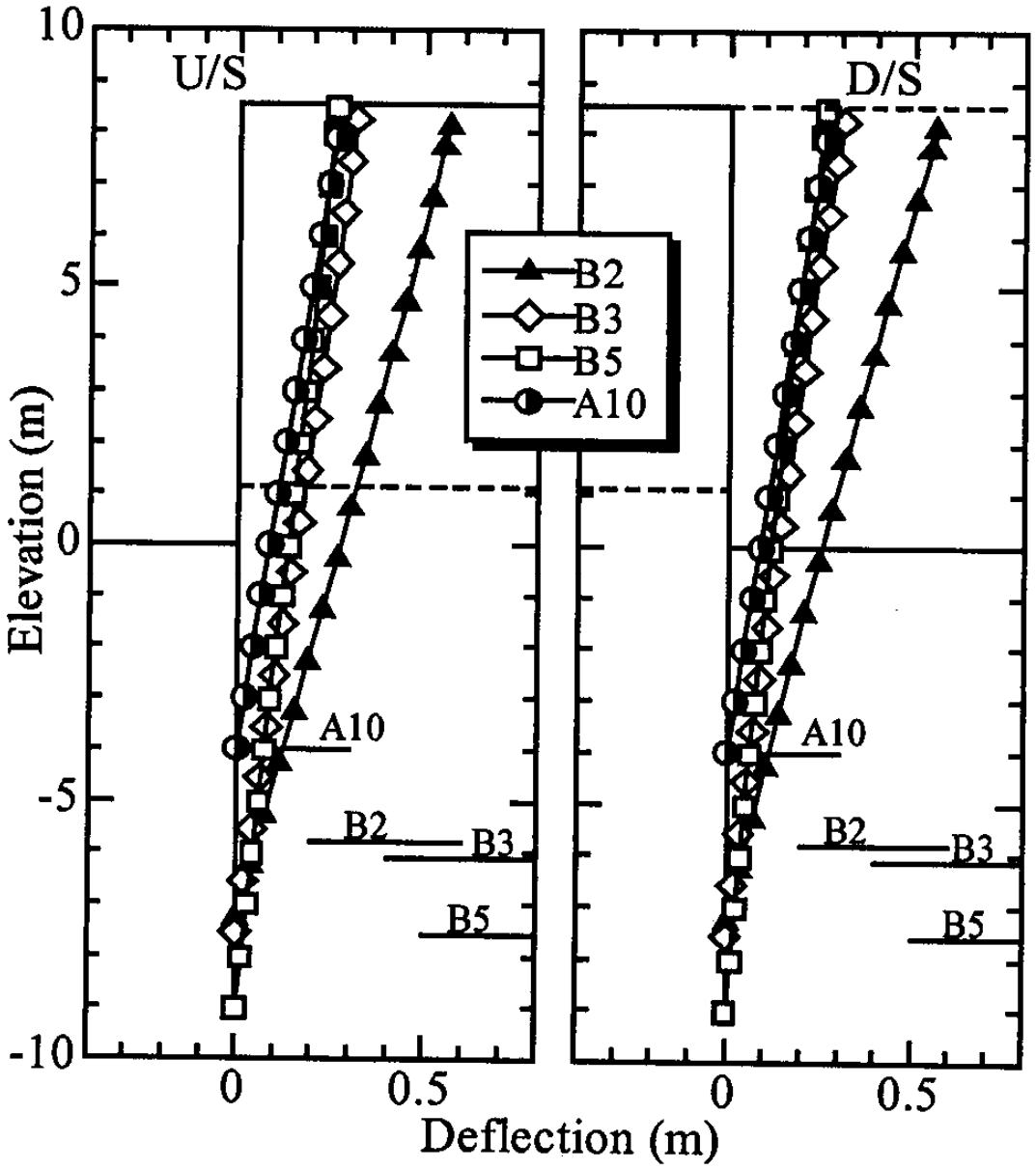

Figure 2-19: Cell wall deflection for the inboard (D/S) and outboard (U/S) wall from centrifuge tests on cofferdam founded on clay foundation (Khan et al., 2006)

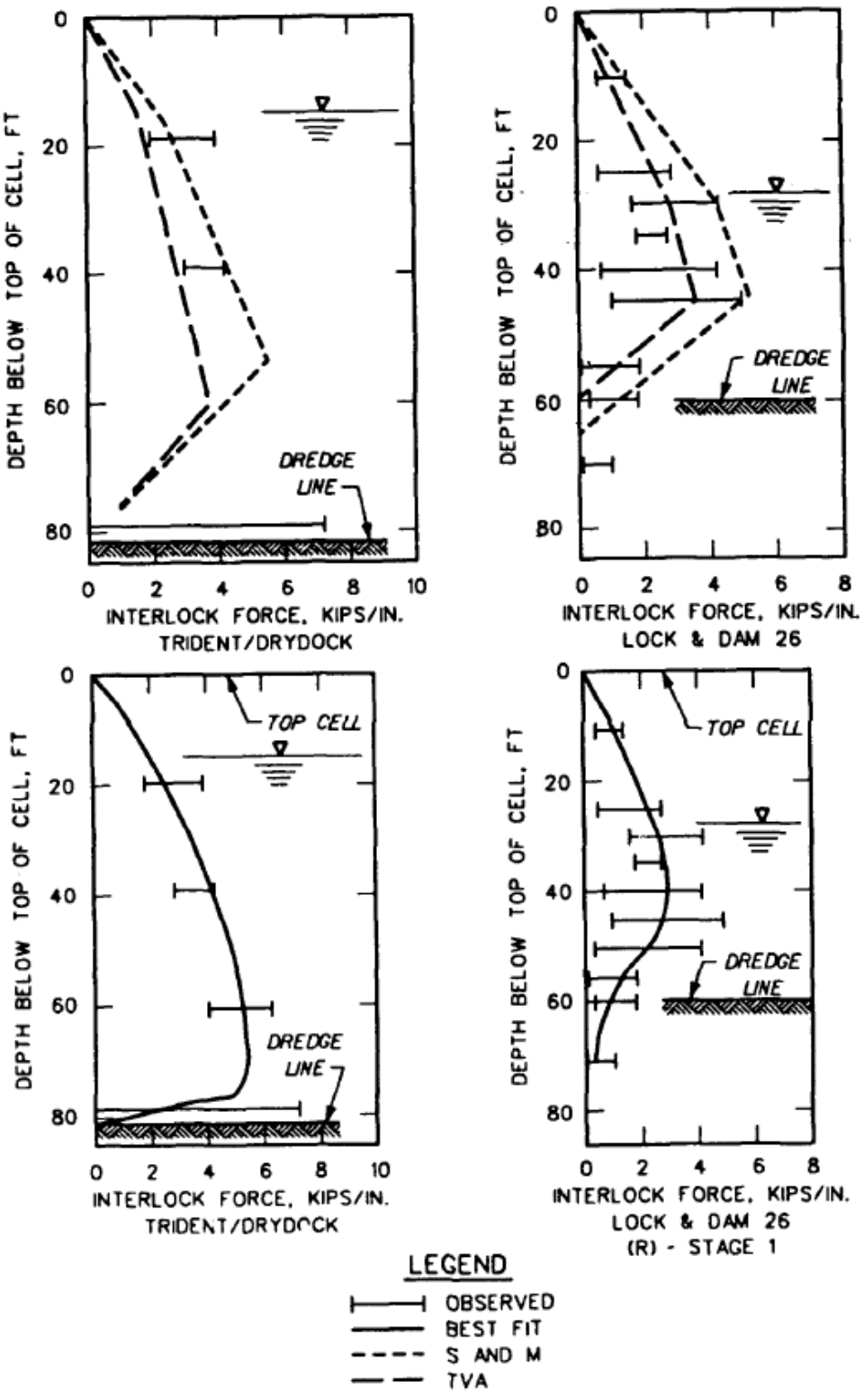

Figure 2-20: Observed interlock forces for Trident and Lock & dam number 26 (Replacement) cofferdams (Martin and Clough 1988)

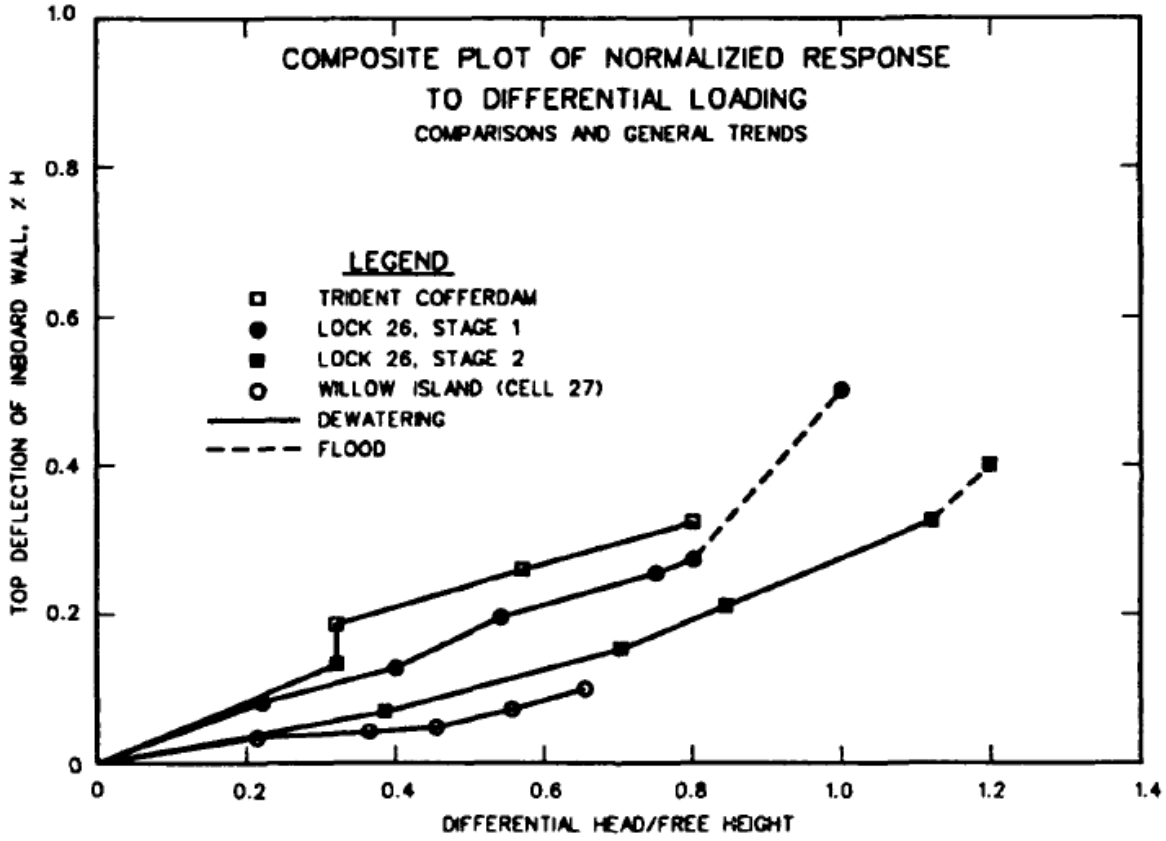

Figure 2-21: Normalised cell wall deflection during differential loading (Mosher, 1992)

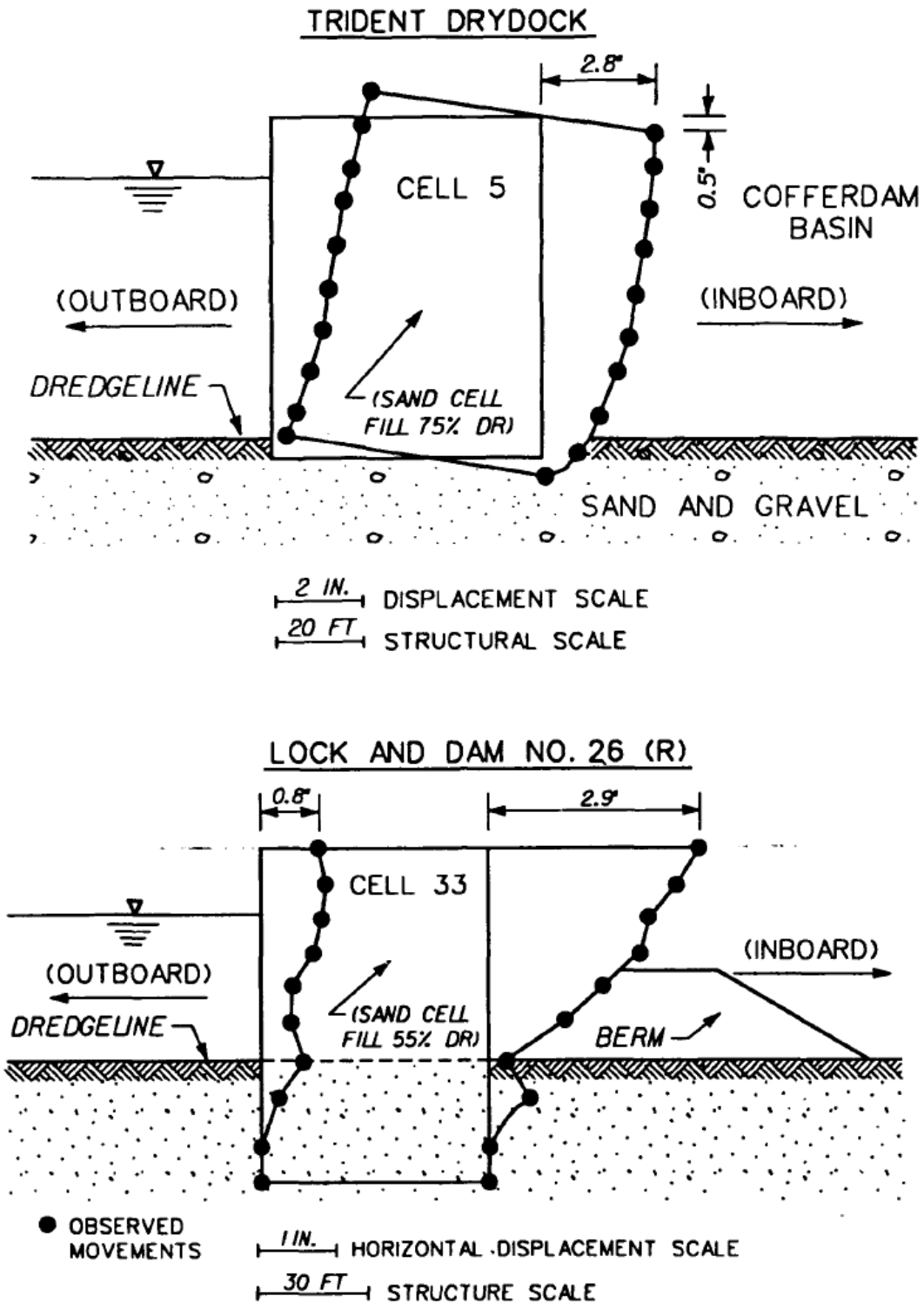

Figure 2-22: Displacement profiles observed at Trident and Lock and Dam No 26 (Replacement) (Martin and Clough 1988)

3 Design and Performance of Cofferdams

3.1 Design Requirements

The cofferdam is typically designed for certain extreme flood levels depending on the type of construction activity within the cofferdam, the sensitivity of the surrounding area and the time during which the structure is to be in service. The flood loading event is usually a short term load and can be treated as an undrained event for cofferdam constructed on a clay foundation. The maximum external water level is assessed and depending on the FoS (factor of safety based on reduced soil strength), a flooding protocol is developed. The cofferdam stability should be checked under highest design water level on the outside and the cofferdam can be flooded after the water level within the river exceeds the design flood. The structure should be analysed for the lowest possible flood level within the cofferdam to prevent damage to the structure and equipment within the cofferdam.

3.2 Overview of cellular cofferdams design standards

A number of design guidelines and standards are available for the design of cellular cofferdams. Guidelines use the stability checks to be applied in a range of combinations to assess the stability of the structure. None of the design standards can be considered to provide a complete assessment of cofferdam stability at this moment due to application of various failure checks independently without mention of type and purpose of the cofferdam. Most of the failure mechanisms considered in these guidelines are not kinematically admissible and not considered critical for all types of cofferdams, some of the current design standards include;

- USACE, US Army Corps of Engineers Design guidelines for design of sheet pile cellular structures, cofferdams and retaining structures (Department of the Army, US Army Corps of Engineers, Washington, DC 20314-1000, 1989);

- NAVFAC, Naval Facilities Engineering Command, Soil mechanics and foundations division (Department of Navy, Design Manual DM-7, 1971);
- CIRIA SP95, Construction Industry Research and Information Association, Special Publication Report 95, (Williams and Waite, 1993);
- BS 8002:1994, Code of practice for earth retaining structures, (British Standards Institution, 1994 amended 2001);
- British Steel Piling Handbook, (2005), Arcelor RPS, Piling handbook, 8th edition;

The US Army Corps of Engineers design guidelines is widely used by designers. This document emerged from field and laboratory studies on a number of cofferdams constructed in US, particularly those constructed on the Mississippi river during the 1960's and 70's. In this document, the geotechnical, analytical, design, and instrumentation issues are discussed in detail and use various stability analysis methods described earlier. This includes the design methods proposed by Terzaghi (1944), Cummings (1957), Schroeder and Maitland (1979), and Hansen (1953). There is also a limited discussion on the use of numerical modelling based on circular cell geometry. The NAVFAC (1971) manual is also widely used for design of cofferdams. The design methods basically take advantage of guidelines proposed by TVA Engineers (1957) for calculation and assessment of cofferdam stability. This document has not been updated for modified cell pressure profiles as described by Maitland and Schroeder (1979), or validated against numerical/field studies. Therefore, it should be used in conjunction with US Army Corps of Engineers guidelines. British Steel Piling Handbook (Schlim & Reuter, 2005) provides details on the size selection and type of sheet piles from a structural capacity viewpoint. It also provides design tables for the selection of embedment depth using pile section modulus, soil strength, type of construction and installation technique. It provides a very limited detail on the overall stability of the structure; therefore it is suggested that this guideline in only used for pile selection and installation technique. Other design standards presented here use fundamentally the same failure checks adopted in USACE and NAVFAC guidelines. These failure checks are discussed in detail in the following section.

3.3 Critical failure mechanisms

3.3.1 Interlock strength of sheet piles

As discussed in section 2.5, the interlock connection strength is one of the most critical failure design considerations, as interlock failure is the prime cause of cofferdam cell failure. To determine the maximum interlock forces, the soil pressures acting on the sheet piles need to be estimated. The soil pressure acting on the cell wall is equal to the sum of the water and soil pressure acting on the wall. The lateral soil pressure is considered to increase with depth, calculated by multiplying overburden with a suitable lateral earth pressure coefficient. Therefore the pressure at any depth H can be calculated as;

$$P = K \times \sigma_v' \qquad \textbf{Equation 3.1}$$

An earth pressure coefficient of K=0.4 was used by Terzaghi (1944), and this was increased to 0.5 by the US Army Corps of Engineers Guidelines (1970). The pressure distribution suggested by Terzaghi (1945) and USACE guidelines (1970) assumed that the pressure increased with the depth and that the maximum pressure acted at the base of excavation, see Figure 3-1(a). Terzaghi's (1945) earth pressure distribution was modified by TVA Engineers guidelines (1957), with maximum pressure acting at 0.75H below the top of the cell, where H is height of the cell above the rock surface, See Figure 3-1(b). The pressure at the base of excavation was reduced to zero as the cell rested on a rock surface without any significant embedment depth. This was applied to a cofferdam founded on the clay/sand where the piles were embedded into the ground to some depth. The assumption that response of clay/soil will be the same as rock foundation is therefore not realistic. The pressure distribution suggested by TVA Engineers was modified in light of field and laboratory studies of circular cells embedded in sand/clay by Maitland and Schroeder (1979). The fill pressure was proposed to be zero at a depth where the sheet piles develop a plastic hinge in their model tests, the depth of this plastic hinge was considered as d′ below the dredge-line, considered as a plane of fixity, see Figure 3-2. The point of maximum pressure was found to be H′/3, where H′=(H+d′), is height of the cell above the plane of fixity. The lateral earth pressure coefficient was calculated as 1.2 to $1.6K_a$, to accommodate the compressibility of the cell due to the applied load. The

Maitland and Schroeder (1979) method was applicable to smaller diameter cells, and can be practically applied to cells founded on rock, clay or sand foundations.

Once the pressure acting on the sheet piles has been calculated the interlock tension can be calculated using an equation for the calculation of hoop stresses (for a circular cell), using equation;

$$t = p_{\max} \times r \qquad \textbf{Equation 3.2}$$

Where

t = maximum interlock pressure

P_{max} = Maximum inboard sheeting pressure

r = Radius of the cell (for circular cells)

The maximum interlock pressure at the connecting arcs between neighbouring cells can be calculated as;

$$t_{\max} = p \times L \times \sec\theta \qquad \textbf{Equation 3.3}$$

Where

L =Distance between centrelines of adjacent cells

θ = Angle between the joint and centreline of the cofferdam, subtended at the centre of the cell

The factor of safety against interlock failure (FoS_{int}) can be calculated as the ratio between the interlock strength, and the maximum interlock tension developed as a result of soil/water pressure acting within the cell.

$$FoS_{\text{int}} = \frac{T}{t_{\max}} \qquad \textbf{Equation 3.4}$$

Where

T = Interlock strength of the piles

3.3.2 Internal Shear Failure within the cell

Internal stability is checked by assuming that a pre-determined shear plane through the centreline and at the base of fill within the individual cell is able to develop. The vertical and horizontal shear failure planes are considered for this purpose to asses the stability against tilting of the cell. The vertical shear resistance was first suggested by Terzaghi (1944), with analyses of development of a shear plane at the centreline of the cell. The results from Terzaghi's method were identified to be overly conservative as they considered a full plastic zone to develop within the limited cell width which will overestimate the centreline pressure within the cell. Terzaghi's (1945) pressure distribution was later modified in light of field and laboratory testing results by Maitland and Schroeder (1979) which will be discussed is section 3.3.2.1 (a) of this document.

The horizontal shear resistance was introduced by Cummings (1957). The concept of horizontal shear resistance is based on the assumption that the cell fill will resist any distortion in the lateral direction by offering horizontal shear resistance against sliding on a horizontal plane. The calculations for the factor of safety against internal cell failure are discussed in the following:

3.3.2.1 Vertical shear failure

(a) Terzaghi method:

Terzaghi (1944), introduced an analytical method for the calculation of internal cell stability of cellular cofferdams in which he suggested that before the cofferdam fails due to excessive deflection or rotation there is a chance that it would have already failed due to shear failure at a pre-determined plane at the centreline of the cell. This assumption in considering the centreline of the cell as the most critical shear plane, was based on the fact that it is the plane of neutral axis for base pressure, and hence the maximum shear force will act at this plane. For stability against such failure, the shearing resistance at the cell centreline combined with the resistance to the movement offered by the interlock joints should be equal or greater than the applied shear force acting on this plane. The total shear force acting on the centreline can be calculated from the pressure distribution

at the base of the cell (Figure 3-3a). From the triangular pressure distribution at the base of the cell the total shear force (Q_T) may be calculated as

$$Q_T = \frac{1}{2} \times \frac{B}{2} \times \frac{6M}{B^2}$$ **Equation 3.5**

Simplifying;

$$Q_T = \frac{3M}{2B}$$ **Equation 3.6**

Where

B = Effective width of the cell

M = Net overturning moment

The shear resistance along the centreline can be calculated from the resistance offered by the cell fill and interlock sliding resistance. The shear force at the centreline of the cell is the fill pressure acting at the centreline multiplied by the angle of internal friction of cell material. The central pressure distribution assumed by Terzaghi (Figure 3-3b) can be used to calculate the centreline pressure.

$$P_s = \frac{1}{2} \times \gamma \times \mathrm{K}(H - H_1)^2 + \gamma \times \mathrm{K}(H - H_1) + \frac{1}{2} \times \gamma \times \mathrm{K} \times H_1^2$$ **Equation 3.7**

P_s = fill pressure at centreline of the cell

H = Height of the cell

H_1 = Height of water table above dredge line

Where

$$\mathrm{K} = \frac{\cos^2 \phi}{2 - \cos^2 \phi}$$ **Equation 3.8**

Where

K = Lateral earth pressure coefficient

Therefore total centreline shear resistance offered by cell fill can be calculated as;

$$S_s = P_s \times \tan\phi \qquad \textbf{Equation 3.9}$$

Where

S_s = Total vertical shear resistance due to fill

The shear resistance offered by interlocks can be calculated from multiplying interlock tension calculated in section (3.2.1), by steel frictional coefficient for interlocks.

$$S_F = f \times P_T \qquad \textbf{Equation 3.10}$$

S_F = Shear resistance of interlocks

P_T = interlock pressure

Therefore the total shearing resistance (S_T) at the central plane will be

$$S_T = P_S \times \tan\theta + f \times P_T \qquad \textbf{Equation 3.11}$$

The factor of safety against shear failure on the vertical plane at the centreline of the cell (FoS_{vs}) can be calculated by dividing the total shear resistance (S_T) by the ultimate load (Q) on the centreline.

$$FoS_{vs} = \frac{S_T}{Q} \qquad \textbf{Equation 3.12}$$

The above equation can be used for a cofferdam cell founded on rock, sand and stiff clay where sufficient foundation stiffness is available to offer equal pressure distribution at the base of the cell. For a cofferdam founded on the soft clay, shear resistance offered by the interlocks should only be used as shear resistance in the fill cannot be mobilised within the cell fill without overstressing the interlocks due to the soft nature of the foundation material. The factor of safety for cell founded on soft clays will be:

$$FoS_{vs} = \frac{P \times R \times f\left(\frac{B}{L}\right)\left(\frac{L + 0.25 \times B}{L + 0.50 \times B}\right)}{M} \qquad \textbf{Equation 3.13}$$

Where

P = Pressure difference of inboard sheeting

R = Radius of the cell

f = Coefficient of internal friction

B = Effective width of the cell

L = distance between centrelines of adjacent cells

M = Net overturning moment

(b) Schroeder and Maitland Method:

The Terzaghi method was found to have reasonable agreement with experimental results when the coefficient of earth pressure was taken as 0.4 to 0.5, but experience shows that for a conventionally sized size cofferdam the values of K are generally above the given limit and hence the Terzaghi method cannot be applied until the cell width is large enough to allow plastic zones to fully mobilise the ordinary active and passive earth pressures (Hansen, 1953). Terzaghi's pressure distribution at the neutral axis of the cell was modified by Schroeder and Maitland (1979), using results from laboratory and field studies. Their pressure distribution used by Tennessee Valley Authority (1957) pressure distributions profile with a redefined pressure depth below the dredge line (Figure 3-2). As a result of cell compression, a lateral earth pressure coefficient (K) of 1 was suggested; this is in agreement with practical values used for smaller diameter cells. The total shear resistance offered by the cell fill (calculated using Figure 3-4b) and interlock resistance can be written as:

$$S_T = \frac{1}{2} \times \gamma \times K\left(H'^2\right) \times \left(\tan\theta + f\right) \qquad \textbf{Equation 3.14}$$

Where

H' = Height of the cell over which vertical shear resistance is applied

The location of point of fixity (Depth d′ below top of overburden) can be calculated as 3.1T with depth of embedment >5T:

$$T = 5 \times \sqrt{\frac{EI}{n_h}}$$ **Equation 3.15**

Where

n_h = constant of horizontal subgrade reaction (See USACE, 1989, for values of n_h for various soil types)

3.3.2.2 Horizontal Shear failure

The stability against horizontal shear failure at the base of the cell is calculated using a method suggested by Cummings (1957). The resistance is offered by the fill in the form of a soil wedge of angle of ϕ' to the horizontal on the inboard side, where ϕ' is equal to angle of internal friction of the fill material. The fill above the wedge will act as an overburden above the failure resisting wedge. The horizontal shear resistance force can be calculated from Figure 3-4a, as:

$$F = \gamma \times H \times B \times \tan\phi$$ **Equation 3.16**

Also

$$H = a + c$$

$$B = \frac{c}{\tan\phi}$$

Replacing the values in the first equation

$$F = a \times c \times \gamma + c^2 \times \gamma$$ **Equation 3.17**

The resisting moment above the base of the cell for the fill material can be calculated from (Figure 3-4b)

$$Mr = \frac{a \times c^2 \times \gamma}{2} + \frac{c^2 \times \gamma}{3}$$ **Equation 3.18**

The horizontal shear resistance provided by interlocks can be calculated as:

$$M_f = P_T \times f \times B$$ **Equation 3.19**

The total resisting moment against horizontal shear failure can be calculated as:

$M_T = M_r + M_f$ **Equation 3.20**

Therefore the factor of safety against horizontal shear failure will be

$$FoS_{h-shear} = \frac{M_r + M_F}{M_o}$$ **Equation 3.21**

Where

M_o = Net overturning moment

The above equation doesn't take into effect of berm in to the calculations. If the berm is provided the resistance against the horizontal shear will increase to:

$$FoS_{hs} = \frac{M_r + M_f + P_R\left(\frac{H_B}{3}\right)}{M_o}$$ **Equation 3.22**

Where

P_R = Passive resistance offered by berm

H_B = Height of the berm

3.3.2.3 Penetration capacity of sheet piles

Both the inboard of outboard piles are checked for adequate penetration to avoid the pull out of the outboard piles and further pushing down of the inboard sheet piles due to unbalanced forces acting on the cell. The capacity of the sheet piles is assessed on the basis of guidelines provided by US Army Corps of Engineers Design Guidelines (1989).

(a) Pull out of outboard sheeting:

The outboard piles are usually designed to increase the seepage path on the wet side to reduce uplift pressure; however its embedment should be checked for pull out due to an overturning moment. The pull out capacity of the outboard sheet pile may be calculated as:

Pull out capacity for cofferdam founded on granular soil,

$$Q_u = \left(\frac{1}{2} \times K_a \times \gamma_e \times D^2 \times \tan\delta \right) \times Perimeter \qquad \textbf{Equation 3.23}$$

Where

Q_u = Ultimate pull out capacity

K_a = Coefficient of active earth pressure coefficient

γ_e = effective unit weight of soil in contact with outboard pile

D = Embedment depth

$\tan\delta$ = Coefficient of friction between soil piles interfaces (Values for various soils provided in table 4-3, of US Army Corps of Engineers Design Guidelines, 1989)

Perimeter = on one foot length of the wall taking the both sides of the walls the perimeter should be 2 times length of the wall.

Pull out capacity of cofferdam founded on clay,

$$Q_u = Ca \times D \times Perimeter \qquad \textbf{Equation 3.24}$$

Where

Ca = Adhesion of soil (see NAVFAC design guidelines for values of C_a for various soil types)

The overturning moment will apply a pull out reaction force (Q_p) in the sheet piles on outboard side. Therefore the factor of safety against pull out of outboard sheet piles will be;

$$FoS_{pull} = \frac{Q_u}{Q_p} \qquad \textbf{Equation 3.25}$$

(b) Penetration of inboard sheet piles:

The unbalanced force acting on the cell will try to push the inboard sheet piles further into the ground by applying an overturning moment on the cell. The sheet piles on the inboard side should not be allowed to penetrate further beyond the designed embedment depth. The resisting moment (M_{pen}) on the sheet piles countering the overturning moment will be;

$$M_{pen} = \left(P_T \times \tan\delta\right) \times D \qquad \textbf{Equation 3.26}$$

Therefore the factor of safety against excessive penetration of the inboard piles will be;

$$FoS_{pen} = \frac{M_{pen}}{M_o} \qquad \textbf{Equation 3.27}$$

3.3.3 External stability analyses

For external stability analyses of cellular cofferdams, the following failure modes should be considered (USACE, 1989).

3.3.3.1 Stability against sliding failure

Sliding failure is considered along a presumed failure surface at the base of the cell. The sliding surfaces can be curved, straight or a combination of both. The stability is assessed by calculating the shear resistance capacity on the assumed planes of maximum shear. The minimum safety factor against sliding failure is calculated using an iterative process for various failure surfaces. The sliding failure will occur along the presumed failure surface only when the failure surface is kinematically admissible. The factor of safety against sliding failure can be calculated as;

$$FoS_{sliding} = \frac{\tau_F}{\tau} \qquad \textbf{Equation 3.28}$$

Where

τ_F = Shear strength of soil at the failure surface

τ = Shear stress developed at the failure surface

The calculations are based on two dimensional analyses and therefore neglect any effect from the three dimensional cell geometry. The calculations only satisfy the force

equilibrium and the moment equilibrium should be calculated separately. The analyses should take into account the uplift pressure by seepage of water at the base of the cell and the seepage pressure acting on the failure plane should be also calculated from flow net calculations. The flooded tension crack development should also be included in the case of short term calculations where a tension crack can develop on the loaded side of the cofferdam (Bolton and Powrie, 1987). The depth of flooded tension crack is calculated by USACE method using following equation;

$$d_c = \frac{2C_d}{\gamma} \times \tan\left(45^\circ - \frac{\phi_d}{2}\right) \qquad \textbf{Equation 3.29}$$

Where

d_c = Depth of flooded tension crack

C_d =Cohesion/ $FoS_{sliding}$

$$\phi_d = \tan^{-1}\left(\frac{\tan\phi}{FoS_{sliding}}\right) \qquad \textbf{Equation 3.30}$$

The presence of a flooded tension crack will require that a full hydrostatic pressure distribution is considered throughout the crack depth, ignoring any shear resistance between soil/pile interfaces. The maximum depth of a flooded tension crack can be up to the depth of embedment of the pile.

In the presence of any weak seam or fracture below the foundation of the cofferdam, a deep seated sliding analysis along this surface will be required. The whole mass of the structure should be considered sliding along this weak surface, using the assumptions considered for general sliding analyses.

3.3.3.2 Stability against bearing failure

Cofferdams are usually founded on rock or sand foundations which provide adequate bearing support for the resulting bearing pressure at the base. However there is a substantial body of evidence to suggest that a number of important cofferdams founded on clay foundations when there is a chance of bearing failure due to inadequate bearing

capacity of the foundation soil. The cell embedment should be sufficient to provide ample bearing support at the base. Bearing failure can result in excessive rotation and sinking of the entire structure. The bearing capacity for a foundation can be calculated using Terzaghi's Bearing capacity equation (Terzaghi and Peck, 1967) with the cell founded on a flat surface. However, Hansen's (1953) method for calculating bearing capacity is considered more suitable, where capacity is calculated as a convex or concave failure surface (whichever is critical for rotational failure), this will be discussed later on in section 3.2.3.3. The ultimate bearing capacity (q_f) from Terzaghi's Method can be calculated as;

for strip loaded area in case of diaphragm cells

$$q_f = \frac{1}{2}\gamma B N_\gamma + C N_c + \gamma D_f N_q \qquad \textbf{Equation 3.31}$$

for circular loaded area in case of circular cells

$$q_f = 0.6\gamma B N_\gamma + 1.3 C N_c + \gamma D_f N_q \qquad \textbf{Equation 3.32}$$

Where

N_γ = Term to account for self weight effects

N_c = Basic bearing capacity factor: for undrained shear strength analysis

N_q = Basic bearing capacity factor: for frictional soil strength analysis

D_f = embedment depth on unloaded side

The total foundation pressure is the sum of the vertical load due to the cell load and pressure due to the net overturning moment acting on the cell. The pressure due to the weight of the cell is W/B, where W and B are weight and width of the cell respectively. The pressure due to the overturning moment can be calculated using a base pressure diagram (Figure 3-3(a)), as $6M/B^2$. Therefore the factor of safety against bearing capacity failure can be calculated as;

$$FoS_{bearing} = \frac{q_f}{\left(\frac{W}{B} + \frac{6M}{B^2}\right)}$$ **Equation 3.33**

3.3.3.3 Overturning stability

The first attempt to asses overturning stability was made by Pennoyer (1934). This considered the cofferdam cell as a rigid body resisting external forces using gravity support provided by the effective cell weight. The cell was assumed to overturn about the lower inner edge of the cell without considering cell deformation or shearing within the cell fill material. The main disadvantage in Pennoyer's (1934) method is that the mechanism of cell rotation about the inner toe is not kinematically admissible. Hansen (1953), introduced a new method for calculating the overturning stability of cellular cofferdams. He assumed a circular failure surface that formed through the toe of the walls with overall rotation about the centreline of the cell (Figure 3-5). The failure circle is considered to be concave for a cell founded on a rock; however it can be either concave or convex for a cofferdam founded on a clay/sand stratum. It was suggested that when the driving depth is shallow the failure surface will be convex (Figure 3-5a). However, when the driving depth is greater than the failure mechanism can be either convex, concave (Figure 3-5b) or combination of both. When the driving depth is considerable, then it is necessary to investigate the development of plastic hinge in sheet piles (Figure 3-7). For kinematic reasons the circular failure plane should meet tangentially at the sheet pile at the point of plastic hinge formation giving $\alpha=90^{o}$, where 2α is the angle subtended at the centre of rotation for failure circle.

If the walls are perfectly smooth each yield point should have a yield moment and no transverse force. In reality this is not possible, but the assumption was considered to be on the safe side. A number of failure circles are considered and a factor of safety against overturning is calculated for each to identify the rupture surface with the lowest factor of safety. The circular failure surface known as the equilibrium method is considered to be a kinematically admissible mechanism, but at the same time it involves complicated calculations involving internal forces acting within a rupture line. Therefore the circular slip surface was replaced by an approximate log spiral surface by Ovesen (1962), known as the extreme method. The gravity and external forces will intersect each other and the

resultant will pass through the locus of the critical log spiral (Figure 3-6), thus eliminating the complicated calculations for unknown forces within slip surface. The logarithmic spiral is assumed to obey the polar equation;

$$r = r_o \times e^{\theta \times \tan\phi} \qquad \textbf{Equation 3.34}$$

Where

θ = Variable in polar coordinates system

r_o = Radius for $\theta = 0$ **Equation 3.35**

ϕ = Angle of internal friction of soil

Various logarithmic spirals are drawn to derive concave (Figure 3-6a) and convex (Figure 3-6b) slip surfaces, and factor of safety is calculated by taking the ratio of the resisting (M_r) and overturning moments (M_o) about the centre of the log spiral.

$$FoS_{overturning} = \frac{M_r}{M_o} \qquad \textbf{Equation 3.36}$$

By plotting the factor of safety against the radius of log spirals a minimum factor of safety is identified. The main drawback of Hansen's (1953) log spiral method is the assumption of uniform stress strain behaviour at all points along the failure curve. The soil at the inner toe is under very high confining pressure in comparison to the toe on the water (loading) side. As the soil behaviour is highly dependent on the confining stress, the stress strain behaviour should vary from point to point along the slip circle, which is not considered in Hansen's (1953) method.

3.3.3.4 Stability against seepage failure

If the soil is permeable and the pressure head is considerable then the stability against seepage failure needs also to be investigated. A flow net is required to calculate the uplift pressure on the soil block on the unloaded side. If the uplift force exceeds the weight of the soil then the structure may fail due to a piping failure on the unloaded side. The factor of safety is calculated using;

$$FoS_{seepage} = \frac{W'}{U}$$ **Equation 3.37**

Where

W' = Weight of soil block on unloaded side

U = Uplift pressure on soil wedge on unloaded side

If a berm is provided for additional support on the dry side then the factor of safety will include the dry weight of berm as the typical material used for the berm is generally a free draining material, therefore;

$$FoS_{seepage} = \frac{W' + W_b}{U}$$ **Equation 3.38**

Where, W_b is weight of berm

3.4 Short comings of current guidance

Although there are number of design guidelines presented for the design of cellular cofferdams there are several short comings in these guidelines. These were investigated with reference to the St. Germans cofferdam case study presented in this thesis. In particular;

- Current design guidelines present a number of possible failure mechanisms, each applied independently. Also, there are no specifications on the application of a particular failure mechanism depending on the cell type, i.e. diaphragm, circular and cloverleaf.

- All field and numerical studies used in the guidance documents are based on a circular type cell configuration; the cofferdam primarily used to construct the lock and dam No. 26 (Clough & Kuppusamy 1985; USACE 1974, 1970 and 1989; Maitland & Schroeder 1979; Marten & Clough 1988; Mosher 1992) and lab studies by Hansen (1953) and Ovesen (1962). The cell pressure calculations in available guidelines are based on circular cells with no ties to connect the two sheet piles as in case of diaphragm type cells, the interlock pressures calculated using these guidelines cannot be applied to diaphragm type cellular cofferdams.

- Only the USACE method advises on the inclusion of a flooded tension crack (Bolton & Powrie, 1987) as a part of the assessment of a sliding analyses. However it ignores the formation of a flooded tension crack for the global check on overturning and sheet pile pull out where this may be critical.

- The sheet piles and steel ties are usually over designed and no guidance is available based on measured bending moments in the piles or tie loads based on field and lab studies for realistic structural loads.

- Construction on the dry side of a cofferdam usually requires excavation to install foundations and embedment for works, such as pumping stations or bridge piers construction etc. The design guidelines are all based on analyses that assume a similar ground level on either side of the cofferdam (Terzaghi, 1945; Hansen 1953; Ovesen 1962; Maitland and Schroeder 1979; Mosher 1992, Khan *et al.,* 2006). Therefore they must not be applied to the cofferdam with excavation on unloaded side to create level difference on either sides of the structure.

- Stability checks during the main construction stages are not suggested by any of the design methods. There are several construction stages (discussed in section 5.2) which are likely to the safer performance of the cofferdam.

- The design & use of a berm support requires further attention as it is costly as well as difficult to construct under balanced water conditions. There is no specific method suggested to determine the dimensions of the berm for cellular cofferdams. The width and height of a berm may be reduced based on the latest design methods (Daly and Powrie, 2001; Smethurst & Powrie, 2008) to optimise construction space.

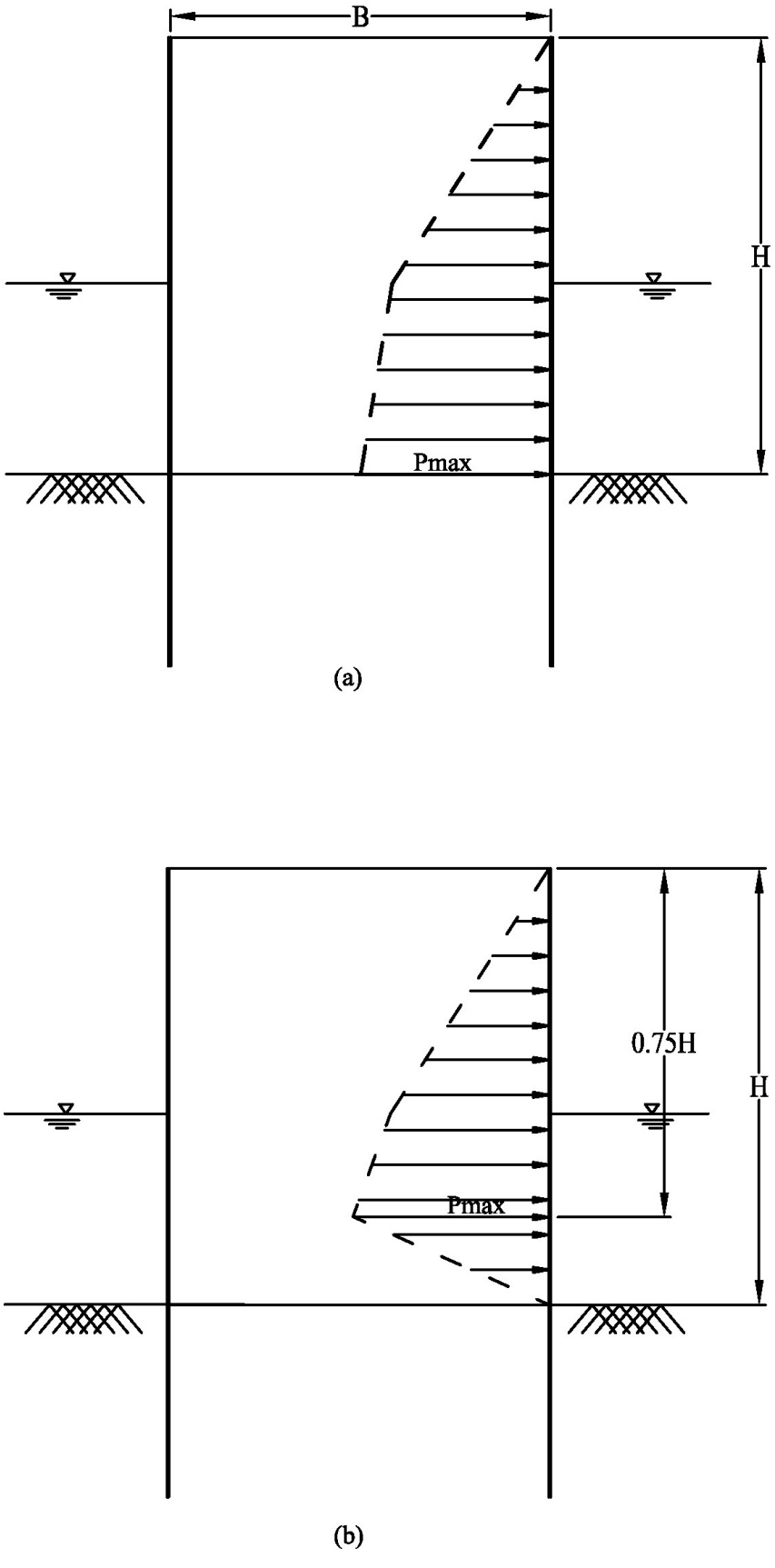

Figure 3-1: Fill pressure acting on cell wall, (a) Terzaghi (1944) method, (b) TVA Method

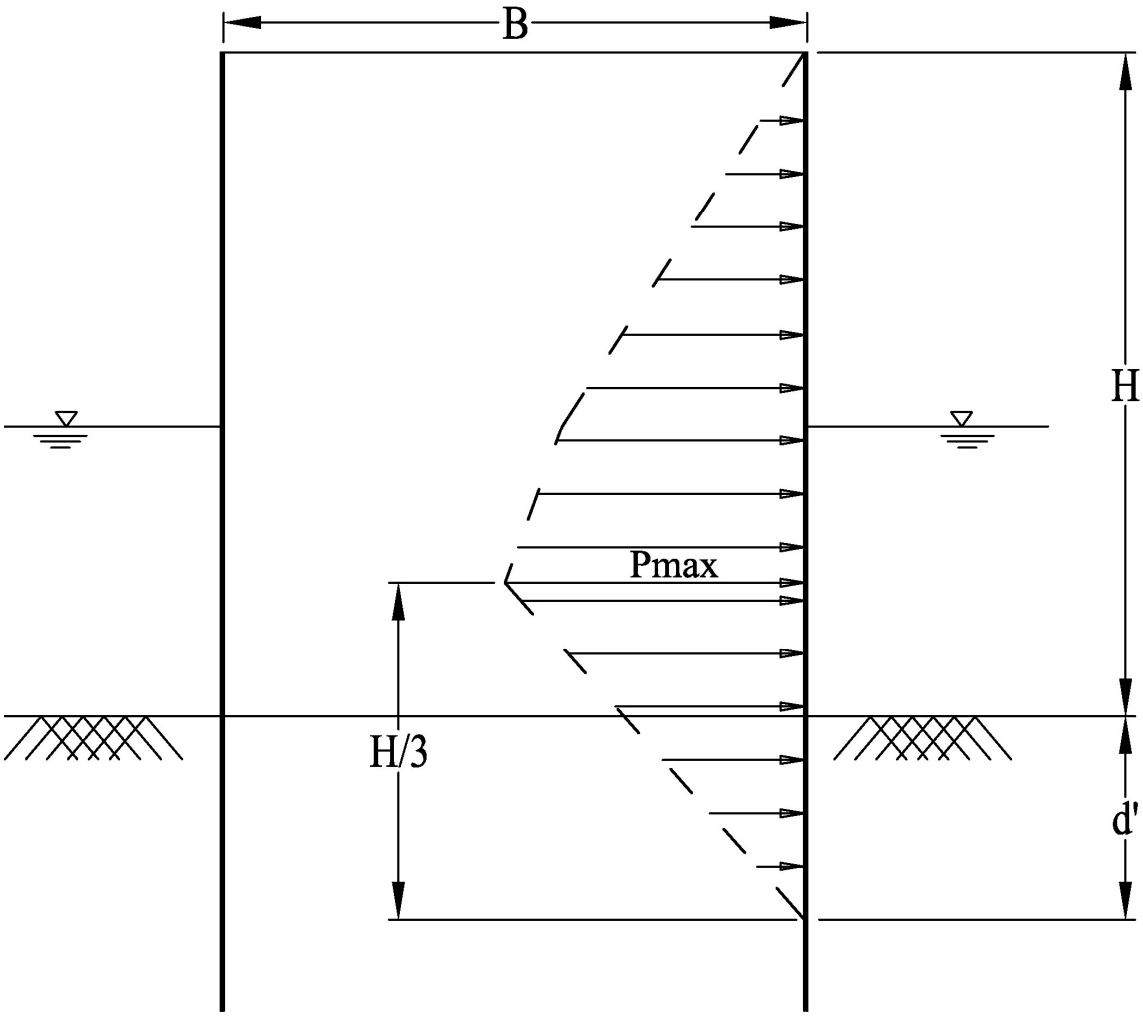

Figure 3-2: Schroeder and Maitland Method for fill pressure calculation on cell wall

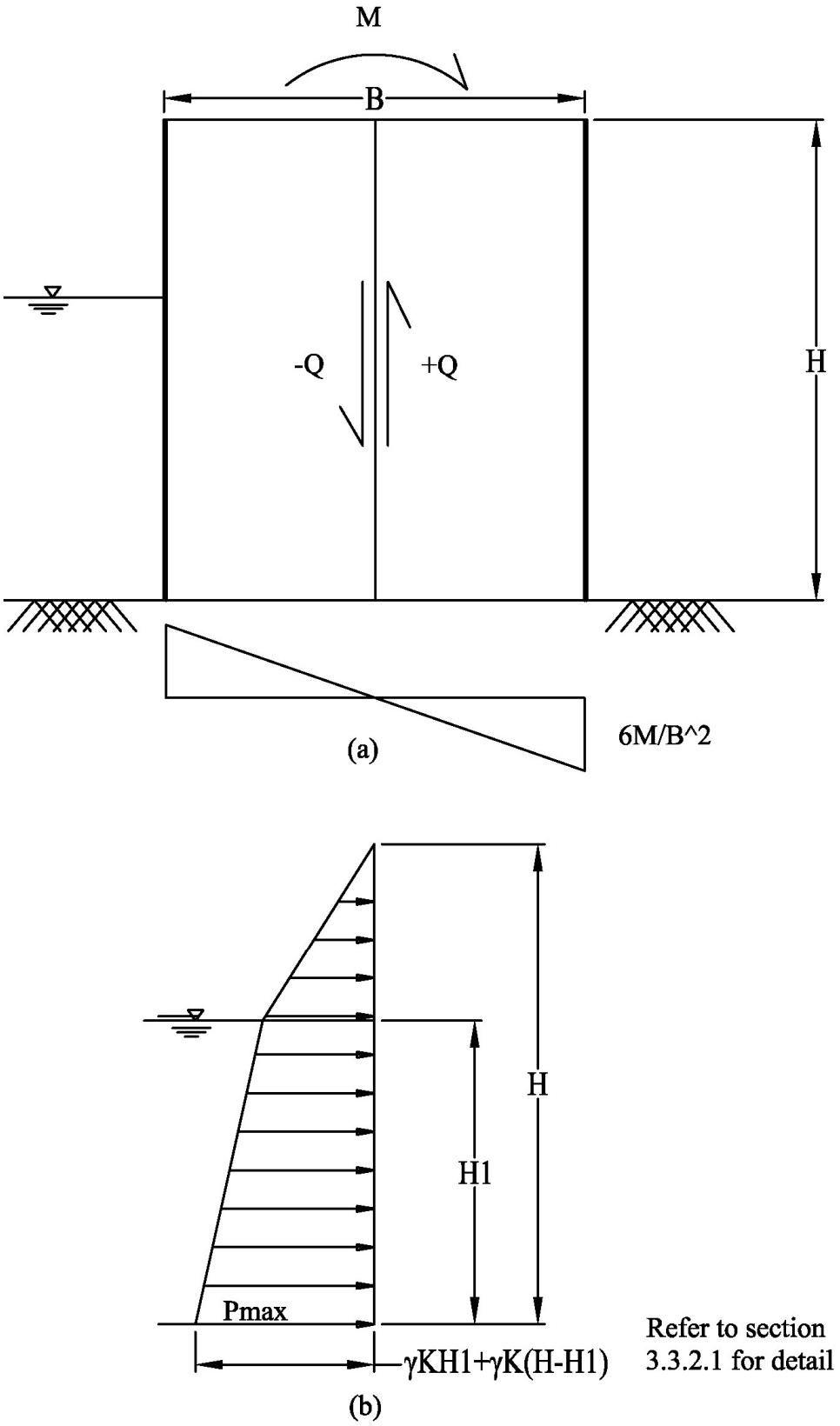

Figure 3-3: Vertical shear resistance (Terzaghi method) (a) Base pressure profile (b) Centreline pressure profile

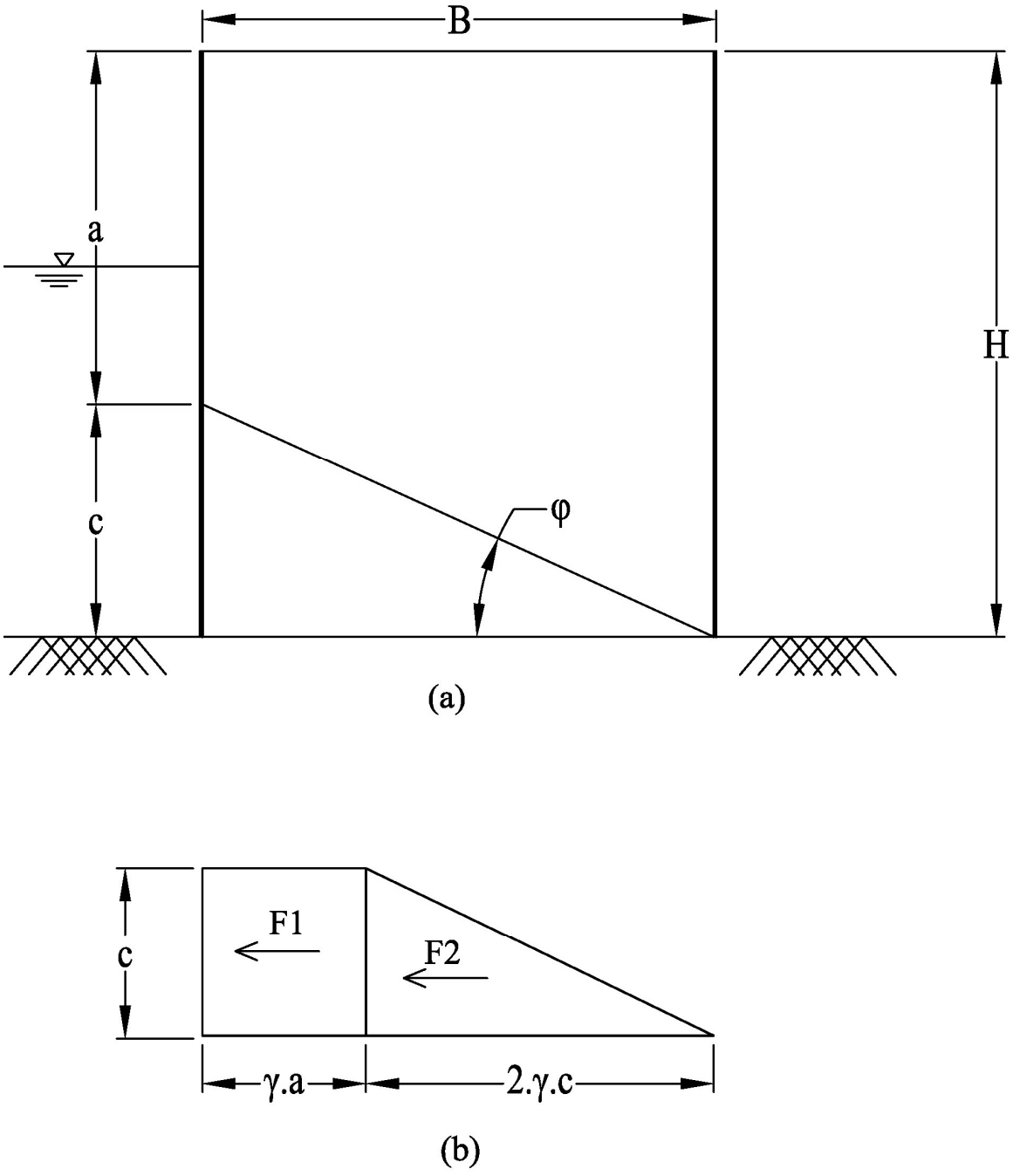

Figure 3-4: Horizontal shear failure, (a) Resisting wedge (b) Pressure diagram

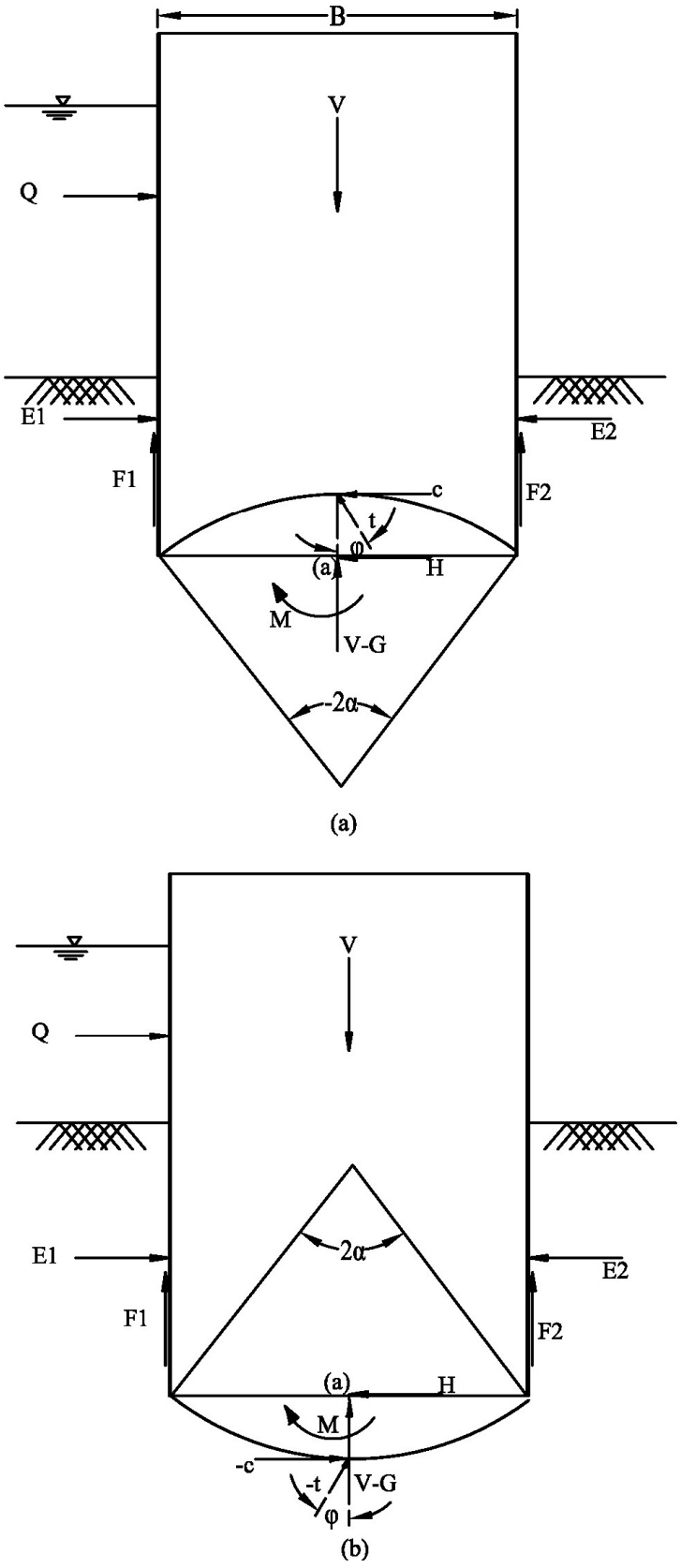

Figure 3-5: Concave and Convex rupture failure surfaces (Equilibrium method) by Hansen 1953.

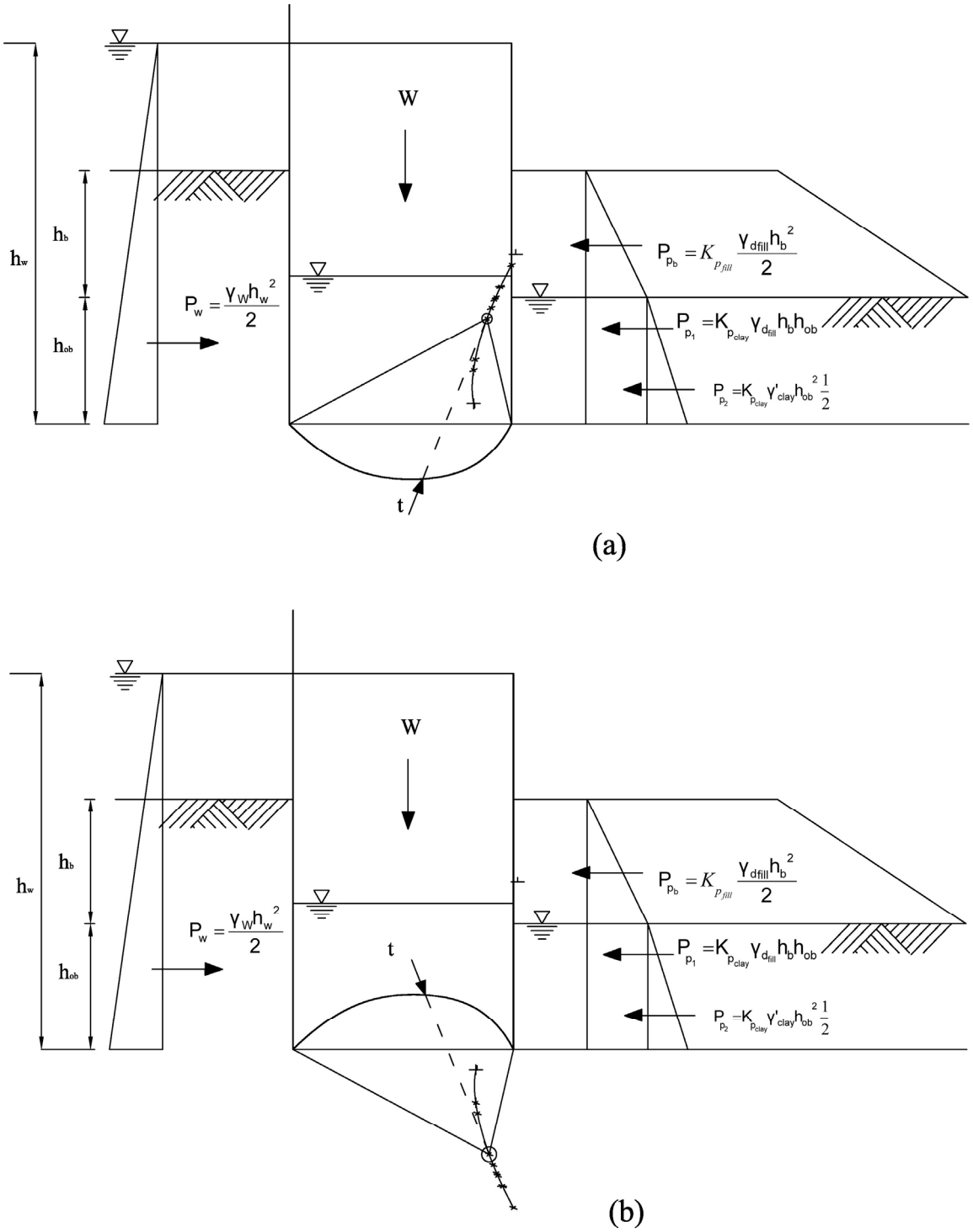

Figure 3-6: Concave and Convex rupture failure surfaces (Extreme method) by Hansen 1953.

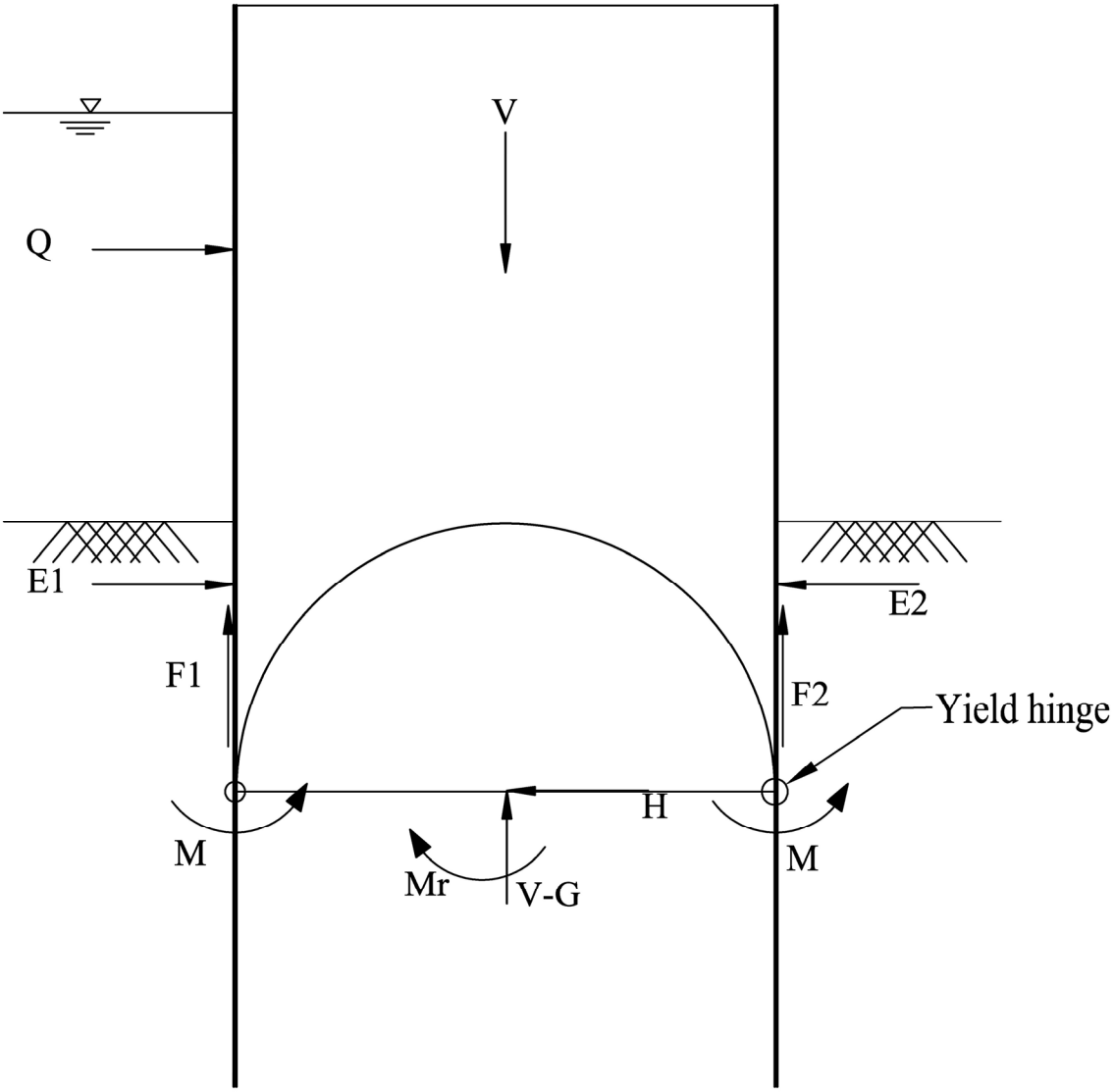

Figure 3-7: Development of yield hinge in sheet piles

4 Case study – St. Germans Cofferdam

4.1 Introduction

This section includes a description of the site geology and the soil testing programme undertaken to determine the engineering properties of the various soil types present at the St. Germans pumping station site at King's Lynn, UK. The geology and soil properties in this area have received relatively little attention compared to other locations within UK e.g. London, Lias, Gault Clays. The soil properties presented include results from soil tests undertaken prior to construction work (Fugro site investigation report, 2004 and Fugro site investigation report, 2005) and include additional tests results from supplementary tests to validate aspects of the original investigation the some of the important aspects arising from the preliminary numerical analyses of the cofferdam.

4.2 The St German's Cofferdam

During 2007 work commenced to replace the pumping station at St. Germans Norfolk, which forms part of the original drainage system (ICE New Civil Engineer, 2007), see Figure 4-1. The new pumping station was constructed 200m downstream from the existing pumping station (Figure 4-2). The new pumping station will be used to pump the water from low lying middle level drain into the Great River Ouse as part of the drainage system south of Kings Lynn.

To enable the existing pumping station to remain operational at all times it was decided that the new pumping station would be constructed downstream (Figure 4-2) within a cofferdam that temporarily diverted the main drainage channel away from the existing west bank. A diaphragm type cellular cofferdam design was developed for this purpose to provide a temporary dry construction area. The ground conditions comprised soft Fen Deposits overlaying stiff overconsolidated Kimmeridge Clay (Atkins Geotechnical Interpretive Report, 2005). This construction provided an opportunity to gain field measurements/observations that could be used to validate numerical analysis of this type of structure.

4.3 Design and layout of St. German's cofferdam

The proposed cofferdam comprised of 18 number of diaphragm type cells (See Figure 4-3). The cross sectional detail and dimensions of a typical 10.5m wide cell is given in Figure 5-2. The flood record and tidal variations in the river showed that the maximum flood level was 106.3m MLD (for a 1:200 years flood event) and the mean high water tide level was approximately 104m MLD. The cells were constructed using AZ 28 (British sheet piling handbook, 2005) tied at 98.5 and 103.5m MLD. A tie spacing of 1.2m for the lower ties, and 2.4m for the upper ties was used. The cells were excavated down to the top of Kimmeridge Clay level (which varies from 91 to 93mMLD through the site) and then backfilled a using granular fill up to the top of inboard pile, i.e. 104m MLD. Cells N0 and S0 which ran into the bank were not excavated and than backfilled in this manner. The central cells (cell C2 to C4) were 13m wide while all other cells were 10.5m in width. The cells were designed using guidelines provided by the US Army Corps of Engineers (1989), and US Naval Facilities Manual (NAVFAC, 1971). The limited knowledge of the behaviour of the Kimmeridge Clay and the behaviour of the diaphragm type cellular cofferdams generally, required more detailed design to be undertaken. Therefore a series of numerical analyses and laboratory soil element tests were conducted to derive the engineering properties of the Kimmeridge Clay and Fen Deposits and to assess the stability of the structure during the staged construction of the cofferdam. To validate the numerical analyses a number of instruments were installed on the inboard and outboard piles on the centre of cell C3 to determine bending moments in the sheet piles. In addition, 15 peizometers were installed within various cells, and on both sides of cofferdam to check the variation in pore water pressures within the cells and to establish drained and undrained soil response.

4.4 Reported geology

The site is located in the reclaimed area of King's Lynn, Norfolk in the east of England (Figure 4-4). The tidal river Ouse is used to drain the area using a number of pumping stations that raise water from lower to the upper level within the middle level catchment area. Historical evidence shows that the River Ouse has altered by approximately in 6 miles length from Wiggenghall St. Germans (the location of the pumping station) to King's Lynn since the early nineteenth century (Skempton, 1945). A detailed description

of the site geology and historic evidence of soil layering presented is based on the work of Skempton (1945) and Godwin (1940).

The Fen Deposits found at the Kings Lynn were deposited between 2000 to 3000 years ago above a thick layer of hard kimmeridge clay. The Fen Deposits were termed “Buttery clay” by Skempton (1945), which is soft plastic clay with traces of peat in the top layers. The borings for the investigation of a cut formed in the slope on the river bank were used to document the soil layering (Figure 4-5) (Skempton, 1945). Three distinctive Fen Deposits layers were identified. The top layer is soft brown silt with traces of peat; the intermediate layer is brown silty clay with many light blue veins along the old root fibres and the lowest layer was identified as grey silt with inclined laminations comprised of alternating silty and clayey silt. Generally the Fen Deposits were identified as normally consolidated. The progressive rise of sea level during past 1000 years at the rate of 0.3m per 100 years has prevented the drying out of Fen and peat soils following their deposition.

The underlying Kimmeridge Clay is of Jurassic origin and is named after the village of Kimmeridge in Dorset England where it is widely exposed at ground level. The BGS map sheet 159 (British Geological Survey, 2008) identifies the Kimmeridge Clay as lithologically similar to the older Jurassic mudstone containing fewer kerogen-rich mudstone and is generally less calcareous. There is very little information available on the Kimmeridge Clay found at King’s Lynn specifically. The Humber bridge foundation (Hull, England) was founded in the Kimmeridge Clay (Simm and Busbridge, 1976) which is about 70 miles to the north of the King’s Lynn. The samples from the excavation at the bridge anchorages showed that the Kimmeridge Clay is a hard, overconsolidated and severely fissured clay with a tendency for rapid disintegration in the presence of water.

4.5 Observed geology

The flood protection channel embankments are constructed up to 106.5m MLD and protect the low lying ground on either side of the middle level drain. A number of boreholes were used to investigate the soil stratum below ground level (Figure 4-6 and appendix A for borehole logs). The cross sectional profiles are provided in Figure 4-7 and

Figure 4-8. The description of various soil layers are presented in Table 4-1 and are based on the geotechnical interpretive report (Atkins, 2005) for the St Germans cofferdam.

Table 4-1: Observed geology (Atkins, 2005)

Geological period	Stratum		Depth to top of the stratum (m below ground level)	Elevation of top (m AOD)	Thickness (m)	Borehole reference
Recently deposited	Made ground		0	3.92 to 7.30	1.2 to 5.5	BH1 to BH3
	Fen Deposits	Clay	1.2 to 5.5	2.72 to 2.3	0 to 5.5	All
		Peat	1.2 to 9.0	2.6 to -1.28	0 to 3.4	BH1 and BH2
	Alluvial sand		3.3 to 11.0	0.62 to -4.3	0 to 4.5	BH1, BH3, BH4, BH5
Jurassic	Kimmeridge clay		10 to 15.5	-5.5 to -8.2	undetermined	All

4.5.1 Made ground

The top soil on both the left and right embankments comprises spoil (made ground) with thickness varying from 1.2 to 5.5m. The made ground is soft to stiff grey silty clay with traces of grey peat. Some construction materials such as concrete and steel pieces were found to be buried under both embankments and may be related to the construction of original pumping station.

4.5.2 Fen Deposits

Fen Deposits were observed in all boreholes across the site. The average thickness of the Fen Deposits layers vary from 0 to 5.5mand are identified as soft laminated grey clay occasional as sandy or silty clay with occasional Peat depositions. The cut in the west slope after the dewatering of the cofferdam shows the Fen Deposits to its full depth (Figure 4-9).

4.5.3 Alluvial sand

Alluvial sand layer is mainly silty sand with some gravel found in boreholes BH1, BH3 and BH5 below the base of Fen Deposits while in BH4 there were some Fen Deposits below the Alluvial Sand layer. This suggests that the Alluvial Sand exists across the site in intermittent layers. It is suggested that it was probably deposited during drainage towards the river Ouse during intermediate sea level falls. The thickness of the alluvial sand varies from 0 within the middle of the channel to 4.5m at the embankments.

4.5.4 Kimmeridge clay

The Kimmeridge Clay was found in all bore holes varying from -5.5 to -8.2m AOD. The thickness of the Kimmeridge Clay layer is unknown as even the deepest bore hole (BH1, see appendix A for detail of borehole logs) did not reach the base of the layer. The Kimmeridge Clay from the site can be described as stiff to becoming very stiff fissured laminated grey clay with depth as indicated by Skempton (1945) and Sim and Busbridge (1976). Thin bands of very weak claystone with occasional decayed shells were also observed within the stiff Kimmeridge clay.

4.6 Geotechnical properties

A range of tests including SPTs, Consolidation tests, index properties tests, UU triaxial tests without pore water pressure measurement and Multistage UU triaxial tests with measurement of pore water pressure were undertaken to determine the engineering properties of the Fen Deposits and Kimmeridge Clay.

4.6.1 Bulk density

The bulk densities for various soil layers are presented in Figure 4-10, and show that the bulk density increases with depth. The average dry densities of the various soil layers for input into the effective stress analyses of the cofferdam are presented in Table 5-2 are based on bulk density from Figure 4-10, with saturation ratio taken as 1 (water table at the top of the soil surface in all boreholes) and porosity of 0.49 calculated from consolidation test on a representative sample.

4.6.2 Plasticity

Plasticity indices (PI) measured using soil samples obtained from BH1, BH3, BH4, BH5 and BH5 together with samples obtained from supplementary boreholes BH1W and BH14 are presented in Figure 4-11. The plot shows that the plasticity for most of the soil samples from both Fen Deposits and Kimmeridge Clay layers lies within a narrow band of 25 to 35%. This suggests that the Fen Deposits and Kimmeridge Clay has approximately uniform plasticity; the scatter in the data can be explained by non-uniformity of strata due to presence occasional clay or silt bands within various soil layers.

4.6.3 Permeability

The hydraulic conductivity (permeability) of a clay deposit is perhaps the major factor controlling its consolidation coefficient, which governs the rate at which excess pore water pressures dissipate and the timescale over which the behavior of the material might reasonably be considered to be "undrained" (i.e., no significant volume change so that the undrained shear strength model of failure may be used in analysis). A single falling head test was carried out in a piezometers installed into the Kimmeridge Clay and the test results are plotted in Figure 4-12. As it was difficult to find the exact initial head due to the low permeability of the soil the time for 90% equalization ($t_{90\%}$) was considered for the calculation of permeability (Hvorslev, 1951). As the soil was considered as an anisotropic material, a transformation factor (x') was calculate using

$$x' = \sqrt{\frac{k_h}{k_v}} \qquad \textbf{Equation 4.1}$$

Based on the evidence of high lateral permeability for fissured clays (Richards *et al.* 2006) the ratio $\frac{k_h}{k_v}$ was considered as 10 in this case.

The piezometer shape factor (F) for a cased borehole (Hvorslev, 1951) with uncased length (L) and diameter (D) in a uniform soil can be calculated using;

$$F = \frac{2\pi L}{\ln\left[\frac{L}{D} + \sqrt{\left(1 + \left(\frac{L}{D}\right)^2\right)}\right]}$$ **Equation 4.2**

The transformed permeability (k_t) was calculated based on BS5930 (BSI, 1981) using the following relationship

$$k_t = \frac{\frac{dy}{dt} A_f}{F}$$ **Equation 4.3**

Where,

A_f = Filter area

$\frac{dy}{dt}$ = gradient of $ln(h/h_o)$ vs *time* line calculated from Figure 4-12

The transformed permeability is also presented as;

$$k_t = \sqrt{k_h k_v}$$ **Equation 4.4**

Where

k_h= horizontal permeability of the soil

k_v = vertical permeability of the soil

Once the transformed permeability is known, the horizontal and vertical permeability can be calculated using;

$$k_h = k_t \cdot x'$$ **Equation 4.5**

$$k_v = \frac{k_t}{x'}$$ **Equation 4.6**

Analysis of this test using equations 4.5 and 4.6 indicated horizontal permeability (k_h) of 1.5 x10^{-7} m/s and vertical permeability (k_v) of 1.5 x10^{-8} m/s respectively. Given that this type of test will normally tend to underestimate the hydraulic conductivity (CIRIA Report

C515; Preene *et al.,* 2000), it was decided not to rely on any period of substantially undrained behavior and to carry out drained (effective stress) analyses, with pore water pressures corresponding to steady state seepage under the highest astronomical tide (105 m MLD and flood tide levels of 106 m MLD and 107 m MLD). This argument is backed up by the piezometers installed within cofferdam cells S4 and N5 before the commissioning of the cofferdam under normal tidal conditions with no cell dewatering. The response from piezometers embedded at 18 and 24m below the top of the cell fill within the Kimmeridge Clay in cells S4 (Figure 4-13) and N5 (Figure 4-14) are showing the pore pressure dissipation when the water level changes within the cell. The pump failure (Figure 4-14) shows that rapid pore water pressure equalization is occurring (approximately 6 days to equalize the pressure) and there is likely to be very little undrained response from Kimmeridge Clay. This approach is considered to be conservative.

4.6.4 Strength

The strength of Kimmeridge Clay was determined as $\phi' = 21^{o}$ with $c' = 6.7$ kN/m^2 from shear box tests while allowing the soil to consolidate for undisturbed samples by Skempton (1945). The values were calculated by drawing an average line for tests conducted at different confining stress while c' as an intercept for the average line. The Fen deposits (identified as Buttery Clay) were found to have strength of $\phi' = 20^{o}$ and $c' =$ 11.01 kN/m^2 under the undrained conditions. The results from weathered samples on the Kimmeridge Clay (Cripps and Taylor, 1987) suggested an effective angle of friction (ϕ') in a range of 14 to 23º with an effective cohesion (c') varying between 14 to 67 kN/m^2.

Based on the moderately high horizontal permeability of the Kimmeridge Clay it was decided to rely on the effective strength of the soil using effective angle of friction ϕ'_{design} with c= 0 kN/m^2. BS8002 (British standards institution, 2001) states that the design strength or effective angle of friction ϕ'_{design} used in the ultimate limit state (ULS) calculation should be the lesser of $\tan^{-1}(\tan \phi'_{peak}/1.2)$ and $\tan\phi'_{crit}$. In both CIRIA Report C580 (Gaba et al., 2003) and Eurocode 7 (BSI, 1995), ϕ'_{design} is taken as $\tan^{-1}(\tan \phi')/1.25$, where ϕ' is a moderately conservative estimate of the strength relevant to the

limit state under consideration, in this case collapse (Eurocode 7 Case C, failure in the ground).

Overconsolidated deposits may have three reasonably well defined effective angles of friction – peak, critical state and residual. The critical state strength is associated with continuum deformation at constant shear stress, normal effective stress and void ratio, while the residual strength is associated with the development and possible polishing of a defined rupture surface. The strength governing the failure of a cofferdam structure is not known, although for embedded retaining walls in mainly granular deposits (sands and gravels), Powrie (1996) argues that the use of a uniform peak strength will be overoptimistic, while the use of the critical state strength will give a close or slightly conservative indication of the onset of large deformations (in both cases, an angle of soil/wall friction $\delta = \phi'_{design}$ was assumed).

It is generally difficult to identify the critical state strength from triaxial tests on samples from overconsolidated deposits, because of their tendency for strain localisation and rupture at or near peak strength. Concentration of deformation along a shear band will result in a relatively rapid post-peak reduction in strength towards the residual. This is evidenced by the final stage shear tests (from an effective cell pressure of 150 kPa) for samples U16, U22 and especially U27.

The average effective stress (p') verses shear stress (t) for effective stress strength data from the Kimmeridge Clay samples U11, U16, U22, U26, U27 and U31 plotted in Figure 4-15 are summarised in Table 4-2.

Table 4-2: Summary of effective stress strength data for the Kimmeridge Clay (stage 3 of shear tests)

Sample	B/H	Depth, m	ϕ'_{peak} °	ε_{ax}, %	ϕ'_{inter} °	ε_{ax}, %	ϕ'_{min} °	ε_{ax}, %	Notes
U11	1W	11.0	30	>8	-	-	28	>8	No sudden fall in strength post-peak
U16	1W	13.0-13.45	42	~6	40	~6	32	~7	

Sample	B/H	Depth, m	ϕ'_{peak} °	ε_{ax}, %	ϕ'_{inter} °	ε_{ax}, %	ϕ'_{min} °	ε_{ax}, %	Notes
U22	1W	15.0-15.45	33	~4	-	-	25	<7	Fall in strength occurred immediately after peak. $\phi' >$ 33° measured in Stage 1
U26	14	14.45	32	~8	-	-	(28)	-	ϕ'_{min} given was measured in stage 2 when the principal stress difference was still rising
U27	1W	17.0	38	~6	35		22	~10	$\phi' >$ 38° measured in Stages 1 and 2
U31	14	16.5	34	~10	-	-	(30)	-	ϕ'_{min} given was measured in Stages 1 and 2. No sudden fall in strength post-peak in Stage 3

The ϕ'_{peak} is the maximum value of ϕ' attained in the third stage of the test. ϕ'_{inter} is the value of ϕ' attained in stage 3 of tests U16, U22 and U27 after peak but before the rapid reduction in stress seen to ϕ'_{min}. ϕ'_{min} is the smallest strength measured in stage 3 post-peak: this was usually at the end of the test, and lower values might have been recorded had the test continued further. Lower strengths were attained in Stage 2 for samples U11 and U26, and in both stages 1 and 2 for sample U31, but in all cases the deviator stress (maximum principal stress difference) was still rising. Strains are cumulative, i.e. they include those that occurred in stages 1 and 2.

Table 4-2 shows peak strengths in the range 30° - 42° (average about 35°), with a rapid fall post-peak towards a residual strength on a rupture surface in some tests. Given

- the inconsistencies and uncertainties in current guidance as to whether the peak or the critical state strength should be used as a basis for design
- the likely conservatism of assuming reduced soil/wall friction (i.e., $\delta < \phi'_{design}$), and

- the fact that the average peak strength is approaching 35°,

It was considered that ϕ' = 30° could represent a suitable basis for ϕ'_{design}.

Another approach can be use of Plasticity index to estimate the effective angle of friction for normally consolidated soils (Kenny, 1959). Figure 4-11 presents the plasticity indices (PI) measured using samples obtained from BH1, BH3, BH4, BH5 and BH5 together with samples obtained from supplementary boreholes BH1W and BH14. A value of ϕ' = 30° is approximately in the middle of the range of values of ϕ' (presumably ϕ'_{crit}) of 27° - 32° that could be inferred for the range of plasticity indices (PI) measured across the site for the Kimmeridge Clay (19 ≤ PI ≤ 39) on the basis of Kenney's (1959) empirical correlation for a normally consolidated clay (Figure 4-16). Given the general lateral distribution of these boreholes relative to the cofferdam a value ϕ' = 30° could represent a suitable basis for ϕ'_{design} across the site with some confidence that this is representative for the site generally.

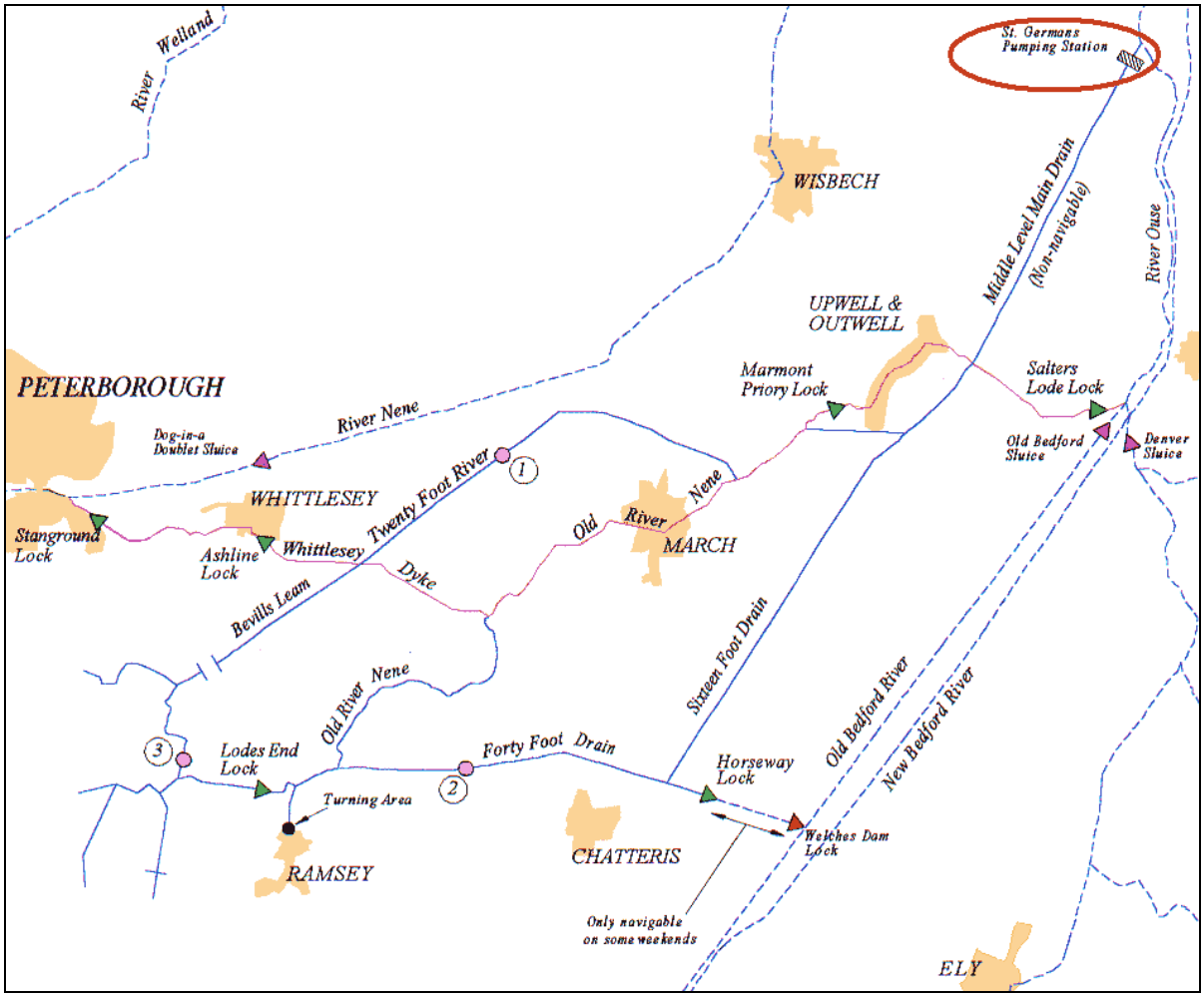

Figure 4-1: Middle level drain, Kings Lynn UK (Middle level commissioners, 1999)

Figure 4-2: Proposed site for new pumping station (Google Earth, 2007)

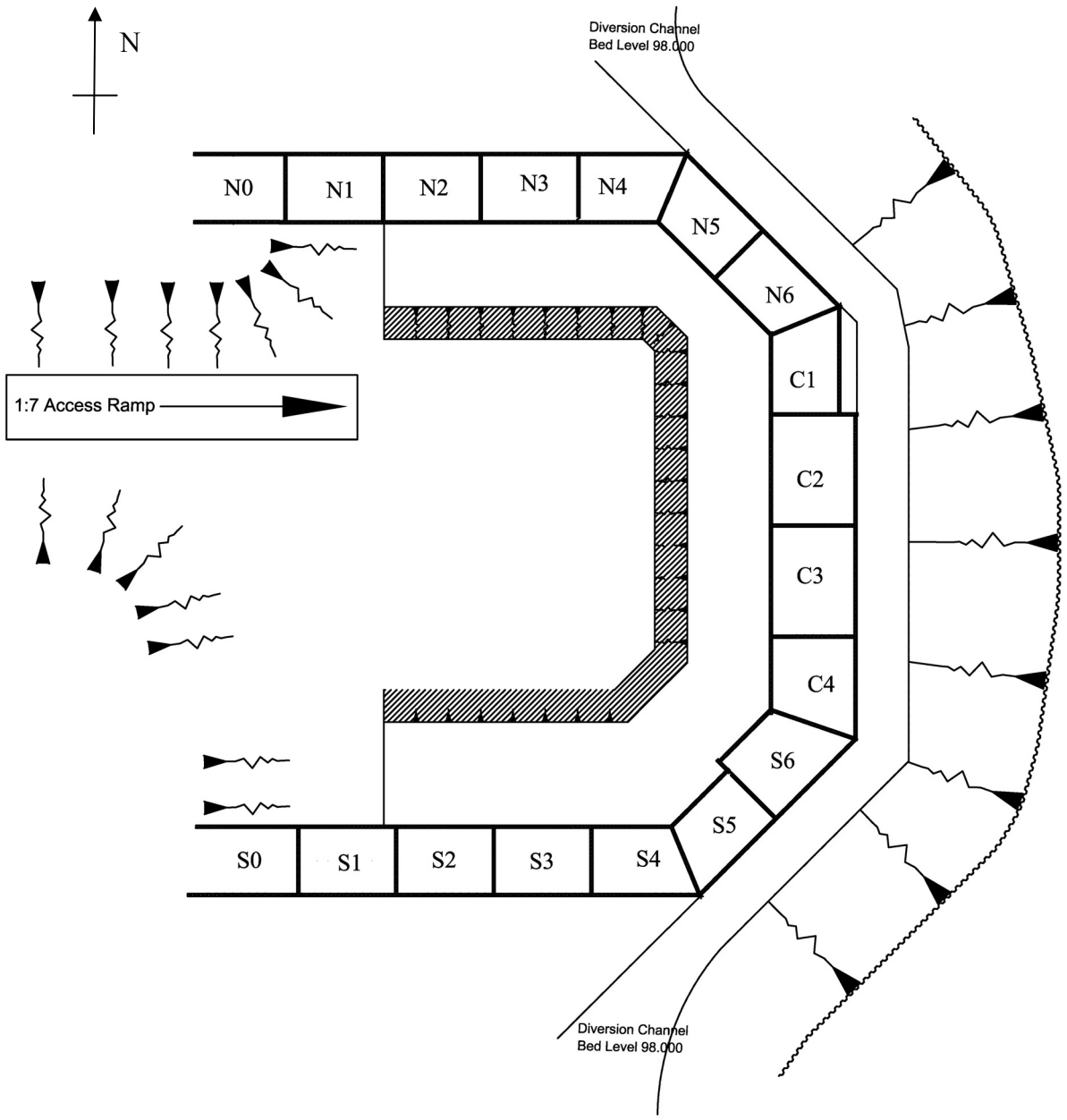

Figure 4-3: St Germans Cofferdam layout

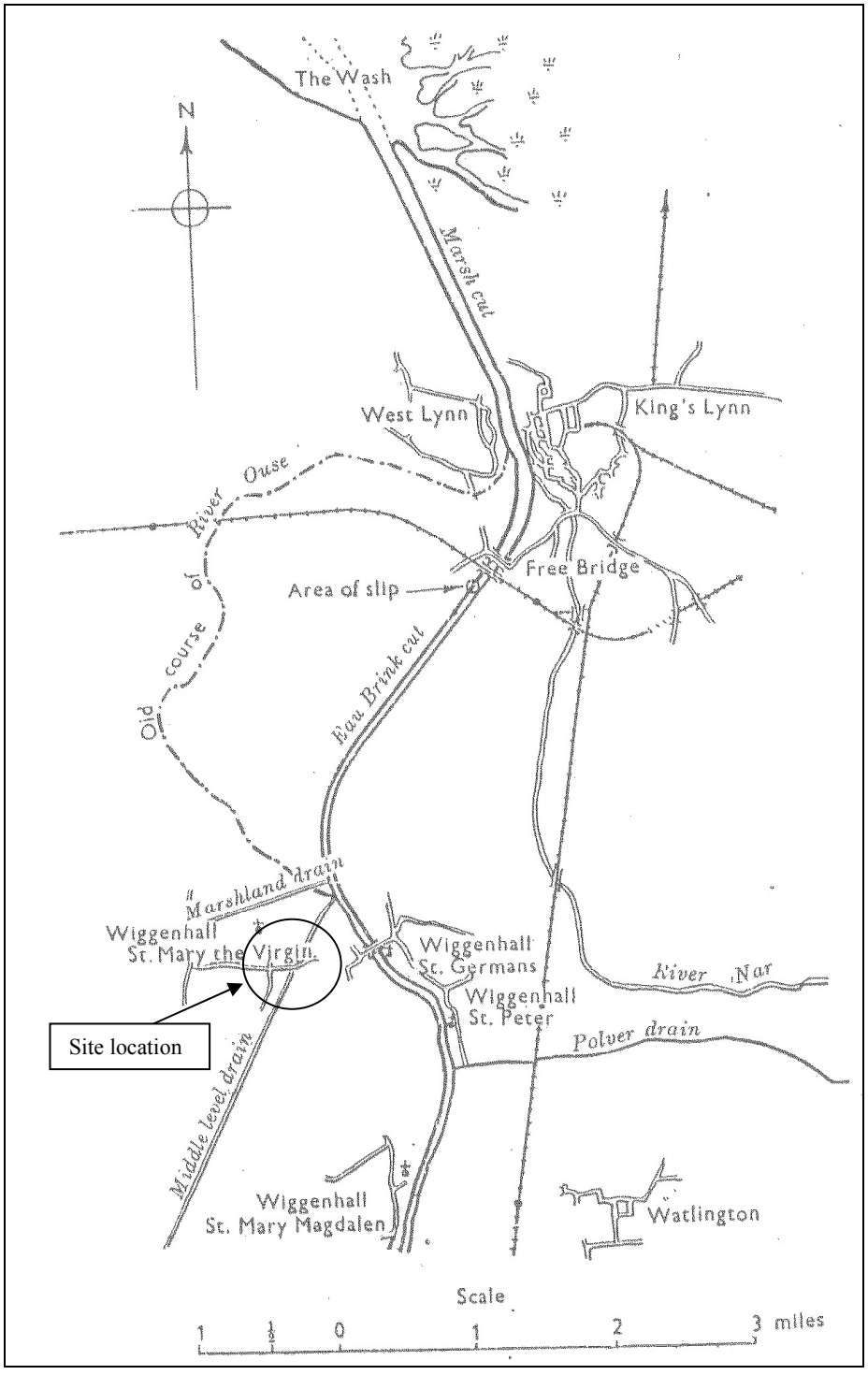

Figure 4-4: Map showing drift of river Ouse and site location (Skempton, 1945)

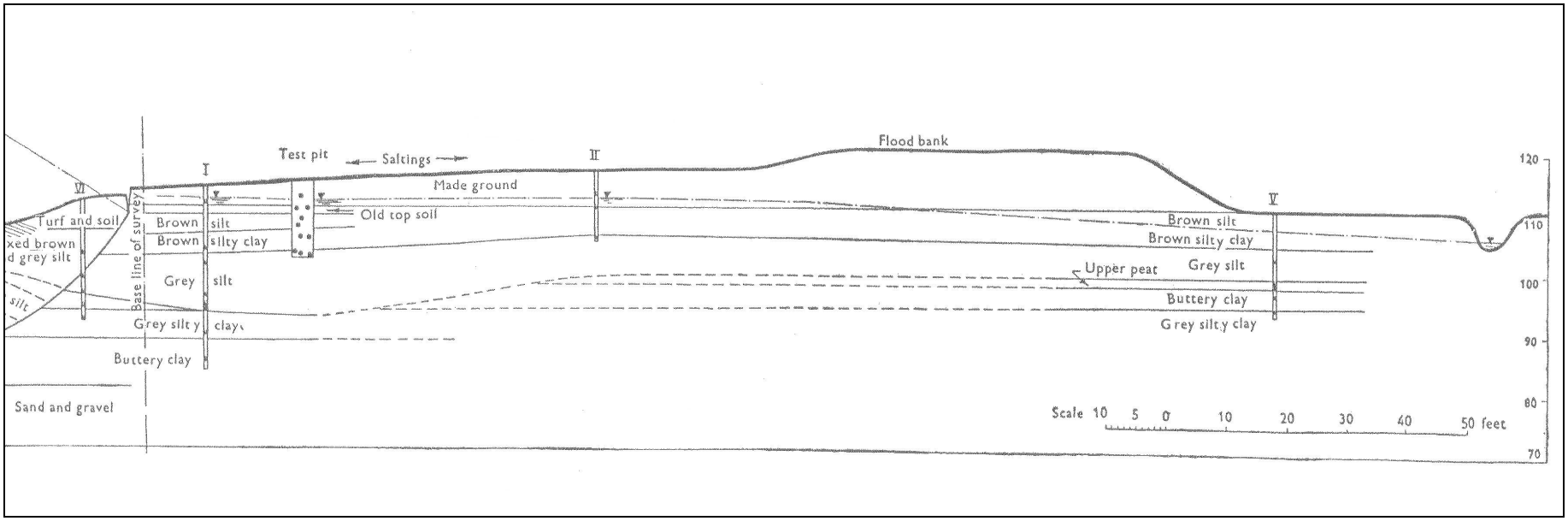

Figure 4-5: Reported soil profile at King's Lynn (Skempton, 1945)

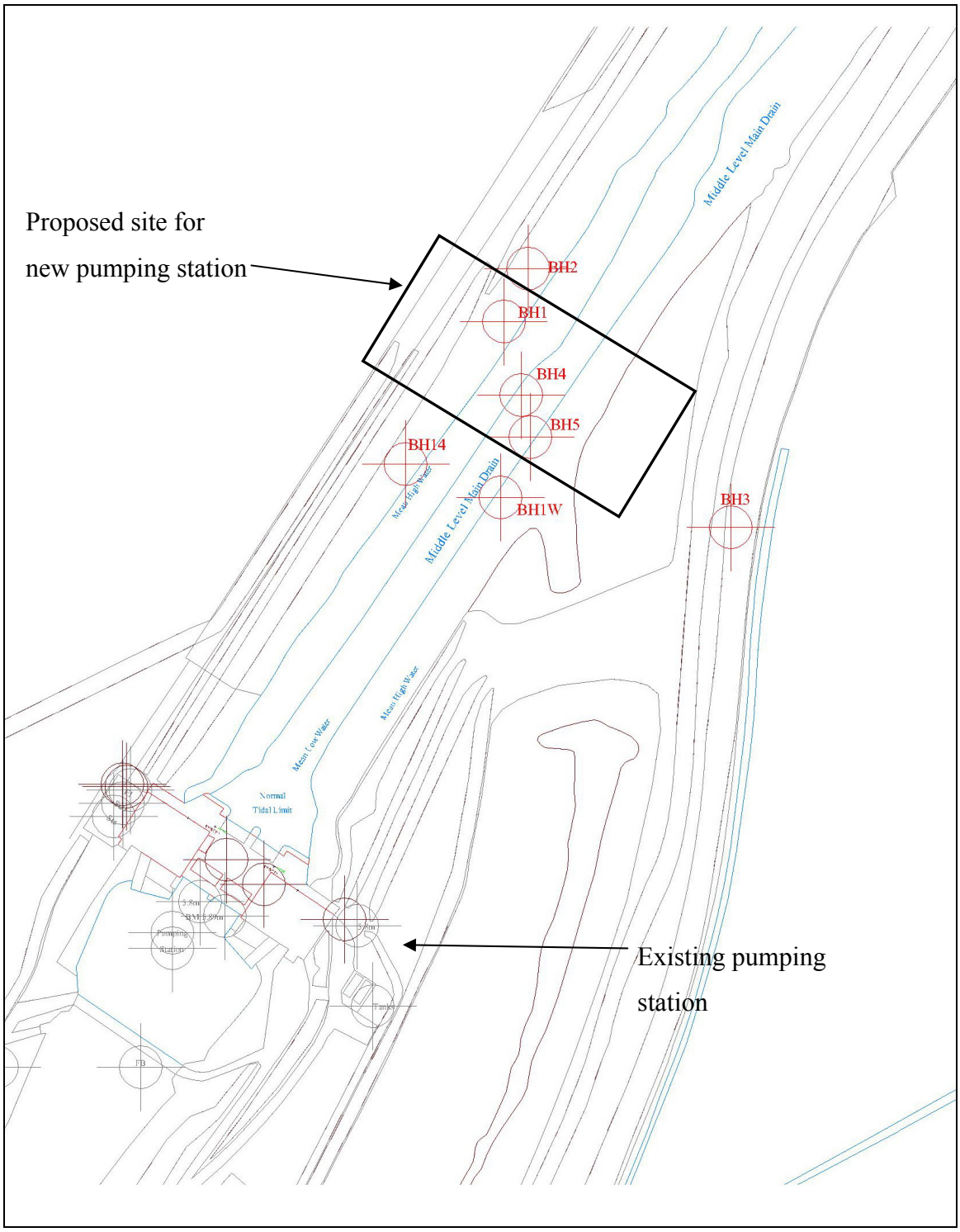

Figure 4-6: Location of boreholes

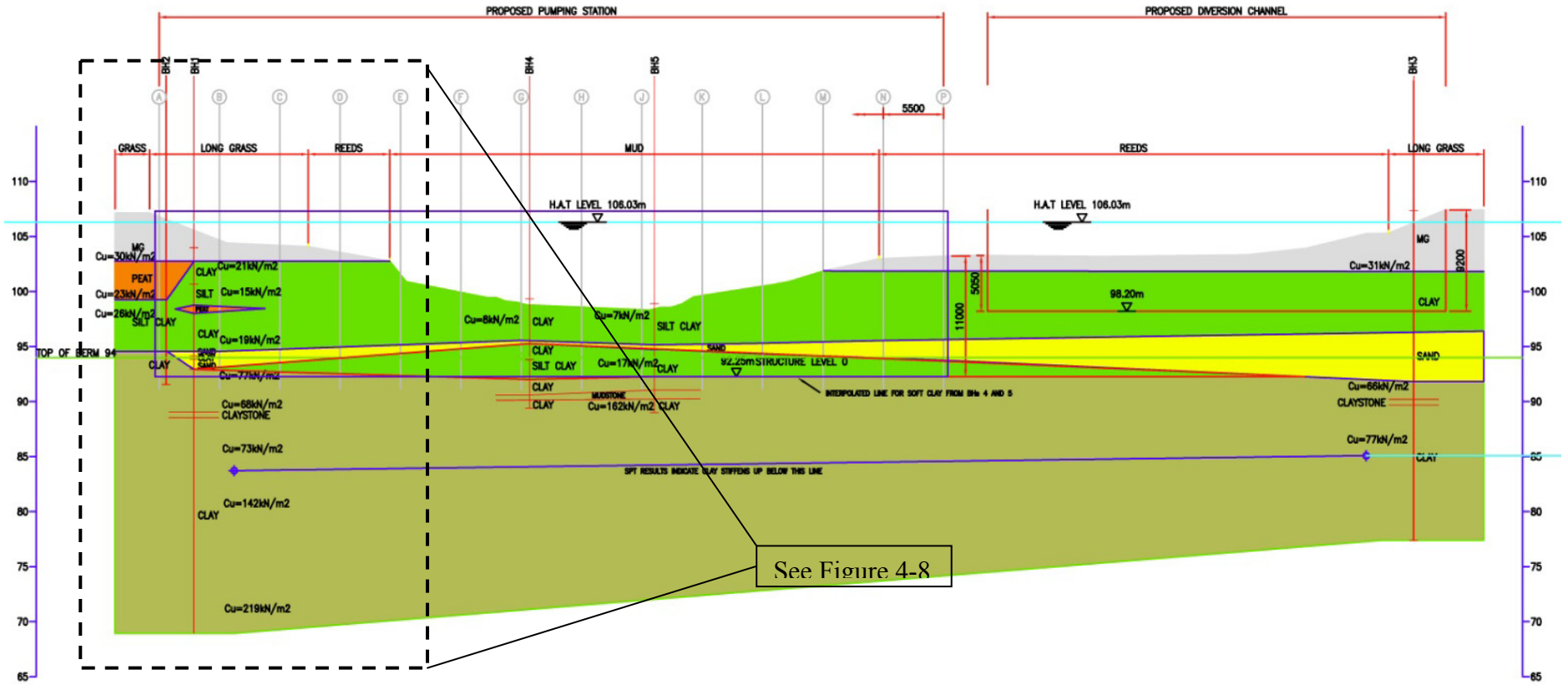

Figure 4-7: Soil profile from site investigation study for the construction of new pumping station (Atkins, 2005)

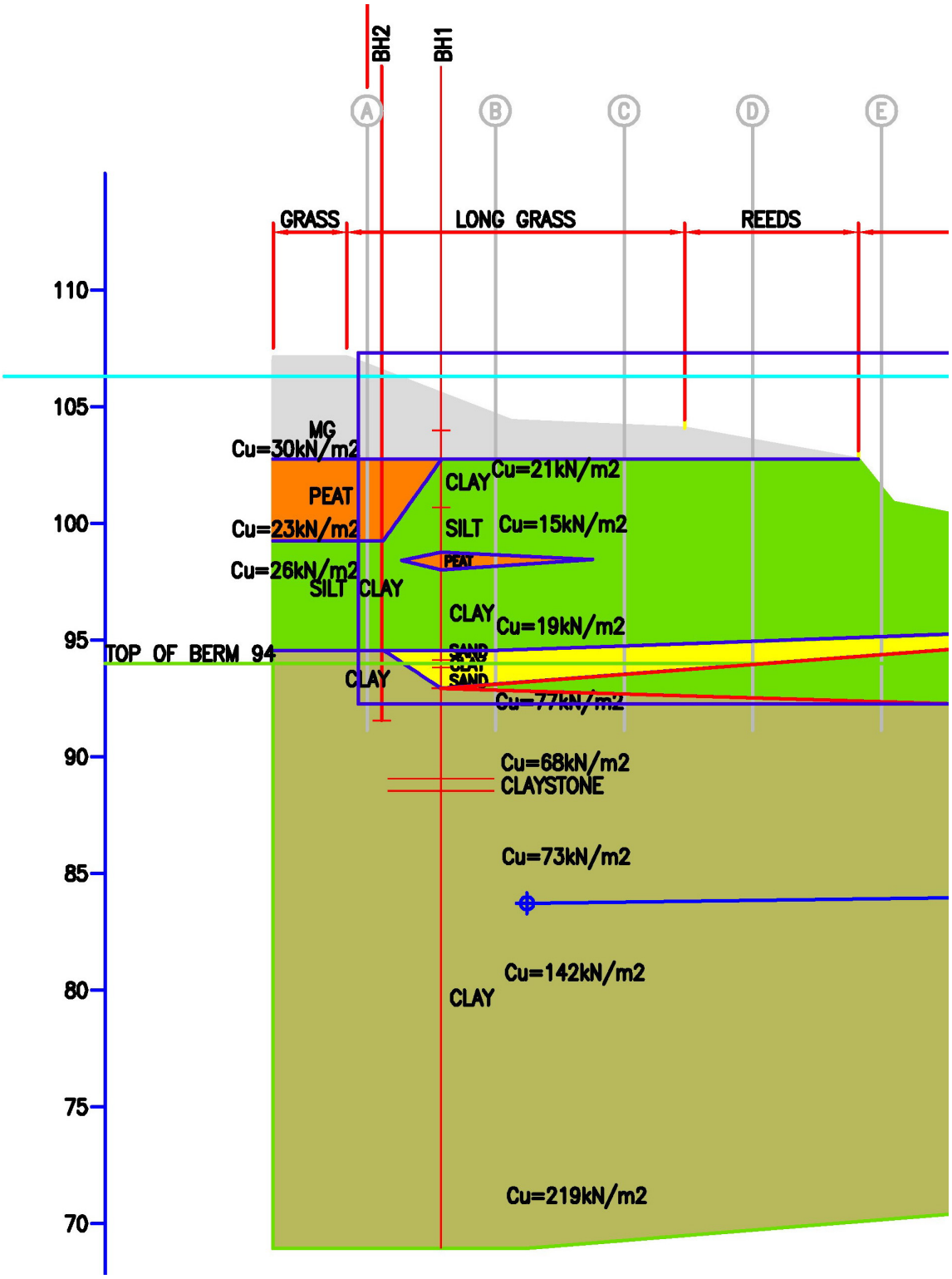

Figure 4-8: Cross section of the soil profile from left bank section of the site (Atkins, 2005)

Figure 4-9: Cut in the west slope showing Fen Deposits

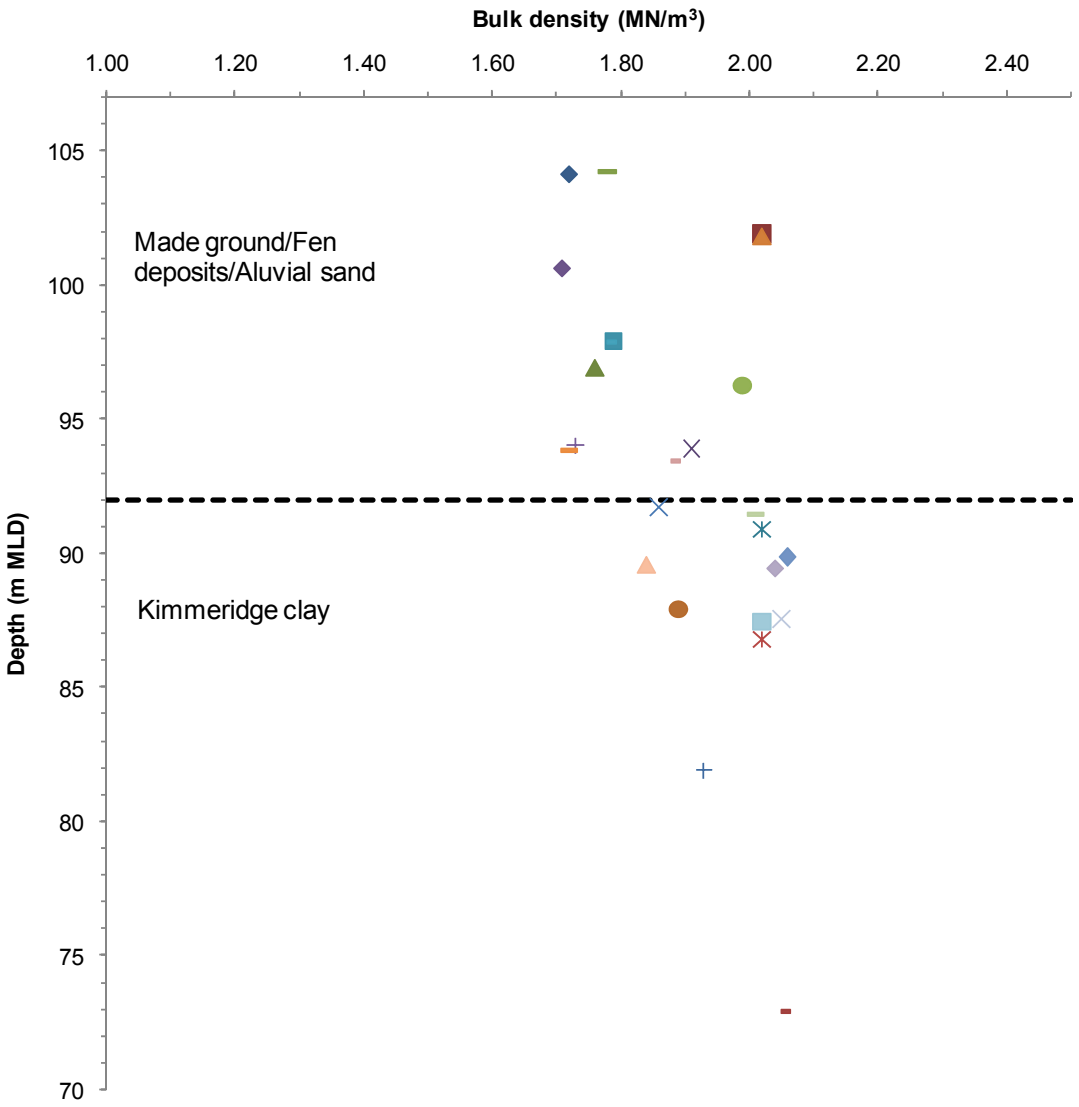

Figure 4-10: Bulk densities for various soil layers

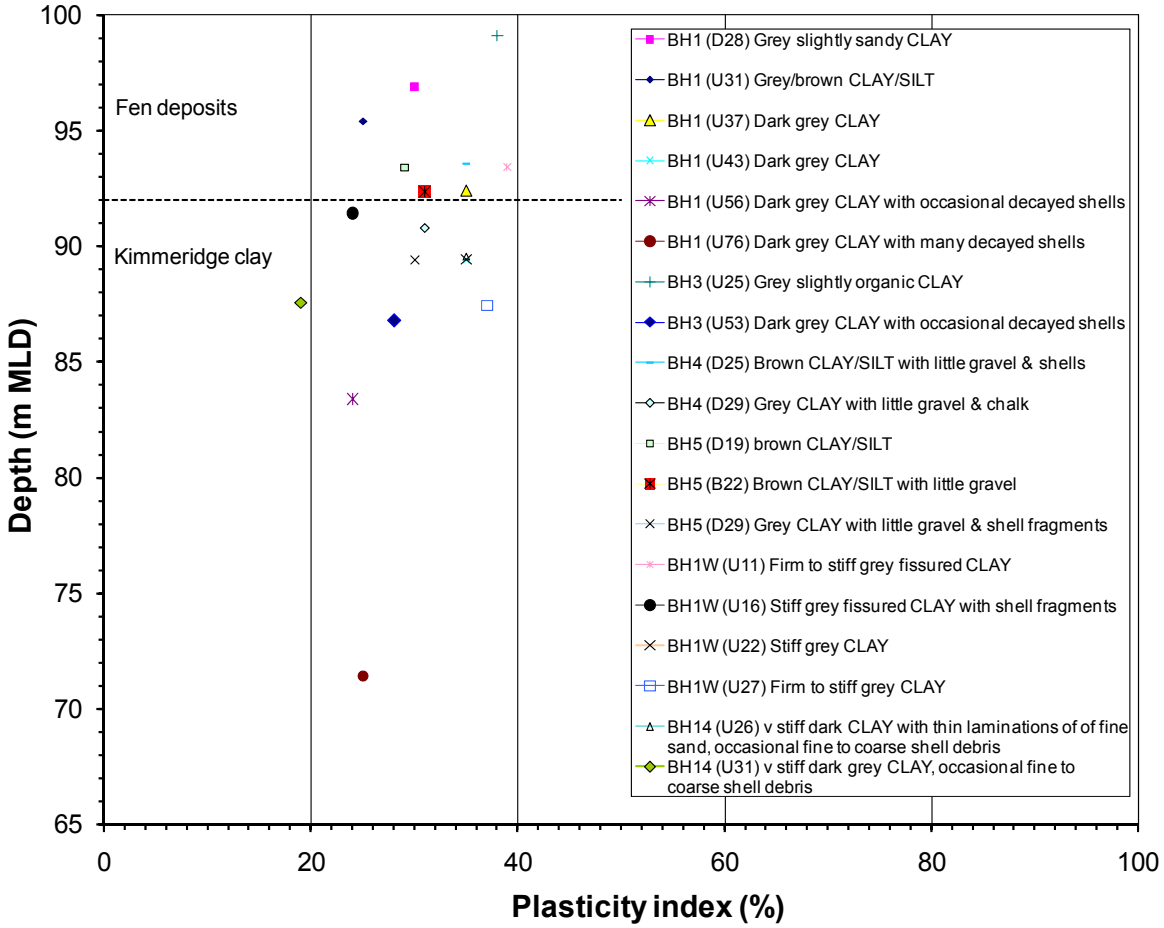

Figure 4-11: Plasticity index data

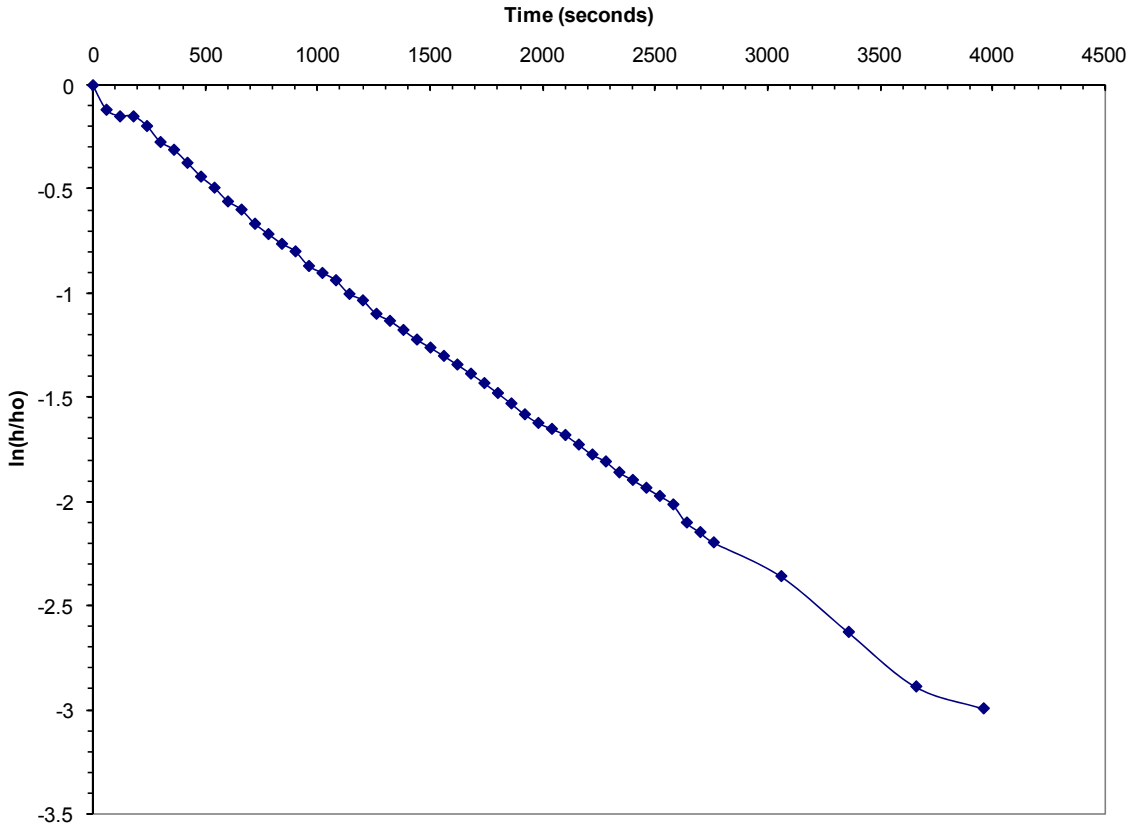

Figure 4-12: Results from falling head test to calculate the basic time lag (T)

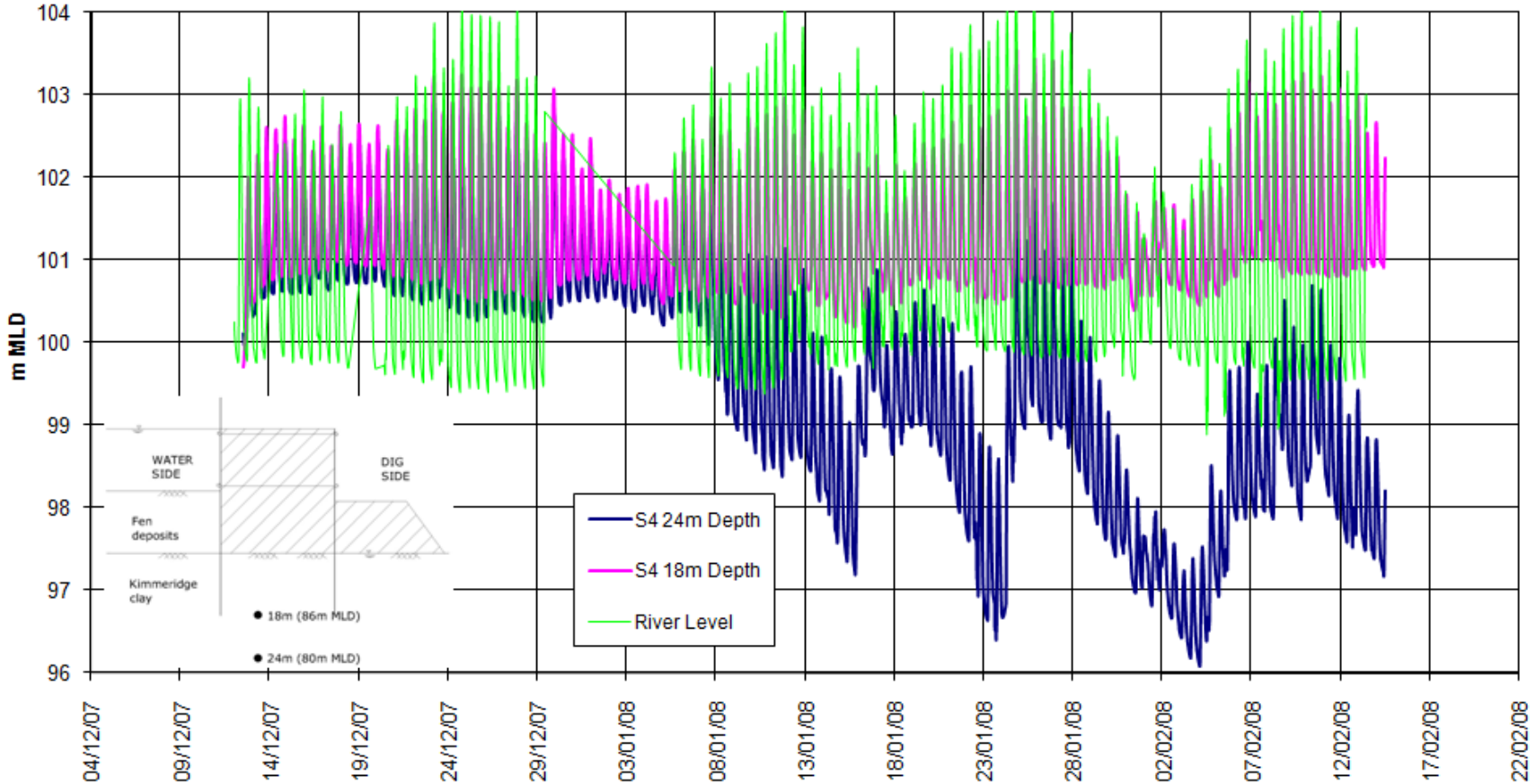

Figure 4-13: Piezometeric results from cell S4

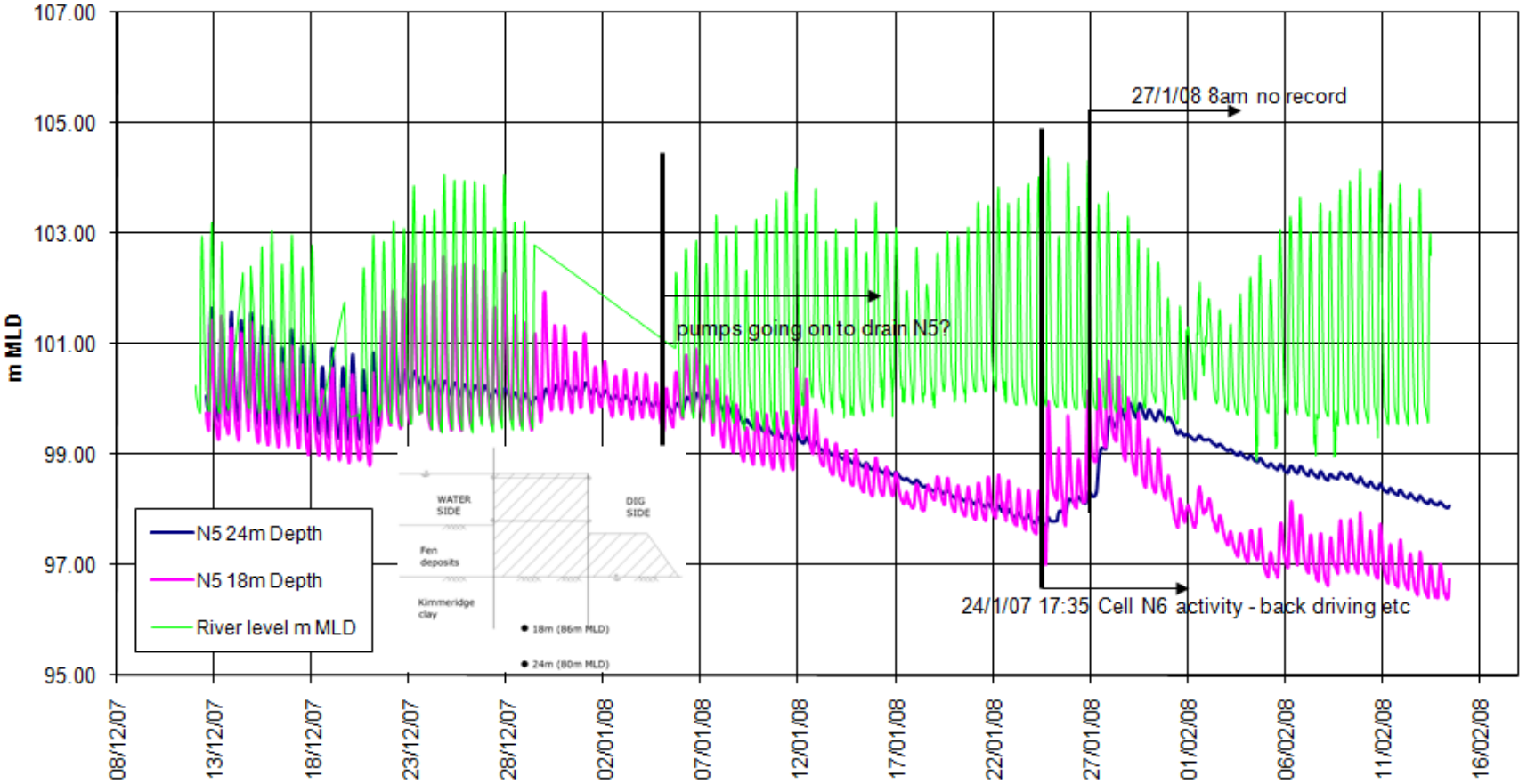

Figure 4-14: Peizometric results from cell N5

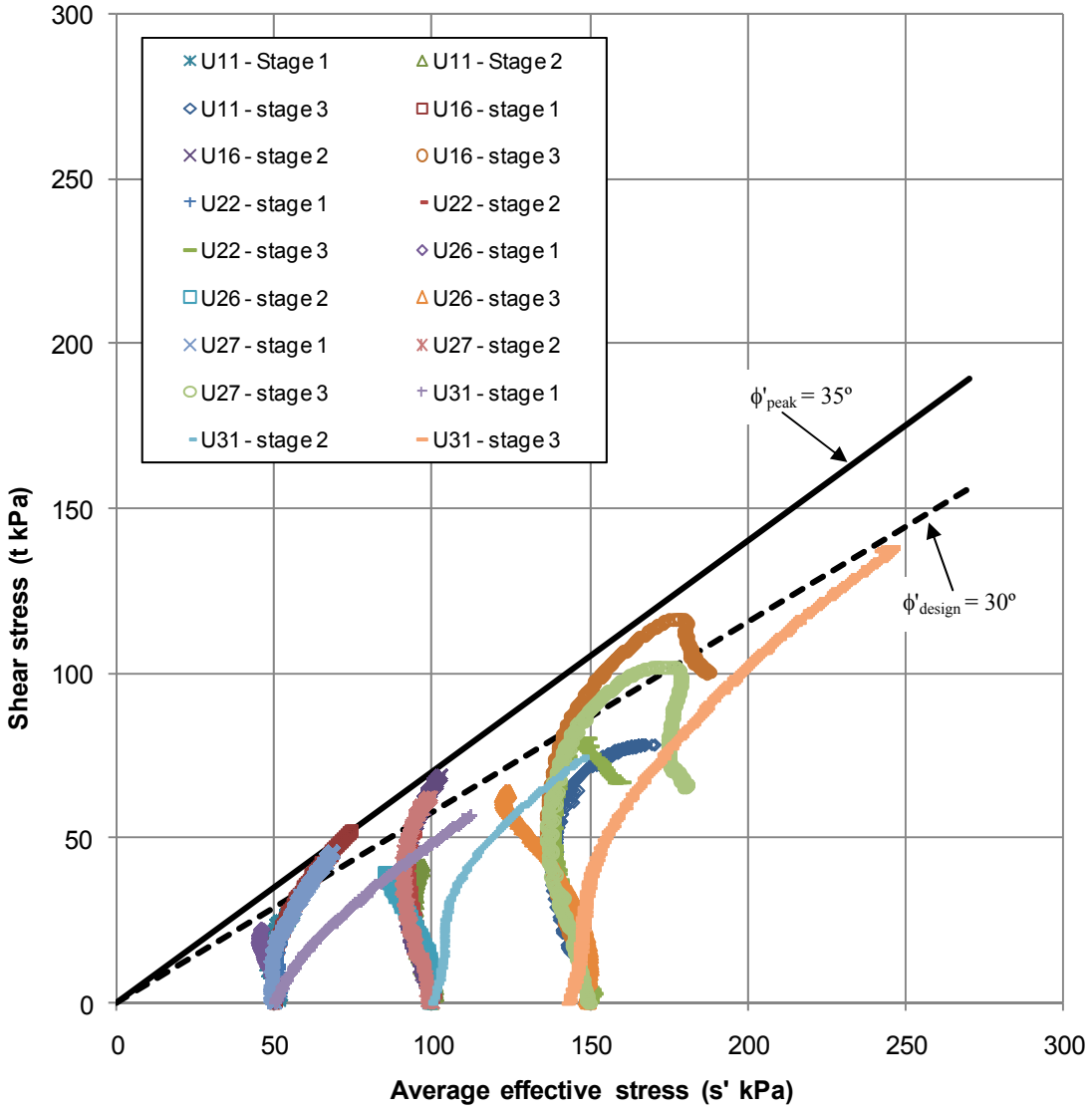

Figure 4-15: Average effective stress (s') plotted against shear stress (t) from multi stage triaxial tests with pore water pressure measurement to investigate the effective angle of friction for kimmeridge clay

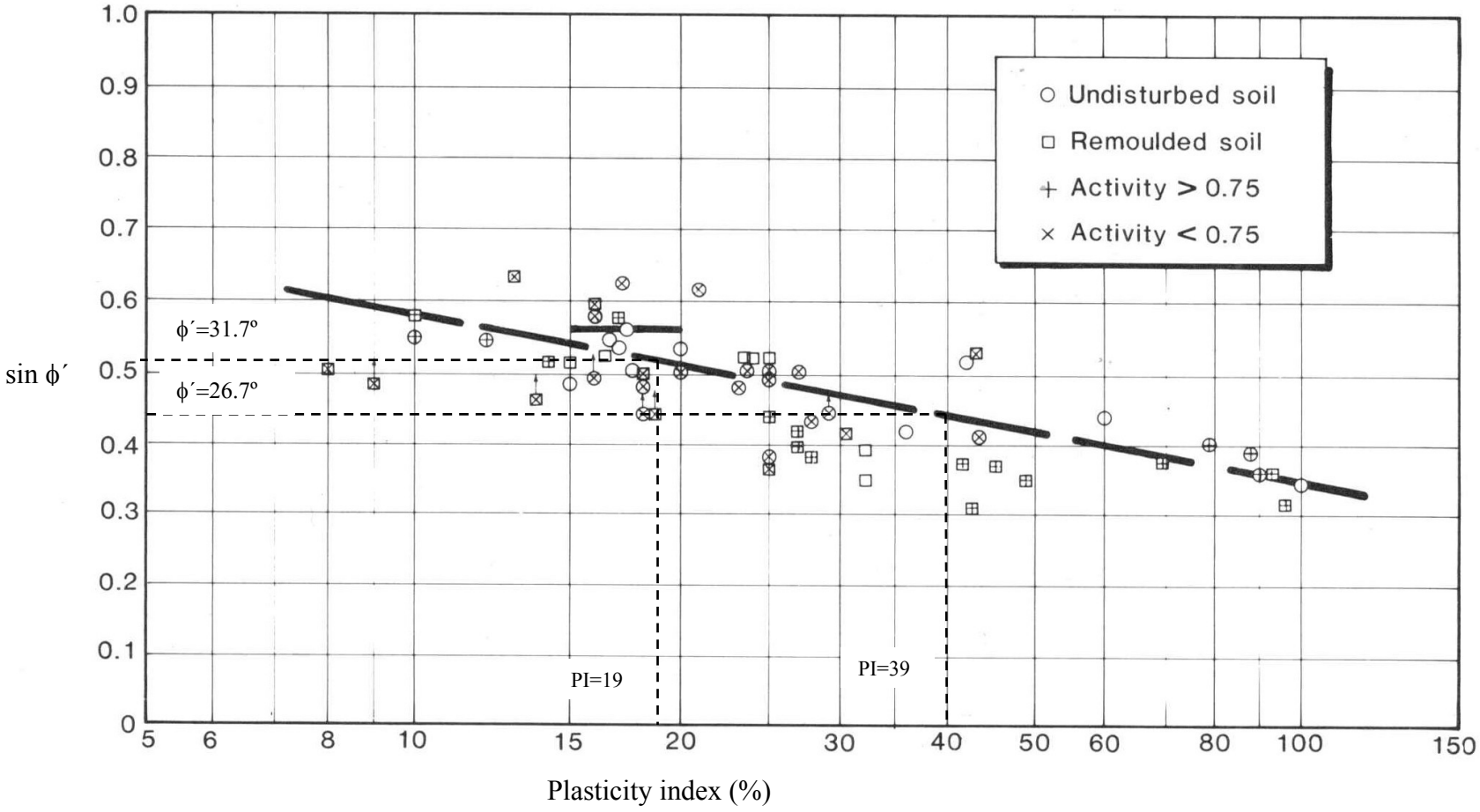

Figure 4-16: Kenny's (1959) relationships between Plasticity index and sinϕ′ for normally consolidated soils

5 Two dimensional numerical analyses

The early numerical analyses of cofferdam performance considered many of the key assumptions regarding the overall failure mechanisms and soil/structure interactions discussed in section 3. The first comprehensive analyses modelled soil structure interactions using a slip surface between the soil & sheet piles and helped identify many of the key aspects of cofferdam modelling (Clough and Hansen, 1977). Due to the complex nature of the failure mechanisms identified and the complex composite behaviour, the US Army Corps of Engineers guidelines (1989) suggested that any numerical analysis cofferdam behaviour should include;

- non-linear stress strain soil behaviour,
- slip (interface) elements between the soil and structural wall elements,
- an ability to simulate the construction sequence, and
- Orthotropic shell response for modelling sheet pile joint flexibility in lateral direction

A finite elements program "Soil-Struct" (Shannon and Wilson, 1982), was developed by Dr. Wayne Clough to model circular type cofferdams specifically for the Lock and Dam No.26 (Replacement). This program provided good agreement between the field and calculated response, but failed to accurately model the response for other types of cofferdams such as the cloverleaf cells employed at the Willow Island cofferdam (Clough and Hansen, 1977).

There have been few reported numerical analyses related to cofferdam performance and no such analyses exist for diaphragm type cofferdams. Therefore a series of preliminary numerical analysis was undertaken. Various numerical codes were initially considered, but following the guidelines set out by USACE (1989), a finite difference formulation FLAC (Fast Lagrangian Analysis of Continua) (Itasca, 2008) was selected to model diaphragm type cofferdam geometry and construction sequence employed at a large cofferdam construction at St. Germans, Norfolk, UK (See section 4).

5.1 The FLAC numerical code

FLAC^{2D} and FLAC^{3D} programmes were originally developed for mining and geotechnical engineers (Coetzee *et al.,* 1998) by Itasca Consultants in 1994. FLAC programs are user-friendly with options for creating complex meshes using a range of mesh generation tools. The basic calculation scheme of FLAC is based on the explicit method, where the variables are at discrete points in space and the shape function is undefined. The one explicit cycle of FLAC can be divided into four sub-steps;

Step 1: The velocities and displacements are calculated from stresses and forces using equations of motion for equilibrium conditions;

Step 2: stresses are determined using constitutive laws;

Step 3: The boundary conditions and newly determined stresses are then used to determine the nodal forces;

Step 4: Equilibrium conditions are used to calculate new velocities at the gridpoints;

The basic concept of this FLAC explicit method is to keep the calculation speed ahead of the physical speed using relatively small time steps in comparison to the implicit method. This enables the code to solve the equations using known values for the fixed duration of calculation step, which considerably increases the calculation speed even though the time step is comparatively small in comparison to finite element codes.

The primary features of FLAC programmes which are considered suitable for solving diaphragm type cofferdam analysis are;

- The ability to assign linear and non linear variation in soil properties with depth,
- Model non-linear soil responses using predefined soil models, or the ability to define bespoke constitutive models using C++ or the FISH programming language (Itasca, 2008),
- FLAC interface elements are available to model soil/structure interactions between the soil and the sheet piles. FLAC interface elements are double sided

allowing different stiffness and strength properties on both sides of the wall to be assigned,

- Steel ties can be modelled using cable elements and be modelled with or without the friction between tie/soil interface,
- It can solve for both short term and long term conditions using fluid flow analyses and may be coupled to calculate consolidation times, or uncoupled to increase the calculation speed, if only the long term conditions are required,
- Construction sequences can be modelled and intermediate stages are saved to allow stability checks during construction stages to be undertaken, and
- Has the ability to model large strain and physical instability of the structure (Coetzee *et al.,* 1998), allowing collapse mechanisms to be identified.

5.2 Load cases

The construction of a cellular cofferdam typically includes a number of key construction stages. Therefore, various load cases should be analysed independently to asses the stability of a cofferdam at each key load stage and after construction together with global stability checks. The following load cases were identified during the design of the diaphragm type cell cofferdam with twin sheet pile walls for the construction of the St. German's cofferdam (for details see section 4.2). This cofferdam was designed to retain soil and water on the loaded side using a diaphragm type cellular cofferdam geometry (see Figure 1-2).

5.2.1 Cell excavation stage

The cell is excavated down to the level where a stiff soil/rock layer is located or the desired bearing capacity is satisfied. The cell is usually excavated under balanced water conditions i.e. the water is at the same level on either side of the cofferdam to avoid the sheet pile moving into the excavation. This also prevents excessive heave and softening of soil plug within the cell in the case of a cofferdam founded on a clay foundation. To stabilise the cells during construction temporary frames are used to tie the two sheet piles

together during cell construction. The structure needs to be investigated for stability under the full cell excavation prior to filling.

5.2.2 Cell filling stage

The interlock forces need to be calculated for the cell filling stage. The water level is usually at the top of the cell fill at the end of this stage. Therefore this is considered to be the most critical stage in terms of interlock stability and is a common reason for cell failure (see section 2.5). The cell stability at this stage is assessed by calculating the factor of safety against the interlock strength (USACE, 1989).

5.2.3 Excavation on the dry (unloaded) side

The cofferdam is excavated on the unloaded (dry) side under balanced water; an earth/fill berm may be placed under water and shaped after dewatering to provide additional support to the wall. The condition with full excavation on the dry side (as was the case with the St. Germans cofferdam) just before the placement of the berm should be analysed for global stability against overturning and sliding to satisfy the stability under this short term loading condition. A tie should also be installed at lowest possible level to stop the movement of the inner piles towards the excavation. The depth of embedment should be sufficient to prevent this movement despite the support provided by the lower ties.

5.2.4 Commissioning of cofferdam

Once the excavation is complete and the berm support is in place, the balanced water loading is no longer required. In the case of the pumping station an additional commissioning stage was required where the water level in the river is considered at the lowest level while the water level on the unloaded side is at the mean high water level. Thus the load on the excavated (dry) side will exceed the load on river (wet) side which is completely opposite to the working loads a cofferdam is typically designed for.

5.2.5 Drawdown stage

The individual cofferdam cells are typically dewatered. The water level on the dry side is reduced to the design level and the structure must be checked for stability under these conditions. The water level within the cell should be taken at the design water level under

the drainage arrangement (weep holes, pumping, berm etc) or through the formation of a sloping phreatic surface between the outer and inboard piles. The interlock stresses, internal and external stability of the cofferdam must be checked under both drained and undrained conditions depending on the type of construction. If the soil permeability is high, the soil surface on the dry side must be checked for piping and boiling failure under the steady state flow under the cofferdam. This will be checked by the analysis implicitly during the flow calculation stage after the soil is excavated on the unloaded side.

5.3 Long term effective stress analyses for St German's Cofferdam

Based on the moderately high permeability of the Kimmeridge Clay (see section 4.6.3) it was decided to conduct a fully drained effective stress analyses without relying on the undrained strength of the soil. FLAC^{2D} finite difference code was used to model the construction sequence and long term response of the cofferdam using the effective stress formulation (Itasca, 2008). A parametric study was conducted to minimise the effect of mesh density and model boundaries. The width of model was fixed as 120 meters horizontally and 85m vertically. A total of 11700 zones were defined, which were immediately reduced to 9360 elements by removing the top 9m of the mesh to model water pressure and any change in initial ground level necessary for further analysis (see Figure 5-1). Six rectangular sub-grids were assigned to achieve the dense mesh (0.5 × 0.5m) in the cell installation zone, while the element sizes outside this subzone were increased in the ratio of 1.05 in both the vertical and horizontal direction using the following relationship.

$$n = \frac{\log\left[-\left(\frac{L}{a}\right)\cdot(1-r)+1\right]}{\log(r)} \qquad \textbf{Equation 5.1}$$

n = Number of elements

L = Length in which mesh is required

a = Fist elements size

r = Ratio for increase element size

A Mohr Coulomb soil model was assigned to all soil elements. A multi-stage analysis was undertaken to capture the short term and then longer term response as changes to the pore water pressure regime occurred due to the removal of water from inside of the cofferdam.

A 10.5m wide section of cofferdam situated in the middle of the river (e.g. cell N3,S3) is considered to be critical in terms of stability (for detail see Figure 1), where the depth of the Kimmeridge Clay is at 92m MLD. The water level used to determine the long term pore water pressure regime is 104m MLD (MHWS) and accounts for the influence of cyclical total pressure head generated across the normal tidal range during the construction stage (under balanced water conditions) and consolidation analysis stage. In the long term, an effective stress analysis using the long term pore pressures (104m MLD), drained material parameters and an impounded water level of 107m MLD (Highest Astronomical Tide) i.e. 1:200 years flood event, allowing ground water to flow and establish a new pore water pressure regime during an increase in the tide level is considered. These modelling stages are summarized in Table 5-1:

Table 5-1: Main Analyses Stages

Stage	Water level	Type of analyses
Cell Construction	104m MLD (Average)	No ground water flow (except cell dewatering stage)
Consolidation	104m MLD (Average)	Uncoupled fluid flow analyses
Effective stress analysis: water level at Highest Astronomical Tide level	Up to 107m MLD (HAT) 1:200 years flood event	Uncoupled fluid flow analyses

5.3.1 Soil properties for effective stress analyses:

The soil profile used for the analyses was derived from the soil investigation report (COSTAIN, 2007; Atkins, 2005). For the critical section (middle of the river) the soil can be divided in two main layers, i.e. Fen Deposits and Kimmeridge Clay (Figure 4-7). The depth of Fen Deposits is 6m below river bed (from 98 to 92M MLD), underlain by

Kimmeridge clay. The soil stiffness values were derived from the Geotechnical Interpretive Report (ATKINS, 2005). As FLAC uses bulk (K) and shear modulus (G) of elasticity as stiffness parameters, drained bulk and shear modulus for the various soil layers were calculated using the following relationships:

Bulk modulus of elasticity K_b,

$$K_b = \frac{E'}{3(1-2\upsilon')} \qquad \textbf{Equation 5.2}$$

Shear modulus of elasticity G,

$$G = \frac{E'}{2(1+2\upsilon')} \qquad \textbf{Equation 5.3}$$

Where,

υ' = Poisson ratio under effective stress conditions

E' = Stiffness of the soil under effective stress conditions

The soil parameters used in the analyses are summarised in Table 5-2.

Table 5-2: Soil parameters used in the analysis

Soil Type	**Depth m MLD**	**E´ drained MPa**	**c´, kN/m^2**	**v'**	**γ_d kN/m^3**	**ϕ'**	**Porosity**
Made Ground	Above 102	4	0	0.2	1410	30°	0.49
Very soft silty clay	102 to 95	0.7		0.2	1110	30°	0.49
Soft silty clay	95 to 92	2		0.2	1210	30°	0.49
Firm to stiff clay	92 to 90.5	10		0.2	1310	30°	0.49
Firm to stiff clay	Below 90.5	22 + 6 z		0.2	1310	30°	0.49
Granular fill (Type I)	Below 99 (within cell)	50	0	0.3	1600	35°	0.3
Granular fill (Type II)	Above 99 (within cell)	25	0	0.3	1600	35°	0.3
Granular fill for berm	berm	25	0	0.3	1600	35°	0.3

As a numerical modelling device a high value of cohesion (1×10^{10} Pa) was specified to prevent soil failure during the accelerated initial consolidation phase; cohesion was changed to zero before the start of the actual construction sequence. The anisotropic soil permeability was assigned on the basis of a falling head test undertaken on site (section 4.6.3);

k_v=1.5 x 10^{-8} m/sec and k_h = 1.5 x 10^{-7} m/sec

FLAC requires that the coefficient of pore pressure term in Darcy's equation (known as mobility coefficient (Itasca, 2008)) is defined as ratio of intrinsic permeability to the fluid dynamic viscosity:

$$K_{FLAC} = \frac{k}{\rho_w \cdot g} \qquad \textbf{Equation 5.4}$$

Where;

k = Permeability of soil

ρ_w = Density of water

From the above, the permeability used for the FLAC analyses was:

$K_{v\,FLAC}$ =1.5 x 10^{-12} m^2/Pa·sec and

$K_{h\,FLAC}$ = 1.5 x 10^{-11} m^2/Pa·sec

5.3.2 Properties of sheet piles and steel ties:

Arcelor AZ28 SP355 piles were used to construct the cofferdam. The sheet piles were considered to be impermeable as the outboard piles were sealed to prevent the ingress of water into the cell. The pile stiffness was calculated from the yield strength of the section as,

σ_y = 355 N/mm^2

ε_y = 0.002 yield strain for steel

$E_{steel} = \sigma_y / \varepsilon_y$ **Equation 5.5**

$E_{steel} = 200 \times 10^9$ N/m^2

(Values taken from British steel piling handbook, 2005)

Table 5-3: section properties for sheet piles

Pile used	Sheet pile Arcelor AZ28
E_{steel} (N/m^2)	200×10^9
Cross sectional Area (m^2) per meter	0.0211
Moment of inertia (m^4) per meter	5.894 X 10^{-4}

Two levels of Macalloy 17MHS (Macalloy Ltd, 2007) steel ties were used to tie the two sheets together in both the lateral and longitudinal direction. The cross sectional areas of the ties were adjusted for pile spacing in the plane strain analyses. The ties detail is given in Table 5-4;

Table 5-4: Section properties for steel ties

Ties used (Macalloy 17MHS)	M48	M76
Location	Upper ties at 103.5m MLD	Lower ties at 98.5m MLD
E_{steel} (N/m^2)	200×10^9	200×10^9
Yield Load (N)	660×10^3	1756×10^3
Diameter (m)	0.045	0.072
Spacing (m)	2.4	1.2

5.3.3 Interface elements for Sheet piles:

FLAC allows the use of interface elements to be connected between the soil and structural elements on either side of the structure. The interface properties include stiffness and shear strength of the interface. The interface stiffness was calculated using the following;

$$K_n, K_s = 10 \cdot \max\left[\frac{\left(K + \frac{4}{3}G\right)}{\Delta Z_{\min}}\right] \qquad \textbf{Equation 5.6}$$

Where,

K_n = Normal stiffness of the interface

K_s = Shear stiffness of the interface

$\Delta Z_{\min}$ = Minimum width of the neighbouring zone

CIRIA SP95 (Williams and Waite, 1993) provide guideline values for the interface friction (δ°) values to be used where δ° is taken as 2/3 of the ϕ' on the active side and ½ of ϕ' on the passive side. For details see Table 5-5 and Figure 5-3.

Table 5-5: Properties of interface elements

Interface location	Interface adjacent to Natural ground	Interface adjacent to Granular Fill
Normal and shear stiffness (MPa)	580	1340 for fill Below 98m MLD 670 for fill above 98m MLD and berm
Adhesion (kN/m^2)	0	0
δ° (Friction)	(2/3 of ϕ') Active (1/2 of ϕ') Passive	(2/3 of ϕ') Active (1/2 of ϕ') Passive

5.3.4 Analyses methodology:

To assess the overall failure mode of the structure, the insitu soil, fill and interface strength was gradually reduced for each set of analyses to check the stability under each reduced strength. Failure was determined from the computed velocity vectors (m/step of run), displacement vectors (total displacement recorded at a grid point), unbalanced force plots and notional maximum displacement of the inboard and outboard walls, plotted against the factored strength ($\tan\phi'_{\text{actual}}/\tan\phi'_{\text{reduced}}$). The detail of soil/fill strength and interface friction reduction used is given in Table 5-6.

Table 5-6: Strength reduction for factor of safety analyses (all values in degrees)

Actual ϕ'_{design} º for soil	30.00				
FoS	1.00	1.10	1.15	1.20	1.25
factored $\phi'_{reduced}$ º for soil	30.0	27.7	26.7	25.7	24.8
δº active (soil)	20.0	18.5	17.8	17.1	16.5
δº passive (soil)	15.0	13.8	13.3	12.8	12.4
actual fill ϕ'_{design} º for fill	35.00				
factored $\phi'_{reduced}$ º for fill	35.0	32.5	31.3	30.3	29.3
δº active (fill)	23.3	21.7	20.9	20.2	19.5
δº active (fill)	17.5	16.2	15.7	15.1	14.6

5.3.5 Detailed analysis steps for modelling the drained response:

The analyses steps are presented graphically in the Figure 5-4 to Figure 5-6. The following is a brief summary of the standard analyses case i.e. full soil strength ϕ'_{design} = 30˚. Each step represents a particular stage executed to model the construction sequence/process towards working conditions following construction of the cofferdam. The model was stepped to equilibrium at the end of each step using an unbalanced force ratio of 1×10^{-3}. Both small and large strain formulations were used to ensure that the cofferdam did not attain a new stability condition under the deformed state in the large strain mode.

Step 1: Generating mesh and applying initial and boundary conditions

FLAC built in options used were:

Configure GW: Ground water flow configuration was used to model the effective stress condition with pore water pressures defined in all mesh zones.

Configure ATS: FLAC function which automatically adjusts total stresses due to any change in pore pressure imposed externally (e.g. due to dewatering or lowering water level manually).

Mesh density:

A minimum element size of 0.5m × 0.5m, with gradually increasing element size outside the cofferdam area was used. The ratio for increasing the element size outside the uniform mesh size was 1.05. A total of 11700 elements were initially defined, and then reduced to 9360 elements by removing the top 9m of the mesh to model water pressure and any change in initial ground level required for further analysis (see Figure 5-1).

Boundary fixities:

The bottom boundary was fixed in the vertical and horizontal direction; the left and right boundaries were fixed in the horizontal direction only.

Installation of Piles and interfaces:

The sheet piles were 'WISHED IN PLACE', with interface elements on both sides connecting the mesh and pile nodes. Beam elements were used to model sheet pile walls of unit width under plane strain conditions. A nodal distance of 0.5m was used to ensure sufficient beam elements were available for each wall in order to capture the correct bending moments and displacements. The self weight of the piles was neglected.

Pore water properties:

The density of the water is taken as 1000 kg/m^3; a water bulk modulus of 0 was used to model a drained response, and 2×10^9 N/m^2, during the fluid flow steps.

Initialisation of stresses and pore water pressures:

In-situ stresses were initialised with the average water level at 104m MLD. This gives a 60 kN/m^2 pore water pressure at the top of the ground level which is modelled by applying a uniform surcharge pressure of 60 kN/m^2. An initial effective insitu stress ratio of 0.6 was adopted for the Fen Deposits above 92m MLD, and 1.0 for Kimmeridge Clay below this level. Pore water pressure was 60 kN/m^2 at the top of the grid (at 98m MLD, as there is 6m of water above ground surface), varying hydrostatically with depth.

Installation of the top truss to model the top support frame:

A single pin ended beam element used to model the truss (top frame) at 104m MLD (top of the inboard pile) providing support to the sheet piles during staged cell excavation.

Step 2: 3m excavation within the cell under a balanced water condition.

The cell was excavated to 3m below ground level to 95m MLD, with a balanced water condition. The pore water pressure at the base of the excavation is taken as 90 kN/m^2 (6m already present plus 3m more due to excavation). This was applied as a surcharge to the excavated surface to model the overburden due to the water inside the cell. The pore pressure within the soil was calculated automatically by FLAC and no change was introduced externally for pore water pressure or stresses within the soil.

Step 3: Excavation of a further 3m to reach the design level within the cell (i.e. 92m MLD or top of stiff kimmeridge clay)

The cofferdam cell was excavated to the design level (92m MLD), and a surcharge pressure of 120 kN/m^2 (6m + 6m of water due to excavation under balanced water) applied to the surface of the excavated face to model the balanced water conditions within the cell. The program is allowed to change any pore pressure due to excavation of the soil, and as mentioned previously the ground water flow is prohibited to model undrained conditions (under balanced water).

Step 4: Filling of the Cell under water up to 98m MLD

The cell is filled under water and the pore water pressure & effective stresses are initialised with $K_o = 1.0$. A uniform surcharge of 60 kN/m^2 was applied at the top of the fill to model the balanced water pressure at the top surface of the fill. New interfaces were introduced to create the link between the soil elements and structural nodes. Pore water pressure was initialised as 120 kN/m^2 at the bottom of the cell (12m column of water above the bottom) and 60 kN/m^2 (6m column of water) at the top of the fill within the cell.

Step 5: Installing the lower level of ties

The first level of ties were installed under balanced water conditions at 98.5m MLD at a tie spacing of 1.2m c/c. The ties used were Macalloy 17MHS, and the specifications provided in Table 5-4.

Step 6: Removing top frame and installing upper level of ties

Once the lower level of ties was installed the top frame was removed whilst maintaining the balanced water conditions within the cell. This avoids any tension in the top frame, as it was not designed to take any tensile load. The top level of ties was installed at this stage with a tie spacing of 2.4m c/c.

Step 7: Filling cell to the top with granular fill material

The cell was filled to the top with compacted fill without any dewatering; therefore the water level within the cell is considered 104m MLD in order to model the extreme case. New interfaces were introduced with the maximum interface friction values for fill the material as detailed in Table 5-5.

Step 8: Dewatering cofferdam cell to 93m MLD

The water level inside the cell was reduced to 93m MLD, i.e. just one meter above the base of the fill design level. Pore water pressure was initialised to zero in the dewatered zones. The "Configure ATS" command automatically adjusts the total stresses following the reduction in pore water pressure. Hydrostatic pore water pressure distribution was initialised in the remaining 1m of granular fill below 93m MLD inside the cell. While the pore pressure below 92m MLD is calculated automatically by FLAC according to the pore water pressure change due to dewatering, and no change is introduced externally below 92m MLD. The model is then solved using uncoupled fluid flow simulation, which means the fluid flow and mechanical forces are calculated in separate stages. The bulk modulus of water was specified as 2×10^9 N/m^2 during the flow calculation stage and set to zero for the stress calculation stage.

Step 9: Excavating underwater to the design level on inner side of the cofferdam

The soil was excavated to 92m MLD, in two stages of 3m each. A uniform surcharge of 120 kN/m^2 due to the water present above the excavated face was applied (120 kN/m^2 for a12m column of water).

Step 10: Installation of berm under water

The height of the berm was 6m (up to 98m MLD), with top width of 10.5m and overall base length of 20.7m. The berm slope was required to be less than ϕ' of the berm material to satisfy the overall stability requirement of the slope. The dry density of the berm material is 16 kN/m^3 with an angle of friction equal to the fill ϕ'. An interface was introduced between the berm and inboard sheeting with an interface friction angle of half of the friction angle of berm material (the maximum recommended by CIRIA SP95 (1992) for an interface on the passive side of a sheet pile wall).

Step 11: Long term consolidation analysis

The excavated (unloaded) side of the cofferdam was dewatered to 92m MLD; fluid flow and mechanical calculation steps were solved separately using the uncoupled fluid flow analyses option in FLAC for the determination of long term effects. The pore water pressure was 60 kN/m^2 at the top surface on the water side with fixed saturation and pore water pressure. The saturation was fixed to zero within the dry cell fill and berm. The model was stepped to equilibrium with an unbalanced force ratio of 1×10^{-3}, and is solved to reach a steady state flow condition at the end of the uncoupled fluid flow simulation stage.

Step 12: Increasing water level above 104m MLD, to simulate the flooding conditions

The water level on the retained side was increased up to a maximum height of 107m MLD, in 1m increments during each stage. The model then solved under drained conditions and pore water flow permitted as an uncoupled simulation to establish a new pore pressure regime according to a rising water level within the river. Both large strain and small strain formulations were adopted separately to ensure that the structure did not attain a new equilibrium state under the deformed shape attained in the large strain mode.

5.3.6 Results from the effective stress analysis

The failure of the structure is assessed by reducing the strength of the soil and the fill, and interfaces by a constant factor ranging from 1 to 1.25. The analysis was allowed to run through to completion for each value of ϕ' and the stability of the structure assessed by

examining the velocity vectors, equilibrium plots and displacement vectors. The maximum notional displacements for both the inboard and outboard wall are plotted against the Factor of Safety;

$$FoS = \frac{\tan \phi'_{design}}{\tan \phi'_{reduced}} \qquad \textbf{Equation 5.7}$$

Where;

FoS = Factor of safety on strength of the soil

$\tan \phi'_{design}$ = Design strength from multi stage consolidated undrained triaxial tests

$\tan \phi'_{reduced}$ = Strength used for the analyses by dividing soil friction angle by suitable factor (see Table 5-6)

Figure 3 shows the Maximum Displacements against *FoS*, for the large strain analyses. The analyses indicate a factor of safety is 1.1 for $\phi'_{reduced}$ =27.7˚ for a water level of 107m MLD (the1:200 years flood event height is 106.3m MLD); 1.2 for $\phi'_{reduced}$ = 25.7˚ for a 106m MLD flood height and a factor of safety greater than1.25 for $\phi'_{reduced}$ = 24.8˚ for flood level of 105m MLD. The analyses were rerun for increasing water levels beyond 104m MLD in the small strain mode to ensure that the structure did not reach a state of equilibrium due to a distorted geometry under a large strain formulation. The results are plotted for Displacement Vs FoS in Figure 5-7, where it can be seen that the factor of safety deduced from the large strain analyses is correct. It should be noted that all the results presented in the Appendix B and C, are derived from the small strain formulation analyses.

Displacement vectors are presented in Figure 5-8 where it can be clearly observed that reducing ϕ' to 24.8° for the 107m MLD flood case will result in failure of the structure due to excessive displacements. The FoS of 1.1 can also be derived from total displacement vectors plots from Figures B.1 to B.5 in Appendix. It is clear from the displacement vectors plots that the structure develops a curved failure surface at the base

of the cell with the soil block sliding towards the excavated side at the level of the toe of the inboard sheet pile, once the FoS falls below 1.10.

To highlight the onset of failure from the maximum displacement of the sheet piles (Figure 5-7) and displacement vectors (Appendix B), the Velocity vectors are presented in Figure 5-9 (see detailed plots for reduction in $\phi'_{reduced}$ values for highest flood level (107m MLD) in Appendix C). Also unbalanced force plots are presented in Figure 5-10. Again it is evident that the unbalanced force does not reach a minimum equilibrium value of 1×10^3 for $\phi'_{reduced}$ less than 27.7° (FoS 1.10) for the 107m MLD flood case. For the 106m MLD flood case, reducing $\phi'_{reduced}$ to 24.8° (FoS 1.25) also results in failure of structure.

The curved failure surface identified from the effective stress analyses (see Figure 5-8 and Figure 5-9) is similar to the analytical circular slip surface (Hansen, 1953) and log spiral failure mechanism identified from laboratory tests by Ovesen (1959); however there is a slight difference in the curvature of the failure curve. The circular type cells and level ground on both sides used in the analysis by Hansen and Ovesen, is significantly different to the case presented here, which used diaphragm type cells retaining both soil and water on the retained side. This suggests that the failure mechanisms previously identified by Hansen and Ovesen may be geometry specific.

5.4 Effective stress analysis of 13m wide section (instrumented cell)

To calculate the maximum structural forces in the sheet piles and ties an effective stress approach was adopted using 13m wide cofferdam cell dimensions from St. Germans cofferdam (cell C3, see Figure 4-3). This section was also instrumented to measure the bending moments and deflections in the sheet piles. The uncoupled effective stress simulation approach available in FLAC^{2D} was utilised for this purpose (Itasca, 2009). The soil properties and interface strength are the same as those used for the 10.5m wide cell analysis presented in Table 5-2 and Table 5-3 respectively.

5.4.1 Analysis steps for 13m wide cell analysis

The analysis procedure for 13m wide cell is different to the 10.5m wide cell. The inboard side on 13m wide cell was excavated under a lower water level, while 10.5m wide cells were excavated on the inboard side under balanced water conditions. Also the berm was removed and the inboard side was excavated for the central cell (C1 to C4; Figure 4-3) to facilitate installation of a series of CFA piles and base slab to provide foundation for the pumping station structure. For the 10.5m wide cells (North and South cells) the berm was in place in the end and remained there during the working of cofferdam. The details of the construction sequence modelled are as follows;

Stage 1: Same mesh density and dimensions were adapted to those used for 10.5m wide cell analysis (see section 5.3.5 and Figure 5-1). The sheet piles were considered wished in place and the model solved for initialisation of initial conditions;

Stage 2: Soil elements between 98 and 95m MLD within the cell were assigned NULL properties, i.e. soil was removed, while a uniform surcharge of 90 kN/m^2 was applied to the excavated face to model the water pressure on the surface to model the balanced water conditions within the cell;

Stage 3: Soil elements between 95 and 92m MLD within the cell were assigned NULL properties to simulate the excavation, while a uniform surcharge of 120 kN/m^2 was applied to the excavated face at 92m MLD to model the water pressure on this surface due to balanced water conditions within the cell;

Stage 4: Soil zones between 95 and 92m MLD were assigned granular fill Mohr Coulomb properties. A total vertical stress of 60 kN/m^2 was initialized in the top (6m of water above the fill), and 180 kN/m^2 at the bottom of the excavated cell to model the fill stresses (12m of water plus 6m of fill). The fill was considered to be compacted to an equivalent horizontal effective stress ratio of 1.0. A uniform surcharge of 60 kN/m^2 was applied at the top of the fill to model the water pressure above the cell fill;

Stage 5: The first level of ties were installed at 98.5m MLD, the properties and spacing of the ties remained the same as those used for 10.5m wide section analysis;

Stage 6: The frame is not designed to take any tension; therefore the frame was removed before filling the cell to the top. The top ties were installed with the same properties as defined in the effective stress analysis;

Stage 7: The cell was backfilled to the top under balanced water conditions. This means that the water level remains at the top of the fill level, i.e. 104m MLD;

Stage 8: Cofferdam cell was dewatered to 95m MLD. The water was allowed to flow to achieve the new pore pressure equilibrium under the reduced cell water level;

Stage 9: The inboard side was excavated down to 94m MLD under the balanced water conditions. The water level was kept as 104m MLD on inboard and outboard side while a lower water level of 95m MLD was kept within the cell;

Stage 10: The water level on inboard side was reduced to 97m MLD and solved to equilibrium allowing the pore fluid to flow and attain a new pore pressure regime under the reduced water level within the cell and cofferdam enclosure;

Stage 11: The berm was constructed up to 97m MLD by using the same granular fill material properties was used for cell backfill;

Stage 12: The cell and inboard side were dewatered to 94m MLD (excavation level) and the model was solved undrained to achieve conditions just after dewatering on dry side;

Stage 13: Fluid flow analysis allowed pore pressure equalisation to model the pore pressure change due to dewatering on the inboard side;

Stage 14: A 120 tonne crane load was applied to the top of cell C3 and solved undrained to model construction load due to construction plant. The crane load was removed once the model reached equilibrium as the crane was only present on the top of the cell C3 for a limited period of time;

Stage 15: The berm was removed to facilitate the construction of CFA piles. The model was solved under undrained conditions first. Once the equilibrium was achieved the fluid flow step was executed to allow pore pressure changes and to arrive at the effective stress conditions after pore pressure stabilisation;

Stage 16: Construction machinery load due to 120 tonne crane load applied and removed once the equilibrium was achieved as in stage 14;

Stage 17: Water level was reduced to 99.5m MLD (average minimum river level) and solved for equilibrium with fluid flow allowed using uncoupled fluid flow analysis;

Stage 18: Water level was increased to 104m MLD (average maximum river level) and solved for equilibrium with fluid flow allowed using uncoupled fluid flow analysis;

Stage 19: The inboard side was excavated down to 92m MLD to construct the base slab;

Stage 20: Base slab was constructed and solved undrained;

Stage 21: The cell pump failure was simulated by increasing the cell water level to 99m MLD and solved for pore water pressure equalisation;

Stage 22: The cell water level was brought down to design level i.e. 94m MLD. Water was allowed to flow to achieve long term conditions where base slab is constructed and river level was kept as 104m MLD. The internal and cell water levels were at 92 and 94m MLD respectively.

5.4.2 Results from 13m wide section analysis

The results from the 13m wide cell analysis are presented; these will be compared with the results from three dimensional analysis (section 6) and field monitoring data (section 7) in section 8 of this document.

5.4.2.1 Bending moment

The bending moment profiles for the outboard and inboard walls are shown in Figure 5-11 and Figure 5-12 respectively. The bending moment with the tension on the wall facing towards the water (outboard) side was considered positive and negative for tension on the face towards the dry (inboard) side of the cell. The bending moments in the upper section of the wall at the end of cell excavation is 94 kN.m for both the walls with opposite sign suggesting that the face of the wall towards inside of the cell is experiencing tension due to removal of soil from within the cell. The lower section of the wall (below 92m MLD) show a change in bending moment sign due to the support provided by the stiff Kimmeridge Clay plug with the cell, which is stopping the inward

movement of the cell walls towards the excavation by providing a support at the lower section of the wall.

When the cofferdam is backfilled to the top while cell pumps are not commissioned and no dewatering is modelled, a change in bending moment profile for the upper section of for both the walls occurs due to restrain provided by the lower steel tie. Due to an increase in tension on the inner side of the cell, a bending moment of 137 kN.m/m for the outer wall and 125 kN.m/m for the inboard wall at the level of lower ties (at 98.5m MLD) was calculated. The section of the wall below the lower tie but above the stiff Kimmeridge Clay (92m MLD) showed an increase in bending moment on the outward face (outside of cell) as a result of increased cell pressure. The increase in cell pressure and bulging of the cell wall due to the poor support provided by the Fen Deposits a slight increase in bending moment to 140 kN.m/m for the outboard and 134 kN.m/m for the inboard wall respectively. The bending moment profile in the lower wall section remained almost unchanged with only a slight increase in bending moment.

After dewatering the cofferdam enclosure and placement of the berm on the inboard side, the highest positive bending moment (220 kN.m/m) was computed at the location of the berm on the inboard side (at 93m MLD). A negative bending moment (tension on the side facing the outboard side) was calculated at the lower steel tie level and where a passive support provided by the Kimmeridge Clay support in front of the wall was also present. For the outboard wall, a maximum positive bending moment of 195 kN.m/m (tension on face towards inboard) was calculated at the level of the lower tie (98.5m MLD) and a maximum negative bending moment of -145 kN.m/m computed just below the level of Kimmeridge Clay level within the cell (92m MLD).

For the long term conditions with no berm in place, the inboard side was excavated to 92m MLD and the pumping station constructed, it was found that the bending moment increased considerably (Figure 5-12); however the bending moment profile remained the same. A maximum positive bending moment of 264 kN.m/m was calculated for the inboard wall at the level of excavation on the inboard side i.e. 92m MLD. The maximum negative bending moments were -125 kN.m/m and -186 kN.m/m at the level of lower ties and on the passive side. For the outboard wall the maximum bending moments are 234kN.m/m and -177kN.m/m at the lower tie level and just below the level of

Kimmeridge Clay within the cell i.e. 92m MLD (Figure 5-11). These results show that the maximum bending moments are calculated at lower tie level and at the level of stiff kimmeridge clay; however they are substantially below the design flexural capacity of 960 kN.m/m for Arcelor AZ28 sheet piles (Schlim and Reuter, 2005) used in the construction of the cell.

5.4.2.2 Wall displacement

The wall displacement plots show that both the inboard and outboard walls move consistently towards the unloaded (inboard) side during the construction of the cofferdam (Figure 5-13 and Figure 5-14). The wall displacement is nominal during the excavation and filling of the cell as the steel truss frame was used during the cell excavation phase under balanced water conditions. The maximum displacement of 109.3mm for the inboard and 104mm for the outboard walls was calculated at the top of the wall. The deflection profile shows that the cell swayed towards the excavated (dry) side.

5.4.2.3 Tie forces

The tie forces at three important stages are presented in Table 5-7. It is clear from the results that during the construction of the cofferdam the tie forces are high for lower ties. The highest tie load was recorded when the cofferdam has just been filled to the top and the dewatering pumps not operational (cell water level is at the top of the fill). When the berm is in place and the cell dewatered, a reduction in tie force is calculated as the cell pressure is reduced due to dewatering the cell and also due to the passive support provided by the berm on the inboard side.

The tie force at the end of construction reduced in the upper ties, due to removal of the berm and further excavated to 92m MLD, which has caused the lower section of the wall to move towards the excavated side. This has caused a slight backward movement of the upper section of the wall (above level of lower tie) resulting in a reduction in the upper tie force and increase in the lower tie forces at the end of construction. Overall, the results show that the tie forces remained well below their yield limit (See Table 5-4).

Table 5-7: Tie forces calculated from plane strain analysis on 13m wide cell

Construction stage	Upper tie (kN)	Lower tie (kN)
At the end of cell filling	0.52	229.83
After placement of the berm	50.47	175.92
End of construction	27.14	205.25

5.5 Summary

A detailed plane strain FLAC^{2D} analyses were conducted to asses the overall stability of a diaphragm type cellular cofferdam and the magnitude of the structural forces. A 10.5m wide section (Cell S3) was analysed for its short and long term stability after pore water pressure equalisation under effective stress conditions. A factor of safety assessment method was introduced based on strength reduction to identify the lowest factor of safety for global failure of cofferdam cell. The study showed that the structure had a FoS greater than 1.25 for working conditions under the mean high water tide of 104m MLD. When the river water level is increased to the highest flood level, i.e. 107m MLD the factor of safety reduces to 1.10. The overall failure mechanism derived from these analyses indicates that the structure develops a curved failure surface at the base of the cell. The failure curve developed in the analysis is similar to the circular slip failure suggested by Hansen (1953) and Log spiral failure surface by Ovesen (1962). However there was no sign of any other type of failure mechanisms suggested in section 3.

Effective stress analyses were conducted to calculate the maximum structural forces at a cross section through the instrumented cell C3 (13m wide cell). The actual construction sequence at cell C3 was adopted to identify any similarity between the simulated and measured results (section 7).The maximum bending moments and tie forces were found to be well below the design capacity of sheet piles and steel cables used in the construction. The bending moments, tie forces and wall deflection calculated from the plane strain analysis are compared with the results from three dimensional analysis and the field monitoring study of the structure in Section 8 to further check the validity of the numerical results.

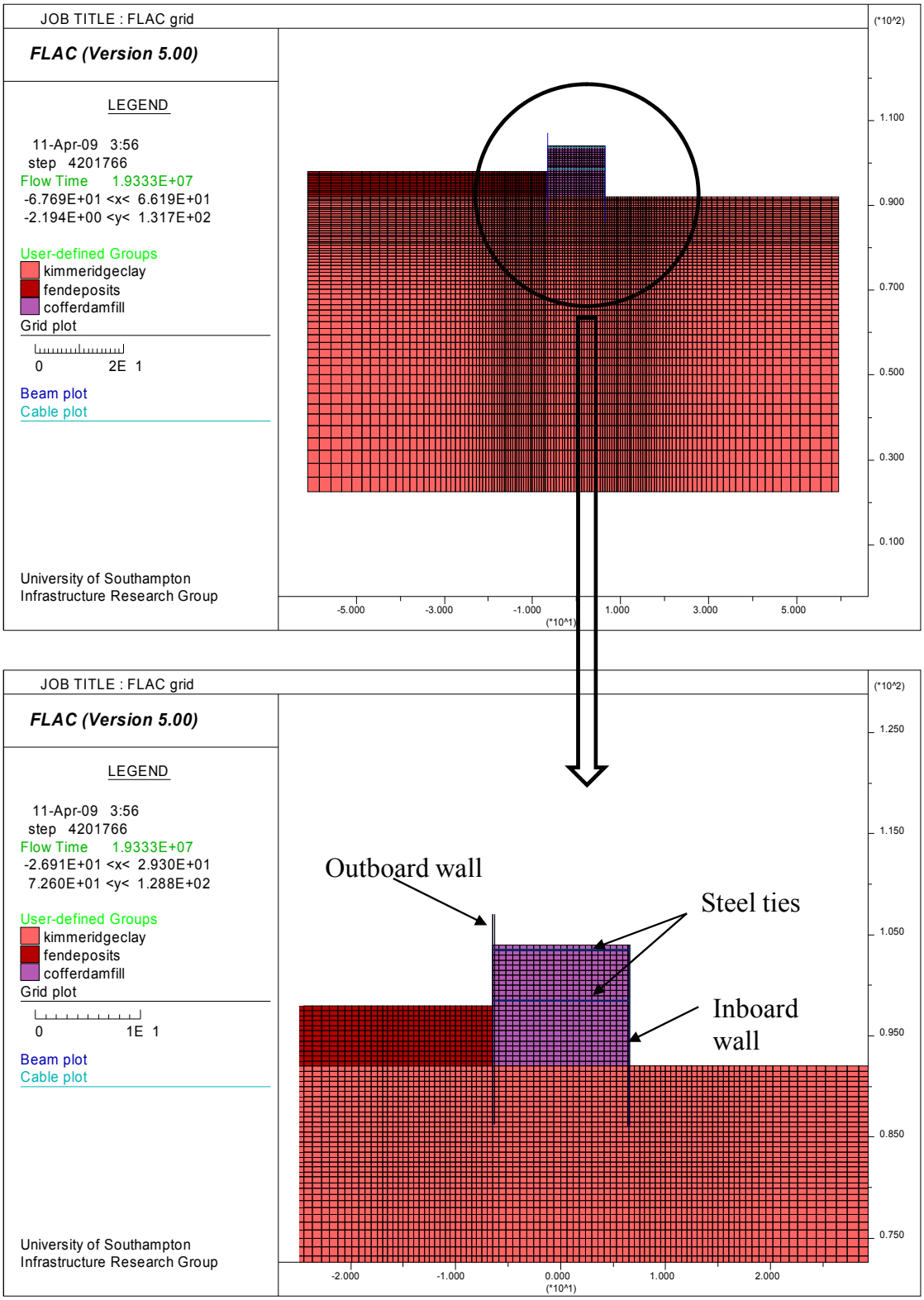

Figure 5-1: FLAC^{2D} mesh used for the plane strain analysis

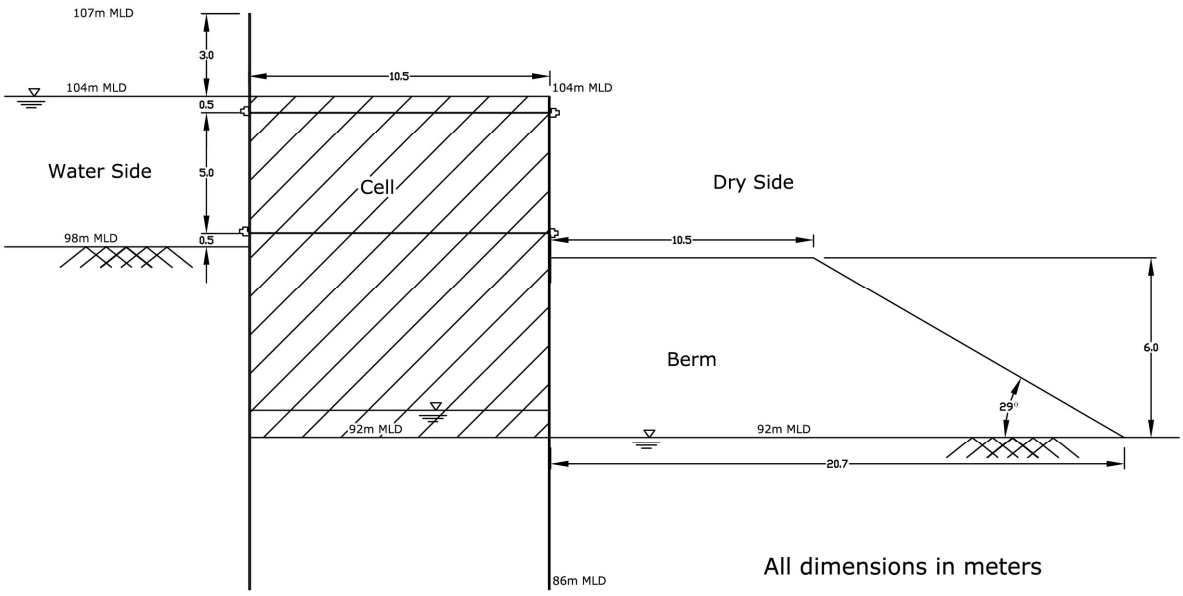

Figure 5-2: Dimensions for critical section used for determination of factor of safety

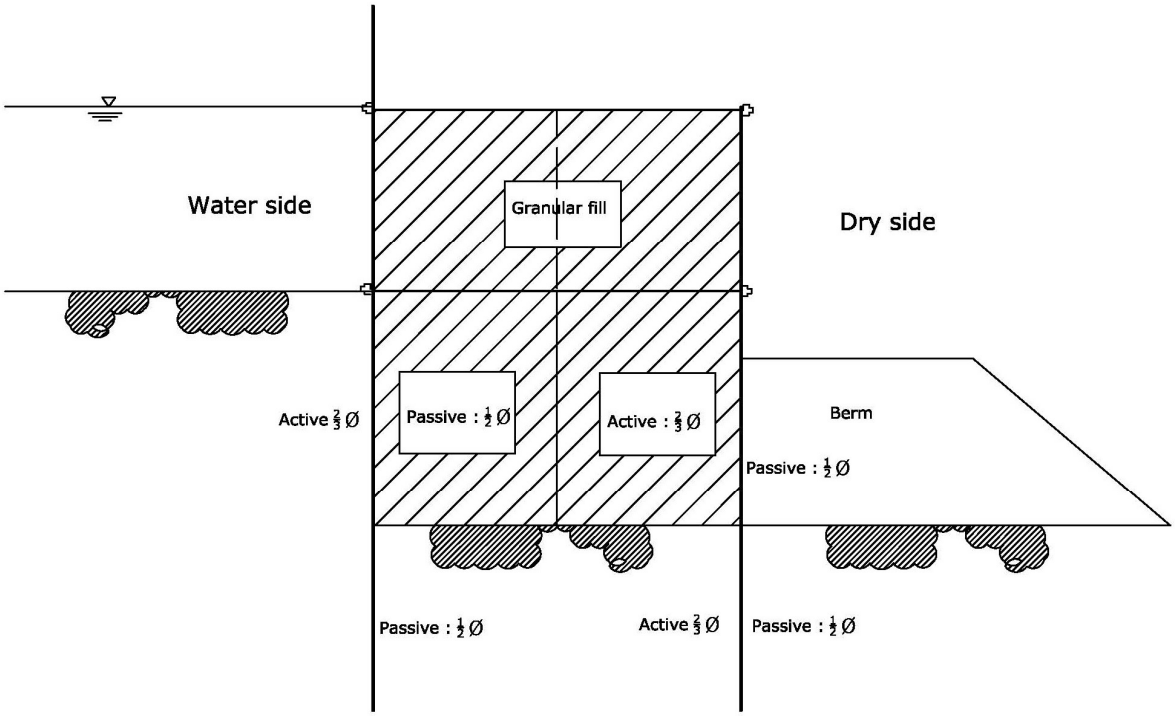

Figure 5-3: Interface friction and location of interfaces for effective stress analysis

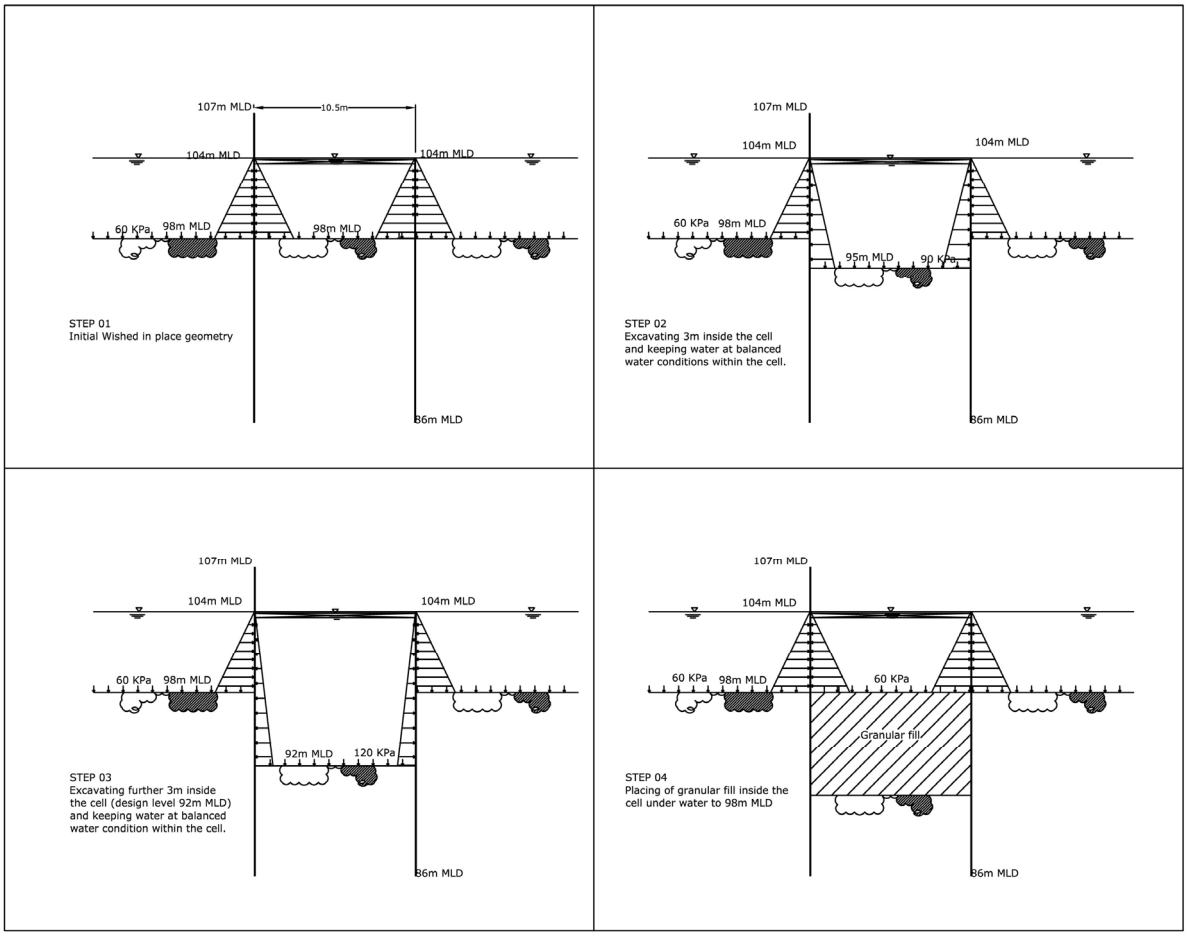

Figure 5-4: Effective stress analysis; construction steps 1 to 4

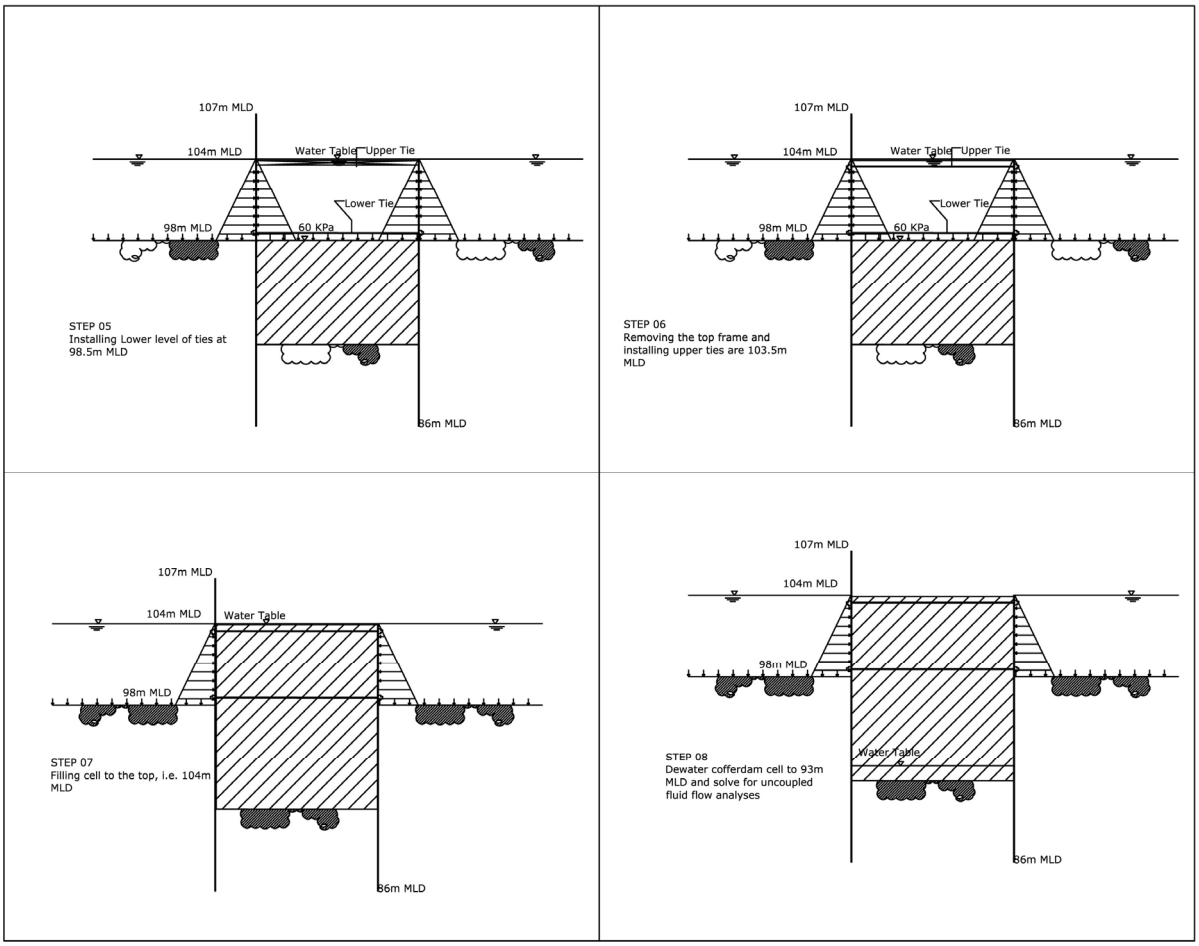

Figure 5-5: Effective stress analysis; construction steps 5 to 8

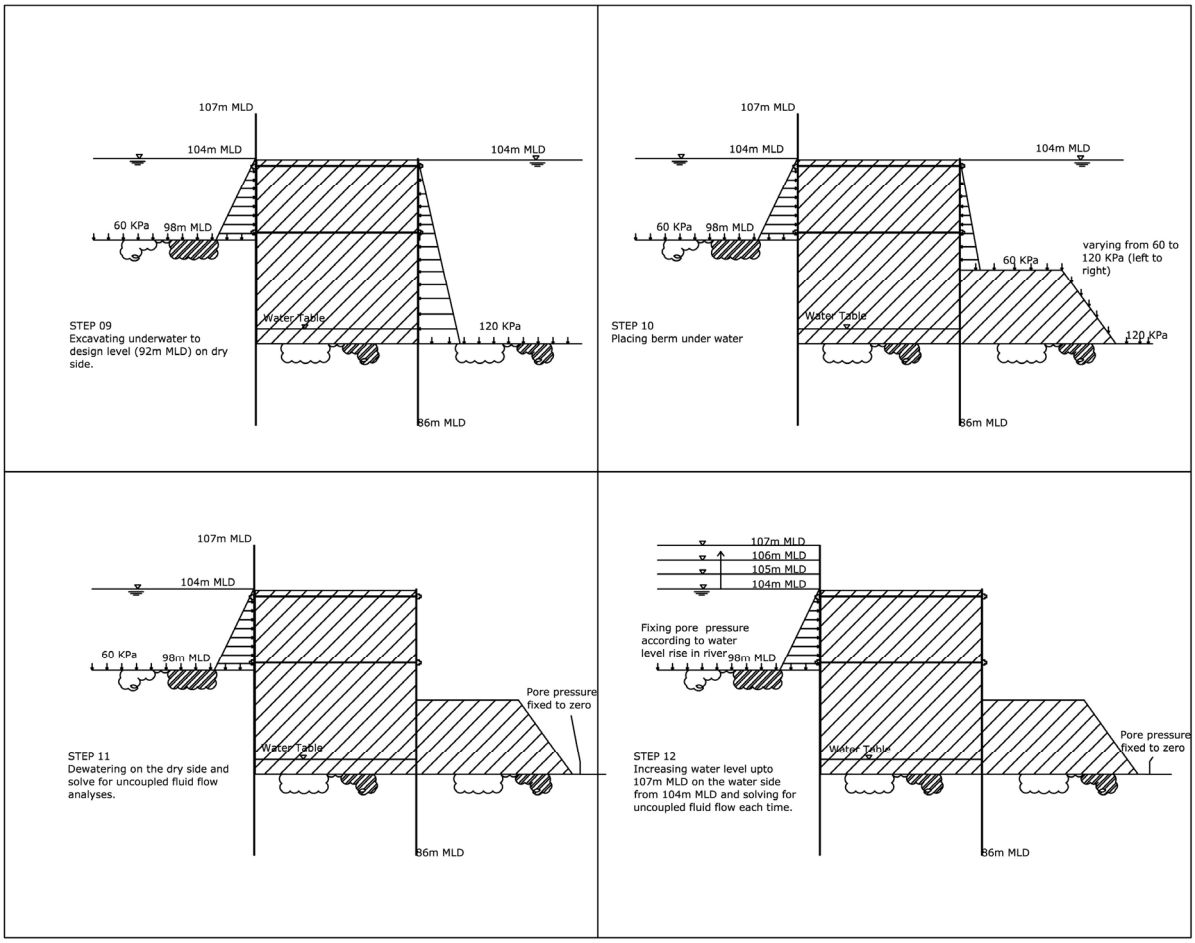

Figure 5-6: Effective stress analysis; construction steps 9 to 12

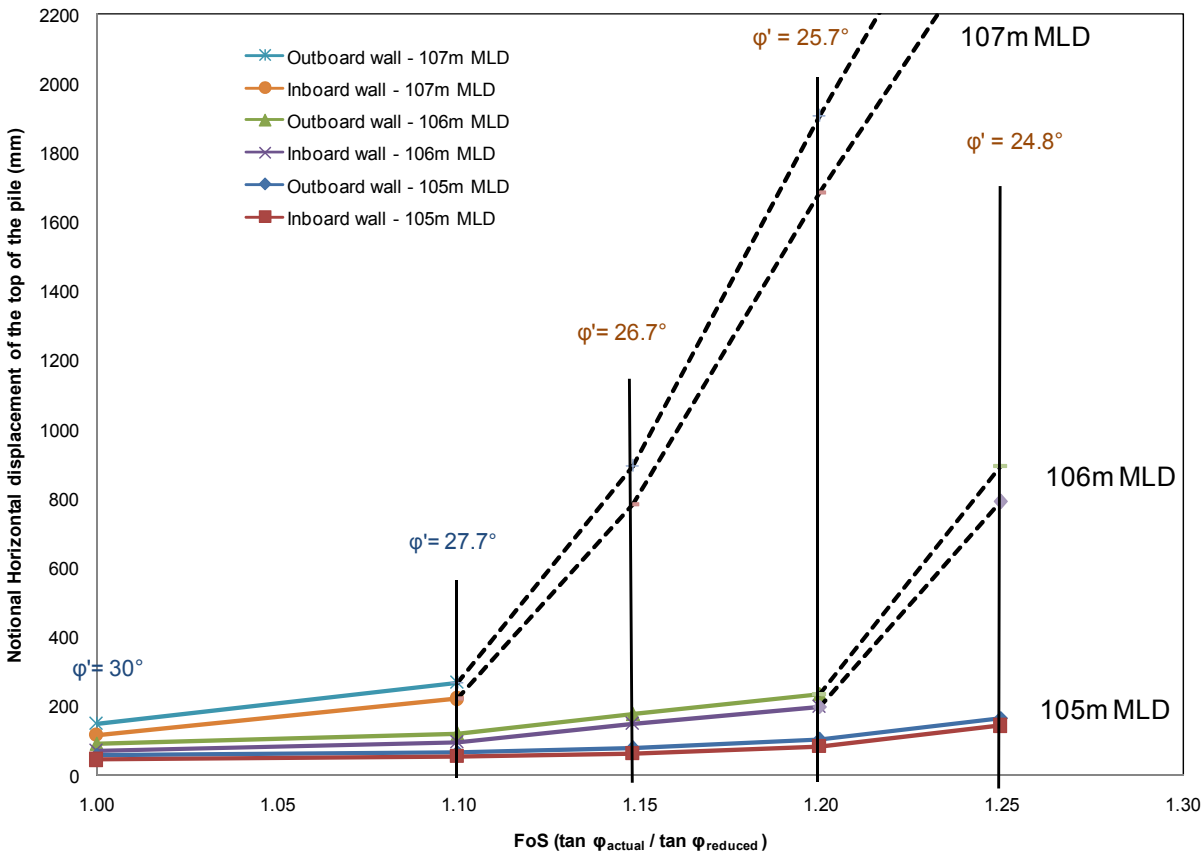

Figure 5-7: Maximum displacement monitoring plot to check the failure under effective stress condition

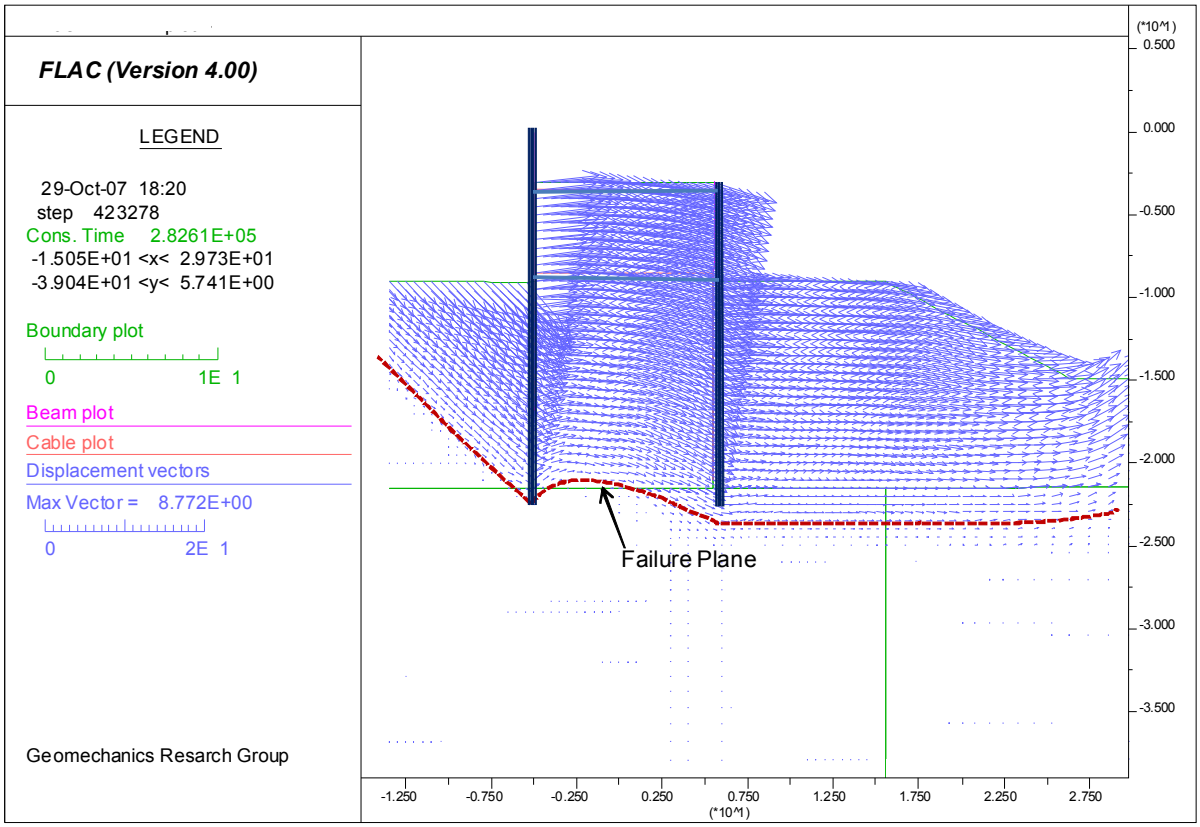

Figure 5-8: Total displacement vectors showing failure mechanism for river water level at 107m MLD and $\phi'_{reduced}$ = 24.8° (FoS = 1.25)

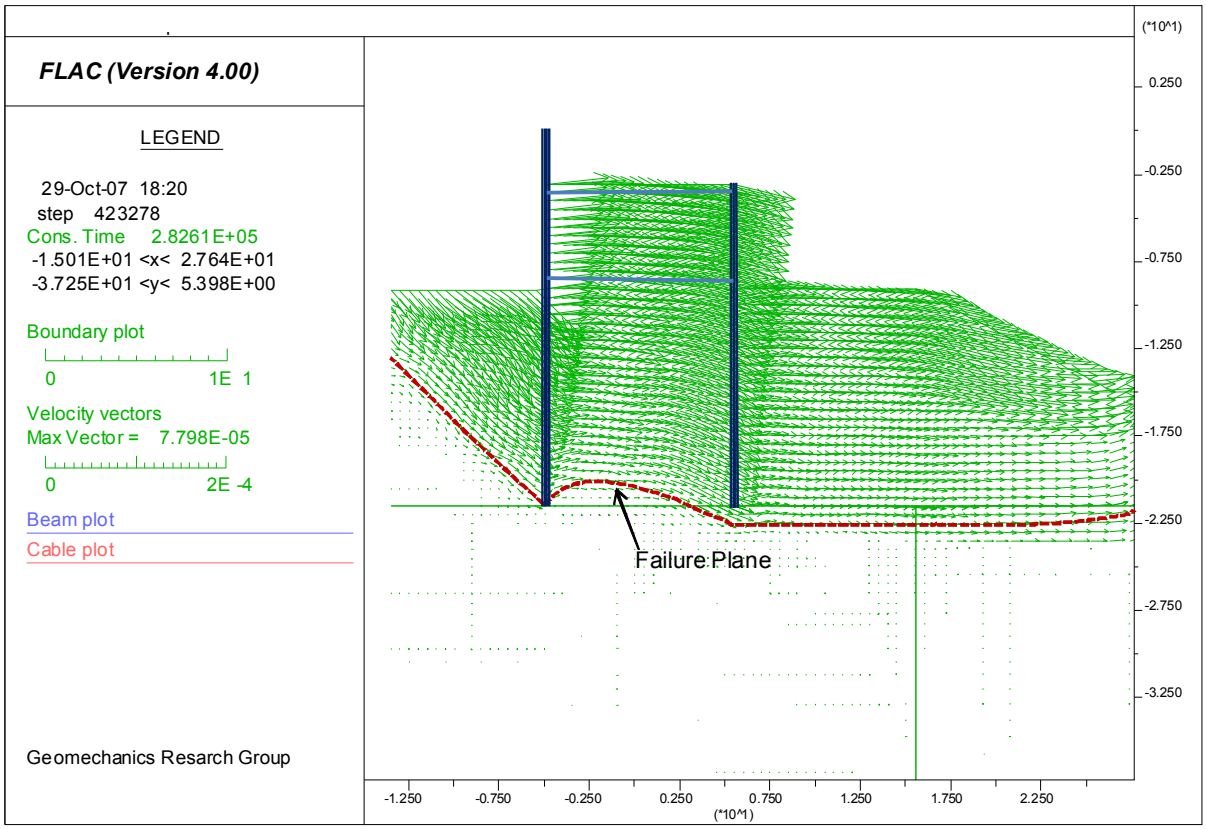

Figure 5-9: Velocity vectors showing mechanism for river water level at 107m MLD and $\phi'_{reduced}$ = 24.8º (FoS = 1.25)

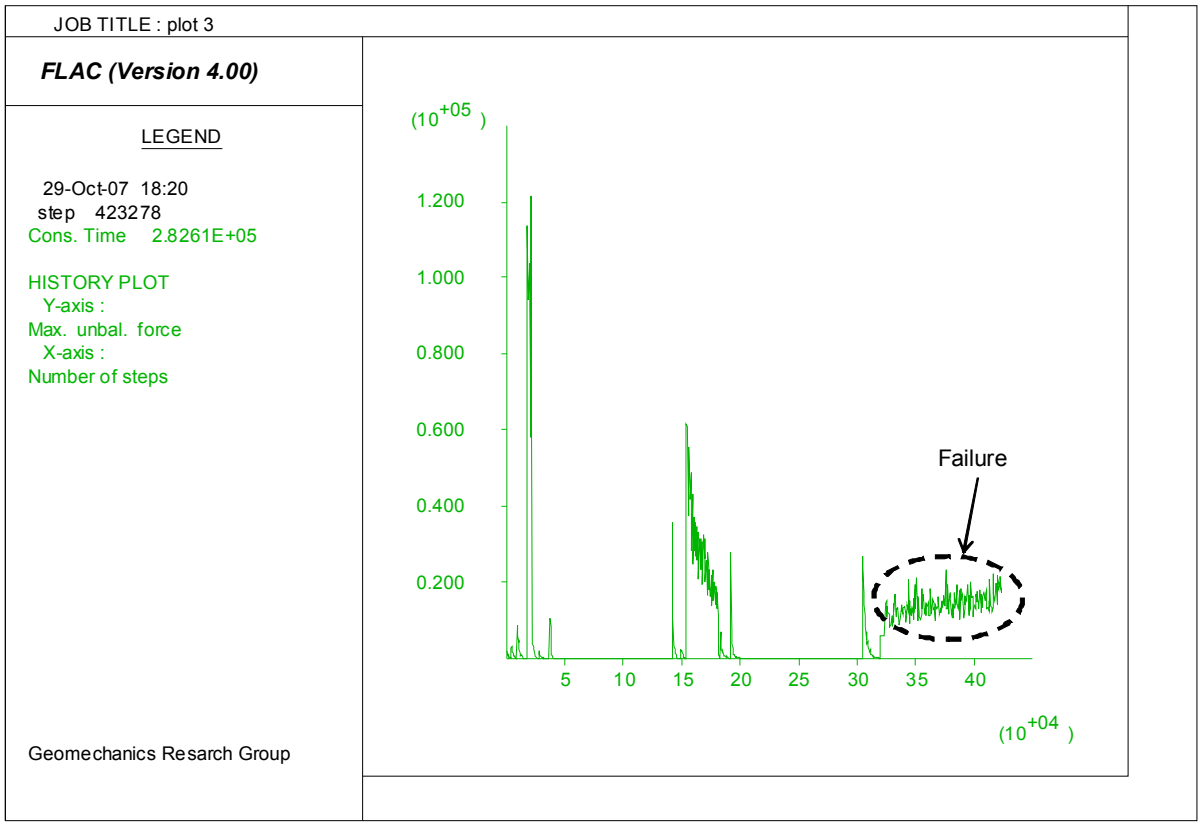

Figure 5-10: Unbalanced force plot for FoS = 1.25 analysis

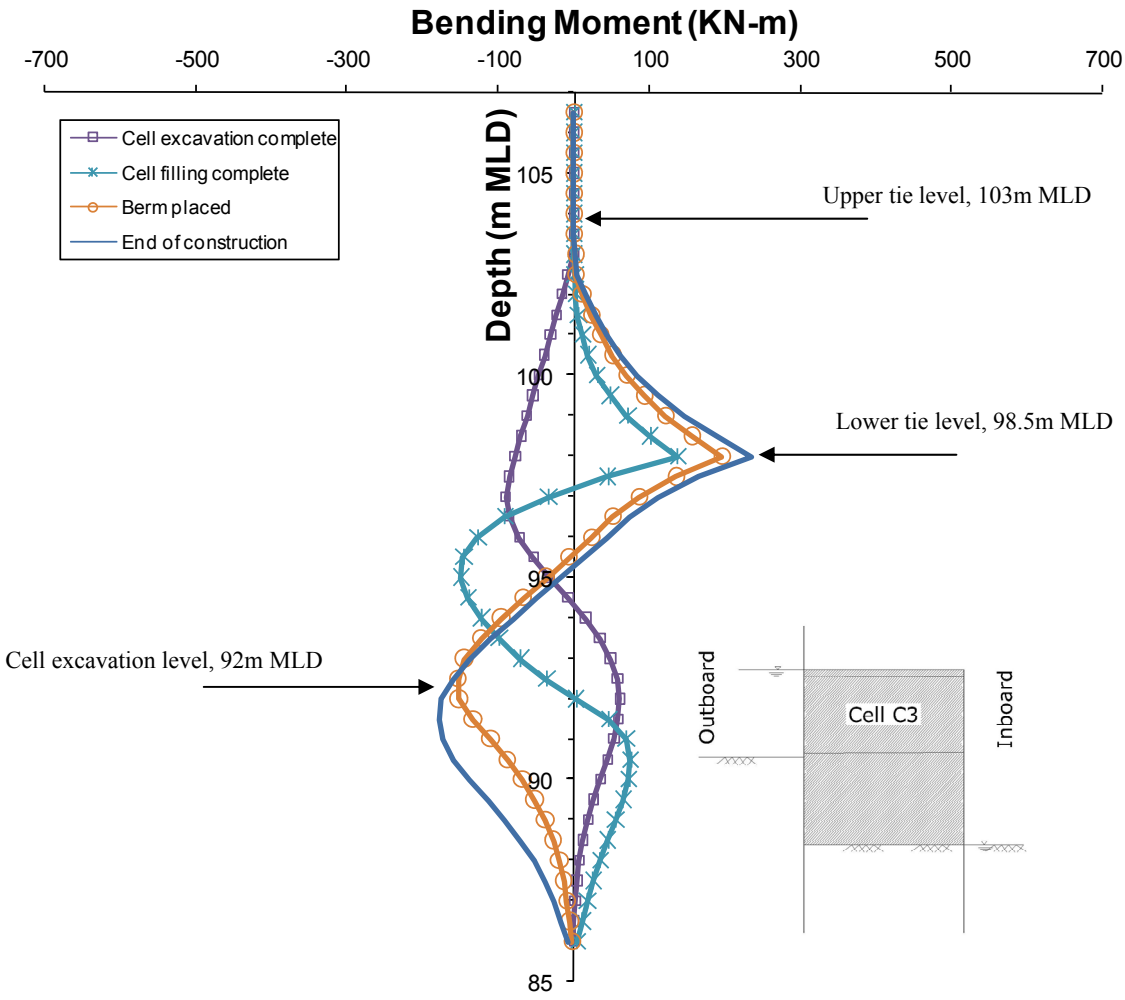

Figure 5-11: Bending moments in outboard wall from analysis of 13m wide cell

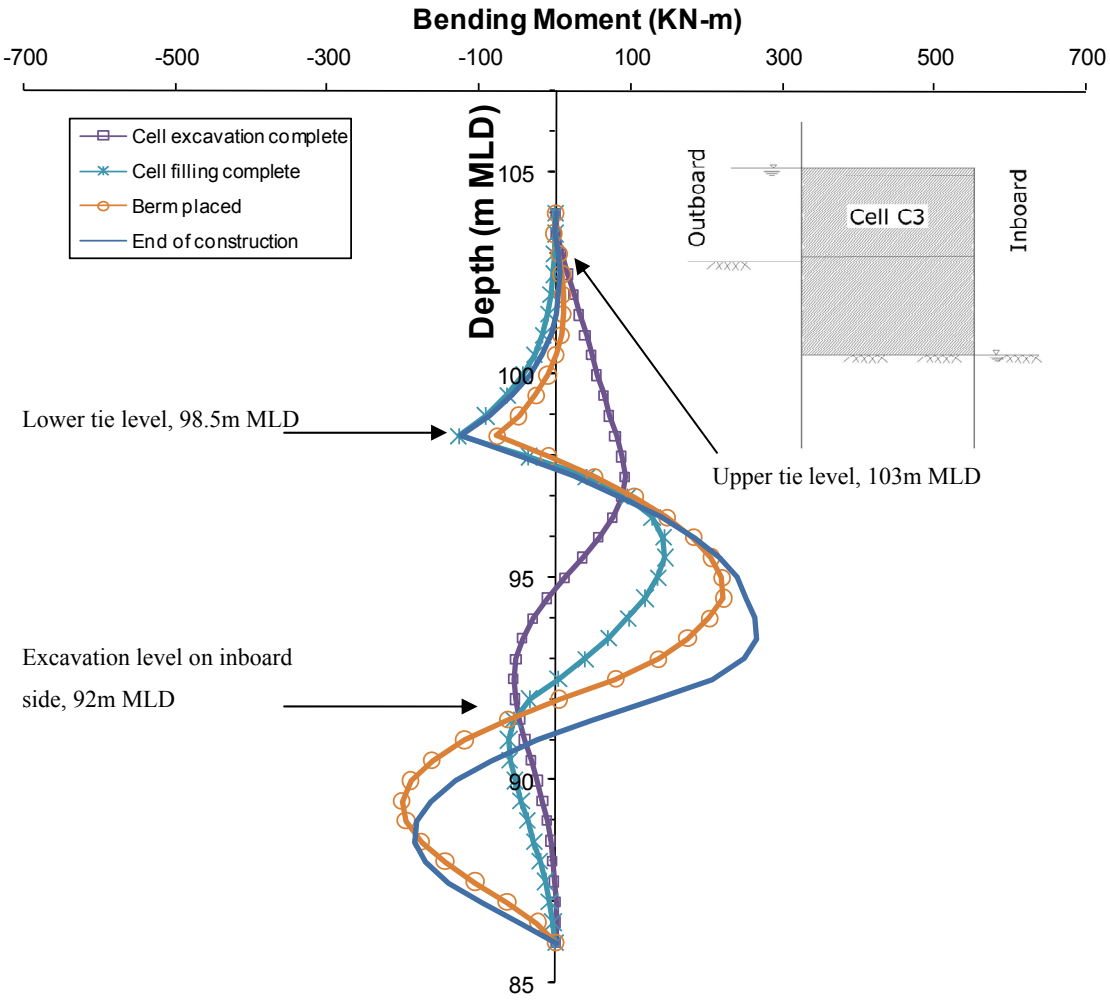

Figure 5-12: Bending moments in inboard wall from analysis of 13m wide cell

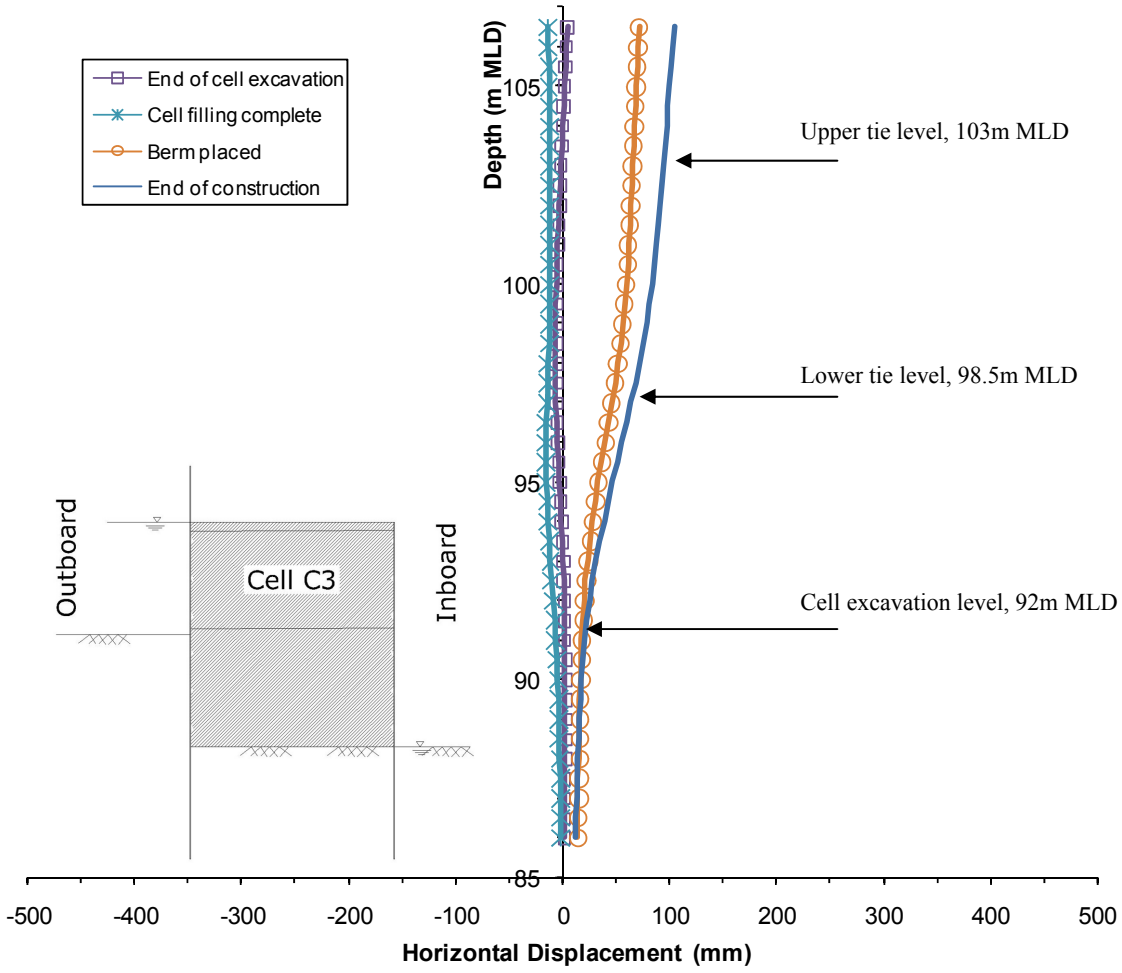

Figure 5-13: Outboard wall displacement from analysis of 13m wide cell

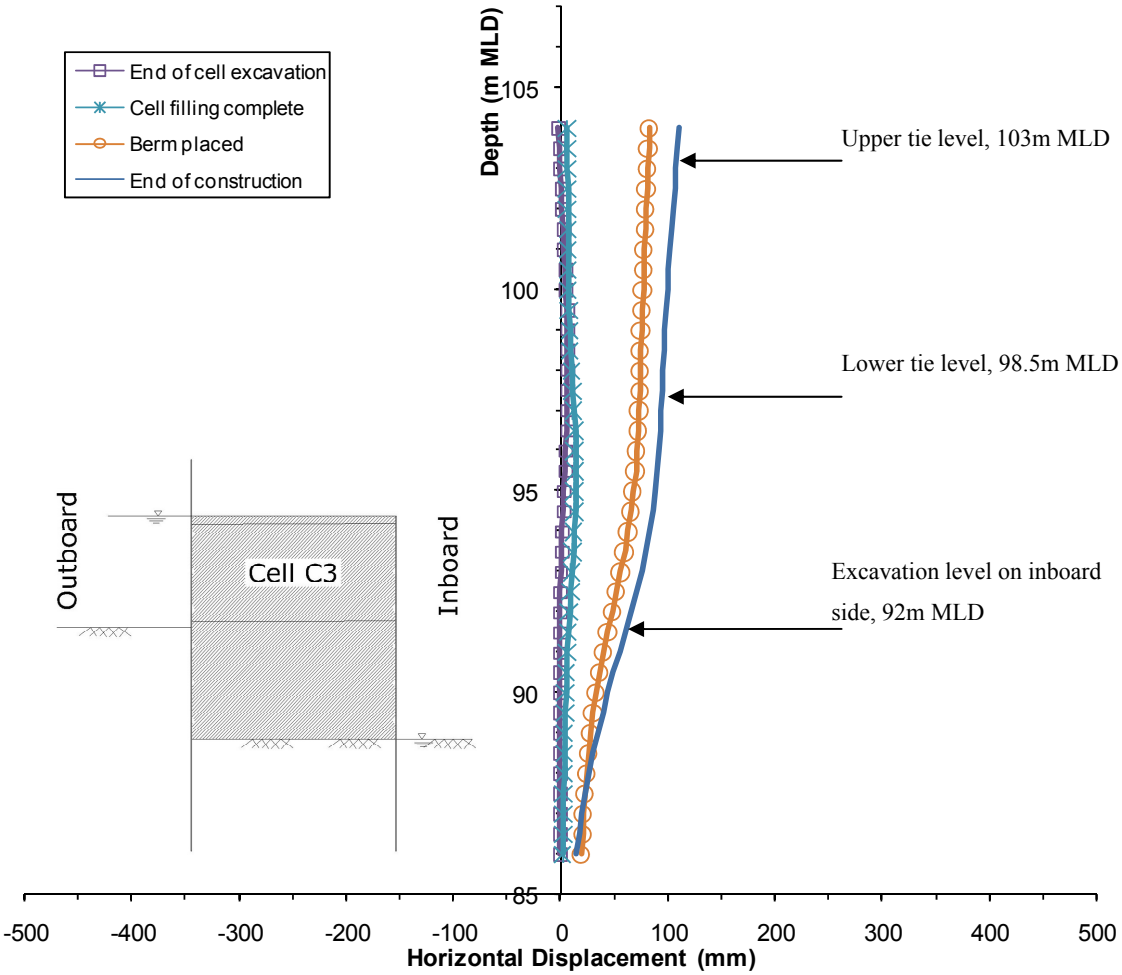

Figure 5-14: Inboard wall displacement from analysis of 13m wide cell

6 Three dimensional numerical analysis

6.1 Introduction

Since the cellular cross walls are not a part of a load bearing structure[2] and do not contribute to the moment resistance, the rectangular/square form may be idealised as plane strain problem in case of diaphragm type cofferdam. However, the presence of interlocks and the lateral distance between the ties suggests there is a case for a full three dimensional analysis to asses the membrane bending in sheet piles to include interlock effects. This will also enable us to determine the load in the lateral ties (connecting cell walls) and to asses if they are really required to be of the same strength as the ties used to connect the inboard and outboard sheet piles. This section presents details of a three dimensional analysis of the 13m wide section (Figure 6-1) to asses bending moments, ties forces and wall deflection. These results are compared with the results from the plane strain analysis and field monitoring data in Section 8.

6.2 Model for 13m wide section to analyse cell C3 behaviour

The effective stress analysis approach available in FLAC^{3D} was used (Itasca, 2009) to simulate construction and performance of a representative cross-section (cell C3) from St. Germans cofferdam (Figure 4-3). A 6m slice was taken from the middle of cell C3 with the same cross sectional dimensions as the plane strain analysis presented in section 5.4. The geometry after construction of the berm and dewatering on the inboard side is provided in Figure 6-1. The berm was then removed and the final section profile analysed to determine the long term structural forces is shown in Figure 6-2.

[2] The cross walls are used to facilitate the construction of the cells (Figure 1-1), as the cells already constructed are required to be filled to the top as they are used as a construction platform to form the neighbouring cells. The interlocks within the sheet piles on the cross walls will slide against each other due to any loading from the water side making them non-load bearing structure in this case.

6.2.1 Grid generation/modification for modelling the construction sequence

The brick type mesh generation facility available in FLAC^{3D} was utilised. A parametric study was conducted to derive the optimum mesh size and boundary locations to minimise their effects on the calculated results. A total of 6324 solid brick elements were used to create the initial mesh. A dense mesh size of 1x1m was used in the area close to the cell and the mesh size was gradually increased in a linear ratio of 1.10 to achieve a large mesh size in the soil zones remote from the area of focus to optimise the calculation time without compromising accuracy (Figure 6-3). The right side of the mesh (with an origin at the centre of the cell) was generated and the reflected using the REFLECT command to create boundaries at -70m and 70m in the horizontal direction. The bottom of the mesh boundary was located at -60m, while the width was kept as 6m in the out of plane direction as the width of the slice analysed. Three zones outboard, inboard and cell were created using the GENERATE ZONE command. The cell zone was then separated to allow the insertion of liner elements to model the sheet piles. Double sided LINER elements were used to facilitate the attachment of sheet pile with soil/pile interface elements on both sides of the sheet piles. Once the piles were installed, the bottom of the cell was connected to the mesh using the MERGE command and the inboard and outboards sides were connected to the liner elements using interface elements with interface friction and stiffness values similar to those used in plane strain analysis (Figure 5-3). The sheet piles and steel ties were considered wished in place and the cell was considered filled to the top due to limitations in FLAC^{3D} to reconnect a mesh back as cell excavation and filling back is not possible in FLAC^{3D}. The initial structural configuration and detailed structural elements etc is shown in Figure 6-4.

6.2.2 Boundary conditions and soil/structure properties

The right and left boundaries were fixed for displacement in the lateral direction and the bottom boundary was fixed in both the lateral and vertical directions. A Mohr-Coulomb failure model was used and the soil properties assigned on the basis of the effective stress analysis approach used in the plane strain analysis in Section 5 (see Table 5-2). A high initial value of cohesion i.e. 1×10^7 kN/m^2 was used to accelerate the model to initial equilibrium. An anisotropic fluid flow option in FLAC^{3D} was used for fluid flow analysis. The permeability was kept the same as in case of the plane strain analysis (section 5.3.1)

with horizontal permeability 10 times the vertical permeability of the soil. The properties for the steel ties were adjusted according to the centre/centre spacing and surface friction ($1/3^{rd}$ of the fill material ϕ') introduced to model the friction between the ties and fill material to model the pull induced by the cell fill material.

The pile stiffness was reduced in the lateral direction to model the stiffness reduction due to presence of interlocks sliding using the orthotropic stiffness option available in FLAC^{3D}. A parametric study was conducted for this purpose by taking the *E-ratio* values suggested by US Army corps of Engineers (1989) i.e. 1.0, 0.1, 0.03, where *E-ratio* is the ratio of horizontal to vertical stiffness of the wall;

$$E-ratio=\frac{E_{SH}}{E_{SV}} \qquad \textbf{Equation 6.1}$$

Where;

E_{SH} =pile stiffness in lateral (in plane) direction

E_{SV} =pile stiffness in vertical direction

Different interface friction values were used on the active and passive sides as detailed for the plane strain analysis (Figure 5-3). Initially the cell was filled up to the top with granular fill under balanced water conditions at 104m MLD with in the cell and on either side of the cofferdam. The initial insitu effective stress ratio was assigned as 1.0 for the Kimmeridge Clay and 0.5 for the overlaying Fen Deposits.

6.2.3 Modelling construction stages

The construction sequence modelled as closely as possible the actual construction of the instrumented cell C3 (Figure 4-3). The fluid flow stages were modelled using the uncoupled fluid flow option available in FLAC^{3D} (Itasca, 2009). In uncoupled fluid flow analysis the mechanical calculations are switched off during the fluid flow analysis and once the pore water pressure equalisation is achieved the fluid flow is switched off and unbalanced mechanical force calculations are made in mechanical calculation step.

Stage 1: Initialisation of initial conditions and solving for initial equilibrium, with cell fill and all the structural elements presented i.e. wished in place.

Stage 2: Cofferdam cell dewatered to 95m MLD. The water was allowed to flow to achieve the new pore pressure equilibrium under the reduced cell water level.

Stage 3: The inboard side was excavated down to 94m MLD under balanced water conditions. The water level was kept 104m MLD on the inboard and outboard walls while a lower level of 95m MLD was maintained within the cell.

Stage 4: The water level on the inboard side was reduced to 97m MLD and solved to equilibrium whilst allowing the fluid flow to attain a new pore pressure regime under the reduced water level within the cell and cofferdam enclosure.

Stage 5: The berm was constructed up to 97m MLD by using the equivalent pressure applied on the inboard side to model the berm pressure acting on the excavated side and inboard sheet pile.

Stage 6: The cell and inboard side were dewatered to 94m MLD (excavation level) and the model solved undrained to achieve conditions just after dewatering on dry side.

Stage 7: Fluid flow was allowed for pore pressure equalisation to model the pore pressure changes due to dewatering on the inboard side.

Stage 8: A 120 tonne crane construction load was applied to the top of cell C3 and was solved undrained to model the load due to construction machinery. The crane load was removed once the model reached equilibrium as the crane usually stayed on the top of C3 for limited period of time.

Stage 9: The berm was removed to facilitate the construction of the CFA piles. The model was solved under undrained conditions first and once equilibrium was achieved the fluid flow step was executed to allow pore pressure change to arrive at effective stress conditions after pore pressure stabilisation.

Stage 10: Construction machinery load was re-applied and removed once the equilibrium was achieved (See stage 8).

Stage 11: Water level was reduced to 99.5m MLD within the river (average minimum river level) and solved for equilibrium with fluid flow allowed (uncoupled fluid flow analysis approach used).

Stage 12: Water level was increased to 104m MLD within the river (average maximum river level) and solved for equilibrium with fluid flow allowed using uncoupled fluid flow analysis.

Stage 13: The inboard side was excavated down to 92m MLD to construct the base slab (Figure 6-2).

Stage 14: Base slab was constructed and solved undrained.

Stage 15: A cell pump failure was simulated by increasing the cell water level to 99m MLD and solved for pore water pressure equalisation

Stage 16: The cell water level was brought down to design level i.e. 94m MLD. Water was allowed to flow to achieve long term conditions where the base slab is constructed and the river level was kept as 104m MLD. The internal and cell water levels were at 92 and 94m MLD respectively.

6.3 Results

6.3.1 Bending moment in sheet piles

Bending moments in the inboard wall from three dimensional analyses at the end of cofferdam construction is plotted in Figure 6-5. Where it can be clearly observed that the reduction in lateral stiffness of the wall results in an increase in bending moment. The maximum negative bending moment (tension on river side face of the wall) coincide with the lower tie level (98.5m MLD). The maximum positive bending moment (tension on inboard side of the wall) is located between 92m MLD (top of excavation level on inboard side), and 98.5m MLD (lower tie level) at 94m MLD which is due to the pressure exerted by the cell fill on the inside of the wall. Passive support was provided by stiff Kimmeridge Clay on inboard side of the wall which resulting in negative bending over the lower end of the wall and below 92m MLD.

The bending moments in the outboard wall at the end of cofferdam construction plane derived from the three dimensional analyses are presented in Figure 6-6. Again the maximum bending moment is calculated at the location of the lower tie i.e. 98.5m MLD. This is due to the lower ties being critical in that it is designed to react to the cell fill

overburden or any increase in cell pressure due to construction trafficking etc. A maximum positive bending moment similar to that calculated in inboard wall was identified at 94m MLD (mid depth of Fen Deposits layer on outboard side). This suggests that the layer of Fen Deposits provides very limited support to the cell material and the similarity with the inboard bending moments suggests that the pressure from within the cell exceeds the pressure exerted by the water column and Fen Deposits from the loaded side of cofferdam. However, both the cell pressure and destabilising load from the river side seems to balance each other below 89m MLD resulting in a very nominal bending moment below this depth.

The results suggest that the maximum bending moment in both inboard and outboard walls is approximately similar (352 and 331 kN.m for inboard and outboard wall respectively). A very nominal bending moment was observed in the wall section between the upper and lower ties (i.e. between 103.5 and 98.5m MLD). The reduction in lateral stiffness results in an increase in bending moment due to a reduction in the overall stiffness of the structure due to moment release at the clutches in the lateral direction. However, the bending moment profile for each wall remains the same in all cases.

6.3.2 Cell displacement

Figure 6-7 shows the calculated displacement of the inboard wall which indicates a sway mechanism for the E-ratio of 1.0 and 0.1 case, while an increased displacement at the unsupported section between the lower tie (98.5m MLD) and excavation level on inboard side (92m MLD) was computed. The effect of lower tie restraint is not significant for E-ratio=1.0 case when the wall is treated as an isotropic material. While for the E-ratio=0.03 case a significant reduction in displacement was calculated at the tie level due to the restraint provided by the lower tie. A maximum deflection of 605.6mm at the end of construction was calculated at the top of the wall for the E-ratio=0.03 case.

The displacement profile for the outboard wall is presented in Figure 6-8. The wall has moved considerably in the upper section i.e. above the stiff Kimmeridge Clay plug within the cell (top of Kimmeridge Clay at 94m MLD) due to the load exerted by the Fen Deposits and rising river level within the river. A similar deflection profile was observed for all cases with changing lateral stiffness and unlike the inboard wall the lower tie was observed to have a very little effect on the deflected wall profile. A maximum deflection

of 678mm was observed at the top of outboard wall (107m MLD) projects a further by 3m above the top of the inboard wall (104m MLD). However the deflection at the same depth as inboard wall (104m MLD) is 604.7mm which is similar to wall displacement for inboard wall i.e. 605.6mm.

It is clear that wall displacements gradually increase with a reduction in lateral stiffness for both the inboard and outboard walls. The reduction in lateral stiffness of the wall has reduced the overall stiffness of the structure which is basically derived from the combined action of cell fill, ties and the sheet piles. This results in an increased structural deflection for the case when the lateral stiffness is taken as 0.03 times the vertical stiffness of the wall.

The displacement contours plot (Figure 6-9) and displacement vectors plot (Figure 6-10), suggests that the overall cell mass is moving on a curved surface within the cell. The top of the cell on the inboard side is identified to experience greater displacement and the vector plot show that there is no sign of pullout of sheet piles on outboard side. The Fen Deposits can be seen slumping on outboard side in a shape of a wedge while the soil wedge on inboard is pushed upward as a result of cell movement towards the unloaded side.

6.3.3 Tie forces

The calculated tensile forces in the steel ties at the end of analyses are presented in Table 6-1. As anticipated, the load in the lower ties is greater in comparison to the upper ties. Also calculated, that reducing the lateral stiffness of the wall results in an increase in tie forces. This is because the lateral load carrying capacity of the wall is reduced as a result of a reduction in the membrane stiffness of the wall. The tie forces presented here are for the ties used to connect outboard and inboard walls. The load in the transverse ties used to connect the cross walls due to the downward pull by the fill material was nominal (almost zero) and are therefore not significant.

Table 6-1: Tie forces at the end of analyses

E-ratio	Lower tie (kN)	Upper tie (kN)
0.03	985.30	66.23
0.1	798.30	52.27
1.0	792.60	0.00

6.4 Summary

Three dimensional representation of the 13m wide cofferdam including tie geometry was used to calculate the structural forces and displacements using FLAC^{3D}. The lateral stiffness was reduced; treating the walls as an orthotropic material to model the interlocks between the sheet pile sections. The outcomes of the analysis are summarised below;

- The highest bending moment for both inboard and outboard walls was calculated at the level of lower tie (98.5m MLD);
- The Kimmeridge Clay in front of the excavation on the inboard side will result in increased bending moment in the supported section of the inboard wall;
- The cell pressure at the level of Fen Deposits (between 92 and 98m MLD) is more than the net pressure exerted by the Fen Deposits and water column at this point, therefore a higher bending moment is recorded in the middle section of outboard wall;
- An increase in structural forces (bending moment and tie forces) was calculated with reduction in lateral stiffness of the sheet piled wall;
- The maximum bending moment and tie forces are significantly below the design capacity of the sheet piles and ties used to construct the actual cofferdam;
- Increase in cell deflection was calculated with reduction in lateral stiffness of the wall;
- The tension in the lower ties is considerably greater in comparison to the upper ties. Therefore a special attention should be provided to the design of the lower ties. It should be also noted that a very high bending moment was observed at the level of lower ties.

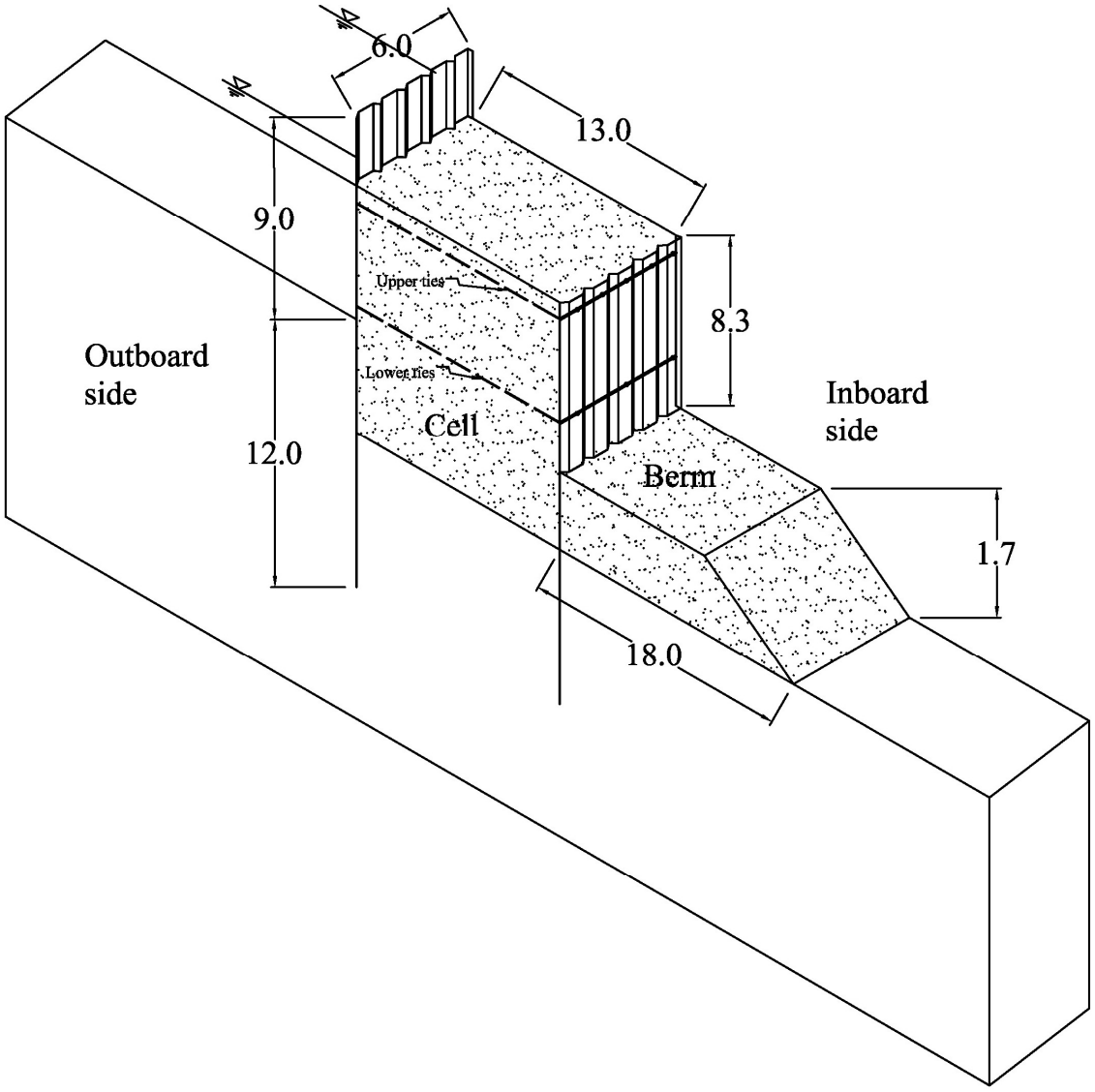

Figure 6-1: cofferdam section used for three dimensional analysis of 13m wide cell where the internal berm is in place.

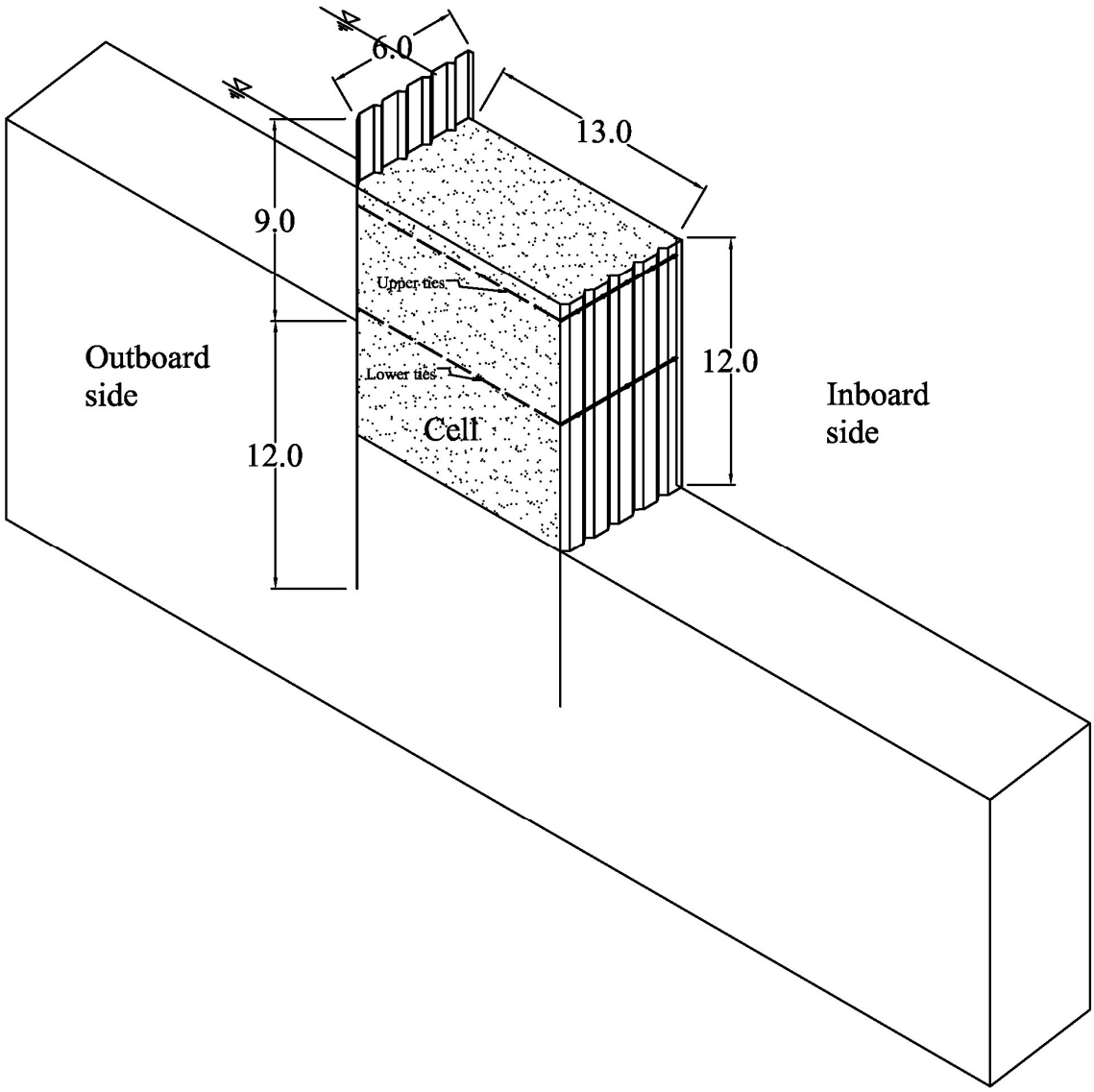

Figure 6-2: Section showing the berm removed and inboard side excavated to 92m MLD to facilitate the construction of base slab

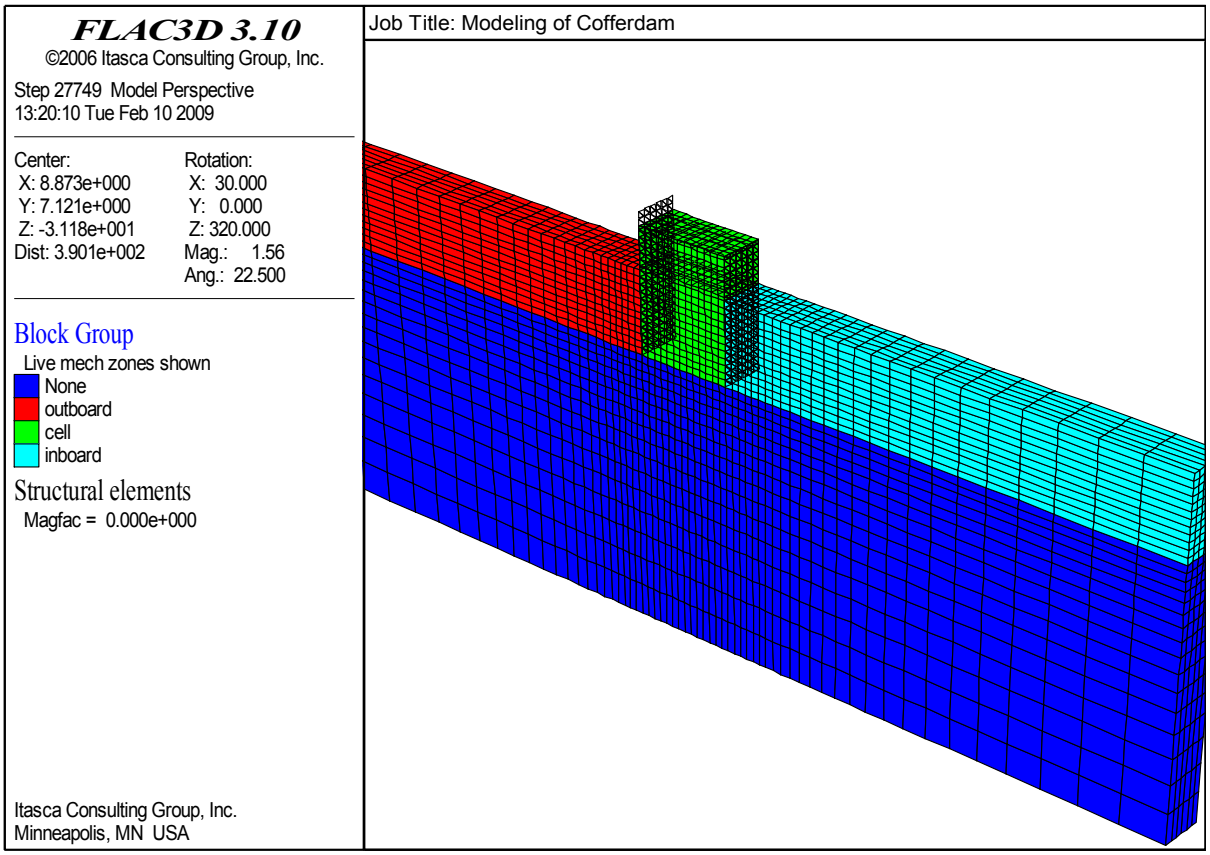

Figure 6-3: FLAC grid showing mesh density and groups

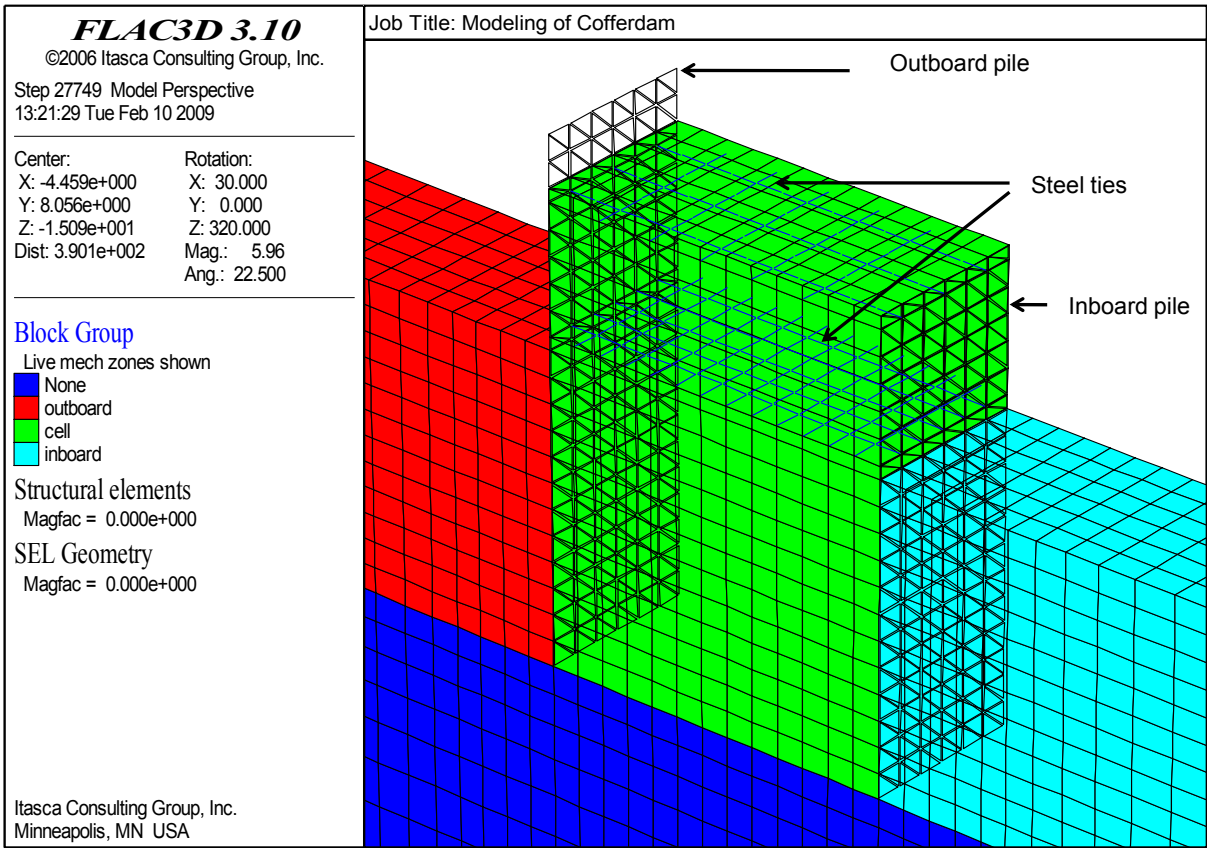

Figure 6-4: FLAC ^{3D} grid showing detail of structural elements used for the analysis

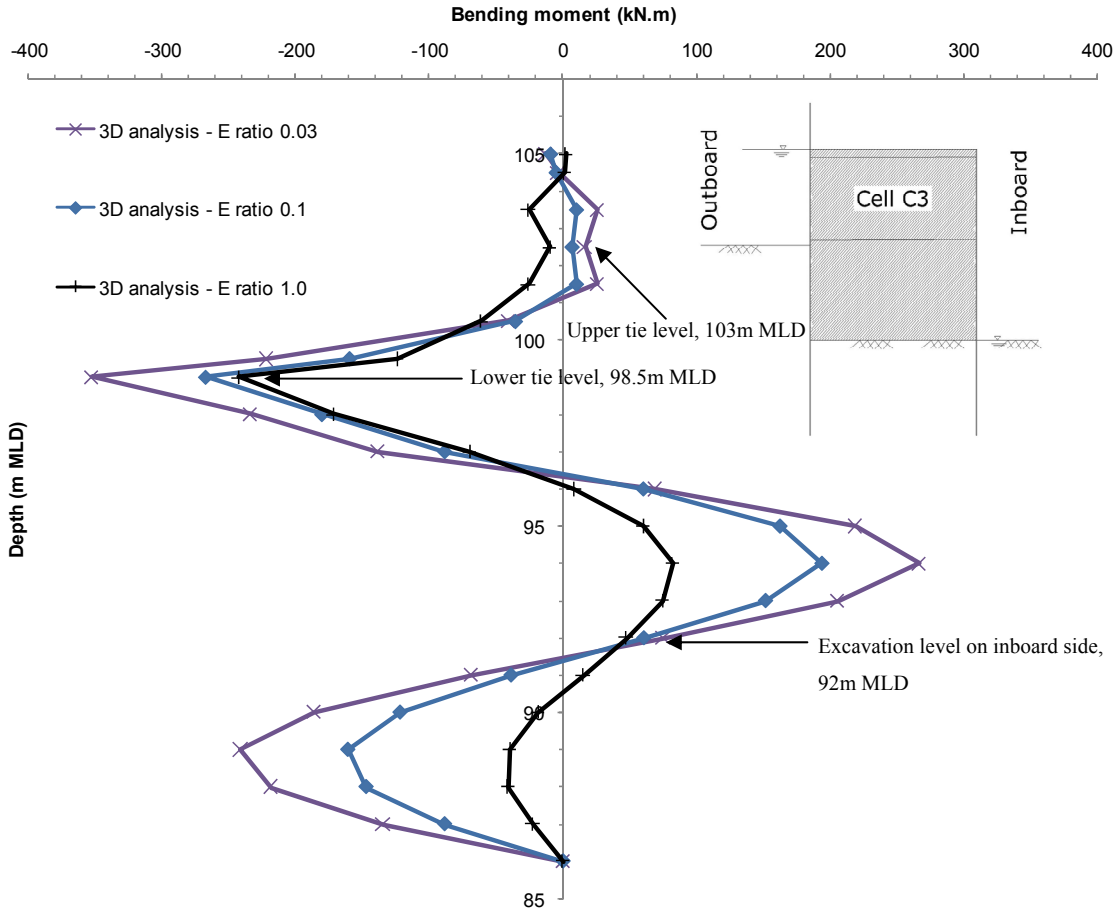

Figure 6-5: Bending moment in inboard wall at the end of cofferdam construction

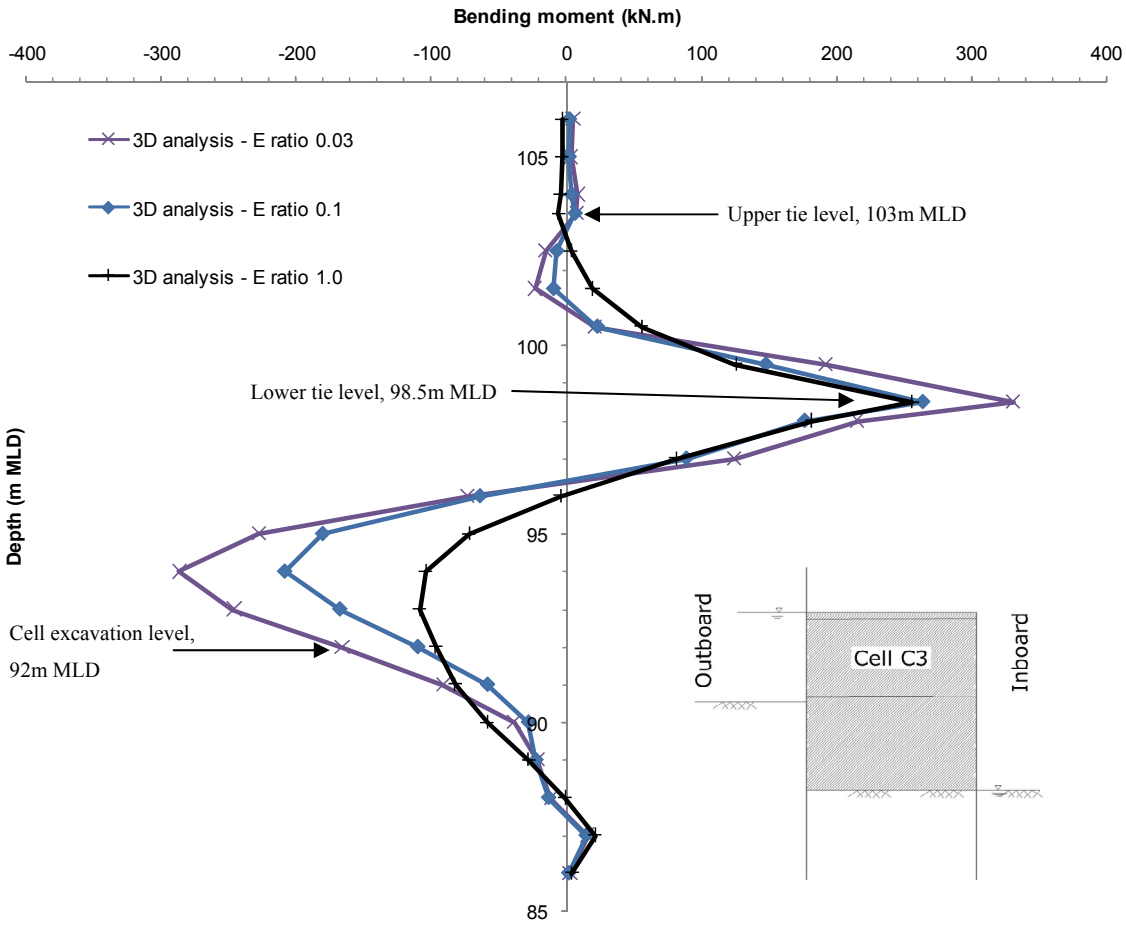

Figure 6-6: Bending moment in outboard wall at the end of cofferdam construction

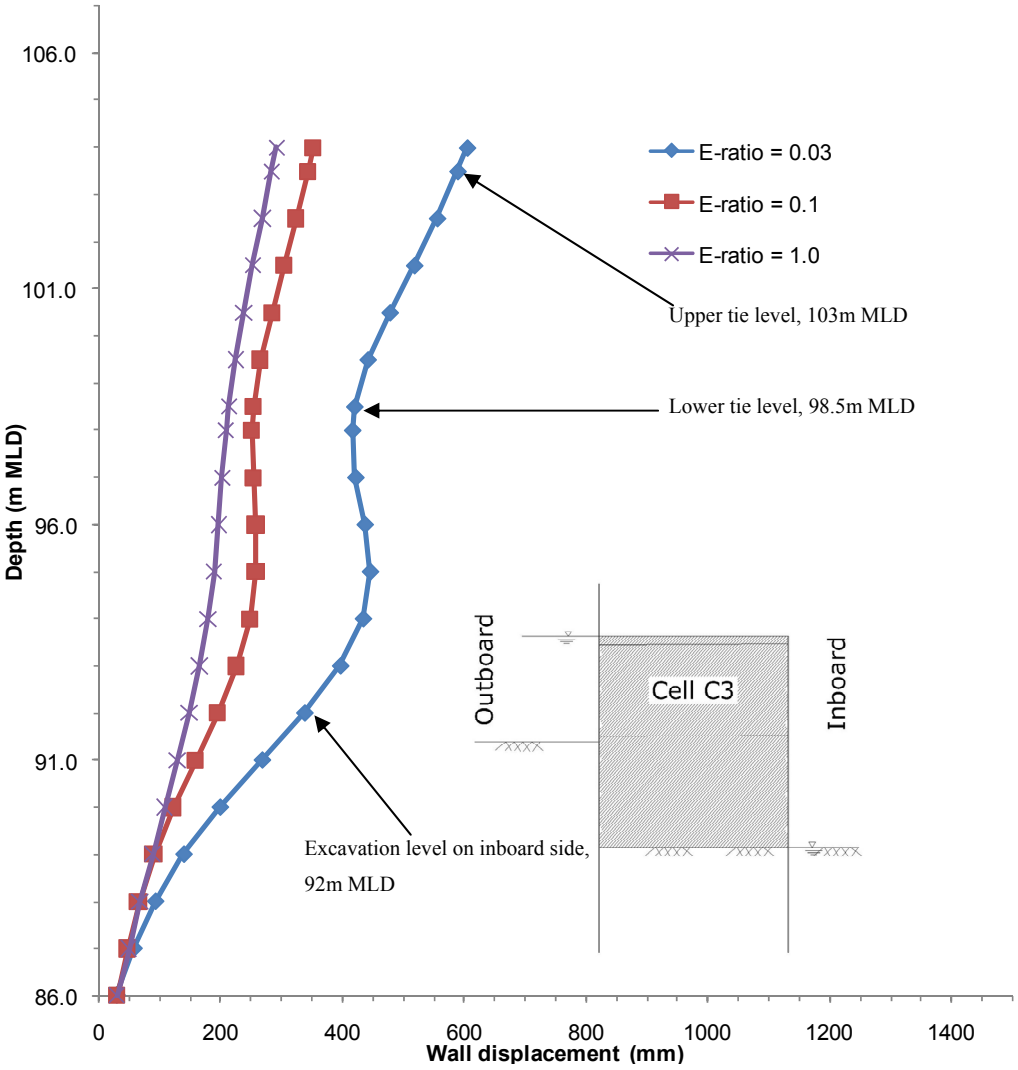

Figure 6-7: Cell displacement for inboard wall at the end of cofferdam construction

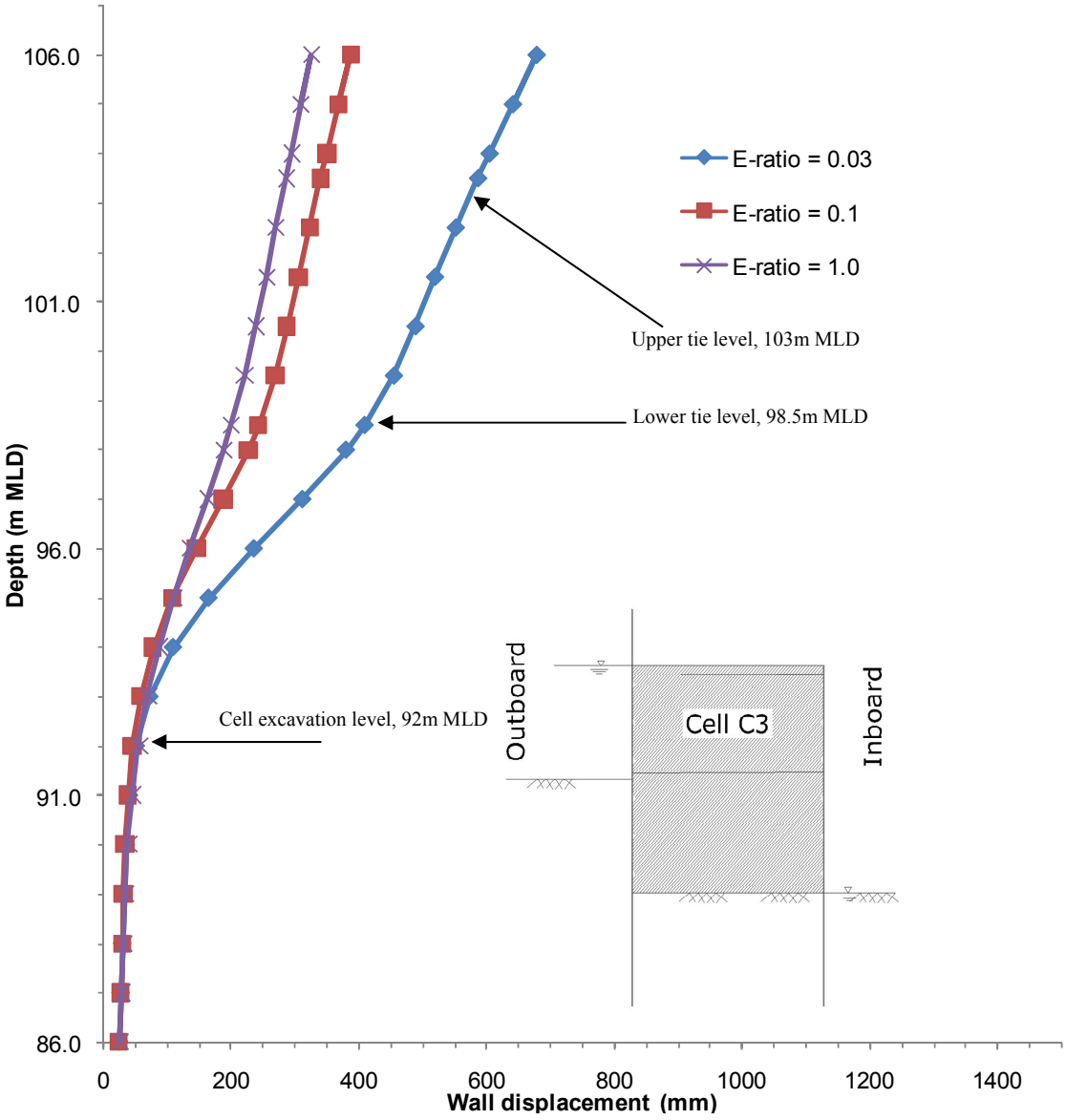

Figure 6-8: Cell displacement for outboard wall at the end of cofferdam construction

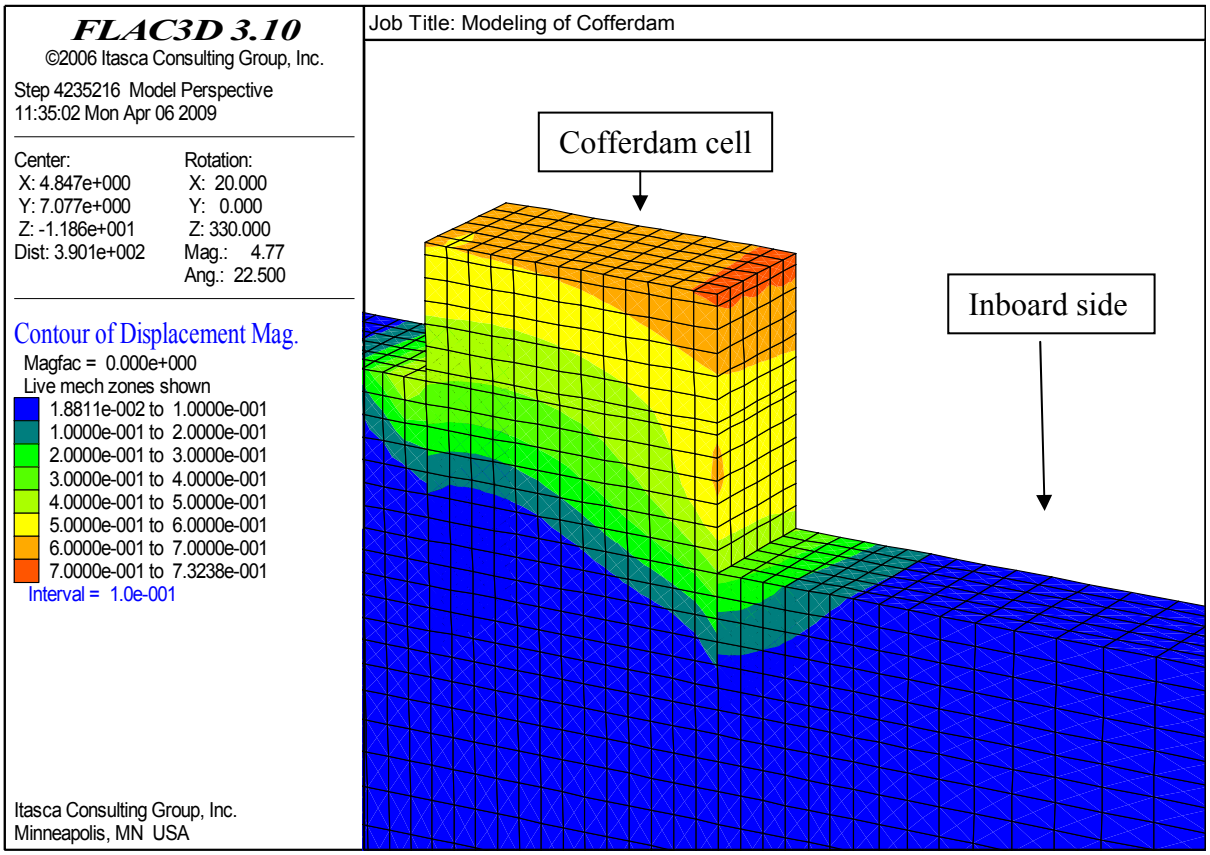

Figure 6-9: Displacement contours for cofferdam at the end of construction (E-ratio=0.03 analysis)

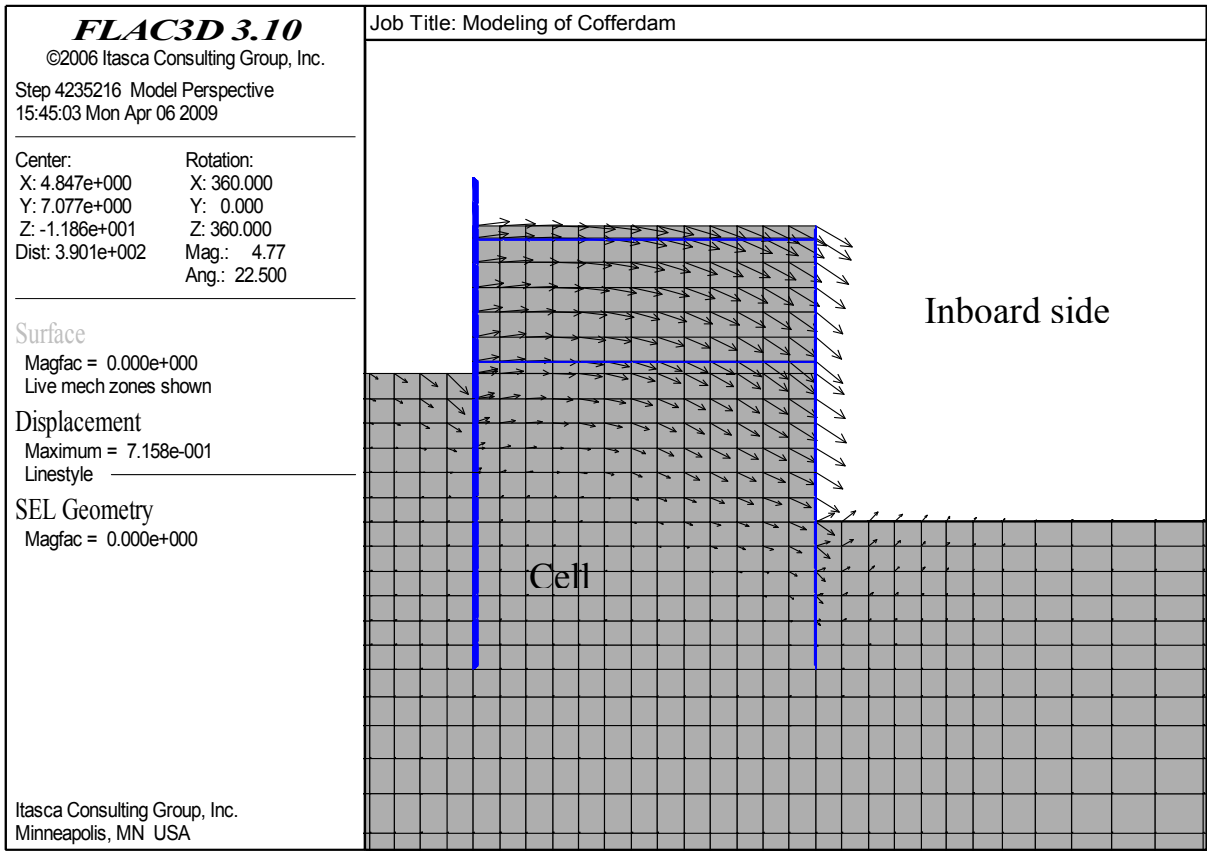

Figure 6-10: Displacement vectors at the end of cofferdam construction (E-ratio = 0.03 analysis)

7 Monitoring of St Germans cofferdam

7.1 Introduction

In this chapter the data acquired from the strain and water levels gauges and cell deflection from total station and manual surveying data are presented. This data was collected using remote monitoring techniques (Richards et al. 2003) and uploaded to a website for constant monitoring by all parties involved in the project. The bending moments from strain gauges installed on cell C3 and the deflection of the cell is of primary importance and will be discussed in detail. These include discussion on changes in bending moments due to a rise in water levels at various monitored locations and tracking the changes in bending moments and deflections at various construction stages.

7.2 Detail of instrumentation

In order to monitor the cofferdam response during construction a number of instruments were installed within cells and on both inside and outside of the cofferdam enclosure. These instruments include electrical resistance type strain gauges, vibrating wire piezometers, water level gauges, standpipes, and total stations. The scope of this research is limited to monitoring an instrumented section (cell C3) only; therefore the following sections will include a discussion on bending moment in cell walls, cell water level, and wall deflection specific to cell C3. The piezometer installed within cell C3 was damaged during construction, therefore the cell water level for C3 presented here will be derived from stand pipe installed within instrumented cell C3 (Figure 4-3).

7.2.1 Strain gauges

In order to calculate the bending moment in sheet piles, electrical resistance type strain gauges (Dunnicliff, 1993) were used. The strain gauges were based on the Wheatstone type circuit configuration. The full bridge type gauge was used where all four circuit elements are active sensing elements (Figure 7-1). The four resistance elements are used in pair of two voltage divider circuits.

R_1 and R_3 = Strain gauge elements used to measure compressive strain

R_2 and R_4 = Strain gauge elements used to measure tensile strain

The R_1 and R_2 pair is the first divider circuit and the pair R_3 and R_4 is the second divider circuit, whereas the output is calculated at the middle of two voltage divider circuits. The voltage ratio (V_r) is acquired from the strain gauge on the basis of change is resistance due to change in imposed phenomenon such as bending moment.

$$V_r = \frac{V_{CH}(strained) - V_{CH}(unstrained)}{V_{EX}} \qquad \textbf{Equation 7.1}$$

Where;

V_{CH} = measured signal voltage

V_{EX} = Excitation voltage

Once the voltage ratio is known the strain can be calculated using the following equation;

$$\varepsilon = \frac{-V_r}{GF} \qquad \textbf{Equation 7.2}$$

Where;

ε = Measured strain

GF = Gauge factor provided by the manufacturer

As only the bending moment was required, a type 1 full bridge strain gauge (National instruments, 2009) was used which only records bending strain and rejects any axial strain (Figure 7-2).

The strain gauges were connected to both inside and outside of the sheet pile to calculate the bending strain in both tension and compression regions (Figure 7-3). Each strain gauge was incorporated with a temperature sensor to exclude the temperature effects from the calculated bending strain (Figure 7-4). There were total 18 numbers of strain gauges installed in pairs (each on inboard and outboard side) to both inboard and outboard sheet piles in the central section of cell C3 (Figure 7-5). The elasticity of the installed strain gauges was approximately similar to the elasticity of the sheet piles as per requirement of British Standards Institution (1986) to exclude error due to stiffness

difference. The bending moment for AZ28 piles (Arcelor steel, 2009) is calculate from the longitudinal bending strain from the pair of strain gauges on the inner face on both sides of sheet pile (Figure 7-6).

$$M = \frac{EI\varepsilon}{y} \qquad \textbf{Equation 7.3}$$

Where;

M = Bending moment in sheet pile

E = Stiffness of sheet pile

I = Moment of inertia for AZ28 section

ε = Bending strain

y = Distance between the neutral axis and the location of strain gauge

Table 7-1: Properties for Arcelor AZ28 sheet pile

E	200×10^6 KN/m^2
I	58940 cm^4/m
y	200×10^{-3} m

The strain gauges and the connecting cables were protected during driving using slotted curved plates welded onto the pile to minimise increase section stiffness in the longitudinal direction. For additional protection and to avoid heat damage during the welding of the covers, the gauges specifically were protected by connecting the cover plate using bolts instead of welding the section at the location of strain gauge (Figure 7-7). The lower end of the cover plate was pointed in shape to facilitate driving and to prevent damage to the strain gauges. Once the installation of the gauges was complete, the covers were installed and the sheet pile in place, they were tested under self bending tests to calibrate the strain gauges and temperature sensors (Figure 7-8). Provided that the

interlocks are able to slide against each other it was considered that the bending stiffness (*EI*) will remain constant in longitudinal direction.

The distributed data management system (DDMS) boxes were connected to the strain gauges to check cable connections to ensure that all the instruments were working properly. After the calibration, the distributed data management system (DDMS) boxes were disconnected again as it was not possible to hammer the piles in with DDMS box installed at the top of the sheet pile. The pitching process for an instrumented 21m (outboard) sheet pile from cell C3 is shown in Figure 7-9.

7.2.2 Water level gauges

Two water level gauges one each within the river and inboard of the cofferdam, were installed on 22nd November 2007. They were used to monitor the tidal water level within the river and impounded water level on inboard side during the balanced water conditions while the dam is being constructed. The river level gauge was installed at the old pumping station structure, while the inboard water level gauge was installed within the cofferdam enclosure in front of instrumented cell C3. The logging frequency of 3 minutes was used for all the water level gages.

7.2.3 Displacement monitoring using ATS and manual surveying

The structural displacement in all three directions at the centre point of the inboard side was monitored using an Automated Total Station (ATS) for the all the cells except cells S0, N0, and C4 (Figure 7-10). Displacement monitoring of the cell C4 was not possible due to the obstruction caused by the jetty installed to facilitate the movement of the crane (Figure 7-11). While the cells S0 and N0 were not expected to experience significant movement as they were adjacent to the west slope with approximately balanced loading conditions on both sides. A raised platform was constructed on the west side (dry side), to locate the automated total station (ATS) (Figure 7-12). The ATS was commissioned on 15th March 2008 and data was collected using ATS until 22nd May 2008. After that the cell displacement was recorded using manual surveying using manually operated total station till 29th of October 2008. It was not possible to collect the cell displacement data once the pumping station structure was constructed due to sight obstruction.

7.3 Data collection and remote monitoring

All the instruments on the site were connected to the on site data collection system which can store the data on a hard drive and forwarded to a remote database system (Figure 7-13). Distributed data management system (DDMS) loggers are used to collect the data from instruments at the 3 minutes interval. The DDMS loggers are connected to onsite computer via cables (Figure 7-15). This computer is located at the old pumping station to avoid any interference with site activities. The onsite computer is used to store data on its hard drive and forward this to site office using Wi-Fi router as a raw file format. This raw data is then downloaded to the remote database using a broadband connection. The remote monitoring system at the University of Southampton is used to collect the data via dialup connection in a raw file format (Richards et al., 2003; Clark, 2005). The raw data is then converted to AGS file format (CIRIA, 2002) and uploaded on to a website (www.monitoringpoint.com) by Dr. Tony Lock (University of Southampton) where it can be viewed by all users. The website allows users set the trigger levels, plot, compare, and download the data in MS Excel file format. The instruments were installed and the data was collected from site by the Structural Statics UK Ltd . My work included regular monitoring, downloading the data to plot trends, comparing changes with field activities/tide levels and calculated response to ensure the safety of the structure at all times.

7.4 Construction detail and sequencing

It took approximately one year from pitching the first pile to completion of the cofferdam enclosing the site. The detail of the construction activity specific to the construction of the cofferdam is outlined below (for the cell reference see the cofferdam plan Figure 4-3).

November 2006 to January 2007

- Site access and foot paths were constructed. Site offices established with facilities e.g. water electricity provided;
- Boundary fencing, site security system, and crane installation was completed;
- Site surveying was completed and environmental barriers were established;

February 2007

- Tubular piles were installed, pile support frames and pile gate installation completed;
- The construction started with pitching first pile to construct cell N1 on the north side of the cofferdam;

March 2007

- Excavation of the first cell (N1) on the north side commenced;
- The flood defence on the west side of the cofferdam was raised to allow the construction machinery to access the top of the cofferdam;
- The sheet piling started on the east training wall on the river bank (Figure 7-49). This was provided as a scour protection and retaining wall for existing flood defence on the opposite (Eastern bank) of the river;
- Construction of the south end started with starting of pitching the sheet piles on cell S1;
- All the sheet piles on cell N1 pitched to the design depth;

April 2007

- All the sheet piles on cell S1 were driven to full depth;
- Excavation was started within cell S1 using a long reach excavator;
- Edge protection was installed all around the site to provide safety during construction;
- By pass channel earthworks commenced;
- Excavation of cell N1 was completed;
- The filling and installation of ties/wailings started on cell N1;

May 2007

- Cell S1 excavation was continued using long reach excavator;
- The sheet piles on cell N2 were driven to full depth;
- Backfilling cell N1 was completed to the top;

June 2007

- First three bents (support for deck slab) with deck slabs installed for construction of jetty. Bent 4 and cross over slab preparation started;
- Pitching of piles was started for Cell N3;
- Filling of Cell N2 was completed to the top and excavation of N3 started;
- Excavation of cell S1 was completed, backfilling and installation of ties was started. The removal of lower bracing frame was difficult due to movement of sheet piles. Remember that the Cells S1 and N1 have only one level of ties (top ties) and higher ground level on outside in comparison to other cells;
- Third front jetty approach ramp earthworks completed on western side to allow access for trafficking on the jetty;

July 2007

- Pitching piles on cell S2 was started;
- All the piles on cell N3 were pitched to full depth and divers started installing ties on cell N3;
- Cell S1 filling was completed to the top of the cell (104m MLD);
- East bypass channel completed, sheet piles were installed to stabilise the slope;

August 2007

- Construction of jetty was completed;
- Cell S2 was excavated, tie bars installed and backfilled to the top;

- Piling started on cell N4 and S3;

September 2007

- Cell N4 piling, excavation and backfilling was completed. Flood pipes were installed within N4 to manage inboard water and flooding the cofferdam in any emergency;
- Excavation within cell S3 was completed and flood pipes and upper ties installed;
- Piling was started on first eastern cell C4;

October 2007

- Backfilling of cell S3 was completed;
- Piling started on cells N5 and S4;
- Piling operation was completed on C4 and cell excavation was commenced;
- Temporary works for construction of cell C3 was started;
- Temporary sheet pile wall was installed on the west side to allow excavation of west slop. As the west slop was cut in the very weak soil (Fen Deposits) therefore the sheet piled wall with dewatering system was introduced to prevent the slop from failure during its excavation;

November 2007

- Cells N5, S4 and C4 were completed and backfilled to the top i.e. 104m MLD;
- All the sheet piles driven on cell C3 including the instrumented piles to monitor the bending moments in sheet piles during construction of the cofferdam;
- Temporary works and advance dig started to construct the cell C2;

December 2007

- The instrumented cell C3 was completed;
- Piling completed for cell C2 and cell excavation was started;

- Temporary works setup for cells N6 and S5;
- Additional site investigation carried out with two boreholes and a falling head test to determine the permeability. Two vibrating wire piezometers were installed within cells N5 and S4;

January 2008

- Piling started and completed for cell C1, N6 and S5;

February 2008

- Cells N6, S5, S6 and C1 completed and backfilled to the top;
- Piling mat installed for wing walls adjacent to cell N0 and piling operation was commenced;
- Cofferdam completed and all ends connected. The construction was undertaken from three sides (North, South and East) simultaneously which connected provides the cofferdam enclosure. This will be dewatered and excavated now to construct the pumping station;

March 2008

- The inboard side on north end excavated to design level under balanced water and berm placement completed;
- Cofferdam snagging complete;
- Jetty removal started to facilitate the construction of east berm;

April 2008

- Jetty removal was completed;
- Ejector wells on eastern cells commenced;
- Excavation and construction of south berm complete, works were slightly delayed on south berm due to failure of long reach excavator;

- Major excavation within the cofferdam started using long reach excavators on temporary access platforms;
- East berm and piling mat installation complete;
- Water level on inboard side was brought down to excavation level;

7.5 Analysis of field data

7.5.1 Bending moment data

The bending moment for both inboard and outboard wall are plotted in two sets of plots for the upper and lower gauges separately. The lower gauges are gauge 1 to 4 and the upper gauges are gauges 5 to 9 (Figure 7-5). This distribution is made as the upper section was more prone to temperature effects and tidal variations. Also there are non-uniform temperature changes because some of the instruments are not in contact with direct sunlight e.g. within the cell and under the ground surface, while others are exposed to direct sunlight, therefore each of the strain gauge was provided with the temperature gauge. All of the upper temperature sensors did not survive the pile pitching process due to the vibration caused during hammering the piles; however three of the lower temperature sensors on each pile are working. The strain gauges were self compensating for temperature effects therefore the data presented here will have to be considered corrected for temperature effects. The actual construction sequence of cofferdam is complex and there are number of factors which might affect the bending moments measured in the sheet piles. The change in river level, cell water level, excavation within and near the cell, CFA piling adjacent to the wall, base slab construction, jetty restraint, and construction equipment moving on top of the cell are some of the important loads imposed on the cell. The construction activities affecting the bending moment are divided in nine stages show in Table 5-1.

Table 7-2: Construction activities affecting the bending moments in sheet piles on cell C3

stage	Dates		Site activity related to cell C3
	From	To	
1	23/11/2007	30/11/2007	On 24/11/2007, a 70 tonne crane was working on the top of cell C3.The excavation started within cell C3 on 23/11/2007.The excavation down to 92m MLD under balanced water conditions was finished within cell C3 on 29/11/2007.
2	01/12/2007	08/12/2007	The backfilling of cell C3 was started on 01/12/2007 and completed to 104m MLD on 08/12/2007.
3	16/01/2008	23/01/2008	Pumps were commissioned with in cell C3 on 13/01/2008 and water level was brought down to 94m MLD on 18/01/2008, while the water level was tidal elsewhere as the cofferdam was still not closed.
4	01/04/2008	24/04/2008	The construction of south berm was started on 01/04/2008. The water level with in cofferdam enclosure was brought down to 98m MLD on 05/04/2008. A very heavy crane (120 tonne) was working on the top of cell C3 on 10/04/2008 and stayed there until 14/04/2008. The excavation in front of C3 was made on 19/04/2008 and inboard water level brought further down to approximately below 97m MLD. The east side excavation within diversion channel on Central cells was made between 11/04/2008 and 25/04/2008. The berm was constructed to 96.5 to 97m MLD on 25/04/2008.
5	24/04/2008	30/04/2008	A heavy (120 tonne) crane working on the top of cell C3 between 25/04/2008 and 30/04/2008. The crane was there to hammer in the steel pipes used for the jetty in front of the central cells. This was done to facilitate the installation of CFA piles and base slab.
6	12/06/2008	26/06/2008	The jetty was connected to the top waling beam on cell C4 on 12/06/2008, thus providing a restraining action on the top to cell C3 which is connected to C4 via waling beam. Excavation down to 92m MLD in front of cell C3 was stared and berm was removed from the front of C3 on 16/06/2008.

stage	Dates		Site activity related to cell C3
	From	To	
7	01/07/2008	08/08/2009	Concrete was poured to construct the base slab supported on the piling mat. The monitoring system was down between 05/07/2008 and 14/08/2008, and once the system was back online the cell water level was at 96m MLD (i.e. 2m above the design level) due to a pump failure within cell C3.
8	17/08/2008	22/08/2008	A heavy crane (120 tonne) was working on the top of cell C3 between 18/08/2008 and 21/08/2008. Pump failure occurred within instrumented cell (C3) and cell water level went up to 99m MLD on 13/08/2008. The pumping station base structure, inlets and outlets were also completed during this period.
9	26/09/2008	28/10/2008	Concrete was poured in most of the formwork used to construct pumping station structure. Pump failure within instrumented cell occurred on 27/09/2008, and cell water level went up to 102m MLD from the design level of 94m MLD.

7.5.1.1 Bending moment in inboard wall

The bending moments calculated from the strain gauges installed on the inboard (dry side) are presented in Figure 7-16. The bending moment data was collected between 22nd November 2007 and 20th January 2009. The change in bending moment during various construction stages (Table 7-2) is provided in Table 7-3. It can be observed from Figure 7-16, that by plotting all the gauges on a same plot for all stages of construction, it is very difficult to identify the changes in bending moment. Therefore the bending moment responses are discussed and plotted as two sets of gauges i.e. lower gauges (bending moment gauges 1 to 4) and upper gauges (bending moment gauges 5 to 9).

Table 7-3: Change in bending moment (kN.m) for inboard during construction of cofferdam

Gauge ID	BMIPL1	BMIPL2	BMIPL3	BMIPL4	BMIPL5	BMIPL6	BMIPL7	BMIPL8	BMIPL9
Depth (m MLD)	87.00	89.00	91.00	93.00	95.00	97.00	99.00	101.00	103.00
stage 1 start	2.38	0.18	4.59	14.17	1.97	-4.41	-1.92	-0.64	-0.35
stage 1 end	-1.80	25.73	53.31	50.81	18.00	-4.47	1.28	-0.35	1.51
Change (δ)	**-4.18**	**25.55**	**48.72**	**36.64**	**16.03**	**-0.06**	**3.19**	**0.29**	**1.86**

Gauge ID	BMIPL1	BMIPL2	BMIPL3	BMIPL4	BMIPL5	BMIPL6	BMIPL7	BMIPL8	BMIPL9
stage 2 start	0.47	22.94	46.11	44.60	23.81	3.54	5.92	3.43	3.54
stage 2 end	-0.17	-9.52	-38.96	7.78	26.42	32.46	0.93	37.80	-13.59
Change (δ)	**-0.64**	**-32.46**	**-85.07**	**-36.82**	**2.61**	**28.92**	**-4.99**	**34.38**	**-17.13**
stage 3 start	4.30	-25.02	-63.59	-0.87	9.52	-1.80	-32.64	74.79	-3.02
stage 3 end	-0.17	-20.15	-58.36	-16.49	-11.91	-1.05	-22.65	79.44	-1.34
Change (δ)	**-4.47**	**4.88**	**5.23**	**-15.62**	**-21.43**	**0.75**	**9.99**	**4.65**	**1.68**
stage 4 start	6.68	-19.51	-89.37	-44.48	-22.94	-25.55	-45.41	58.36	-9.41
stage 4 end	9.70	-99.06	-221.07	-78.28	57.37	43.96	-16.72	68.06	-9.35
Change (δ)	**3.02**	**-79.55**	**-131.70**	**-33.80**	**80.31**	**69.51**	**28.69**	**9.70**	**0.06**
stage 5 start	9.70	-99.06	-221.07	-78.28	57.37	43.96	-16.72	68.06	-9.35
stage 5 end	7.38	-86.00	-205.85	-109.69	19.97	41.29	6.85	88.96	-6.16
Change (δ)	**-2.32**	**13.07**	**15.21**	**-31.42**	**-37.40**	**-2.67**	**23.58**	**20.90**	**3.19**
stage 6 start	8.13	-111.60	-228.50	-111.14	31.53	55.98	8.65	83.56	-8.07
stage 6 end	6.85	-143.14	-248.07	-59.46	49.47	61.20	6.62	84.49	-1.51
Change (δ)	**-1.28**	**-31.53**	**-19.57**	**51.68**	**17.94**	**5.23**	**-2.03**	**0.93**	**6.56**
stage 7 start	7.72	-158.41	-264.74	-42.80	53.65	58.59	5.17	80.48	-1.16
stage 7 end	10.45	-209.86	-271.24	-1.45	91.98	62.77	-1.28	71.66	-6.45
Change (δ)	**2.73**	**-51.45**	**-6.50**	**41.34**	**38.33**	**4.18**	**-6.45**	**-8.83**	**-5.28**
stage 8 start	9.52	-209.86	-268.22	2.90	96.51	63.24	0.81	71.89	-7.96
stage 8 end	12.25	-235.46	-291.39	4.24	129.43	95.93	13.70	77.87	1.68
Change (δ)	**2.73**	**-25.61**	**-23.17**	**1.34**	**32.93**	**32.69**	**12.89**	**5.98**	**9.64**
stage 9 start	8.89	-231.81	-295.45	0.58	128.04	93.61	18.17	73.05	-1.16
stage 9 end	11.33	-246.27	-297.26	11.61	152.31	111.90	26.77	80.77	8.13
Change (δ)	**2.44**	**-14.46**	**-1.80**	**11.03**	**24.27**	**18.29**	**8.59**	**7.72**	**9.29**
stage 9 end	11.33	-246.27	-297.26	11.61	152.31	111.90	26.77	80.77	8.13
10/01/2009	2.85	-237.50	-296.15	5.81	147.84	99.65	39.08	85.30	10.45
Change (δ)	**-8.48**	**8.77**	**1.10**	**-5.81**	**-4.47**	**-12.25**	**12.31**	**4.53**	**2.32**

Stage 1:

Figure 7-17 shows the bending moments changes for gauges 1 to 4 during construction stages 1 to 3 (Table 7-2). The bending moment with the tension on the river side face of the wall is a negative bending moment and positive when the tension is on the face towards the dry side (inboard). A nominal bending moment in the sheet piled wall can be observed prior to excavation or any major construction activity i.e. stage 1. This nominal moment was due to installation of support frame and the crane moving on the jetty. Bending moments in the lower gauges (1 to 4) are plotted in Figure 7-17 and upper

gauges (5 to 9) in Figure 7-18, while the bending profile is shown in Figure 7-25. The bending moment started increasing as the excavation started on 23/11/2007 under balanced water conditions. Table 7-3 shows that positive bending moment was recorded at gauge locations 2 to 5 (i.e. below 93m MLD) as the support provided by the soil plug with in the cell (Kimmeridge clay) when cell is excavated down to 94m MLD and negative bending moment in gauge 6 as the sheet piles move inwards towards the excavated cell. The maximum change (48.72 kN.m) in bending moment was observed in gauge 3 (at 91m MLD). The rest of the gauges (1, 6, 8, and 9) did not show much change in bending moment at the end of stage 1 after the cell excavation was completed on 29/11/2007.

Stage 2:

The bending moments change significantly once the cell filling and compaction commences from 01/12/2007. The gauge 3 from lower set of gauges (Figure 7-17) and gauges 6 and 8 from the upper set show an immediate response to the cell filling (Figure 7-18). The greatest change was revealed by gauges 2, 3 and 4 with maximum change of -85.07 kN.m from the lower set of gauges, and gauge 6 (34.38 kN.m change). As the filling process pushed the piles towards the outside of the cell the bending moment changed on gauges 1, 2, 3, and 9 (Figure 7-25) once the cell filling process was complete (08/12/2007). The upper gauges did not show a significant decrease in bending moment due to the excavation under balanced water, the restraint provided by the steel ties and the use of the top frame to facilitate the cell excavation.

Stage 3:

Cell dewatering reduced the cell water level to 94m MLD within the cofferdam cell on 18/01/2008. The bending moment at depth 93m MLD (gauge 4) (Figure 7-17) and 95m MLD (gauge 5) (Figure 7-18) recorded increase in negative bending moment. This is due to a reduction in the pressure within the cell as the cell water level is reduced, while the water level is balanced elsewhere as the cofferdam is still not closed. The greatest change was revealed by gauge 5 (95m MLD) (Table 7-3) installed at 1m above the reduced cell water level (Figure 7-25).

Stage 4:

The water level within the cofferdam enclosure ceased being tidal on 01/04/2008 following a low tide. The remaining water was pumped to 97m MLD within the cofferdam enclosure (Figure 7-40), and excavation continued to 94m MLD in front of C3 on the inboard side using a long reach excavator (Figure 7-41). The excavation in front of the central cells (C1 to C4) was made between 11/04/2008 and 25/04/2008; however, it was not possible to identify the exact date for excavation of cell C3. Lowering the water level increased the bending moment in the lower set of gauges (Figure 7-31), the greatest increase was observed in gauge 3 (91m MLD) i.e. from -89.3 kN.m to -221.07 kN.m (Table 7-3). The increase in negative bending moment in the lower gauges is due to the support provided by the stiff Kimmeridge Clay in front of the cell. From the upper set of gauges, an increase in bending moment was observed in gauge 5 (95m MLD) and 6 (97m MLD) due to the removal of water pressure and excavating the Fen Deposits which were balancing the cell load by providing support on the inboard side (Figure 7-20). While the bending moment gauges 8 (101m MLD), and 9 (103m MLD) did not show significant change as they were not dependent on the support provided by the inboard water/soil as they were above 101m MLD and were also restrained by the steel ties (Figure 7-25). It is interesting to note that the bending moment change due to dewatering was greater in comparison to the change due to excavation in front of the cells. The reason may be very poor shear strength and stiffness of the Fen Deposits. Also a very heavy crane (weighing 120 tonne) was working on the top of cell C3 during 11 to 14th April 2008, which may have affected the bending moments caused by such a high live load trafficking on the top of the cell.

Stage 5:

Two factors were identified to have affected bending moments in the inboard wall during this stage. Firstly the cofferdam was dewatered and excavated to 94m MLD and the berm was emplaced. Secondly, a 120 tonne crane was working on the top of the cell installing the steel pipes used to construct jetty (removed later to facilitate the installation of CFA piles and base slab) (Figure 7-42). The bending moments recorded in gauge 3 (91m MLD) and 4 (93m MLD) recorded a small reduction in bending moment (Figure 7-19 and Figure 7-26). The upper gauges showed an increase in bending moment except for gauge 5 (Table 7-3 and Figure 7-20). This is probably due to the energy transferred to the

sheet pile due to hammering in the pile sleeves in front of the cell and the weight of the crane itself. This can be clearly observed in the response of gauge 7 (99m MLD) and 8 (101m MLD) (Figure 7-26), which show an increase in tension on the inboard side of the sheet pile by increase in positive bending moment due to increased pressure within the cell.

Stage 6:

The front jetty was connected to the top wailing beam on cell C4 on 12/06/2008 (Figure 7-44). The berm was removed and the Kimmeridge Clay in front of central cells (C1 to C4) was excavated down to 92m MLD (Figure 7-45) under the lower tide identified from the tidal data to ensure low tide windows for the placement of the piling mat in front of the central cells (C1, C4). As the soil was excavated and the berm removed, an increase in negative bending moment for gauge 2 (89m MLD), and 3 (91m MLD) was recorded (tension on face towards cell) (Figure 7-21) due to support provided by the stiff Kimmeridge Clay on inboard side. While the positive bending moment change was recorded on gauges 4 (93m MLD) and 5 (95m MLD) (Figure 7-22; Figure 7-26). This may be partly because the soil excavated in front of these gauges at this level and partly because of the jetty connected to the top of adjacent cell (C4), provided a restraining action to the top of the cell leading to an increase in tension on the dry side face of the inboard wall due to the movement of middle section of the wall towards the excavation. The rest of bending moment gauges from upper set of gauges (gauges 6 to 9) did not show any noticeable change.

Stage 7:

The monitoring system was down during 05/07/2008 and 14/08/2008, and no strain gauge or river level data was collected over this period. Unfortunately some on the important construction stages such as excavation down to 92m MLD and the piling mat construction occurred during this period (Figure 7-46). Once the monitoring system was back online on 14/08/2008, the cell water level was recorded at 96m MLD which is 2m above the design cell water level, indicating a pump failure within cell C3. The bending moment gauge 2 (89m MLD) has shown a continued increase in bending moment from the previous stage (Table 7-3) indicative of an increase in tension on the pile face towards

cell fill (Figure 7-21). This is due to increase in pressure due to a rise in cell water level and the negative bending moment is a result of the passive pressure offered by stiff Kimmeridge Clay in front of the cell below 92m MLD (excavation level). The increase in cell pressure has also resulted in an increase in the tension on the dry side of the wall above 92m MLD; this is indicated by bending moment gauge 4 (93m MLD) and 5 (95m MLD) (Figure 7-21; Figure 7-22) with increase in positive bending moment during this stage. The top 2m of Kimmeridge Clay on inboard side was recently excavated (stage 6), but still there is no unbending action indicated by gauge 1, 2 and 3 (the gauges in contact with Kimmeridge Clay supporting cell on dry side between 87 and 91m MLD), representative of softening of the Kimmeridge Clay (Figure 7-27).

Stage 8:

The pump failure continued and the water cell level reached 99m MLD within the cell on 13/08/2008 and remained there until the pumps came back online on 05/09/2008 and cell water level was brought down to 94m MLD. This resulted in a further increase in negative bending moment (tension on wall face towards the cell) in gauges 2 (89m MLD) and 3 (91m MLD) (Figure 7-23) which were at the level of the Kimmeridge Clay on inboard (dry) side. There might be some effect due to heavy pumping station structure constructed on the top of the piling mat (Figure 7-48), but this is actually supported on the CFA piles therefore it is difficult to quantify this change. The bending moment gauges below 99m MLD i.e. gauge 5 (95m MLD) and 6 (97m MLD) (Figure 7-24) which have no support on the inboard side recorded an increase in the tension on the dry side face of the sheet pile with increase of 32 kN.m in bending moment for both the gauges (Table 7-3). The gauges above 99m MLD are less affected (Figure 7-27), as the lower steel ties installed at 98.5m MLD are supposed to take much of the load increase due to cell pressure below this level.

Stage 9:

The majority of the pumping station structure was completed during this period. A pump failure on 28/09/2008 allowed the cell water level to increase up to 102m MLD within the cell, this water level was brought down to design level of 94m MLD on 28/10/2008. A small increase in negative bending in lower gauges i.e. gauge 2 (89m MLD), and 3 (91m

MLD) (Table 7-3; Figure 7-23) was recorded in comparison to the previous pump failure (stage 8). An increase in positive bending moment was also observed in the upper set of gauges i.e. 5, 6, 7, 8, and 9 (from 95 to 103m MLD) (Figure 7-24 and Figure 7-27), as the increase in cell water level resulted in an increase in cell pressure. The greatest response to the rising and falling cell water level with change in river tide was indicated by gauges 2, 3, 5 and 6 (installed between 89 and 97m MLD).

Bending moment change between the end of stage 9 and end of monitoring

The bending moment profiles in Figure 7-16, Figure 7-23, Figure 7-24, Figure 7-27 and net change in bending moment values shown in Table 5-1 indicates that since the major geotechnical works are complete the bending moments have stabilised and there is very little change in bending moment particularly for the gauges in contact with the Kimmeridge Clay supporting the cell (below 92m MLD) on the dry side of the cofferdam. There are possibly two reasons for this behaviour. The CFA piles are constructed in front of the instrumented section (at 2m c/c) (Figure 7-45) and the base slab at 0.3m from the inboard wall. These may be acting as a low level prop preventing the wall movement on the inboard side of the cofferdam.

7.5.1.2 Bending moment in outboard wall

Figure 7-28 shows the change in bending moment in the outboard (water side) wall on the primary vertical axis plotted against dates when the readings were taken, and cell, river level plotted on the secondary vertical axis. The sign convention is same as the inboard wall, i.e. tension on the water (outboard) side will be considered as the negative bending moment and positive if the tension is on the dry (inboard side) face of the sheet pile (Figure 7-5). The dates during which the data was collected are same as the inboard wall discussed in previous section. Net change in bending moment during identified constructions stages (Table 7-2) is provided in Table 7-4. To plot the bending moment data, a similar approach used for inner wall was adopted, i.e. the gauges were divided in the lower set of gauges (bending moment gauges 1 to 4) and the upper set of gauges (bending moment gauges 5 to 9). The change in bending moment in outboard wall during construction stage indentified in Table 7-2 will be discussed separately for each stage in the following;

Table 7-4: Change in bending moment (kN.m) for the outboard wall during construction of cofferdam

Gauge ID	BMOPL1	BMOPL2	BMOPL3	BMOPL4	BMOPL5	BMOPL6	BMOPL7	BMOPL8	BMOPL9
Depth (m MLD)	87	89	91	93	95	97	99	101	103
stage 1 start	0.46	2.32	0.70	-1.34	-0.23	-0.64	0.11	0.70	5.57
stage 1 end	-10.98	-45.82	-20.21	-1.34	15.39	11.21	20.38	13.12	4.88
Change (δ)	**-11.44**	**-48.14**	**-20.90**	**0.00**	**15.62**	**11.85**	**20.27**	**12.43**	**-0.70**
stage 2 start	-8.59	-45.52	-20.21	-4.82	20.32	5.81	16.31	9.58	8.59
stage 2 end	-1.97	-28.86	36.06	40.18	102.95	37.16	-8.31	-22.59	6.27
Change (δ)	**6.62**	**16.67**	**56.27**	**45.00**	**82.63**	**31.36**	**-24.62**	**-32.17**	**-2.32**
stage 3 start	-2.21	-29.09	56.56	79.78	150.98	94.24	17.65	-15.39	33.45
stage 3 end	-3.02	-38.79	54.12	93.78	177.11	114.57	18.64	-15.97	14.75
Change (δ)	**-0.81**	**-9.70**	**-2.44**	**13.99**	**26.13**	**20.32**	**0.99**	**-0.58**	**-18.70**
stage 4 start	-10.68	-52.61	66.37	134.25	207.83	130.42	18.69	-35.83	20.61
stage 4 end	-21.78	-90.64	4.59	102.43	198.88	123.16	21.02	-37.28	7.37
Change (δ)	**-11.09**	**-38.04**	**-61.79**	**-31.82**	**-8.94**	**-7.26**	**2.32**	**-1.45**	**-13.24**
stage 5 start	-21.78	-90.64	NA	102.43	198.88	123.16	21.02	-37.28	7.37
stage 5 end	-23.34	-93.26	NA	63.58	167.53	106.50	39.72	-12.89	9.93
Change (δ)	**-1.57**	**-2.61**	NA	**-38.85**	**-31.36**	**-16.67**	**18.70**	**24.39**	**2.55**
stage 6 start	-29.44	-105.39	NA	57.25	163.00	105.45	27.81	-19.11	12.31
stage 6 end	-30.89	-109.11	NA	58.99	162.36	106.32	30.77	-15.27	8.59
Change (δ)	**-1.45**	**-3.72**	NA	**1.74**	**-0.64**	**0.87**	**2.96**	**3.83**	**-3.72**
stage 7 start	-33.74	-113.87	NA	57.89	165.38	111.90	44.19	-8.54	10.57
stage 7 end	-39.37	-128.68	NA	38.96	161.78	111.66	43.55	-16.90	-0.18
Change (δ)	**-5.63**	**-14.81**	NA	**-18.93**	**-3.60**	**-0.23**	**-0.64**	**-8.36**	**-10.74**
stage 8 start	-36.70	-123.98	NA	36.46	153.01	107.60	33.10	-19.98	3.37
stage 8 end	-37.45	-128.33	NA	24.56	139.36	100.69	36.17	-18.41	3.54
Change (δ)	**-0.75**	**-4.36**	NA	**-11.90**	**-13.65**	**-6.91**	**3.08**	**1.57**	**0.17**
stage 9 start	-42.33	-135.82	NA	27.99	148.65	108.70	49.06	-15.04	9.87
stage 9 end	-44.07	-139.65	NA	17.53	137.85	102.26	36.75	-29.50	4.35
Change (δ)	**-1.74**	**-3.83**	NA	**-10.45**	**-10.80**	**-6.45**	**-12.31**	**-14.46**	**-5.52**
stage 9 end	-44.07	-139.65	NA	17.53	137.85	102.26	36.75	-29.50	4.35
10/01/2009	-50.35	-145.29	NA	18.11	143.43	108.30	51.33	-28.22	1.80
Change (δ)	**-6.27**	**-5.63**	NA	**0.58**	**5.57**	**6.04**	**14.58**	**1.28**	**-2.56**

Stage 1:

The excavation within the cell C3 was started (23/11/2007) under the balanced water conditions with top frame in place to support the cell walls during excavation. The cell

excavation down to 94m MLD (top of Kimmeridge Clay) was completed on 29/11/2007. Change in bending moment during stage 1 is provided in Table 7-4. The lower bending moment gauges 1, 2, and 3 (between 87 and 91m MLD) recorded negative bending moment (Figure 7-29; Figure 7-37) due to the restraint provided by the stiff Kimmeridge Clay soil plug at the lower end of the wall (below 94m MLD). Figure 7-30 shows the bending moment change in upper set of gauges. The gauges 5, 6, 7, and 8 (95 to 101m MLD) recorded positive bending moment (Table 7-4). This is not consistent with the upper set of gauges on the inboard side (Table 7-3) as the cell is still considered to be under balanced loading conditions on both the inboard and outboard of the cell. The reason for this may be the load from the east slope (Figure 7-49) from the right bank across the river (opposite to the cell wall), which may be applying some unbalanced loading on the outboard wall in comparison to the inboard side.

Stage 2:

Table 7-4 provides the change in bending moment in the outboard wall during filling of the cell C3. The bending moment gauges 2, 3, 4 (89 to 93m MLD) from the lower set (Figure 7-29) and 5, 6 (95 and 97m MLD) from the upper set of gauges (Figure 7-30) show change in bending moment towards positive side (Figure 7-37) i.e. tension has increased on the cell side face of the wall. The reason for this is that, when the top frame is removed and once the cell is half filled, the Fen Deposits (having very poor undrained strength and stiffness) will push the outboard wall towards the inside of the cell. There might be some effect from the east slope (Figure 7-49) as observed in stage 1 (during excavation of cell) increasing the pressure on the river (outboard) side of the outboard wall. The bending moment gauges 7 and 8 (99 and 101m MLD) recorded change in bending moment on negative side (Table 7-4). This is due to the increased cell pressure by the cell fill. This increase in the cell pressure is not transferred completely below the level of gauge 7 (99m MLD) the lower steel tie was installed at 98.5m MLD, which is supposed to take most of the cell pressure above this level (Figure 7-5).

Stage 3:

The cell pressure was reduced as a result of dewatering the cell by commissioning the pumps (18/01/2008). The bending moment change in the lower set of gauges is presented

in Figure 7-29 and upper set in Figure 7-30. This reduction in cell pressure resulted in tension on the cell side face of the sheet pile which is revealed by the gauges 4, 5 and 6 (93 to 97m MLD) with increase in bending moment on positive side (Table 7-4). The greatest change in bending moment can be observed at gauge 5 (95m MLD) which is just 1m above the reduced water level within the cell (Figure 7-37).

Stage 4:

Once the water level within the cofferdam enclosure was reduced from balanced water condition (01/04/2008) the cofferdam started moving towards the unloaded (dry) side. This results in an increased negative bending moment (tension on the river side of the wall) recorded by gauges 1 to 7 (87 to 99m MLD) (Table 7-4). The table shows that bending moment gauges 1 (87m MLD) and 2 (89m MLD) recorded increase in negative bending moment (tension on water side) as that part of the wall is supported by the stiff Kimmeridge Clay, while the gauges 3, 4, 5, and 6 (91 to 97m MLD) recorded reduction in net positive bending moment. The change in bending moment from upper set of gauges (Figure 7-32) for outboard wall (gauges 5 to 9) is compared to the gauges on inner wall (Figure 7-19) as the loading conditions have changed (Figure 7-5). The outboard wall is under tidal river level, and retaining 4m of the Fen Deposits (from 98 to 94m MLD) in comparison to inboard wall where there is no tidal pressure and the Fen Deposits were excavated down to 94 MLD (top of the Kimmeridge Clay) between 11 to 25th of April 2008. The overall change in bending moment for the inboard wall is greater in comparison to the outboard wall (compare Table 7-3 and Table 7-4).

Stage 5:

Table 7-4 provides change in bending moment during stage 5 of cofferdam construction. As the inboard side was recently excavated and dewatered (See stage 4) the cell is still showing some defection towards the excavated side. A heavy crane (120 tonne) was working on the top of the cell C3 during this period to hammer-in the steel pipes used for jetty which was no longer required (Figure 7-42), this was to facilitate the installation of the CFA piles later on. The hammering process was expected to have transferred a lot of energy to the structure which has damaged the bending moment gauge 3 in the process (Figure 7-31). Gauges 1 (87m MLD) and 2 (89m MLD) did not show visible change from

the lower set of gauges while gauge 4 (93m MLD) recorded change in bending moment on the negative side (tension on river side); however, the net bending moment is still positive. From upper set (Figure 7-32), the gauges 5 (95m MLD) and 6 (97m MLD) recorded a negative change while the gauges 7 (99m MLD) and 8 (101m MLD) which are above the lower tie level (98.5m MLD) recorded change in bending moment towards the positive side (tension on cell side face).

Stage 6:

Figure 7-33 and Figure 7-34 show change in bending moment in the upper and lower sets of bending moment gauges during stage 6 of the construction of cofferdam (Table 7-2). The change in bending moment profile for the outboard pile recorded before and after the completion of the construction stage 6 is plotted in Figure 7-38. There was a negligible change for bending moment in the inboard wall during jetty connection to the wailing to the inboard pile and the excavation in front of cell on dry side (Table 7-4). This is mainly because the jetty is preventing the top of inboard pile which is connected to the outboard pile by means of flexible ties; therefore the bending moment profile for outboard pile should largely remain unaffected. Removal of the berm and excavation down to 92m MLD in front of inboard wall was undertaken during the low tide windows; therefore, the effect of excavation on the outboard wall is minimal.

Stage 7:

The monitoring system was down between 05/07/2008 and 14/08/2008, therefore no bending moment and river data is available for this period (Figure 7-33 and Figure 7-34). The base slab was poured during this stage to support the construction of pumping station. A small increase in negative bending moment (tension on water side face) can be observed for gauges 2 (89m MLD) and 4 (93m MLD) only (Table 7-4); however, the net bending moment in gauge 4 was positive. This increase is due to rise in water level to 96m MLD (2m above design level) within the cell which has increased the pressure within the cell resulting in an increased tension on the water side face of the outboard wall. The bending moment gauge 3 (91m MLD) was damaged during stage 5 and is not plotted in profile plot (Figure 7-39).

Stages 8 and 9:

Figure 7-35 and Figure 7-36 show the change in bending moment for the outboard wall during stages 8 and 9 (Table 5-1) of the construction of cofferdam. Two consecutive pump failures have affected the bending moment in the gauges above the design water level (94m MLD), i.e. gauges 4 to 8 (93 to 101m MLD) (Table 7-4). The change in bending moment is due to increase in the cell pressure due to rising water level within the cell. There was no effect due to construction of pumping station structure and other activates as they are mainly taking place in front of the inboard wall.

Bending moment change between end of stage 9 and end of monitoring

The bending moment profile in Figure 7-39 and data in Table 7-4 shows that there is very little change in bending moment at the end of the stage 9 and two months after the major geotechnical/structural works were completed once the data collection was stopped (10/01/2009).

7.5.2 Cell displacement data

Cell displacement data for Cell C3 is illustrated in Figure 7-50 showing that the cell deflected continuously towards the inboard side as the construction of the cofferdam progressed. The displacement was negligible during the period when the water level was balanced on both side of the cell i.e. until 1st of April 2008. The lower displacement gauge readings shows some error in recording the cell displacement which is mainly due to obstruction due to the construction activities in front of the cell, and the data was taken by the Automated total station which automatically records the displacement without any knowledge of obstruction. Most of the cell deflection accumulated when water level was brought down to within the cofferdam (e.g. between 01/04/2009 and 11/04/2009), with maximum deflection of 25mm for the outboard pile. The lower section on the inboard wall revealed a lesser deflection in comparison to the top of the inboard wall, which suggests that the cell has swayed towards the inboard side. Very little displacement was recorded during excavation of Fen Deposits; however the outboard wall has shown a slightly greater displacement in comparison to the inboard wall. This is because the height of the outboard wall is greater (107m MLD, overhanging 3m above the cell, see

Figure 7-6) in comparison to inboard wall (104m MLD) therefore any sway in the cell will result in greater displacement for outboard wall.

Once the inboard side was excavated down to 94m MLD (top of kimmeridge clay) and berm was placed the cell has showed some consistent deflection until hammering of the steel pipes was completed on 01/05/2009 (Figure 7-42) which were used to support the jetty in front on central cells (C1 to C4). The jetty was connected to the top wailing beam on cell C4 (adjacent to instrumented cell C3, Figure 7-10) on 12/06/2009; this will have some restraining action on the top of cell C3. This might be the reason the bending moment gauges have shown substantial change in bending moment during excavation down to 92m MLD for placement of base slab (Table 7-3), but a very little in cell displacement is observed from cell displacement data during this period (stage 6 on Figure 7-50). The displacement monitoring for lower point on inboard wall was stopped on 15/09/2009 as the construction of pumping station was causing the obstruction to the total station sight to take the readings for lower displacement point. The displacements for upper points on the inboard and outboard walls were taken until 29/10/2008, and showed a little change. At the end of displacement monitoring, a maximum deflection of 148mm, and 119mm towards the inboard (dry) side was recorded for outboard and inboard walls respectively.

7.5.3 Water levels data

River and cell water levels recorded during the cofferdam construction are presented in Figure 7-51. The inboard (dry) side water level gauge malfunctioned soon after installation and therefore no data on the impounded water level is available. To test the pumping system, the cell water level was pumped down to design level i.e. 94m MLD on 18/01/2008 once the cell filling was complete for a period of three weeks. Once the cofferdam was complete and all the cells were connected, the pumping system was commissioned for continuous operation on 23/02/2008 to keep the cell water level at the design level during construction within the cofferdam. There were two pump failures during the cofferdam construction and it can be clearly seen that the cell water level is responding to the river tide when all the pumps are stopped during the second pump failure (Figure 7-52). However, the cell water level was considerably lower than the river

level as the clutches between the sheet piles on both the inboard and outboard walls permit inflow and outflow from the cell.

The highest and lowest river tides recorded during construction were 104.9 and 99m MLD respectively and generally the water stayed around these levels for all higher and lower tides. The 1:200 years river flood level is 106.3m MLD (for which the cofferdam was actually designed). The return period for the higher/lower tide was around two weeks. This return period was very helpful in identifying lower tide windows in which the removal of the berm and excavation for placement of base slab which was a critical part in the construction of central cells (cells C1 to C4). As far as daily variation is concerned two higher and lower peaks were observed one each during day and night time.

7.6 Summary

The bending moments measured on the inboard and outboard piles have revealed some of the important aspects of the structural forces and impact of construction sequence on the these forces. The bending moment profiles (Figure 7-27 and Figure 7-39) shows that the inboard wall has a higher net bending moment of 297 kN.m in bending moment (gauge 3, 91m MLD) in comparison to a maximum bending of -139 kN.m for the outboard wall from bending moment gauge 2 (installed at 89m MLD). It should be also noted that the bending moment gauge 3 was non functional for the outboard wall and keeping in mind the highest bending moment in the inboard wall at that level there is a probability that the recorded bending moment from gauge 2 on the inboard is less than the actual bending moment if gauge 3 was working. However for both inboard and outboard walls the maximum bending moment was in a section where it was primarily supported by the stiff kimmeridge clay. The bending moment once reached the maximum value, did not show any reduction in bending moment which suggests that there is no unbending effect due to undrained behaviour of the soil as the reduction in bending moment is observed when pore water pressure equalisation takes place (Richards and Powrie, 1998). This is consistent with the higher Kimmeridge Clay permeability derived from the falling head test. However, the constant bending moment at the final stage may include the effect due to the CFA piles and base slab constructed close (0.3m) to the inboard wall.

The bending moment profile indicates that the bending moment reduction at the point where the steel ties are installed is not significant. Especially at the outboard pile where there is no change in profile due to the lower tie at 98.5m MLD. This suggests that there might be clutches in the steel ties connection or probably the ties were very loose at the time of installation. It was understood from centrifuge model tests on the cofferdams that the net bending for inboard and outboard wall for cofferdam founded on clay is similar (Khan *et al.,* 2006), however we have observed here that the bending moment in inboard wall is significantly higher in comparison to the outboard wall. The is justified by the argument that most of the construction activities and excavation on dry side affects the inboard wall more in comparison to the outboard therefore much attention should be provided to the design of the inboard wall. The overall bending moment in both the walls is well below the design capacity of 960 kN.m for the Arcelor AZ28 sheet piles (Schlim and Reuter, 2005) used for the construction of cofferdam.

The river tide level has a very little effect on the bending moment. There is some effect of changing tide during the pump failure within the cell on the bending moment gauges above the design water level (which is also top of Kimmeridge Clay within the cell), i.e. bending moment gauges 4 to 9.

The cofferdam displacement data has revealed overall sway towards the inboard (dry) side of the cofferdam. The cell displacement during dewatering was greater than the displacement during excavation of 3m of the Fen Deposits in front of the instrumented cell. This suggests that the support provided by the Fen deposits on the unloaded side was very poor due to very weak stiffness and strength of the Fen Deposits. It was also noticed that the cofferdam was stable in the end and there is no sign of continued deflection of the cell.

7.7 Conclusions

The instrumentation of the Cell C3 at the St. Germans cofferdam was used to collect the bending moment and cell deflection data during construction and once the cofferdam was complete. The following conclusions can be drawn on the basis of the study conducted:

- Use of the electrical resistance type strain gauges, ATS and remote monitoring system collecting data at regular intervals has allowed round the clock monitoring of the structure at construction site 180 miles away from the monitoring database;
- The monitoring data has helped identification of changes during construction of cofferdam. This also helped in optimising the design and undertaking some of the important construction works such as removal of the berm to place the base slab under low tide;
- Maximum bending moment coincided with the level of stiff Kimmeridge Clay, suggesting a strong passive response from the Kimmeridge Clay to the unbalanced loading of the cell;
- The bending moment in the inboard wall is greater in comparison than that measured in the outboard wall;
- Identification of various construction stages has revealed additional causal effects such as construction machinery loadings, dewatering and impact loads due to hammering of adjacent piles;
- The deflection profile revealed sway of the cell by showing greater displacement at the top of the cell in comparison to the lower level of cell;
- The cell water level was responding to the tide level with in the river once all the pumps with the cofferdam stopped working.

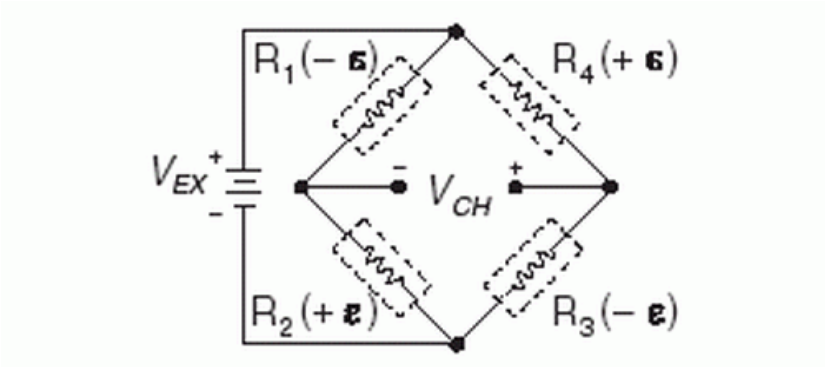

Figure 7-1: Full bridge type 1 circuit diagram for the strain gauges used to calculate bending strain (National instruments, 2009)

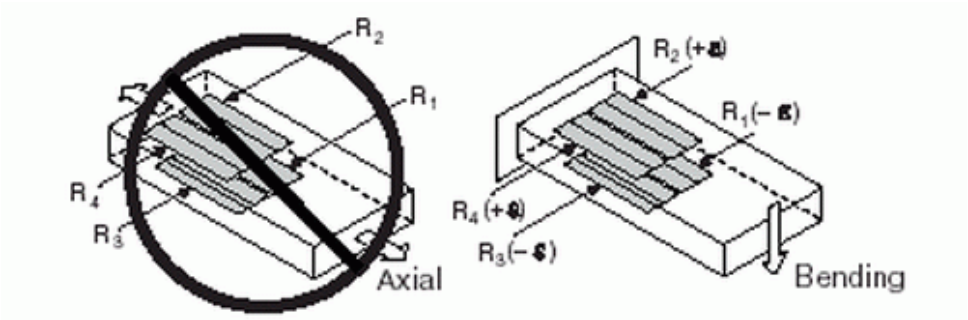

Figure 7-2: Full bridge type 1 strain gauge used to measure bending strain while rejecting axial strain (National instruments, 2009)

Figure 7-3: Instrumented section of the pile showing the cover plates and pointed tip (Structural statics, 2008)

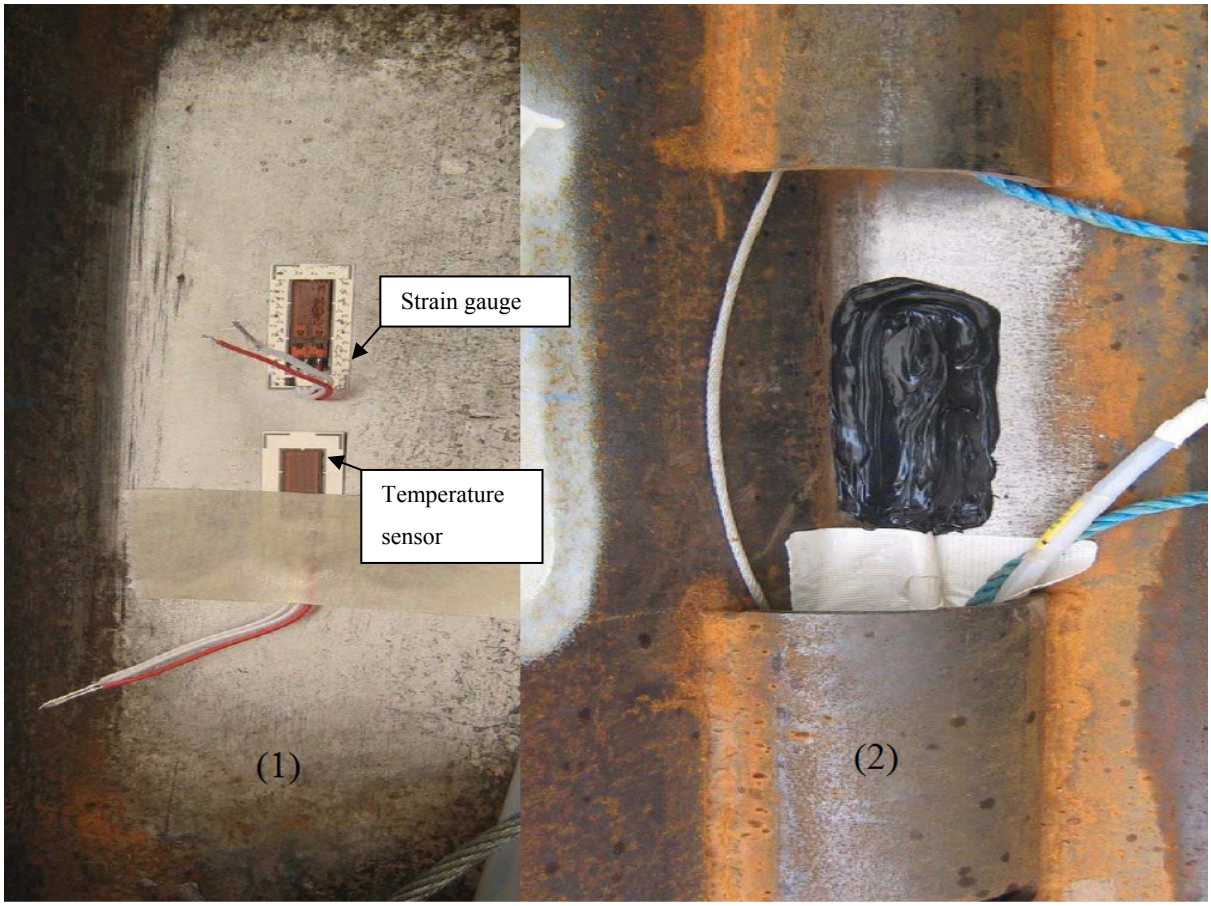

Figure 7-4: Temperature and resistance type strain sensors embedded together

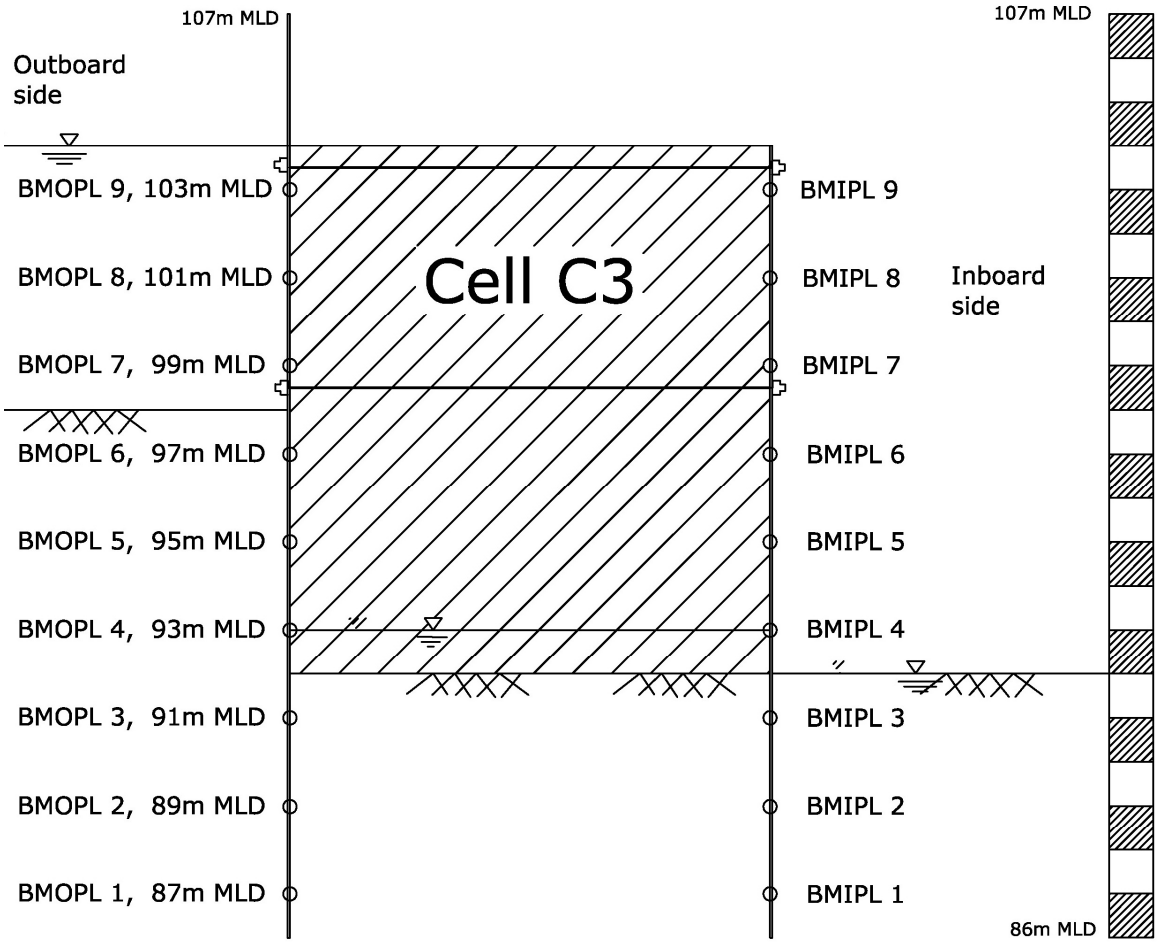

Figure 7-5: Location of strain gauges installed onto cell C3

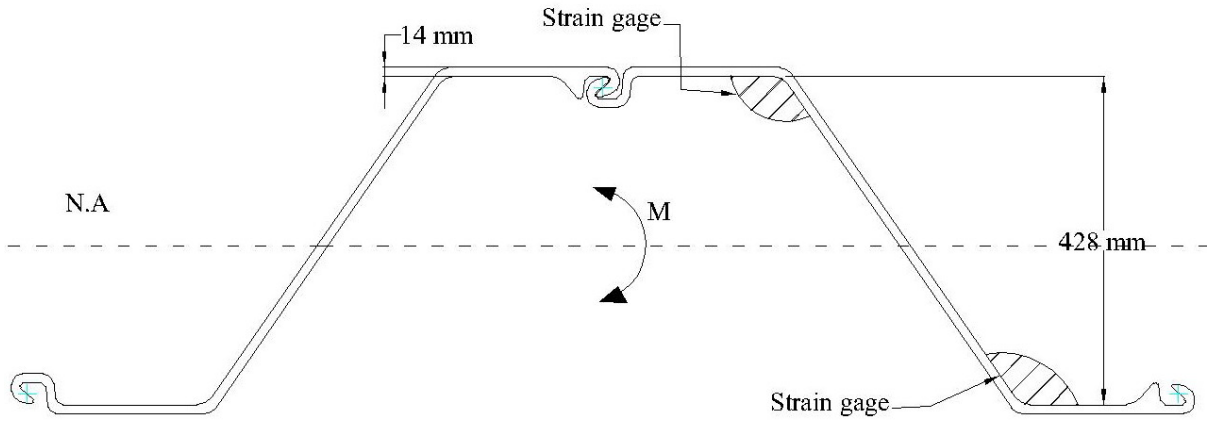

Figure 7-6: AZ28 sheet pile showing location of strain gauges

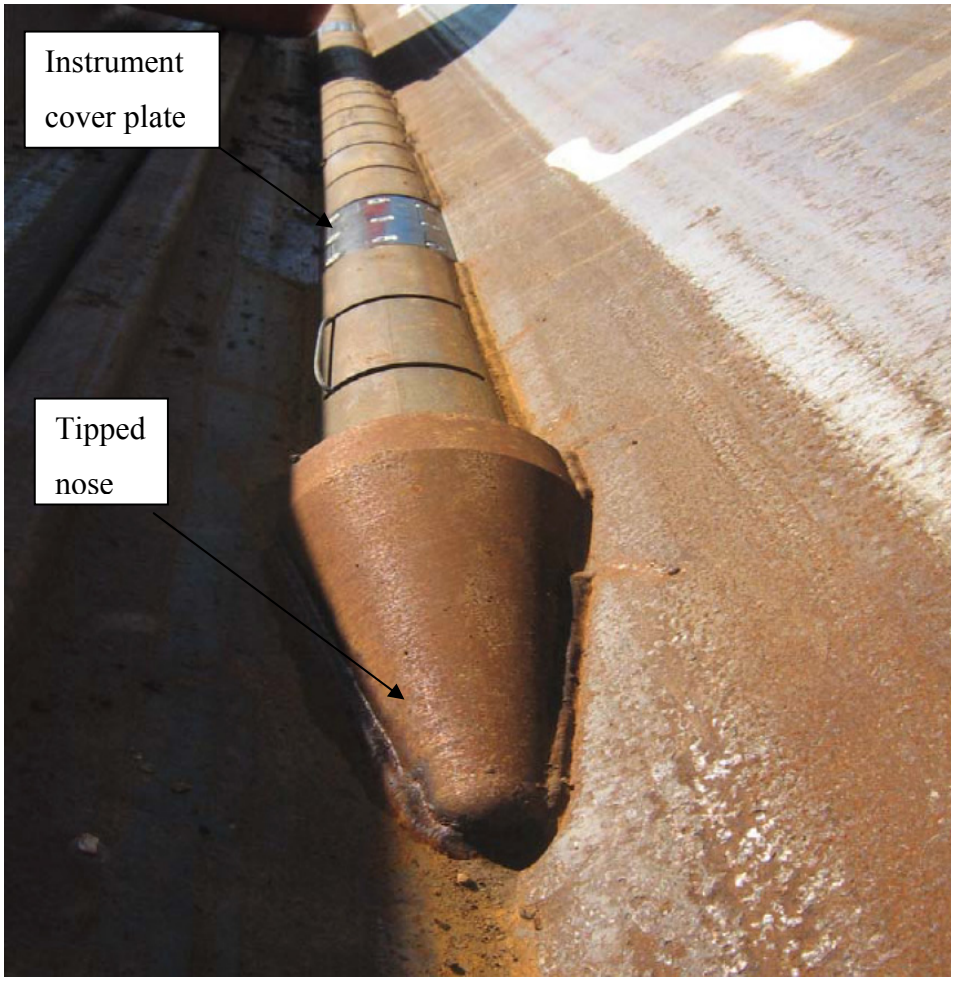

Figure 7-7: The bolted plates at the location of strain gauge pointed tip to facilitate pitching

Figure 7-8: Self bending test to calibrate and check the strain gauges and temperature sensors

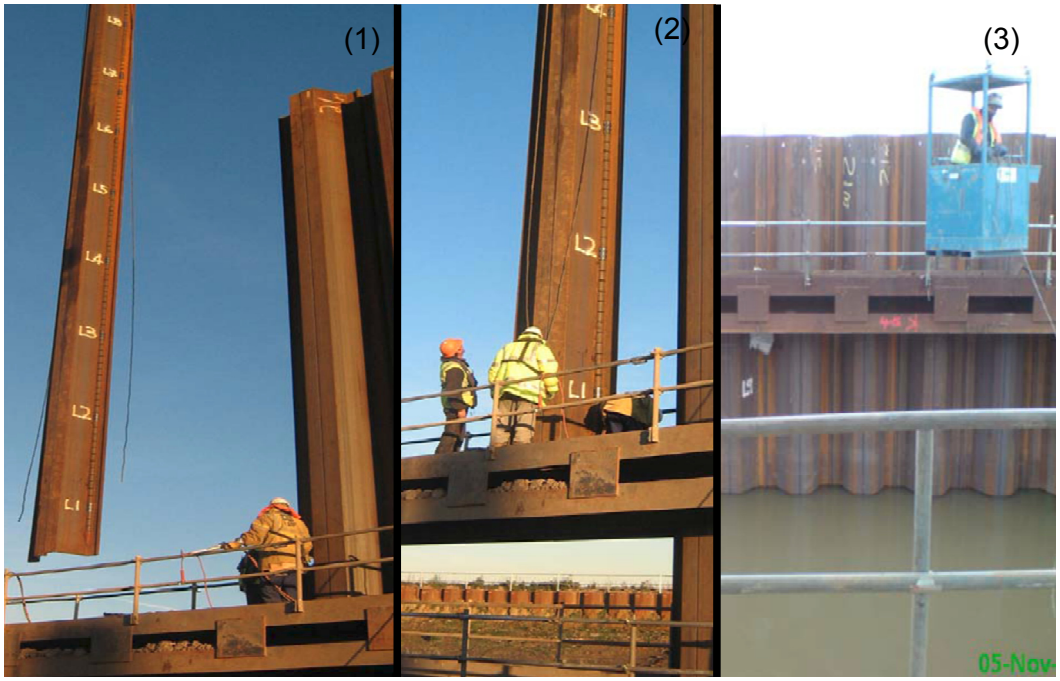

Figure 7-9: Outboard instrumented pile pitching process (1) Pile lifted (2) Insertion into pile guide (3) Pile installation complete

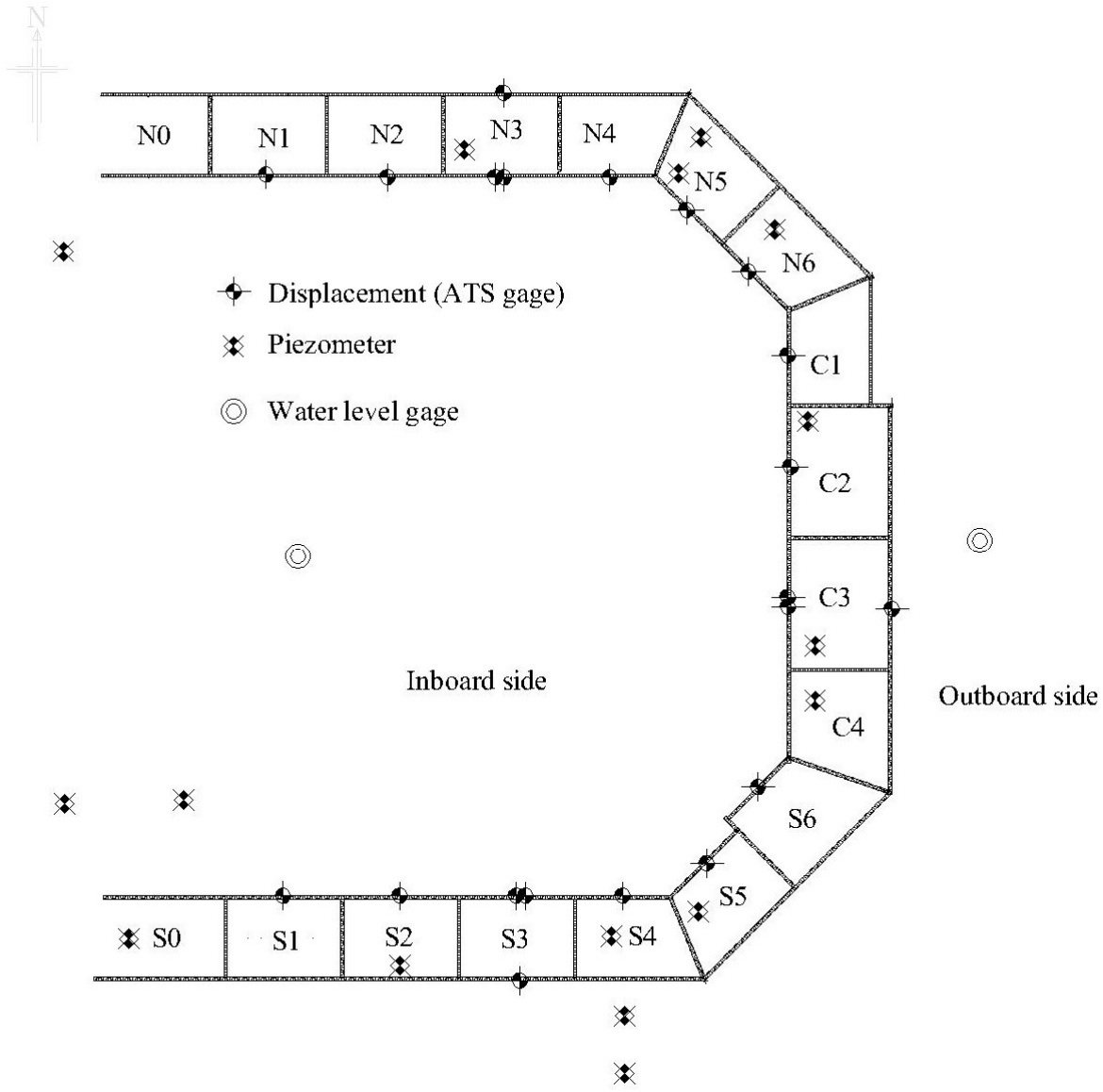

Figure 7-10: Location of ATS points, piezometers and water level gauges on plan of the cofferdam

Figure 7-11: Jetty connected to Cell C3

Figure 7-12: Platform constructed on west side to facilitate installation of ATS

Figure 7-13: Data collection and remote monitoring system

Figure 7-14: Data loggers installed on cell C3

Figure 7-15: Site computer, used for data storage and communication

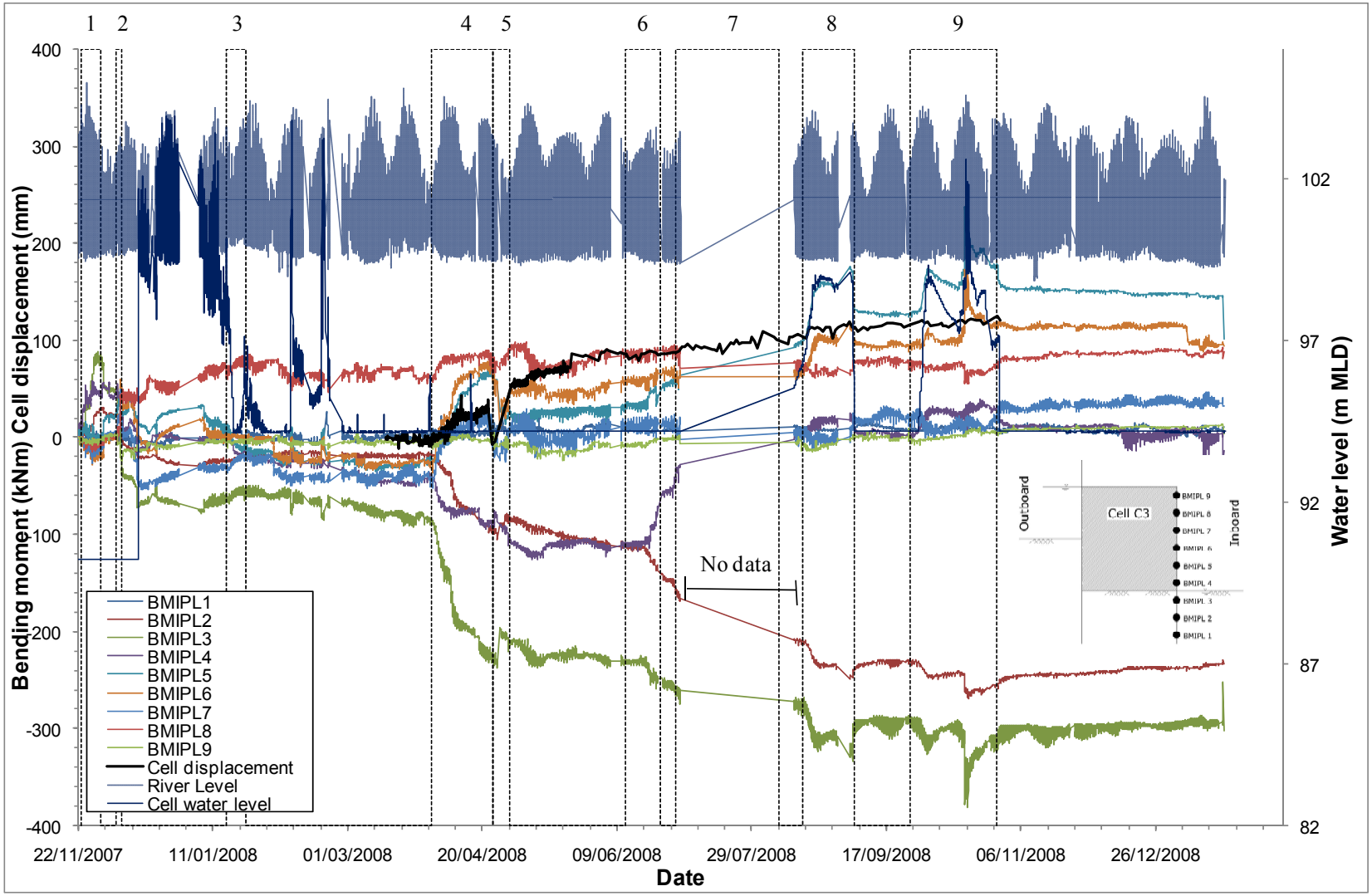

Figure 7-16: Bending moment in inner pile, cell displacement, river and cell water levels (for detail of construction stages see Table 7-2

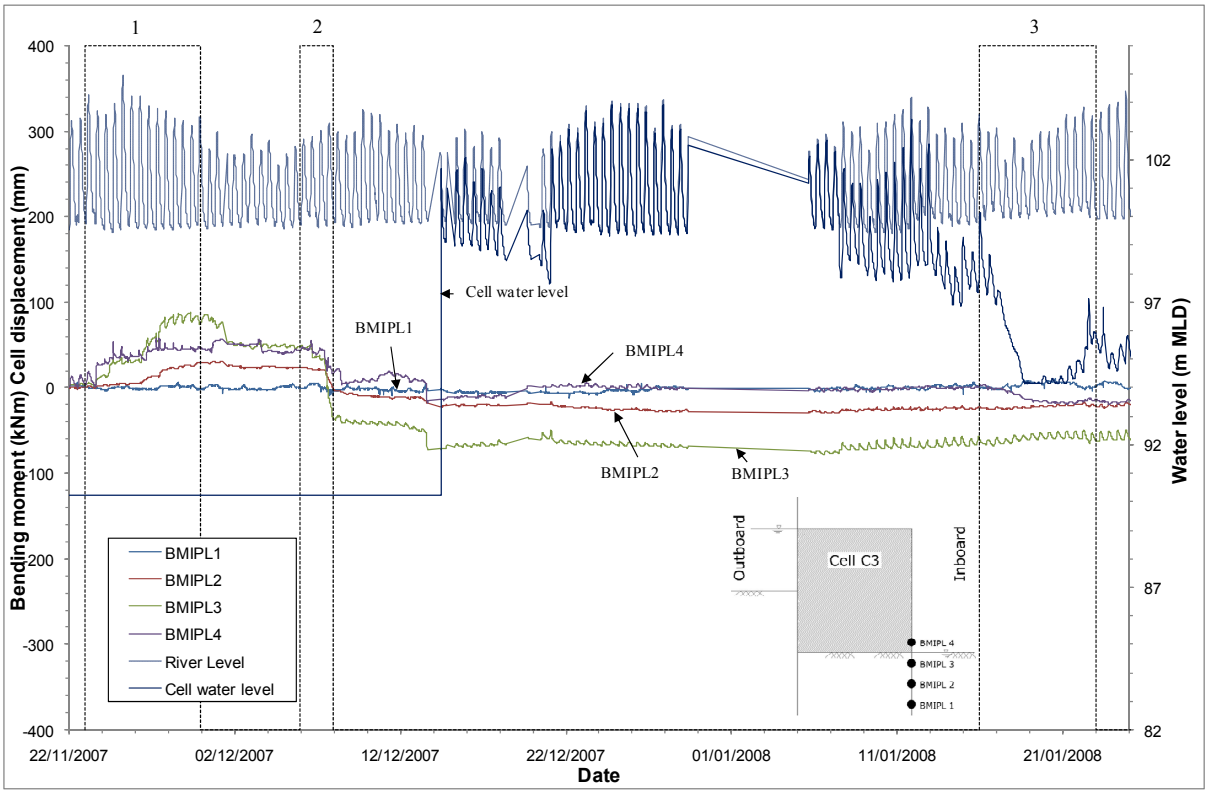

Figure 7-17: Bending moments in inner pile during stages 1, 2, and 3 for gauges 1 to 4

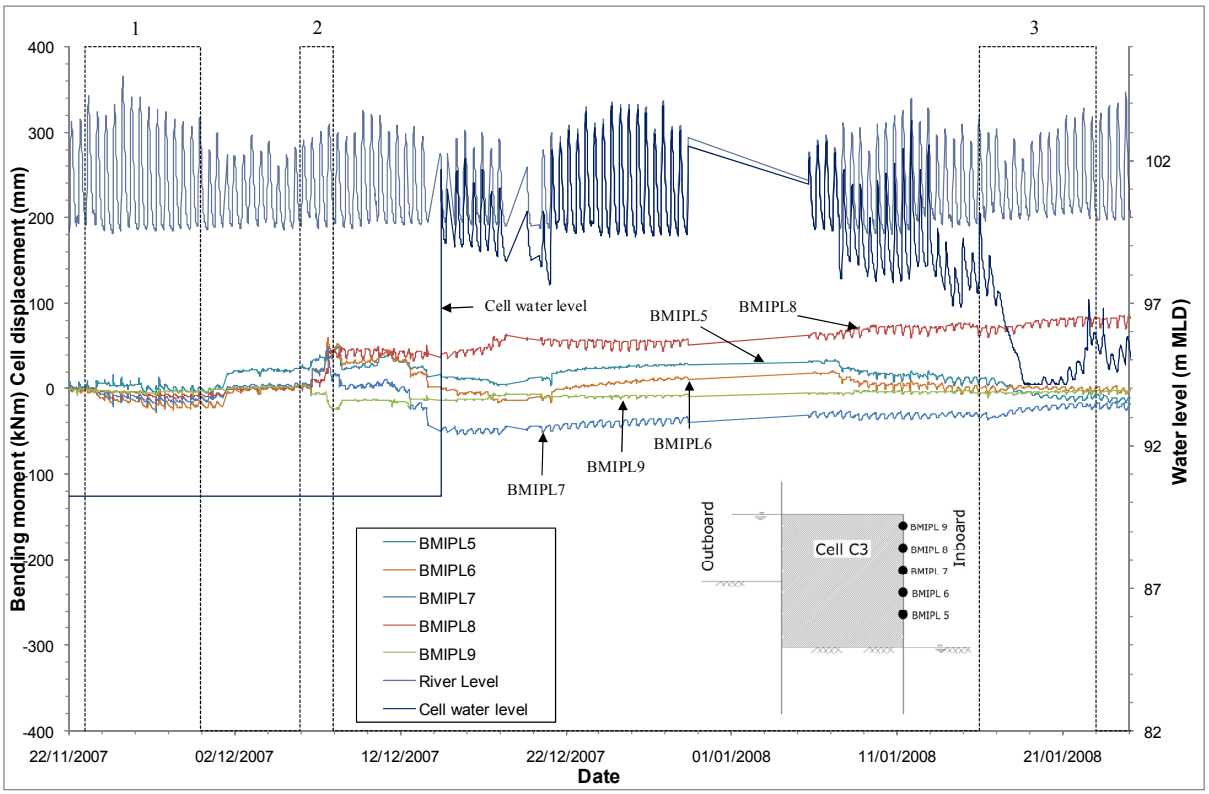

Figure 7-18: Bending moments in inner pile during stages 1, 2 and 3 for gauges 5 to 9

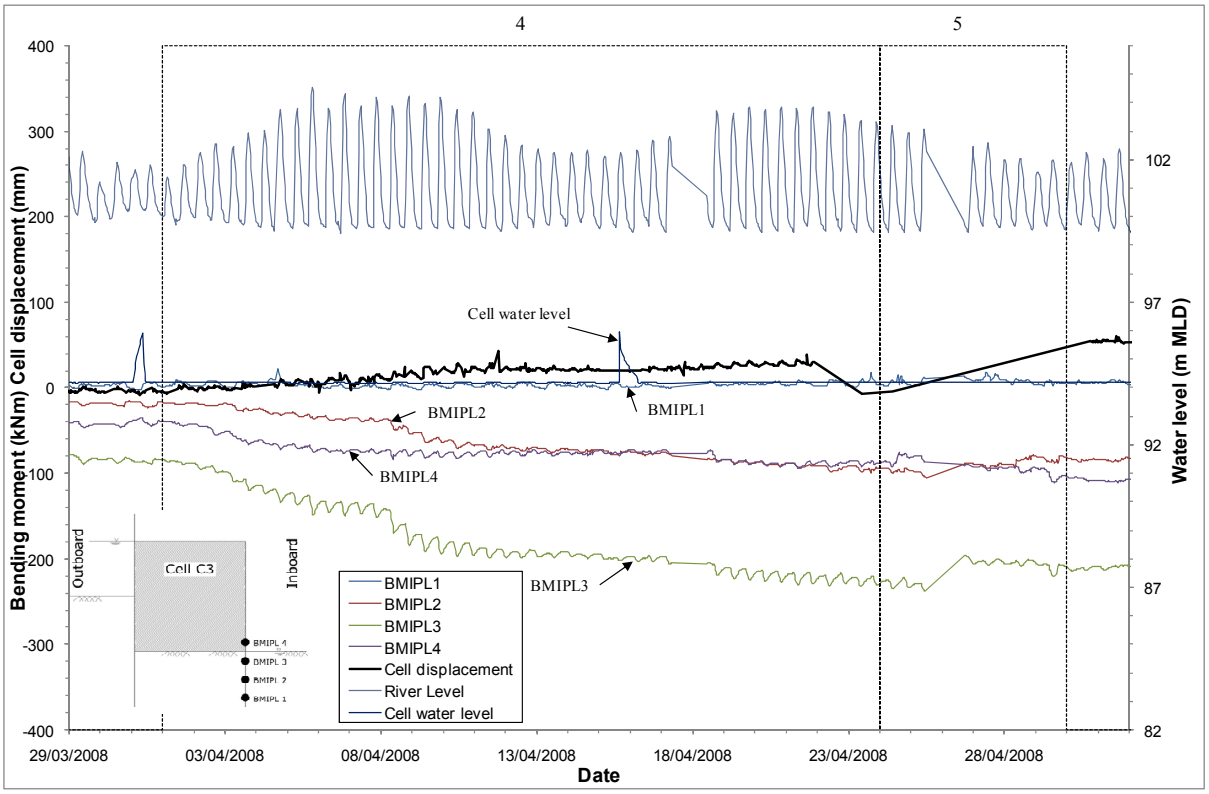

Figure 7-19: Bending moments in inner pile during stages 4 and 5 for gauges 1 to 4

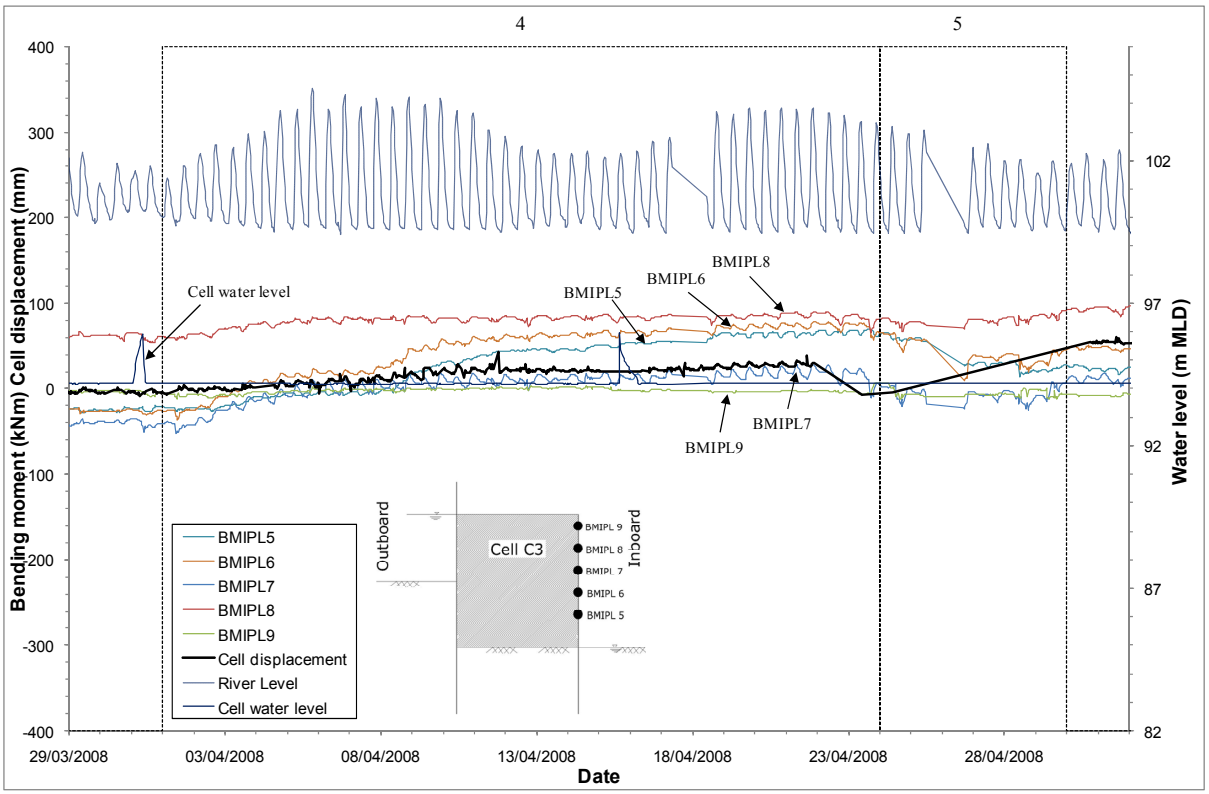

Figure 7-20: Bending moments in inner pile during stages 4 and 5 for gauges 5 to 9

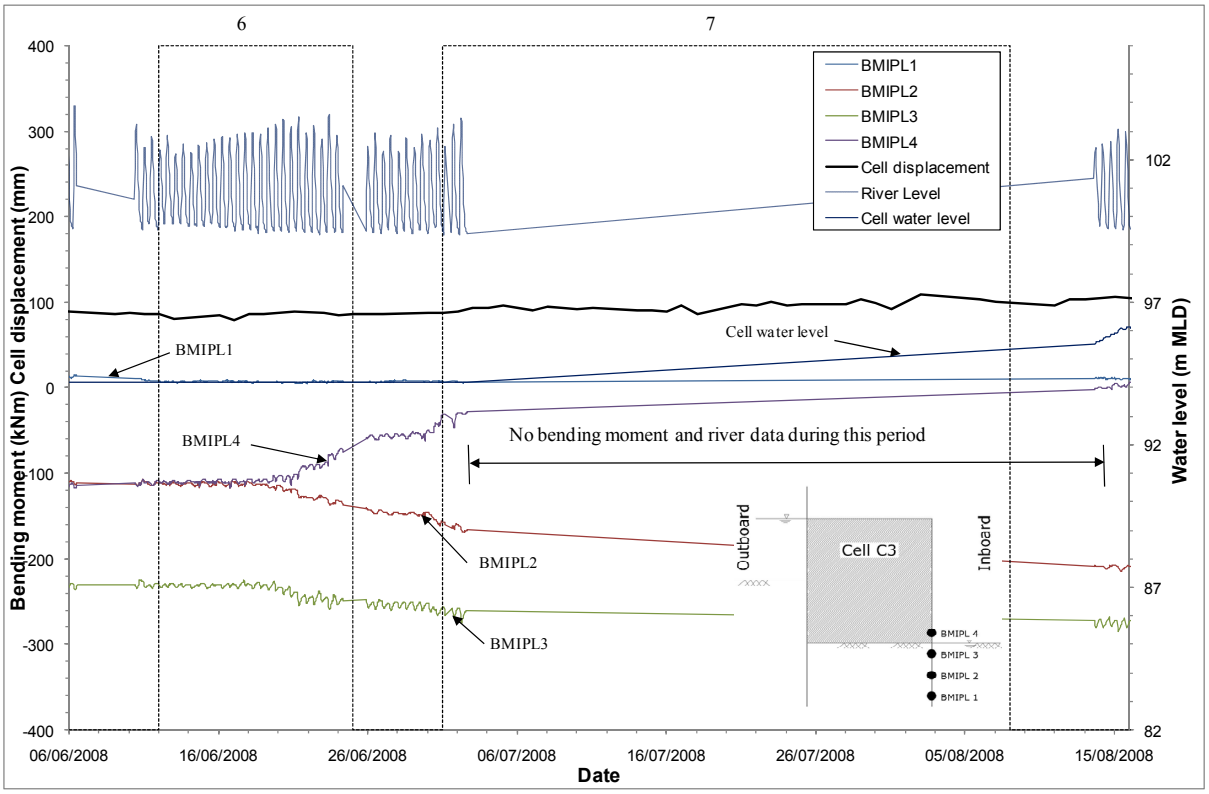

Figure 7-21: Bending moments in inner pile during stages 6 and 7 for gauges 1 to 4

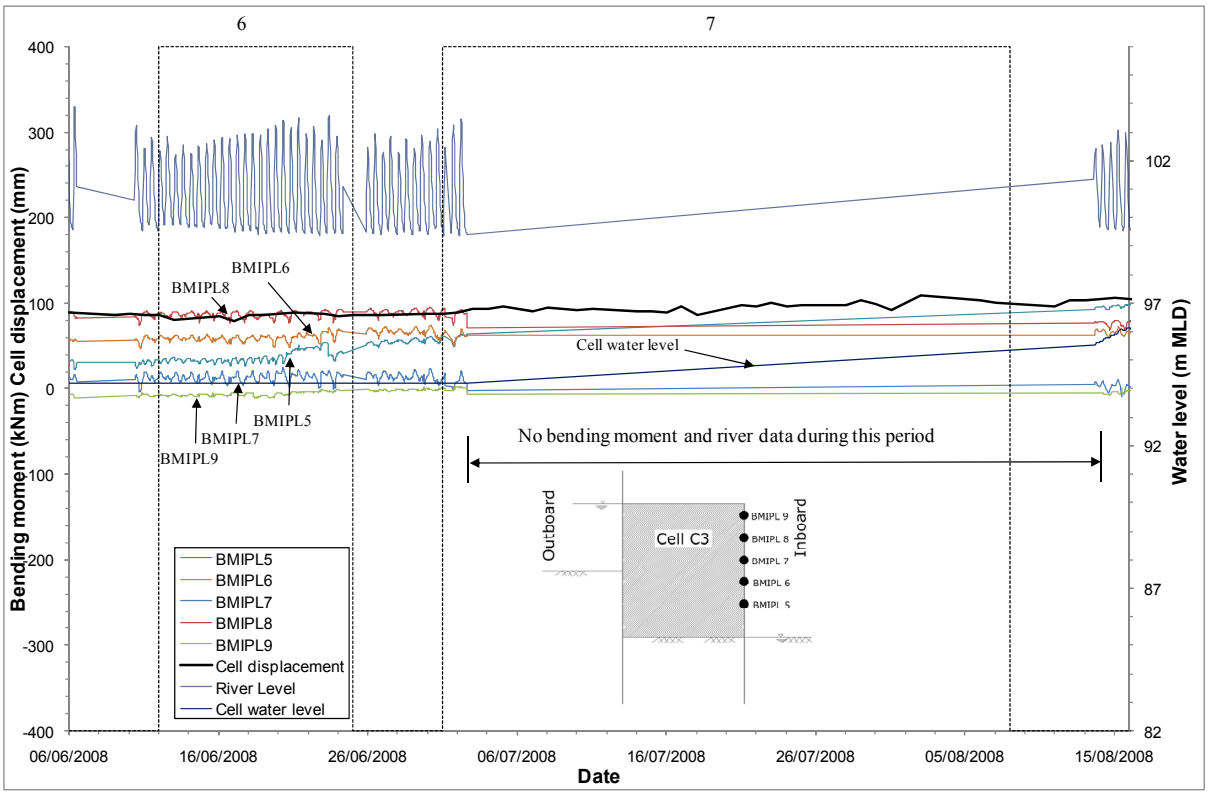

Figure 7-22: Bending moments in inner pile during stages 6 and 7 for gauges 5 to 9

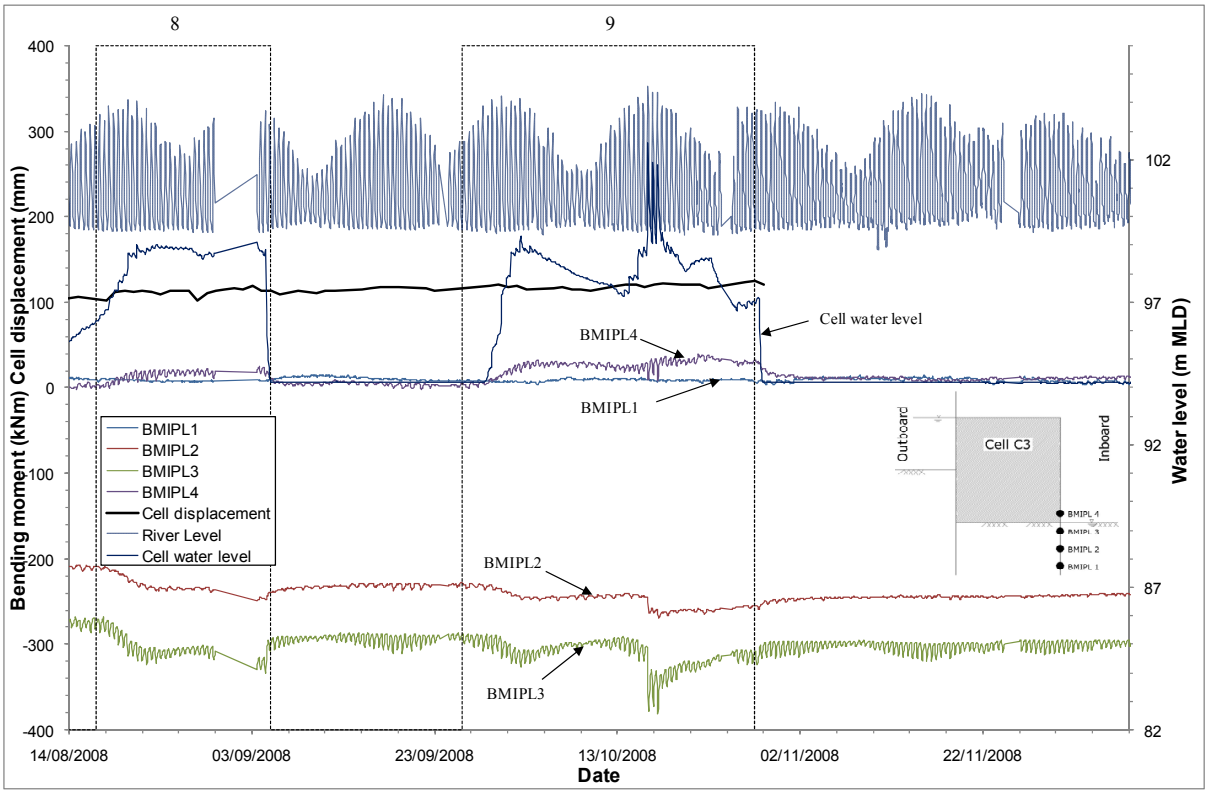

Figure 7-23: Bending moments in inner pile during stages 8 and 9 for gauges 1 to 4

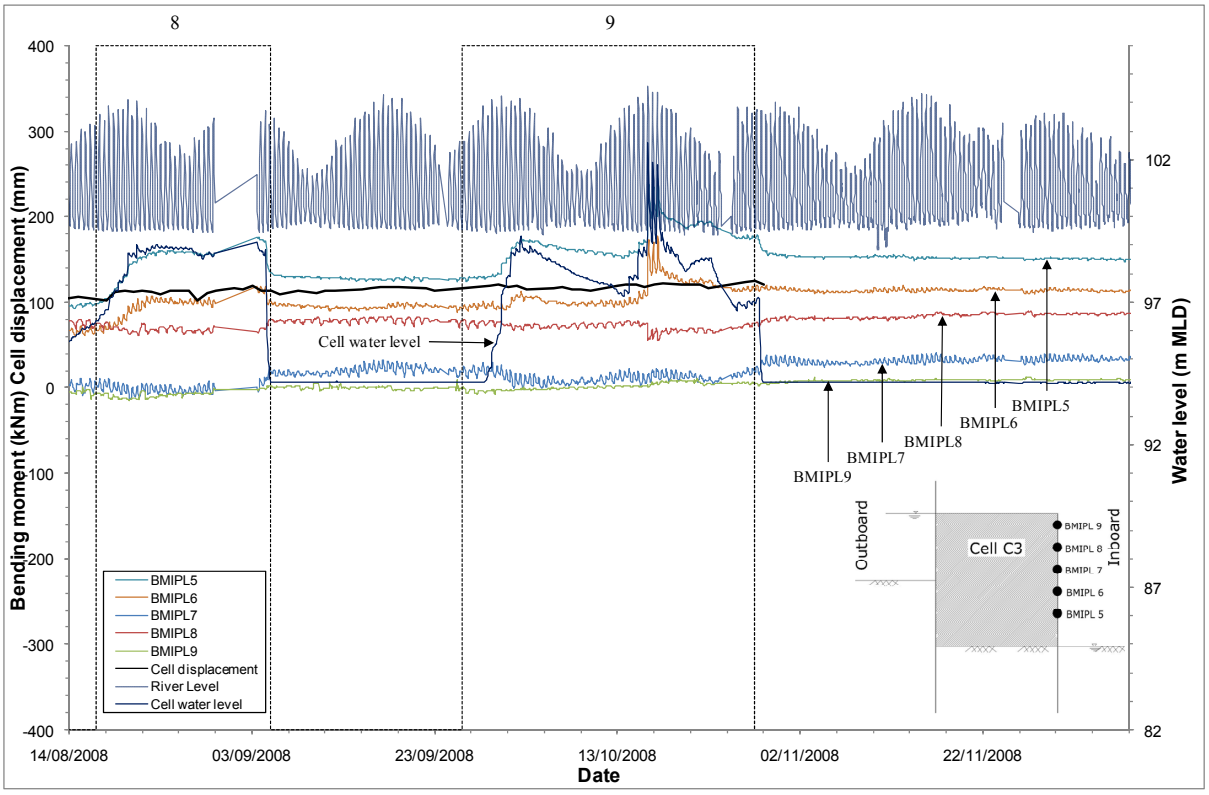

Figure 7-24: Bending moments in inner pile during stages 8 and 9 for gauges 5 to 9

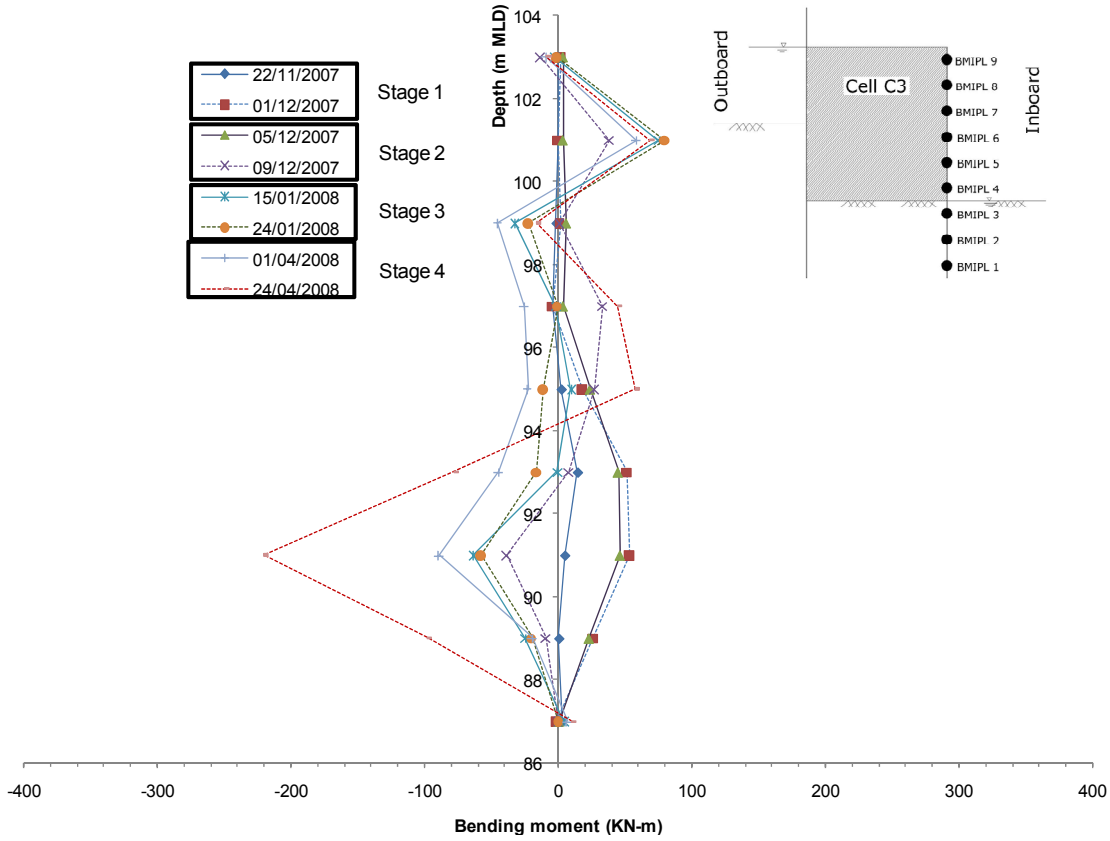

Figure 7-25: Bending moment profile for inboard pile (stages 1 to 4)

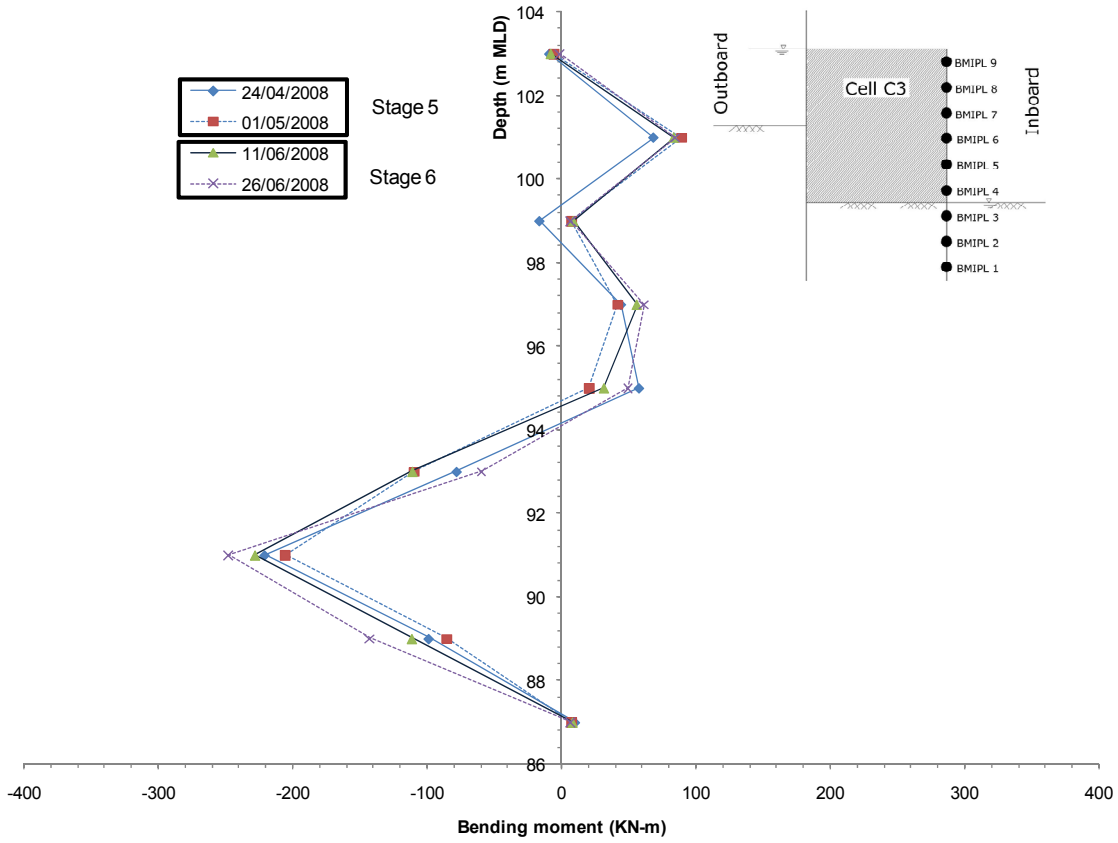

Figure 7-26: Bending moment profile for inboard pile (stages 5 to 6)

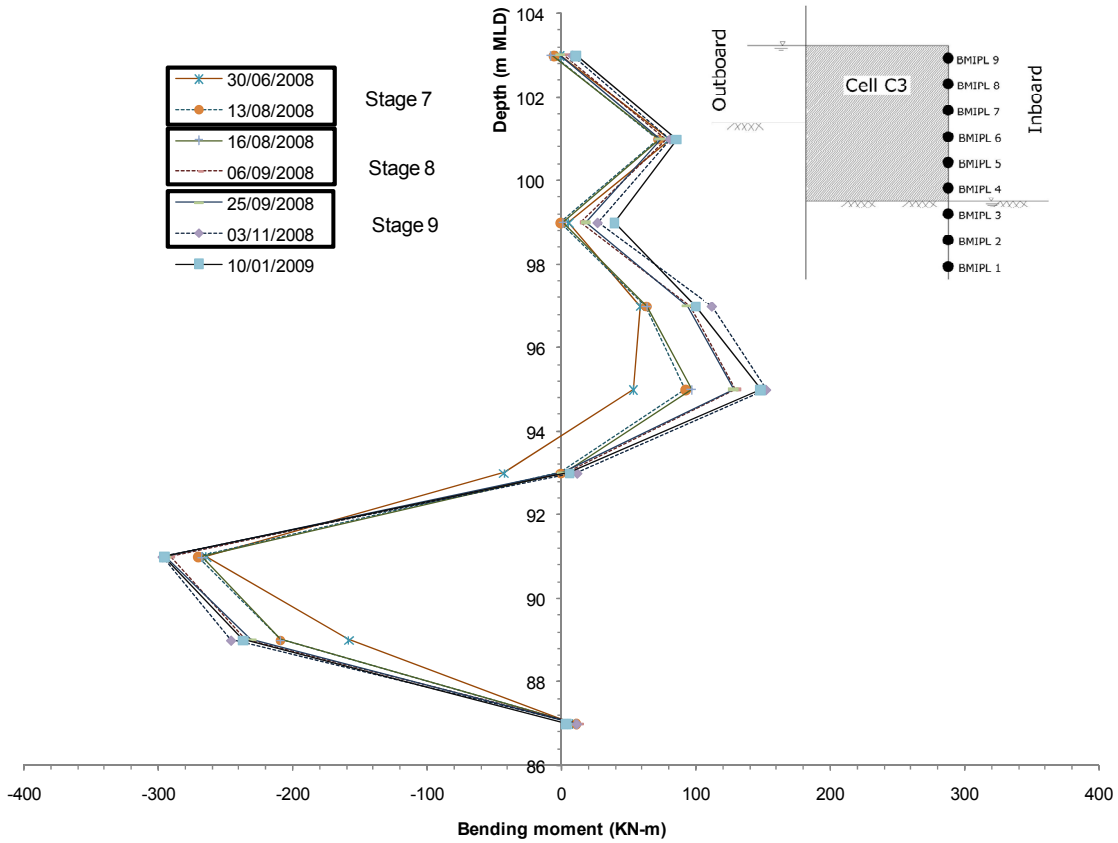

Figure 7-27: Bending moment profile for inboard pile (stages 7 to 9)

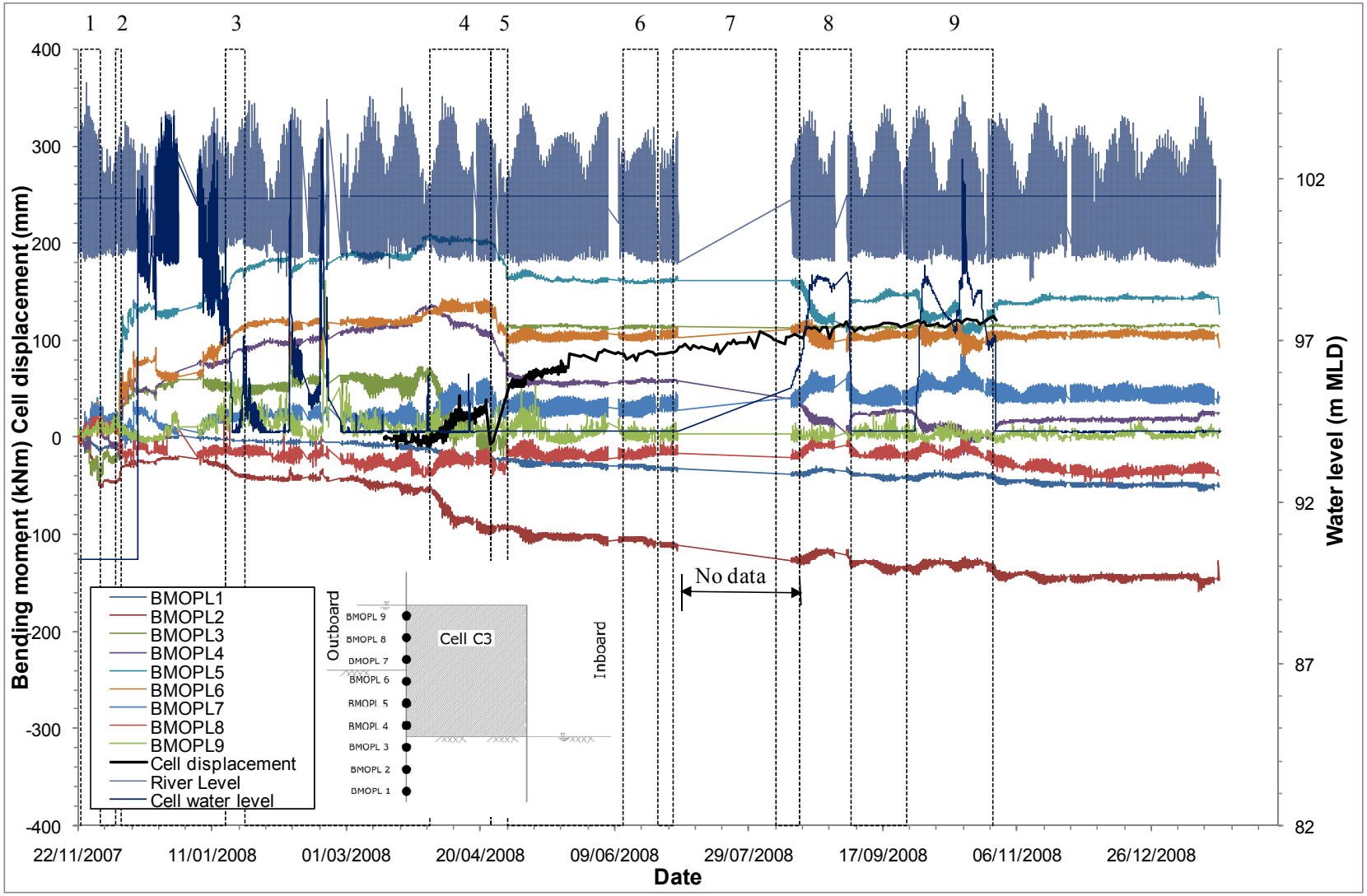

Figure 7-28: Bending moment in outer pile, displacement, river and cell water levels (for detail of construction stages see Table 7-2

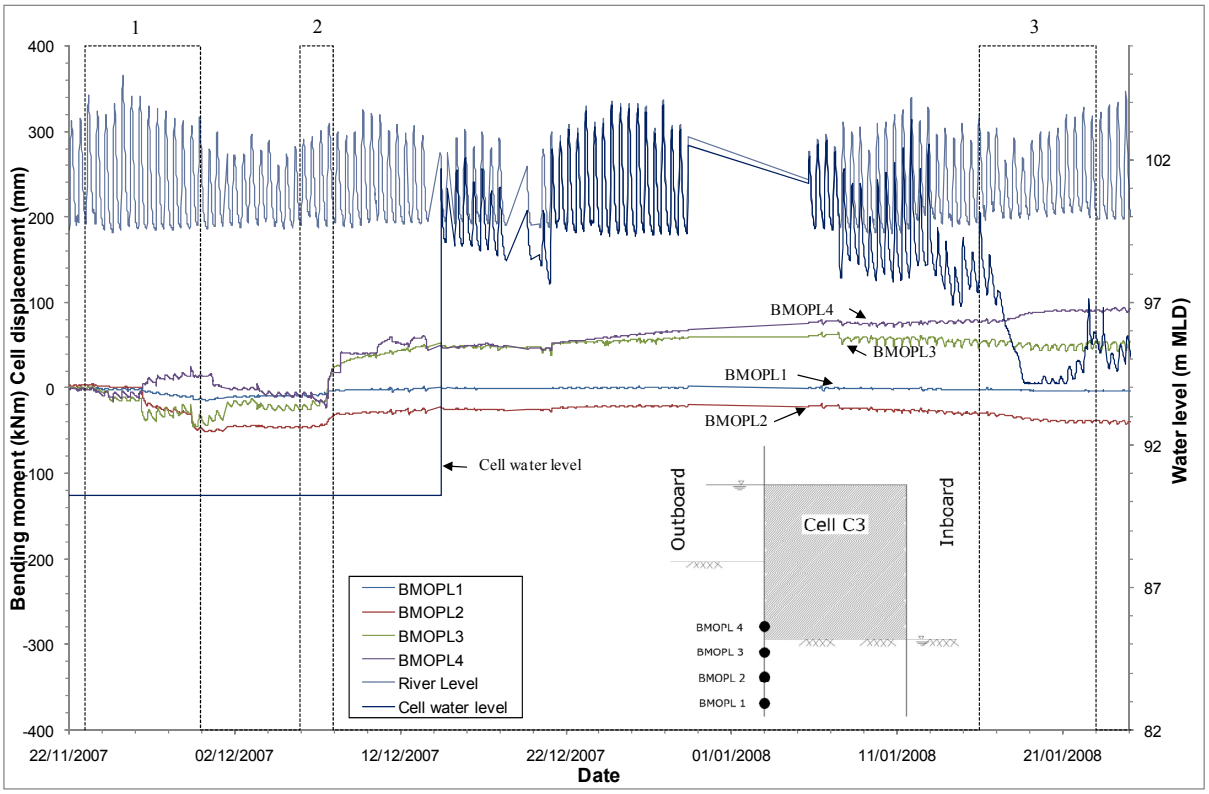

Figure 7-29: Bending moments in outer pile during stages 1, 2 and 3 for gauges 1 to 4

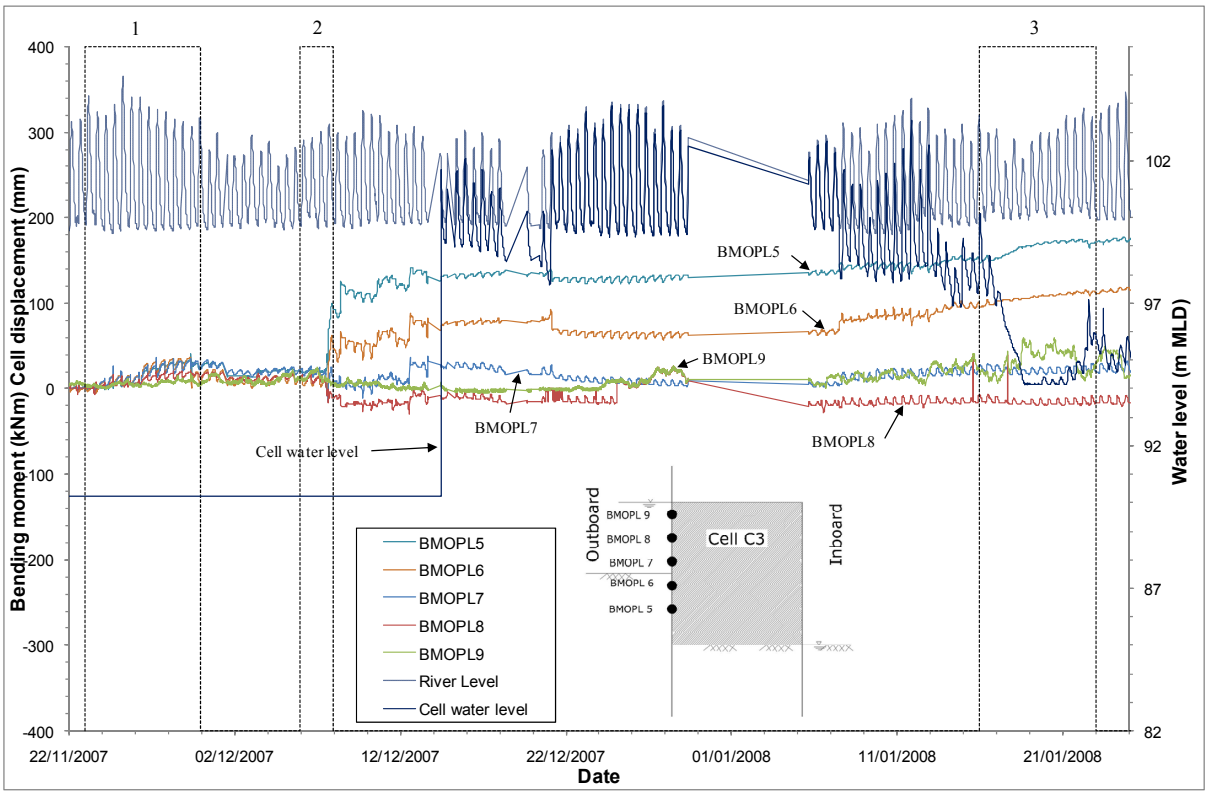

Figure 7-30: Bending moments in outer pile during stages 1, 2 and 3 for gauges 5 to 9

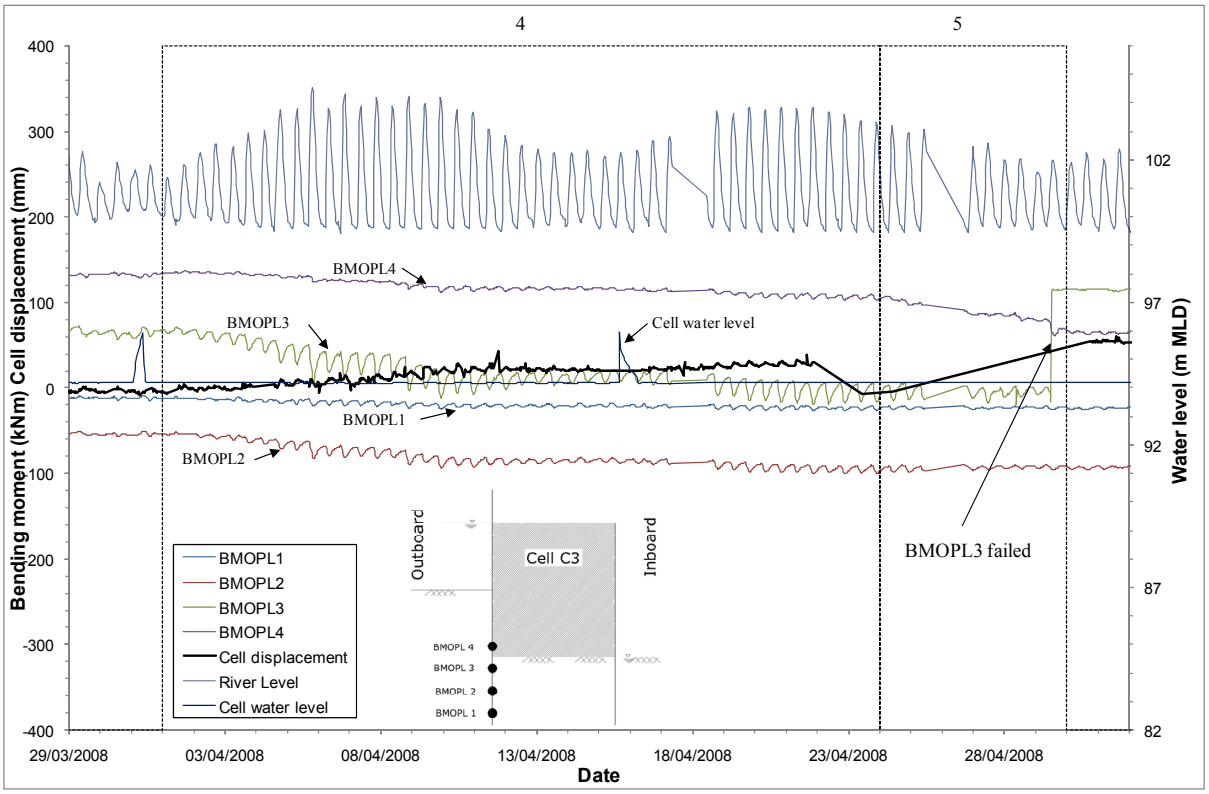

Figure 7-31: Bending moments in outer pile during stages 4 and 5 for gauges 1 to 4

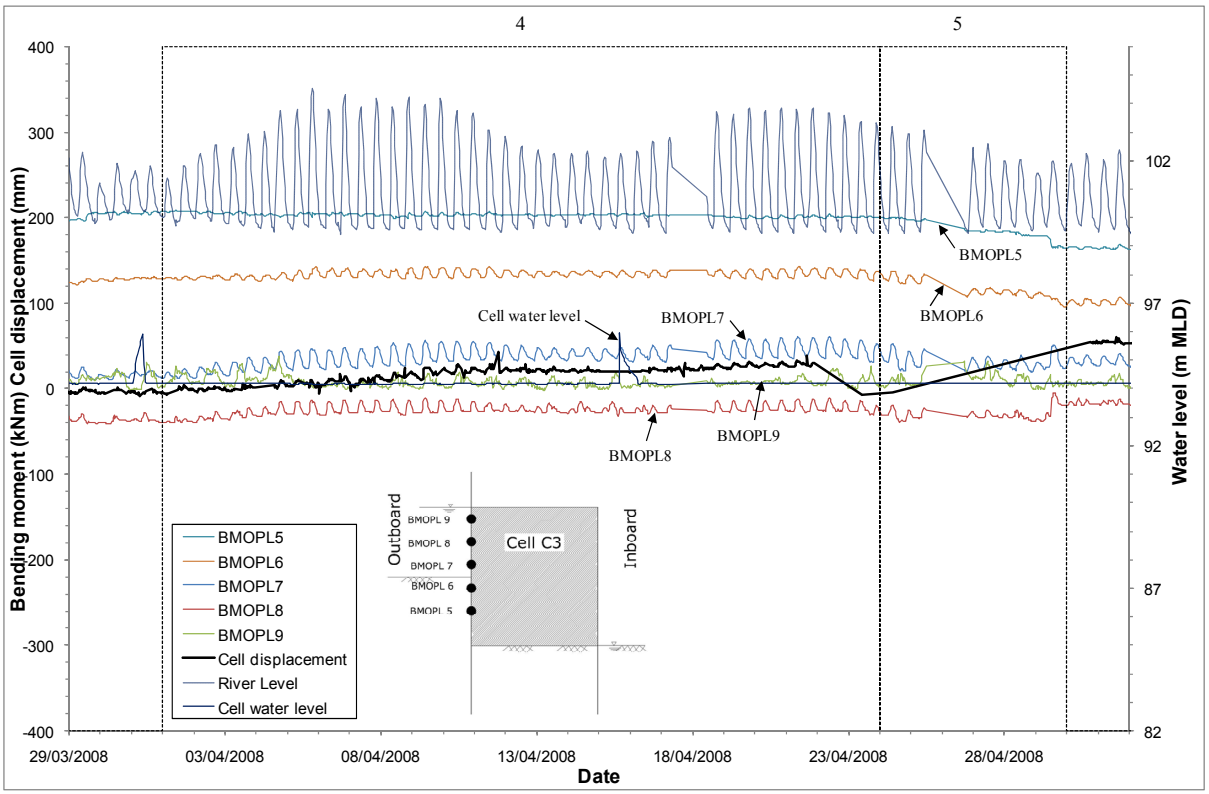

Figure 7-32: Bending moments in outer pile during stages 4 and 5 for gauges 5 to 9

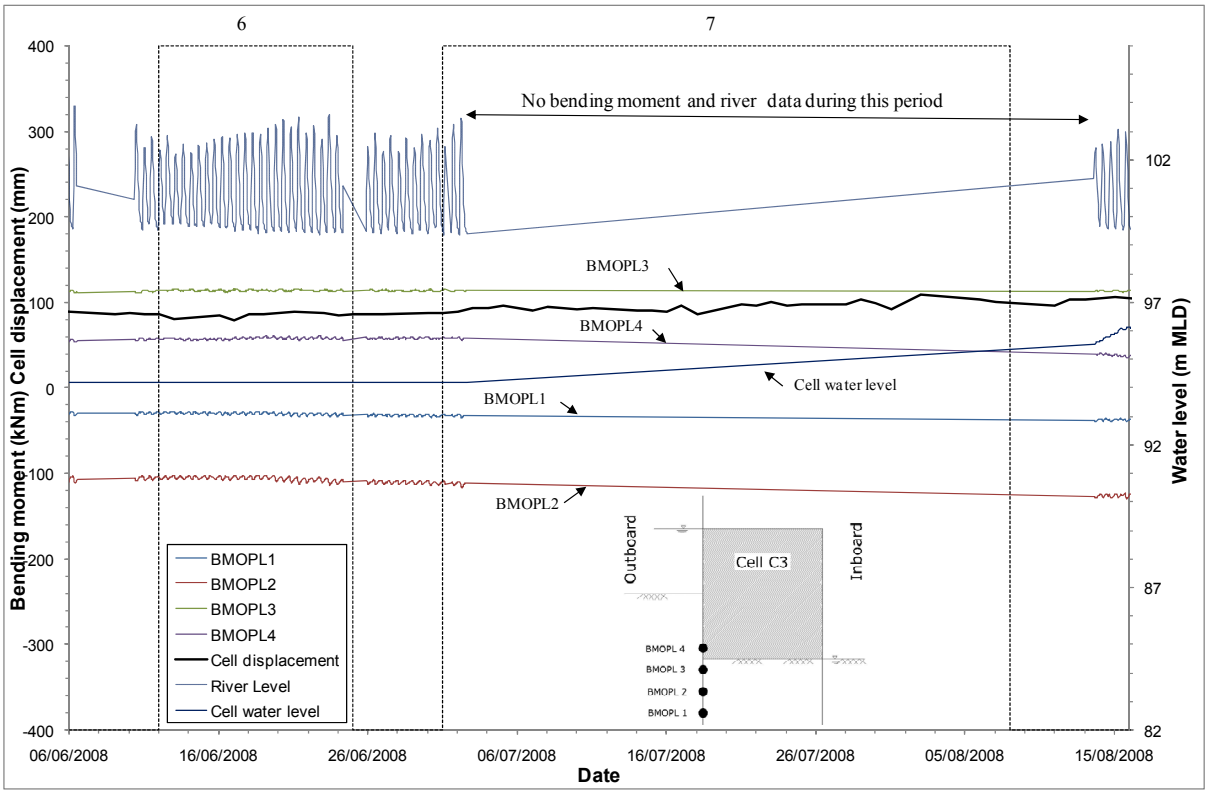

Figure 7-33: Bending moments in outer pile during stages 6 and 7 for gauges 1 to 4

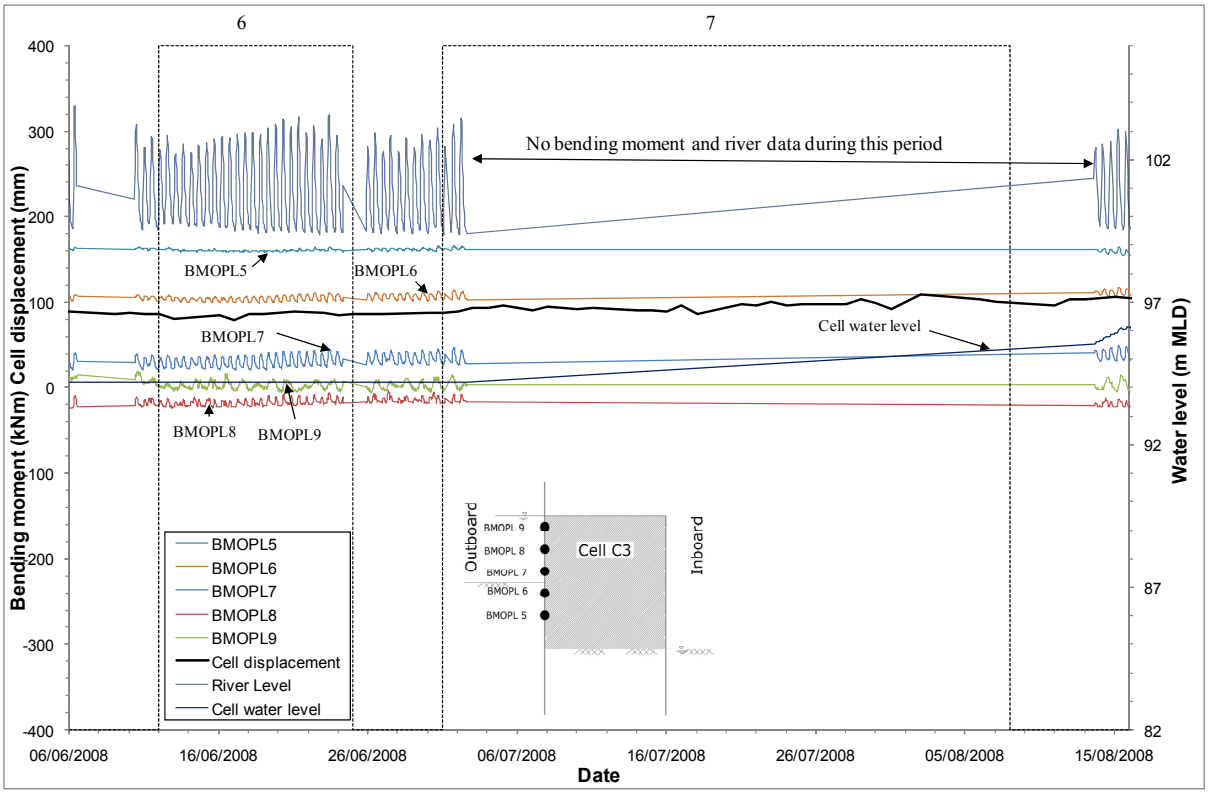

Figure 7-34: Bending moments in outer pile during stages 6 and 7 for gauges 5 to 9

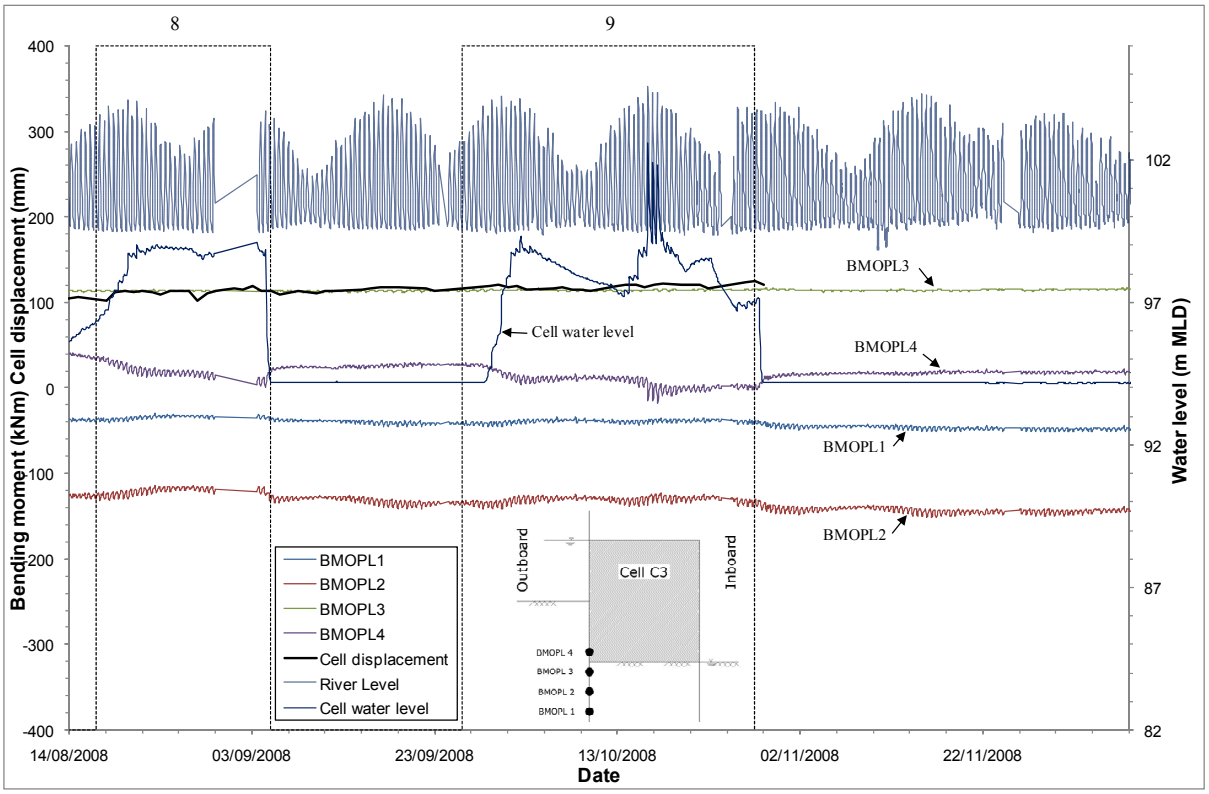

Figure 7-35: Bending moments in outer pile during stages 8 and 9 for gauges 1 to 4

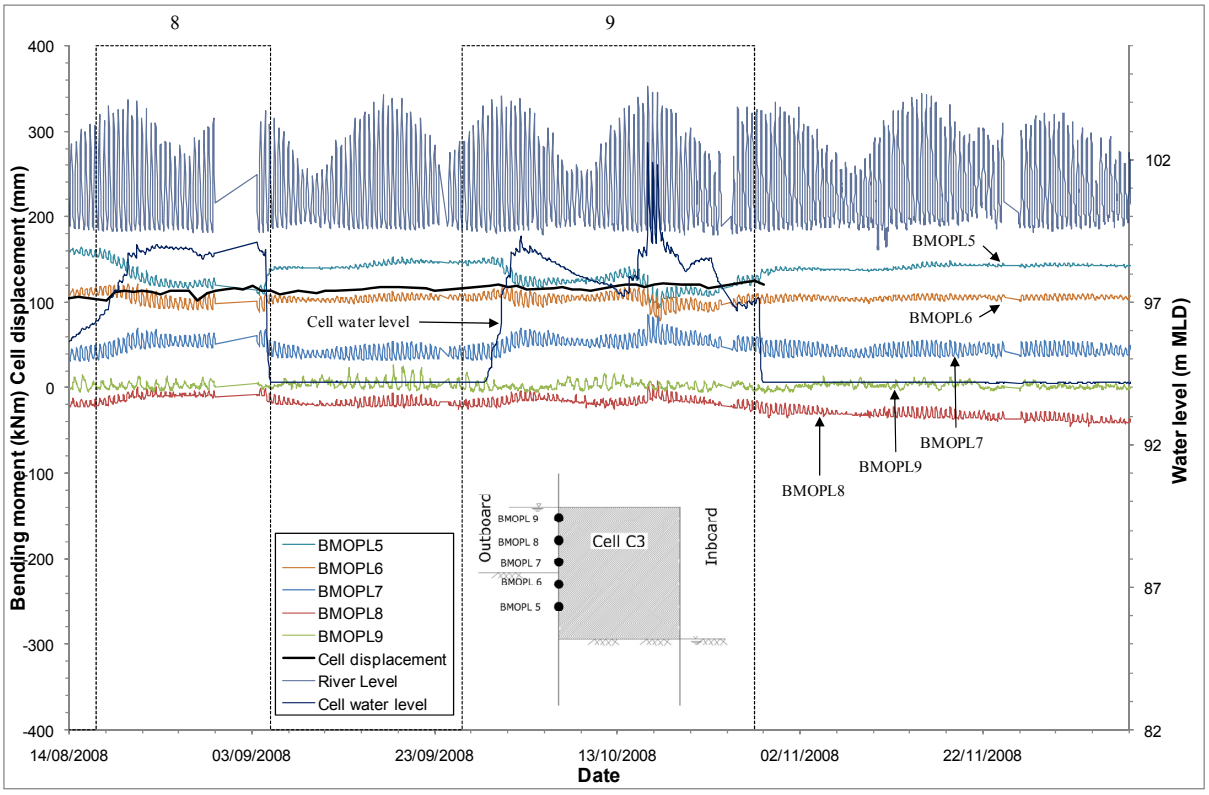

Figure 7-36: Bending moments in outer pile during stages 8 and 9 for gauges 5 to 9

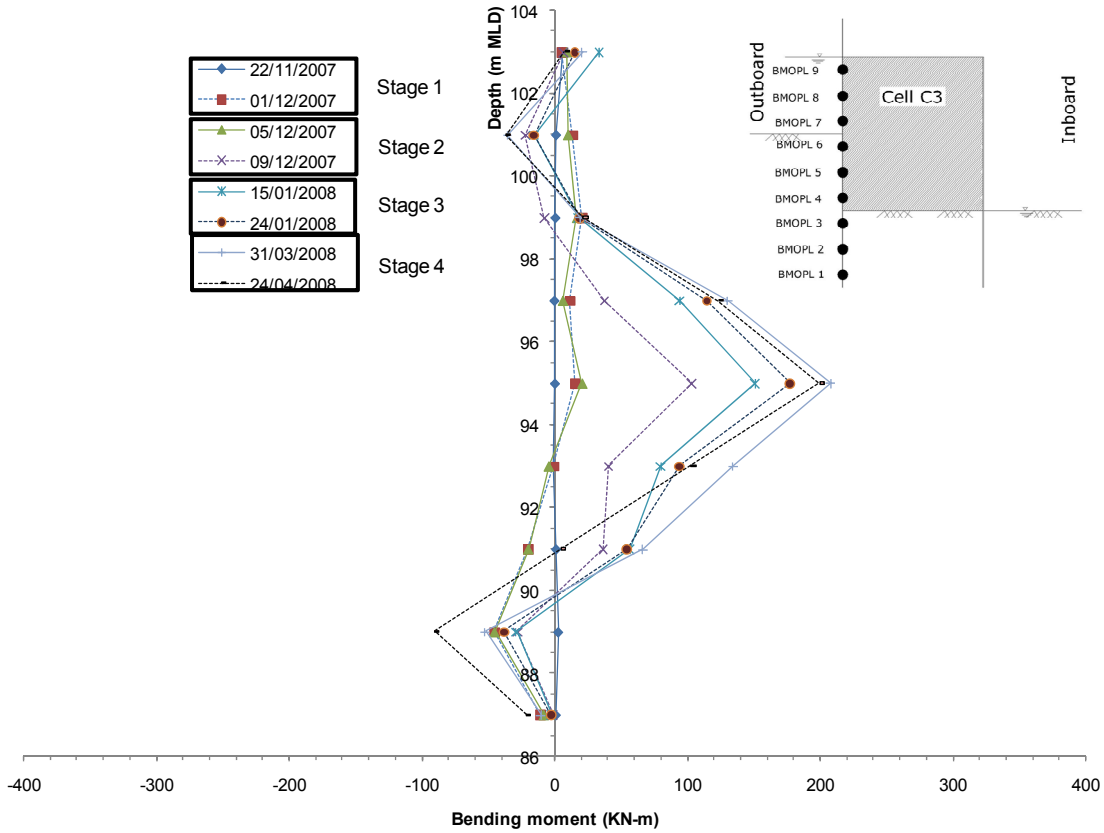

Figure 7-37: Bending moment profile for outboard pile (stages 1 to 4)

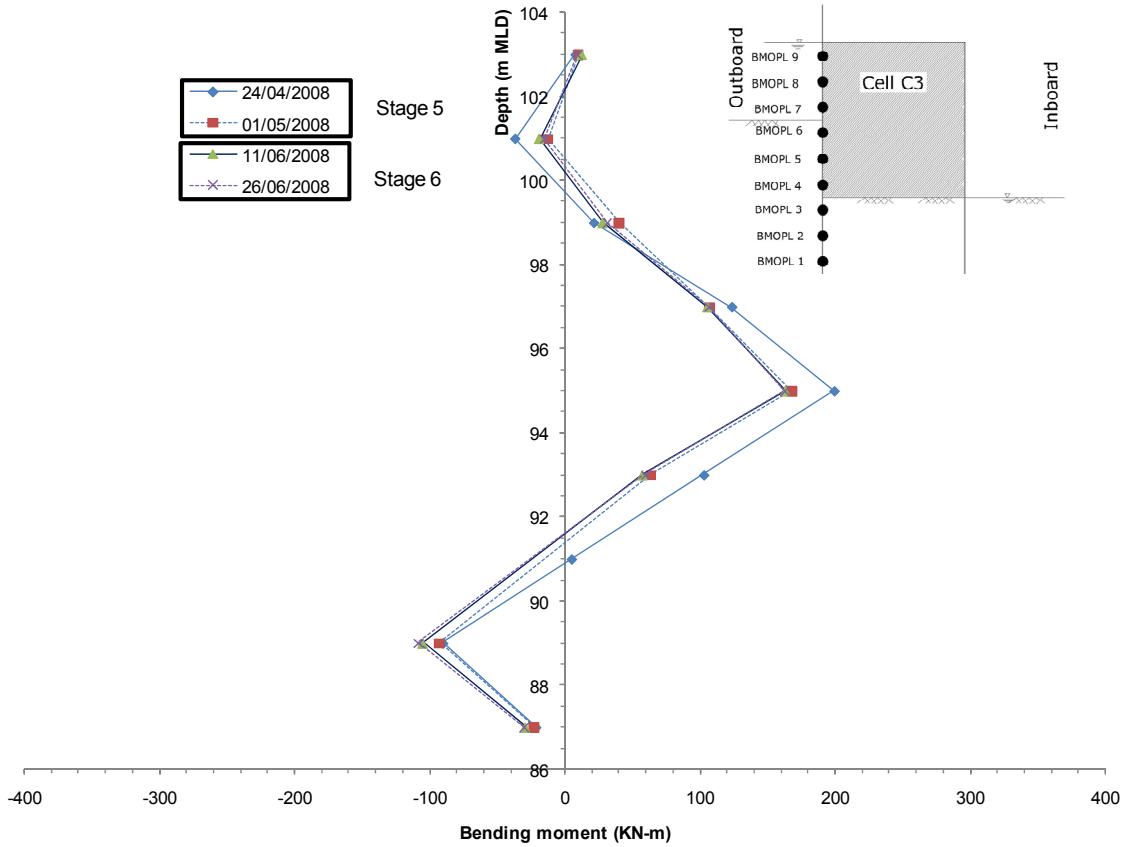

Figure 7-38: Bending moment profile for outboard pile (stages 5 and 6)

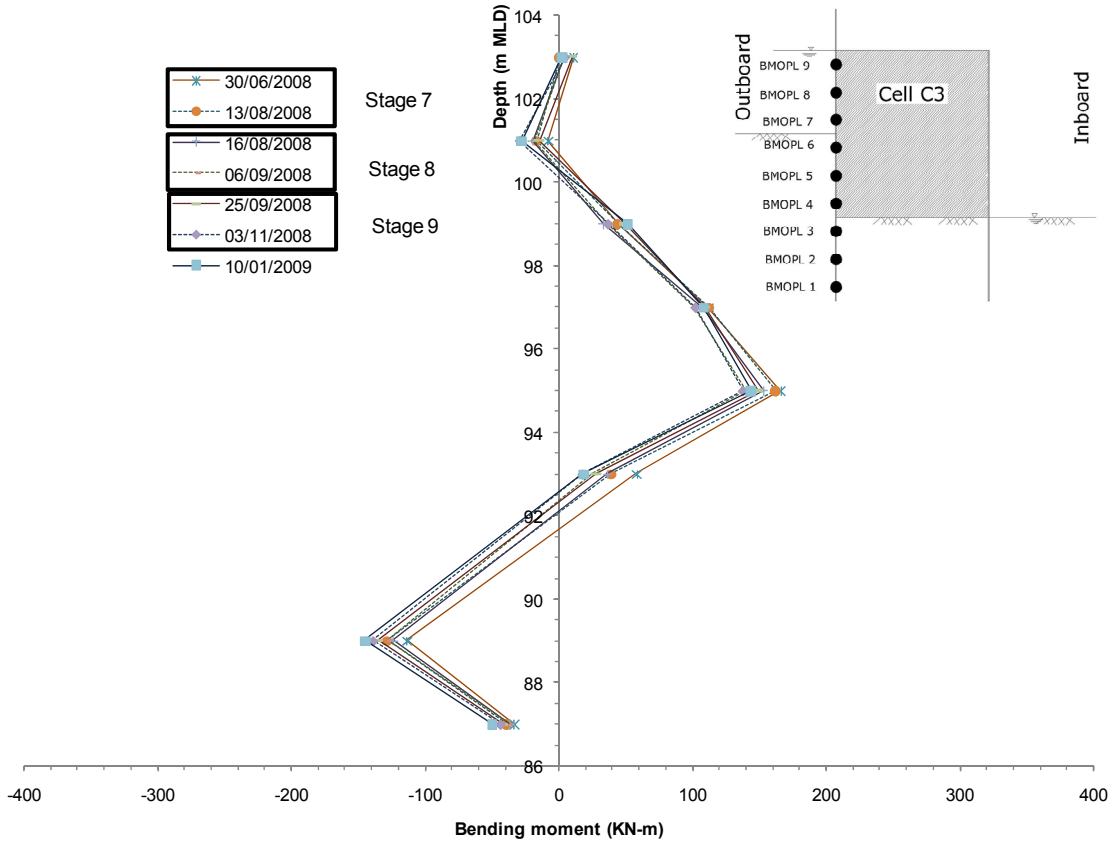

Figure 7-39: Bending moment profile for outboard pile (stages 7 to 9)

Figure 7-40: Water being pumped out of the cofferdam enclosure (10/04/2008)

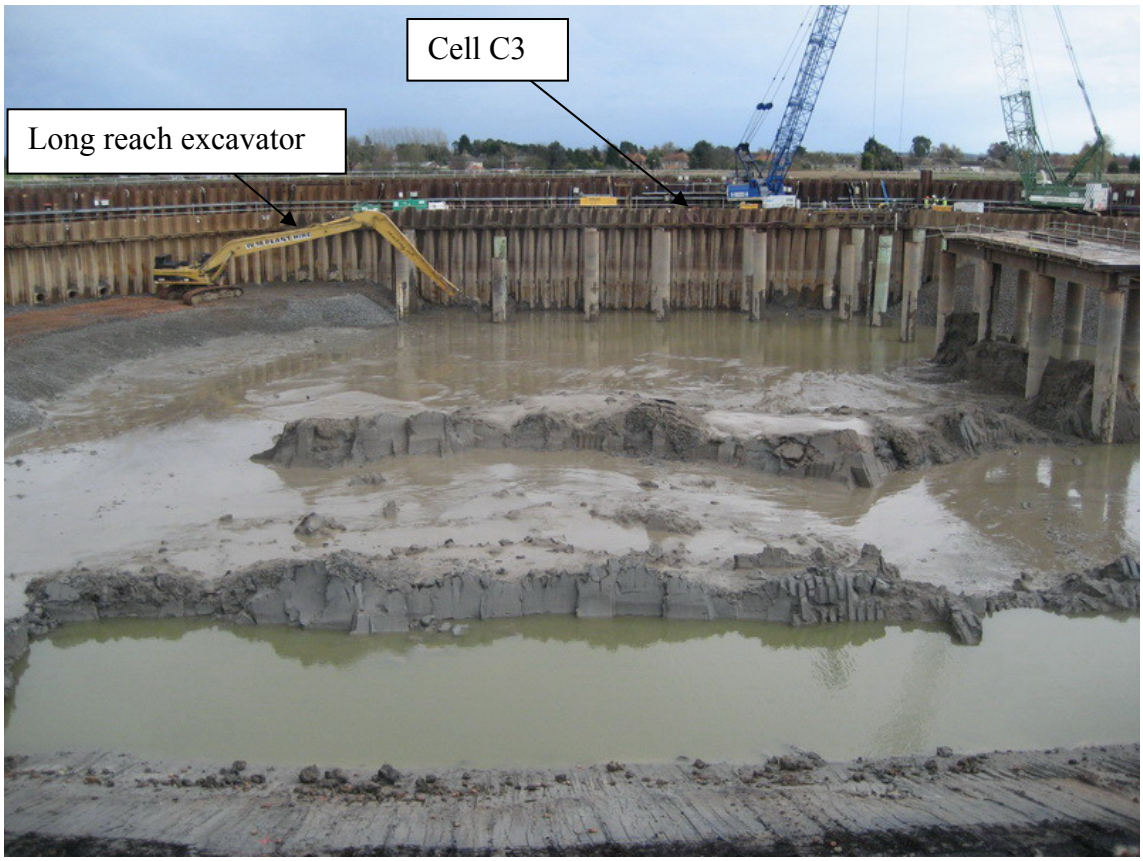

Figure 7-41: Long reach excavator used to excavate down to 94m MLD in front of central cells, i.e. C1 to C4 (11/04/2008)

Figure 7-42: Steel pipes used for jetty are hammered in to facilitate installation CFA piles once the jetty was removed (25/04/2008)

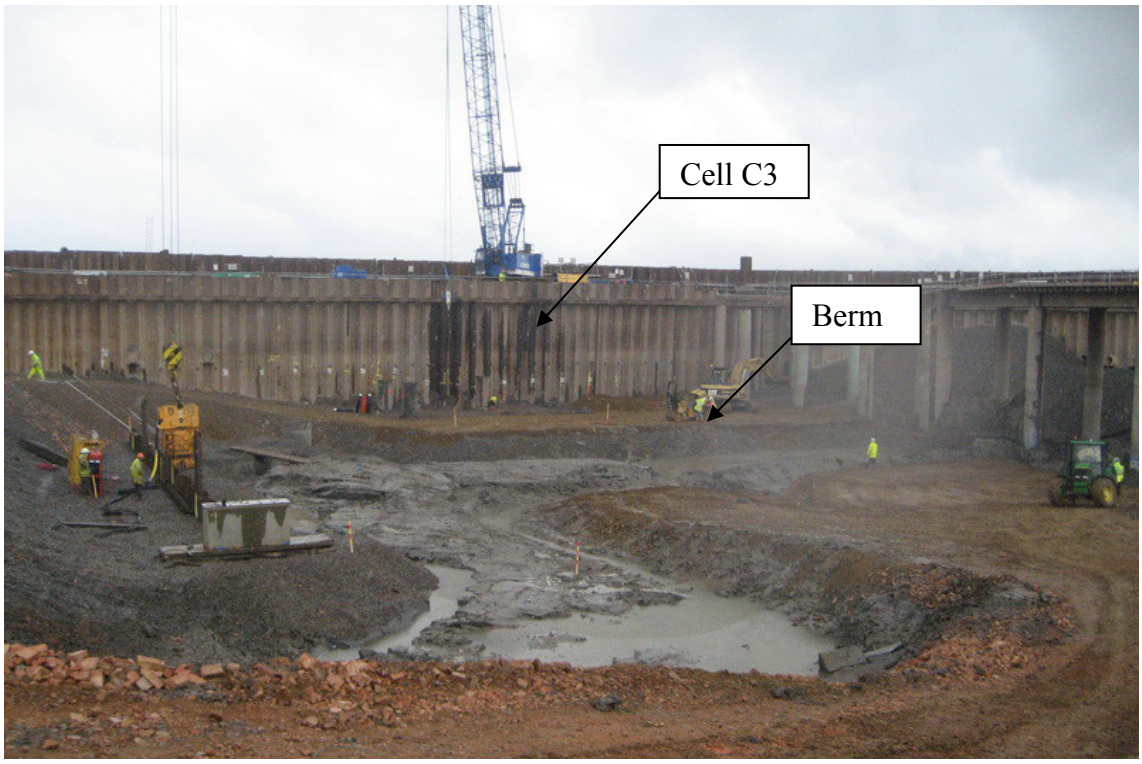

Figure 7-43: Cofferdam dewatering and berm installation complete (30/04/2008)

Figure 7-44: Front jetty connected to walling beam on cell C4 (12/06/2008)

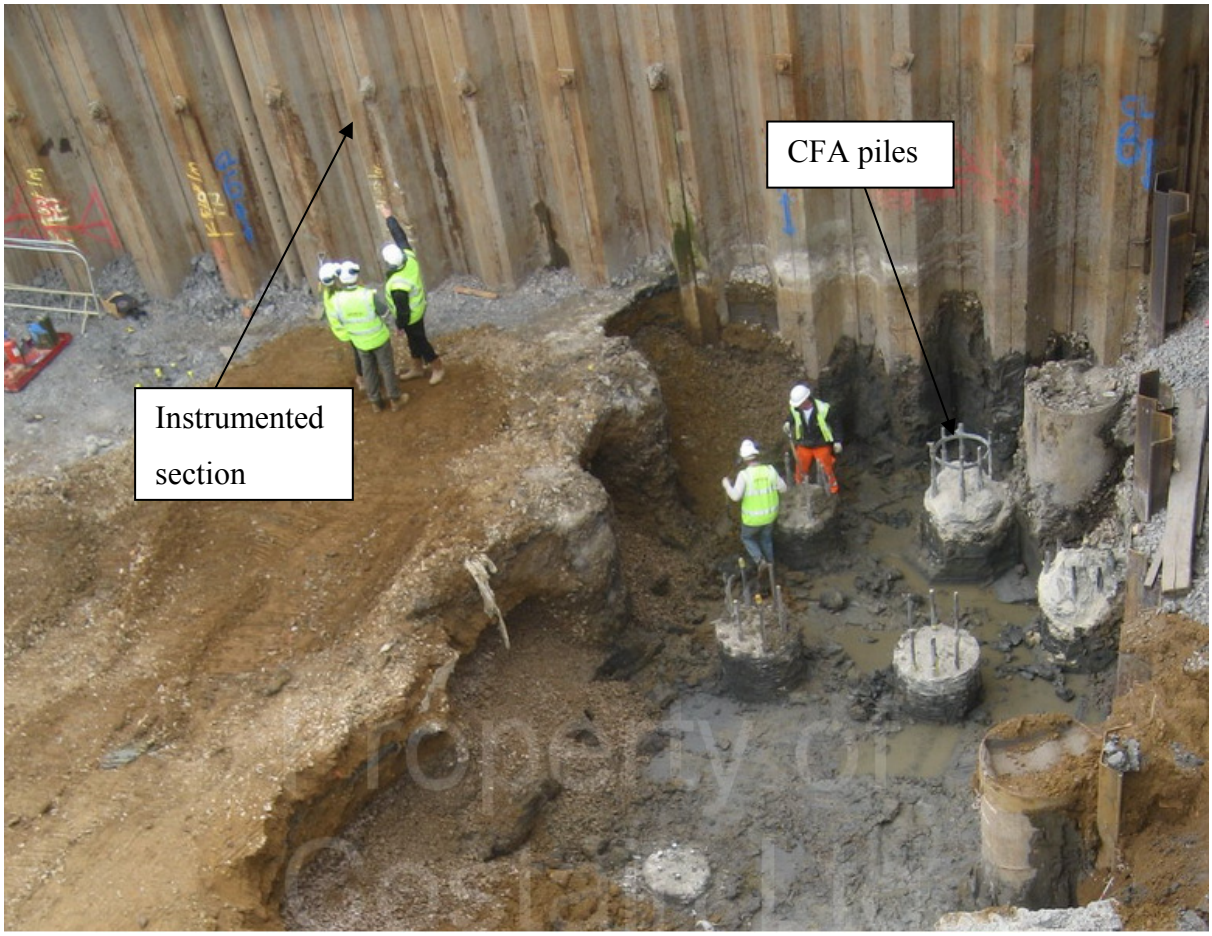

Figure 7-45: Excavation to 92m MLD in front of Cell C3 to facilitate placement of piling mat (16/06/2008)

Figure 7-46: Piling mat completed in front of cell C3 (Date 03/07/2008)

Figure 7-47: Base slab poured (Date 15/07/2008)

Figure 7-48: Pump base completed (Date 18/08/2008)

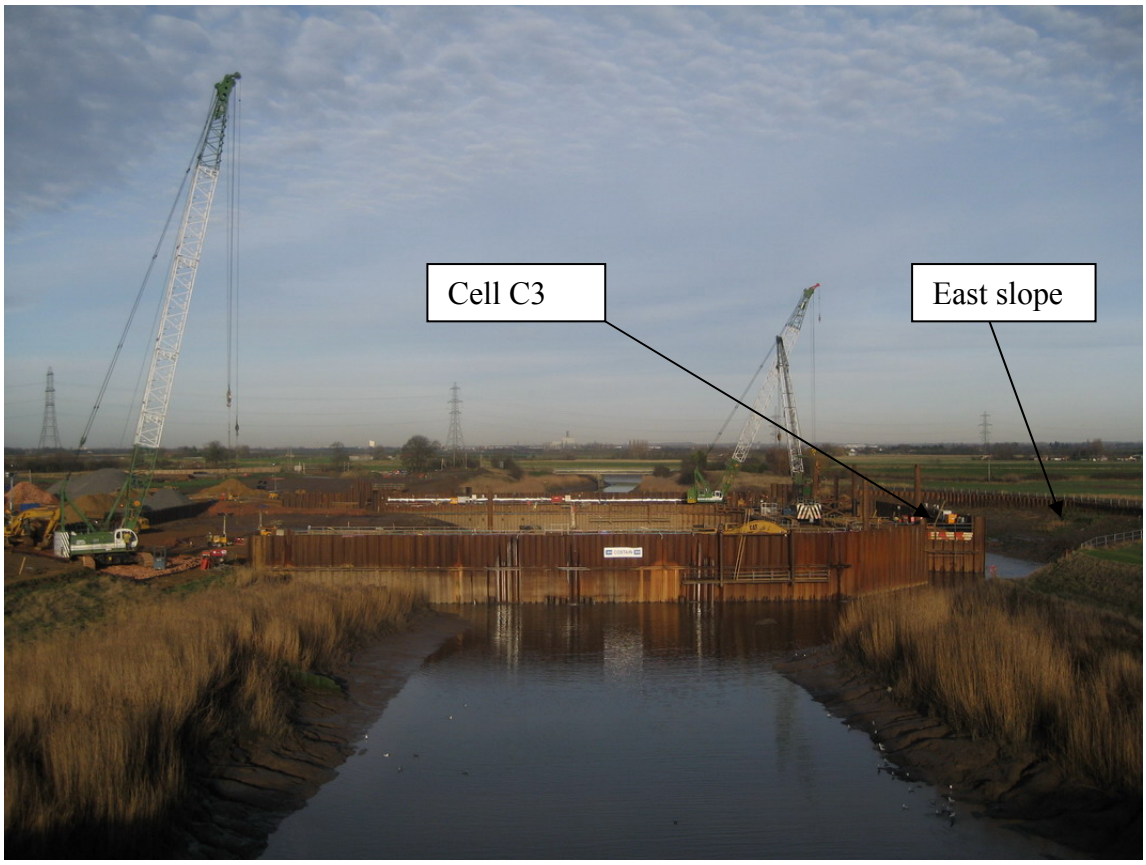

Figure 7-49: East slope and central cells construction

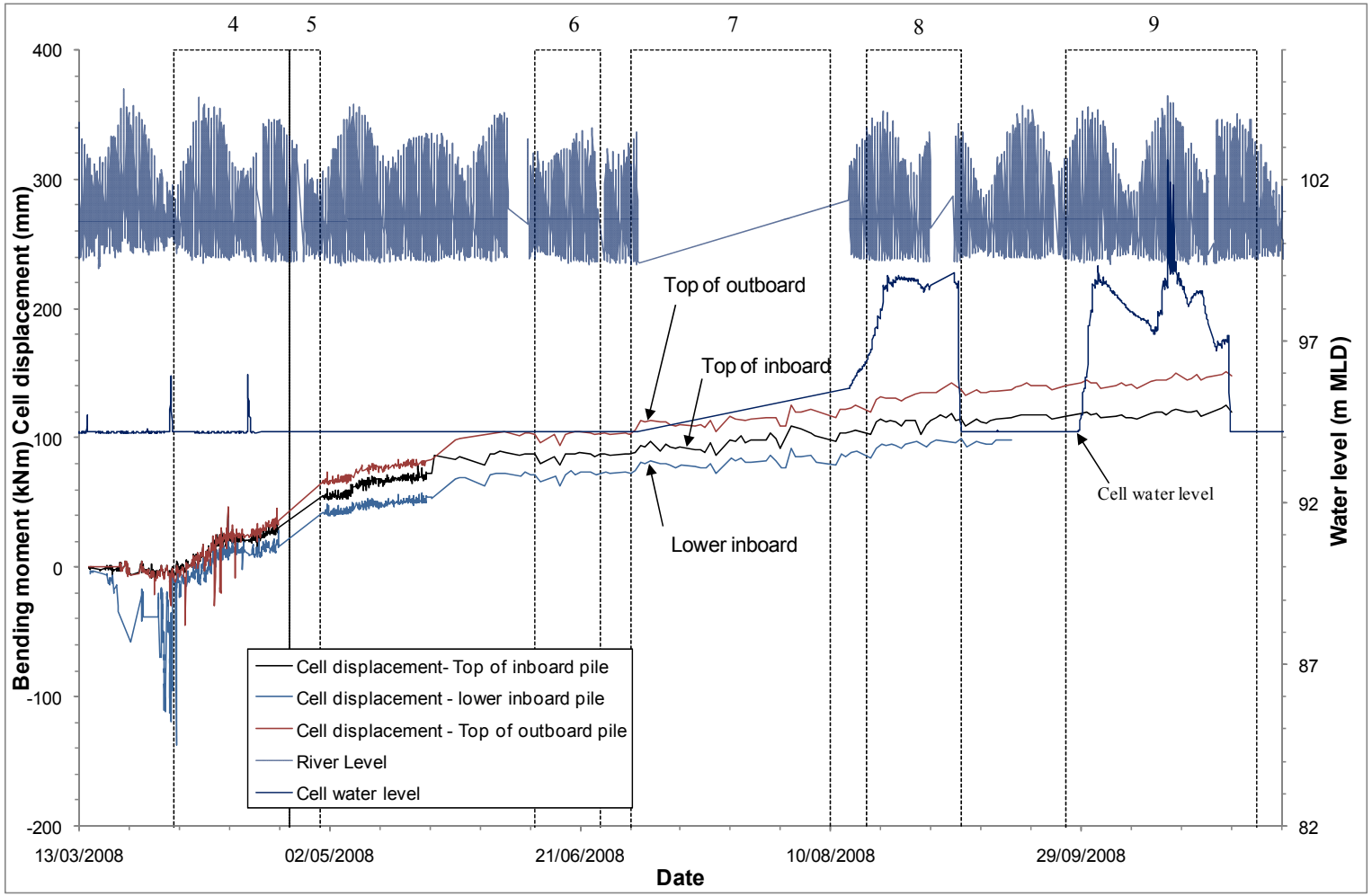

Figure 7-50: Cell displacement for C3

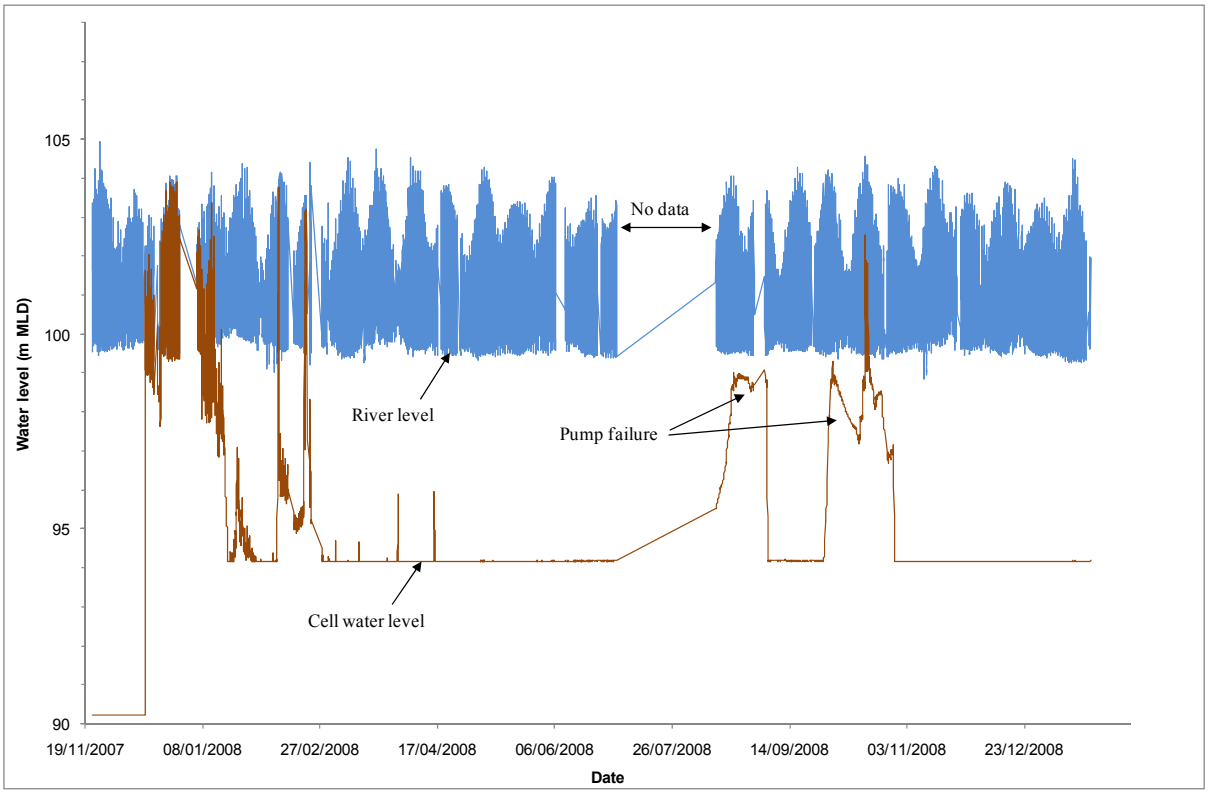

Figure 7-51: Cell (C3) and river water level data

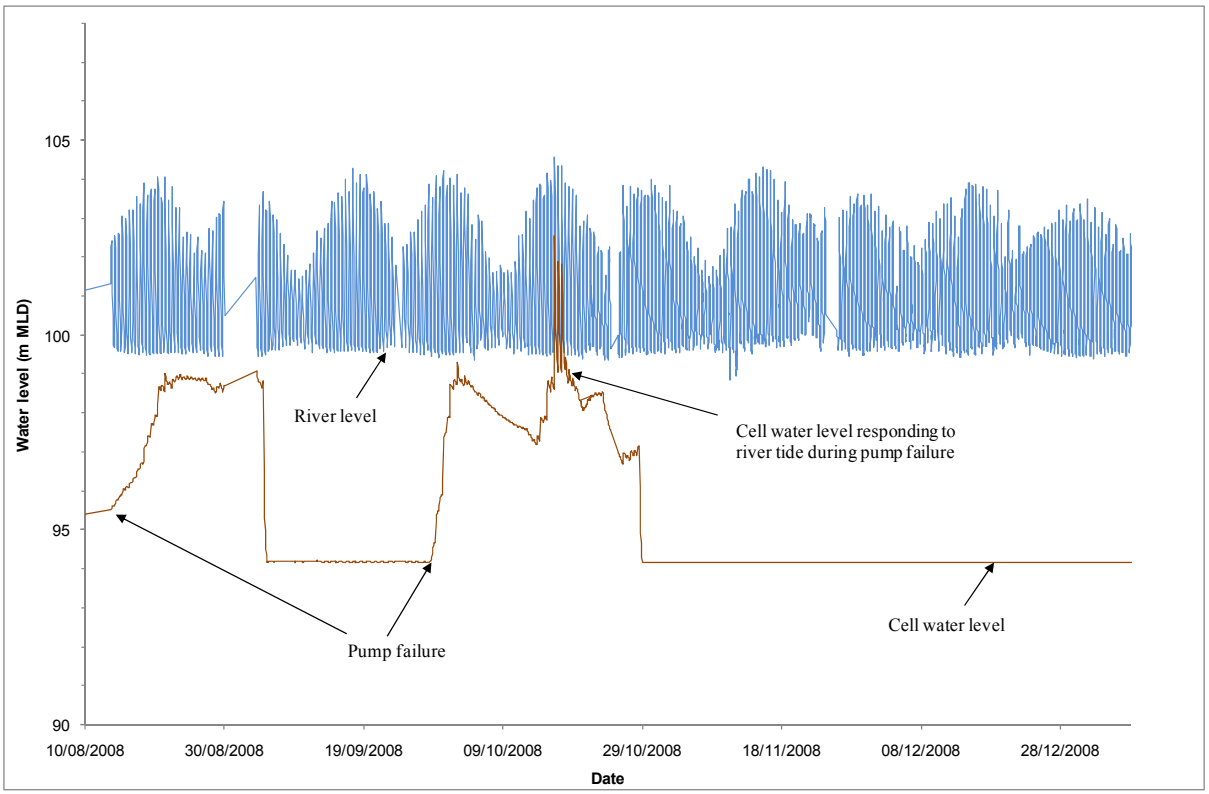

Figure 7-52: Cell water level response to river level during pump failure for cell C3

8 Comparison of numerical and field results

8.1 Introduction

A numerical study was conducted that modelled the structural response due to the construction sequence and geometry of cell C3. The cell C3 geometry was selected as this cell had been instrumented to monitor bending moments and wall deflections. FLAC (Itasca 2009) was used for both 2D (Section 5) and 3D (Section 6) analyses of the diaphragm type cellular cofferdam.

In this chapter, the results from these analyses (2D and 3D) are compared with the field measurements (Section 7) to identify the similarities and differences between the field results.

8.2 Comparison of calculated and measured results

8.2.1 Bending moments

The computed (2D and 3D) and measured bending moments at the end of construction for the inboard wall are shown in Figure 8-1. The bending moment at the level of top tie and 1m below that depth remained unchanged for all cases. The magnitude of bending moment derived from numerical analyses at the level of the lower tie is plausible as the wall would be expected to show some negative bending moment at this level due to the tie restraint to cell fill pressure on the inside face of the wall. However, the field measurements do not show this which suggests that at the time of installation the ties may not have provided full restraint and there was some play in the connections. At 95m MLD the measured bending moment and those derived from three dimensional analysis with an E-ratio of 0.1 are similar. Using an E-ratio 0.03 (3D) and two dimensional plane strain analysis over predicts the magnitude of bending moment, however an E-ratio 1.0 analysis under predicts the magnitude of bending moment. The measured bending moment profile indicates that the actual excavation level may be above 92m MLD or the load transmitted to the structure may have pushed the maximum bending moments to the top of

excavation level on inboard side. The similarity between the E-ratio 0.03 (3D) and measured results for the depth below excavation level suggests that interlock tensions within the wall below that depth where passive support is provided by the stiff Kimmeridge Clay is lower in comparison to the free face above the excavation level where the wall is unrestrained on the inboard side thereby increasing tension within interlocks.

The bending moment response for the outboard wall is presented in Figure 8-2. A zero bending moment was recorded above 103.5 m MLD as this section is the 3m overhang used to prevent the inundation in times of high flood. As previously seen the calculated and measured results between the upper tie level and 101m MLD are similar (E-ratio of 0.03, and 0.1 analyses (3D)). The bending moments below 101m MLD and above 93m MLD diverge with the numerical results indicating that the lower ties take considerable more load resulting in a high positive bending moment (tension on the cell side face of the wall) due to the restraint provided by the lower steel ties. This is in contrast to the measured response and again is indicative of limited restraint actually provided by the tie. In retrospect it would have been very informative to have instrumented the ties to determine loads and improve the interpretation of the overall structural response of the cofferdam. Below cell excavation level with the cell (92m MLD) good agreement is observed between the two dimensional analysis and the measured results. It should be noted that the gauge BMOPL3 (for gauge references see Figure 7-5) was damaged during the construction of the cofferdam and therefore an idealised value for bending moment profile was drawn using gauge BMOPL2 on the basis of difference between the bending moment gauges BMIPL2 and BMIPL3 on the same level (89m MLD) from inboard wall.

8.2.2 Wall displacement

The computed (2D and 3D) and measured displacements are shown in Figure 8-3 and Figure 8-4 for the inboard and outboard walls respectively. The measured wall displacements were only obtained at the top of each respective wall. Therefore, for comparison with the numerical results an idealised toe displacement of 10mm was used to obtain a straight line deflection profile. The maximum measured displacement at the top of the inboard wall was 120mm which is similar to the displacement calculated from the two dimensional analysis. However the three dimensional analysis has over predicted

the displacement by a considerable amount with maximum deflection of 293, 353 and 605mm form the analyses with E-ratio values of 1.0, 0.1 and 0.03 respectively.

Lateral displacement towards the excavated side at the top of outboard wall was measured as 149mm which is under predicted by the two dimensional analysis (maximum wall deflection of 104mm) as shown in Figure 8-4. The maximum deflection was substantially over predicted by the three dimensional analyses with maximum outboard wall displacement of 326, 388 and 678mm form E-ratio of 1.0, 0.1 and 0.03 analyses. The reason for this was identified to be the difference between the plane strain and three dimensional approaches (See Section 8.3).

8.2.3 Tie loads

The tie loads calculated from the two and three dimensional numerical analysis are presented in Table 8-1. Unfortunately force in steel ties was not monitored and no comparison with the numerical results is possible. The Table 8-1 indicates the tension in lower steel ties from 2D analysis is much lower than 3D results. Two dimensional analyses include the excavation and backfilling of the cell which was not possible for three dimensional cases due to software limitations. That is why that the tie forces in two dimensional analysis are much lower in comparison to the three dimensional analysis with same cofferdam dimensions and soil properties. The force in the upper ties was found to be very low in all cases and well below the yield strength of the ties used (Table 5-4).

Table 8-1: Comparison of tie loads from the two and three dimensional analyses

		Lower tie (kN)	Upper tie (kN)
3D analysis	E-ratio 0.03	985.3	66.23
	E-ratio 0.1	798.3	52.27
	E-ratio 1	792.6	0
2D analysis		295.56	27.14

8.3 Discussion

In comparison to the three dimensional analyses, the bending moment profile from the two dimensional analyses provides a relatively better fit for both the inboard and

outboard walls with the exception of the lower tie section. The tension in steel ties was not monitored but the steel tie tensions calculated from the two dimensional analysis of the problem are well below the three dimensional analysis results.

The wall displacement profiles computed from the two dimensional analyses compare well with the field data for both the inboard and outboard walls. The three dimensional analysis have over predicted moment by more than a factor of two. The reasons behind identified difference between the numerical calculated and measured structural forces and displacement may be summarised as:

- There is clear indication from the bending moment plots (Figure 8-1 and Figure 8-2) that the restraint actually provided by the steel ties is not substantial as a negative bending moment is expected at the level of lower ties as indicated by two and three dimensional analyses. Lack of fit in tie connections and any sag or flexibility in the cables (the ties were not pre-tensioned so may contribute a low level of restraint). The true response of the ties and their effect on wall bending moment can not be easily modelled in the numerical analyses as steel tie tensions were not directly monitored to quantify the connection and installation effects in the ties.

- Construction effects such as over dig within the cell as the cell was excavated under balanced water conditions may also be influential. Slight discrepancies may have shifted the maximum measured bending moment to a level which is slightly below the location of the maximum calculated bending moment from numerical analysis for inboard wall. Similarly, the location of the maximum measured bending moment in the outboard wall is slightly above the point of maximum bending from the numerical study suggesting that there may be an under dig or some load from base slab affecting the bending moments in the embedded section of the wall. However the magnitude of the maximum bending moment obtained from the 3D (E-ratio 0.03) analysis for inboard wall, 3D (E-ratio 0.1), and 2D analysis for outboard are close to the maximum measured bending moments.

- The front jetty was connected to the top wailing beam on the cell C4 (adjacent to the instrumented cell C3, Figure 7-44). This may have caused some restraint to

the top section of the wall as the wailing beam is connecting all the central cell cells (C1 to C4) affecting the structural forces and wall deflection. It has not been possible to quantify this effect in the analyses as these only include analysis of a section (the instrumented section) and there is no consideration of the effects of neighbouring cells.

- The pumping station base slab is supported on CFA piles consequently there may be some load transfer from the cofferdam to these piles in front of the wall and may behave as a formation level prop. This may substantially alter the structural behaviour of the wall in the longer term.

- The construction sequence adopted for the analyses was identified from the site construction diary which provides more general cofferdam construction details but lack detail specific to the instrumented cell. Therefore, there is a possibility that the analyses may not include all the important construction events/loads and precise excavation/water levels. Modelling these construction effects is challenging and not usually done.

The results from 3D analysis using an E-ratio of 1.0 and the 2D analysis should give similar output when treating the sheet piles as an isotropic material. However, there are a number of reasons why this has not been the case;

- The three dimensional analysis include use of LINER membrane elements (Itasca, 2009) which can take both membrane and nodal forces and the tie spacing is based on actual spacing used to construct the cofferdam. The two dimensional analysis uses BEAM structure elements (Itasca, 2009) to model the sheet piles where the loads are only applied at the nodes and the steel tie spacing is therefore considered to be 1m centre to centre for both lower and upper ties with the structural properties adjusted to match the actual tie spacing (1.2m c/c for lower and 2.4m c/c for the upper ties).

- The two dimensional analyses models all the important construction stages including the excavation and backfilling process of the cofferdam cell. It was well established from these analyses that cell excavation and backfilling have a significant effect on the computed soil stresses and the structural forces (Figure

5-11 and Figure 5-12). In the case of the three dimensional analyses the cell excavation and backfilling processes were not modelled due to limitations with the program that allow the reinstatement/creation of links between the soil and structure elements once they are deleted during excavation stage.

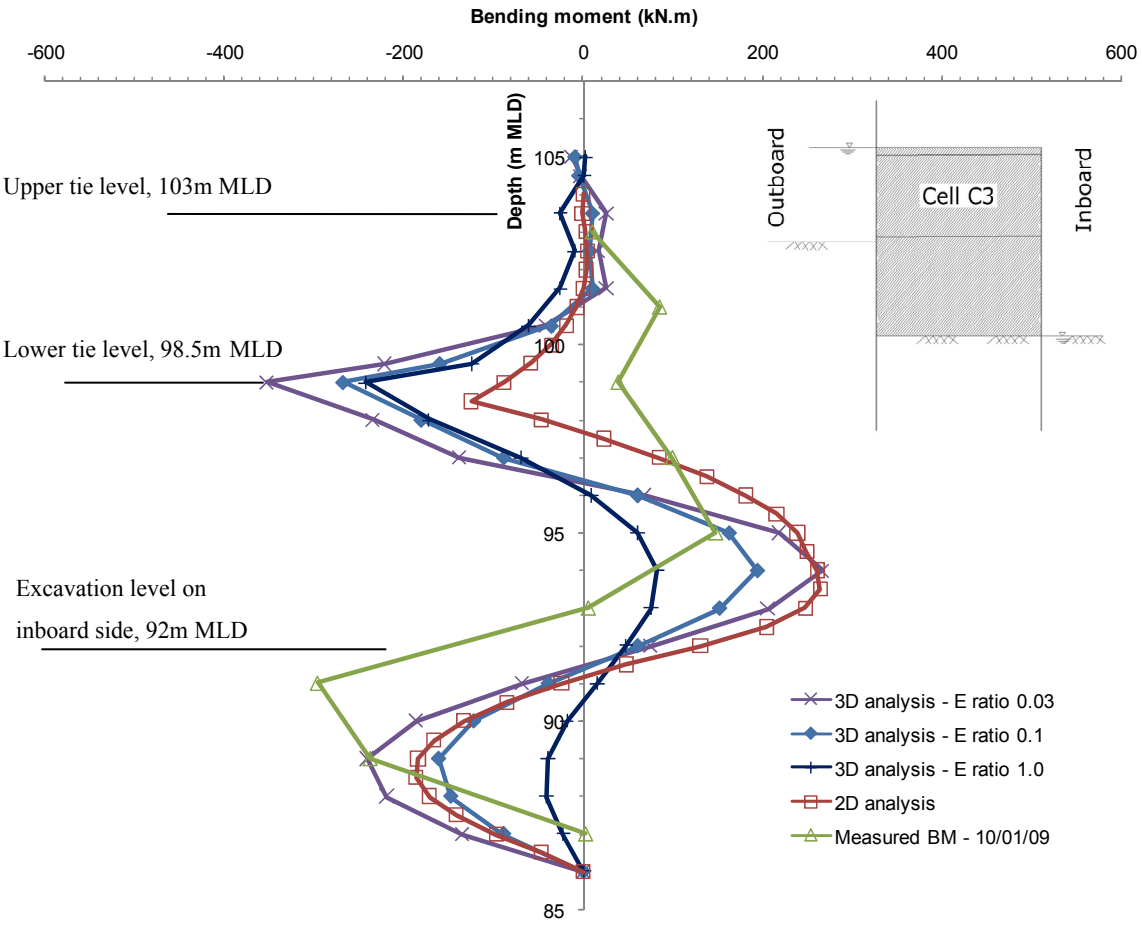

Figure 8-1 : Comparison of bending moment in inboard wall from numerical (2D and 3D) and measured bending moment from instruments

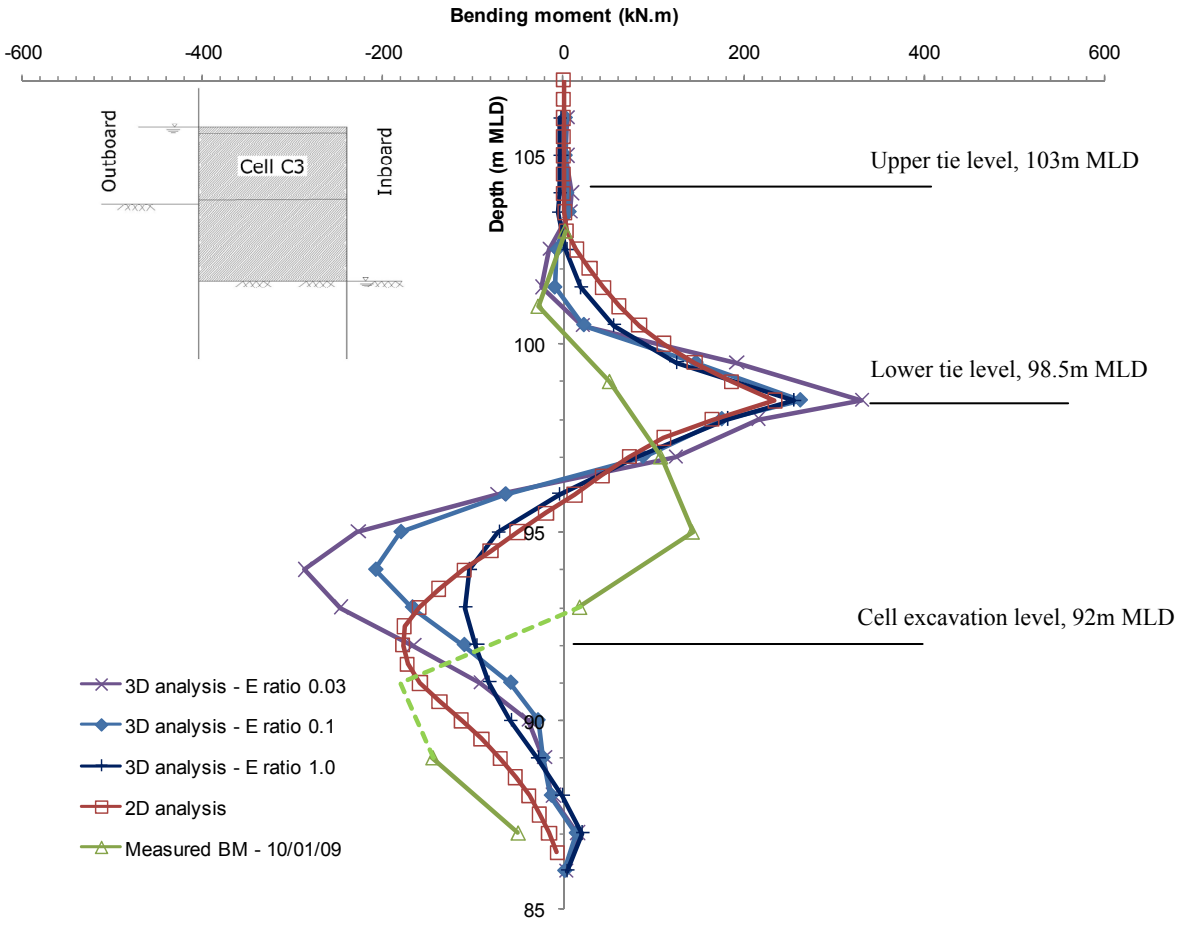

Figure 8-2: Comparison of bending moment in outboard wall from numerical (2D and 3D) and measured bending moment from instruments

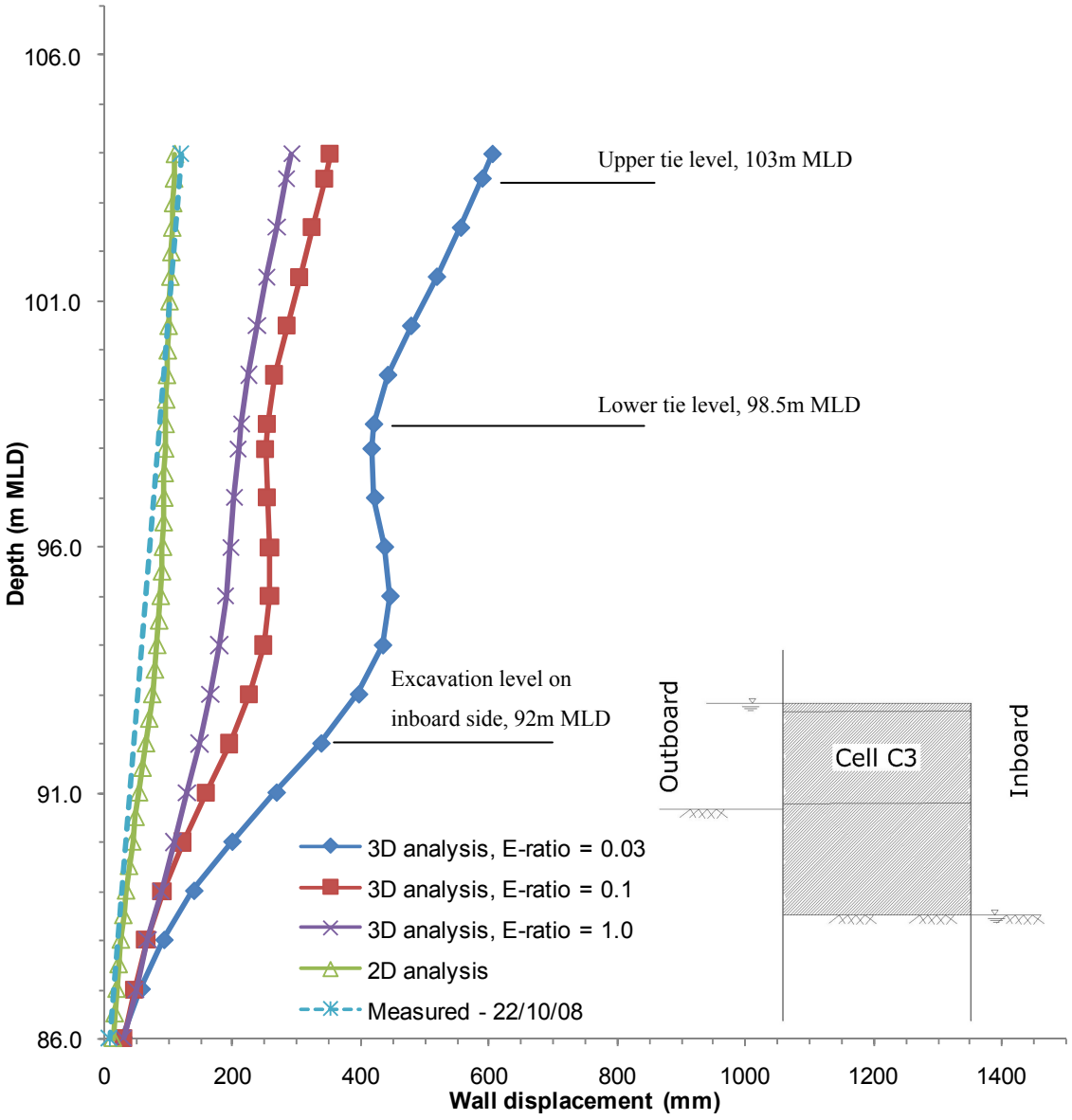

Figure 8-3: Comparison of lateral displacement of inboard wall from numerical (2D and 3D) and measured wall displacement from monitoring data

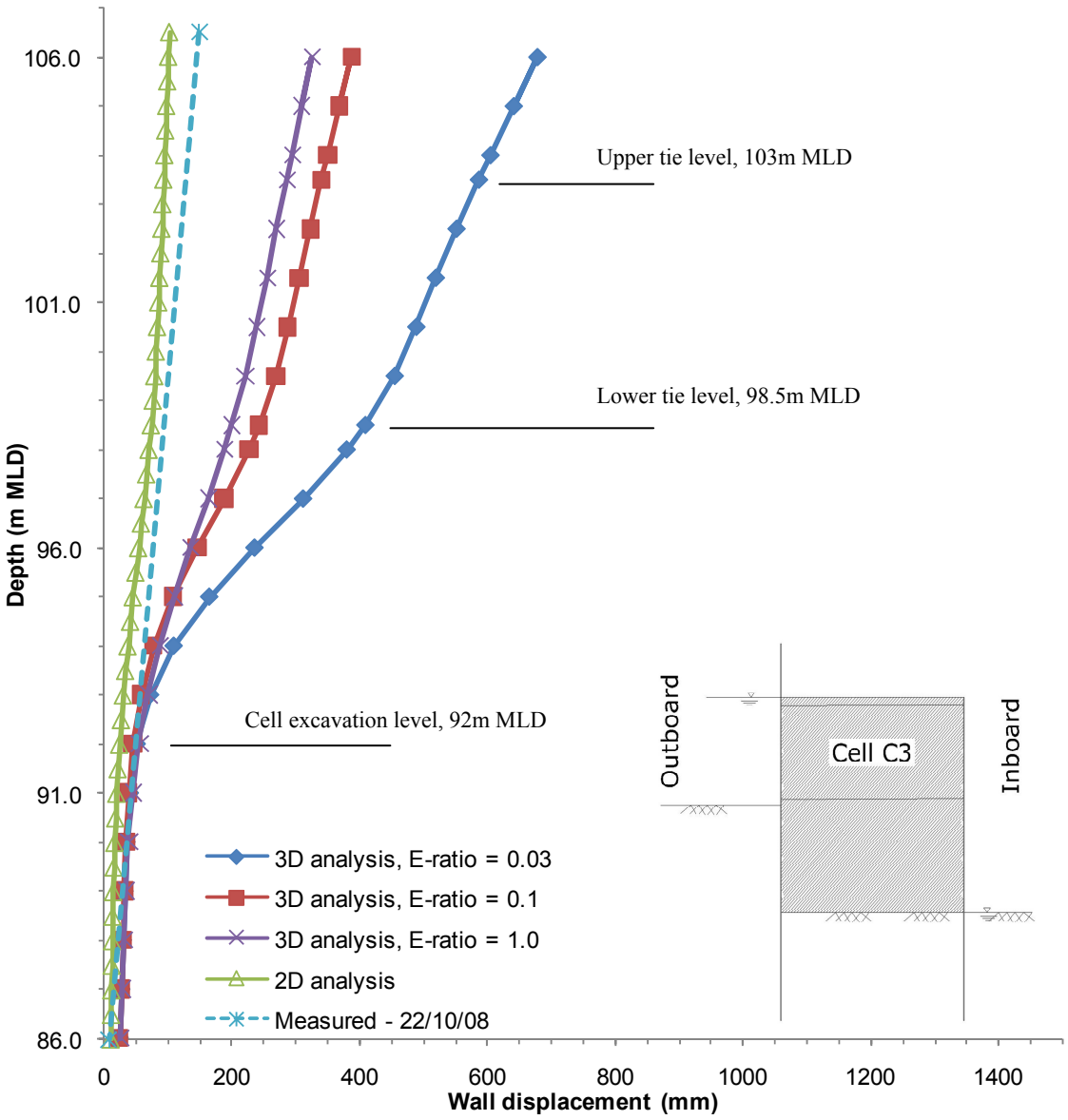

Figure 8-4: Comparison of lateral displacement of outboard wall from numerical (2D and 3D) and measured wall displacement from monitoring data

9 Conclusions and recommendations

The research work presented in this thesis provides a case study related to the behaviour of a diaphragm type cellular cofferdam. The aim of the research was to evaluate existing design guidelines for the design of diaphragm type cofferdams using a series of numerical analyses and the measured performance from a field study since existing design guidelines were derived from model tests on circular cofferdams. The two dimensional analyses were conducted to identify the failure mechanism and factor of safety against failure for a critical cofferdam section. A relatively larger cofferdam cell (which was instrumented) was modelled to verify the structural forces and deflection in the sheet pile walls considering construction events. Three dimensional analyses were conducted to identify the effect of using a modified orthotropic stiffness and tie spacing on the calculated response of the structure.

The field study comprised near continuous measurement of bending moments in the sheet piles, wall deflections, and water levels in and around the instrumented cell. The important construction stages were identified and changes in the various measured quantities were back analysed to further understand the performance of the cofferdam throughout the construction phase and once the cofferdam is operational.

9.1 Conclusions

The general conclusions derived on the basis of research presented in this thesis are:

- Engineering properties for Kimmeridge Clay have been derived from high quality samples and multistage triaxial tests. The stiff Kimmeridge Clay was found to have moderately high permeability and higher drained shear strength in comparison to the tests conducted on the remoulded soil samples (Cripps and Taylor, 1987);
- A methodology based on reducing the shear strength of the soil was used to identify the failure factor of safety for the diaphragm type cellular cofferdams;
- The predicted failure mechanism suggests a curved failure surface at the bottom of the cofferdam which is similar to Hansen (1953) log spiral failure mechanism.

There was no sign of any other failure mechanisms presented in section 5. Therefore this mechanism is confirmed as a relevant and most important failure mechanism for diaphragm type cofferdams;

- Detailed two and three dimensional numerical analyses of cellular cofferdams were undertaken and results presented. These analyses modelled aspects of the actual construction sequence of the cofferdam construction and were used to compute the structural forces in the cofferdam at key construction stages. The reduction in lateral stiffness to include for wall flexibility in the lateral direction resulted in an increase in the structural forces and wall deflections in case of three dimensional analyses;

- Structural monitoring was of significant benefit in helping to understand the behaviour of cofferdam during construction and after it was commissioned to support the construction of pumping station. In particular the effects of construction traffic loading had a significant influence on bending moments;

- Some of the relatively less important loads such as construction machinery loading and cell pump failure were observed as having a significant effect on the measured structural forces. However, when applied in an overall stability analysis the construction load will have a stabilising effect therefore it was concluded that the construction load should not be used in the 'failure factor of safety' analysis as the construction load is not always present at the top if the cell;

- The maximum bending moment from the numerical analyses compared well with the measured results in most cases. For the upper section of the wall, an agreement was identified between the results from 2D and 3D analyses; however, they differ significantly from the measured bending moments due to uncertainty in the lower tie behaviour; Although the three dimensional analysis are helpful in understanding the three dimensional nature of the problem due to the inclusion of the actual tie spacing and orthotropic wall stiffness to account for interlock effects, the two dimensional analysis provided a good fit to structural and wall displacements. Therefore on the basis of this study it is suggested that in contrast to the circular type cofferdams, the diaphragm type cellular cofferdams may be

analysed as a two dimensional problem. This helpfully reduces the computational effort required to undertake a full three dimensional study of the problem.

9.2 Recommendations for future work

On the basis of research work presented in this thesis a number of important issues were identified related to modelling and measurement of cofferdam performance. Further investigation for improving the design and understanding of cellular diaphragm type cofferdams is required in order that;

- The failure factor of safety and slip surfaces identified were from the specific cell and construction geometry used at the St. Germans cofferdam. A more detailed parametric numerical study using general cross section is required to identify more general failure criteria;

- Cell excavation and backfilling were identified as having a significant effect on structural forces following assessment of the two dimensional analyses. However, it was not possible to model this for three dimensional analyses due to software limitations. Further investigation using three dimensional analysis that include the modelling of the cell excavation and backfilling stages is suggested;

- The use of an orthotropic stiffness to accommodate interlock effects has a significant effect in the case of diaphragm type cellular cofferdams. Further analyses should focus on using different E-ratio values for the embedded and free height sections due to the non-uniformity of the applied pressure at these sections. It is also suggested that a check on the cell interaction effects. The restraint provided by the neighbouring cells and any support provided by other structures such as jetties, formation level props etc should be undertaken. This will assist in identifying the load in the lateral ties as they are expected to have no effect on the load bearing capacity of the cell during the working life of the cofferdam;

- Wherever possible, tie loads should be measured as these have been identified as being highly significant in terms of their effect on bending moments and cell deflection in this study. This will help understanding of bending moment in upper section of the wall, with the inclusion of any play or flexibility in tie connections.

Furthermore, there are no recorded cases in the literature where tie forces have been measured directly;

- Although the site diary was available to identify the various construction stages to identify the loads affecting the structural forces, it proved very difficult to identify the exact dates and water/excavation levels specific to the instrumented cell. It is suggested that a live cam is installed to record construction activity to allow a more precise interpretation of the load changes during construction of the cofferdam.

Appendices:

Appendix A: Borehole logs

Drilling Method Cable Percussion
Equipment Dando 2000
Dates Drilled Start 03/03/2004 End 08/03/2004
Borehole Diameter 200mm to 11.10m, 150mm to 35.00m
Casing Diameter 200mm to 11.10m, 150mm to 15.00m
Logged by JG 03/03/2004
Compiled by pb 10/03/2004
Checked by 12.05.04

BOREHOLE No. BH1

Coordinates (National Grid) 558953.9 E, 314408.2 N
Ground Level 3.90 m OD

Date & Time	Casing Depth (m)	Depth to Water (m)	Sample Details: Depth (m) From	To	Type	No	SPT Blows/N Drive mm: Test	U100 Blows/ Recovery mm: Result	Description of Strata	Depth (Thickness) (m)	Level	Legend
03/03									TOPSOIL	(0.40) 0.40	3.50	
			0.40		D	1			MADE GROUND: Firm grey mottled orange and brown clay with occasional limestone cobbles.			
			0.50	1.00	B	2				(0.80)		
			1.00		CD	3						
03/03			1.00		K	4						
			1.00		V	5						
04/03			1.20		D	6			Soft orange, brown and grey sandy SILT.	1.20	2.70	
	Nil	Dry	1.30	1.75	U	7		18/ 450		(0.50)		
			1.75		D	8			Soft grey CLAY.	1.70 (0.40)	2.20	
			2.00		D	9						
			2.10		CD	10			Soft fissile grey sandy CLAY. Sand is fine.	2.10	1.80	
			2.10		K	11						
			2.20		V	12						
			2.50	2.95	D	13						
	1.60	Dry	2.50	2.95			S2					
			2.50	3.00	B	14				(1.20)		
			3.30		D	15			Very soft brown sandy CLAY. Sand is fine.	3.30	0.60	
			3.40		W	18						
	3.10	Dry	3.50	3.85	U	16		10/ 350				
			3.85		D	17						
			3.90		CD	19						
			3.90		K	20						
			3.90		V	21				(1.90)		
			4.50		D	22						
	4.40	GL	4.50	4.50			S0/ 0					
			4.50	5.00	B	23						
			5.30		D	24			Very soft light brown PEAT.	5.20	-1.30	
	Nil	Dry	5.50	5.95	U	25		20/ 450		(0.70)		
			5.95		D	26			Very soft and soft blue grey CLAY.	5.90	-2.00	
			7.00	7.50	D	28			At 7.00m; Slightly sandy clay. Sand is fine.			
	6.80	1.00	7.00	7.45			S2					
			7.00	7.50	B	29				(3.60)		
			8.00		D	30						
	8.30	1.00	8.50	8.90	U	31		11/ 400	At 8.50m; CLAY/SILT.			
			8.90		D	32						
			9.60		D	33			Brown and blue grey SAND with occasional coarse gravel.	9.50 (0.30)	-5.60	
			9.80	10.25	D	34			Firm to stiff grey slightly sandy CLAY. Sand is fine to coarse. Rare fine and medium	9.80 (0.30)	-5.90	
	9.70	GL	9.80	10.25			S24					

Remarks (See notes & keysheets)
1 Groundwater was encountered at 3.40m.
2 Prior to boring a Cable Avoidance Tool (CAT) survey was carried out. An inspection pit was hand-dug to 1.20m depth and rescanned using the CAT to check for services. Services were not located.
3 The borehole was advanced by chiselling methods from 14.20m to 14.50m (1 hour).
4 An amount of water was added to facilitate boring and to maintain a positive hydrostatic head in granular strata from 3.85m to 5.30m and 9.60m to 9.80m.
5 The borehole was backfilled on completion with cement bentonite grout.

Scale 1:50

FUGRO

Project: ST GERMANS PUMPING STATION, KINGS LYNN, Middle Level Commissioners, W S Atkins Limited
Contract No. BAS040046
Figure No. FR1 (1 of 4)
301/04

Figure A.1: Borehole 1 – page 1 of 4

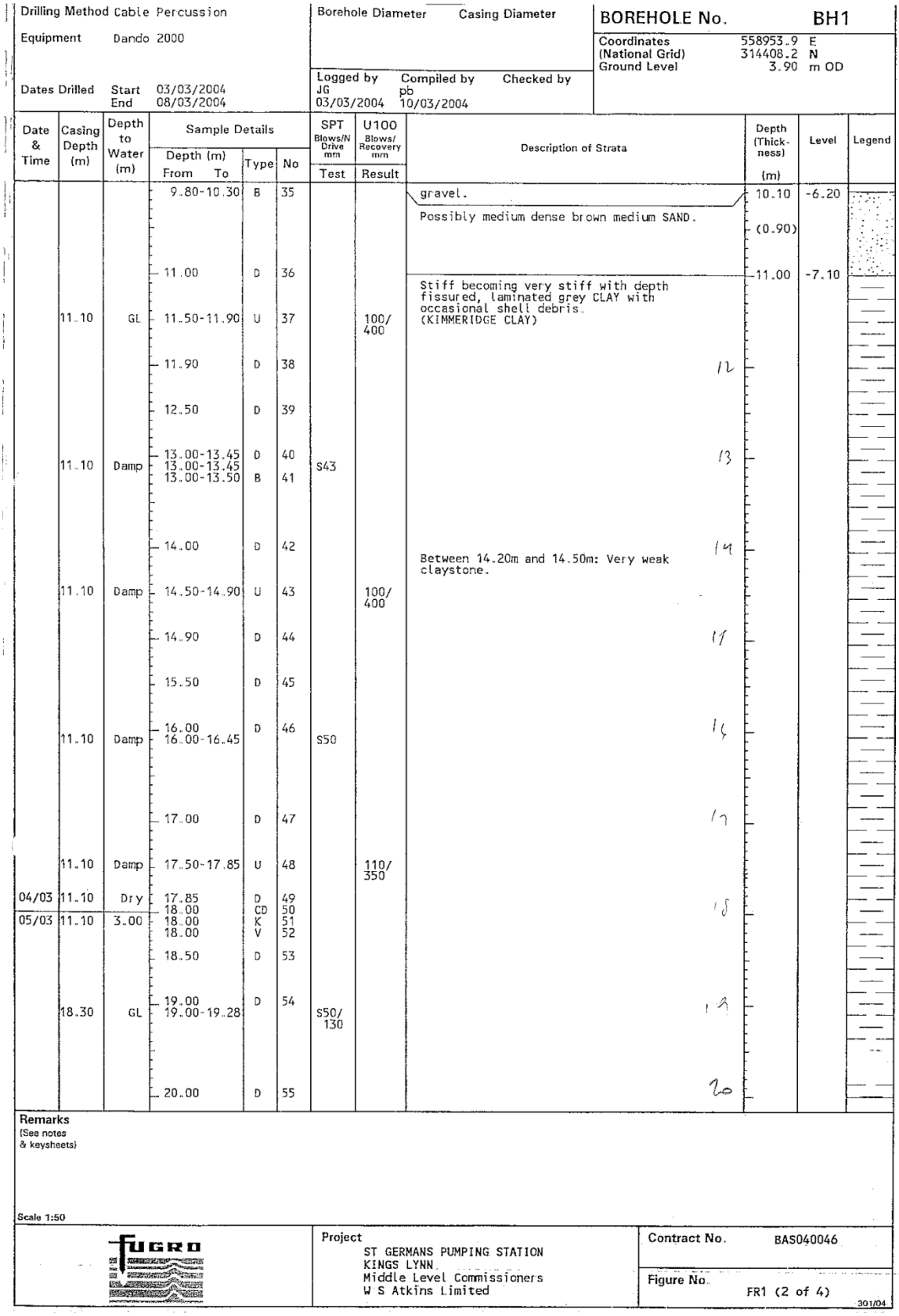

Drilling Method Cable Percussion
Equipment Dando 2000
Dates Drilled Start 03/03/2004 End 08/03/2004
Borehole Diameter Casing Diameter
Logged by JG 03/03/2004 Compiled by pb 10/03/2004 Checked by 10/03/2004

BOREHOLE No. BH1
Coordinates (National Grid) 558953.9 E 314408.2 N
Ground Level 3.90 m OD

Date & Time	Casing Depth (m)	Depth to Water (m)	Sample Details: Depth (m) From	To	Type	No	SPT Blows/N Drive mm Test	U100 Blows/ Recovery mm Result	Description of Strata	Depth (Thick-ness) (m)	Level	Legend
			9.80	10.30	B	35			gravel.	10.10	-6.20	
									Possibly medium dense brown medium SAND.	(0.90)		
			11.00		D	36				11.00	-7.10	
	11.10	GL	11.50	11.90	U	37		100/ 400	Stiff becoming very stiff with depth fissured, laminated grey CLAY with occasional shell debris. (KIMMERIDGE CLAY)			
			11.90		D	38						
			12.50		D	39						
	11.10	Damp	13.00	13.45	D	40						
			13.00	13.45			S43					
			13.00	13.50	B	41						
			14.00		D	42			Between 14.20m and 14.50m: Very weak claystone.			
	11.10	Damp	14.50	14.90	U	43		100/ 400				
			14.90		D	44						
			15.50		D	45						
	11.10	Damp	16.00		D	46						
			16.00	16.45			S50					
			17.00		D	47						
	11.10	Damp	17.50	17.85	U	48		110/ 350				
04/03	11.10	Dry	17.85		D	49						
			18.00		CD	50						
05/03	11.10	3.00	18.00		K	51						
			18.00		V	52						
			18.50		D	53						
			19.00		D	54						
	18.30	GL	19.00	19.28			S50/ 130					
			20.00		D	55						

Remarks
(See notes & keysheets)

Scale 1:50

FUGRO

Project
ST GERMANS PUMPING STATION
KINGS LYNN
Middle Level Commissioners
W S Atkins Limited

Contract No. BAS040046

Figure No. FR1 (2 of 4)

301/04

Figure A.2: Borehole 1 – page 2 of 4

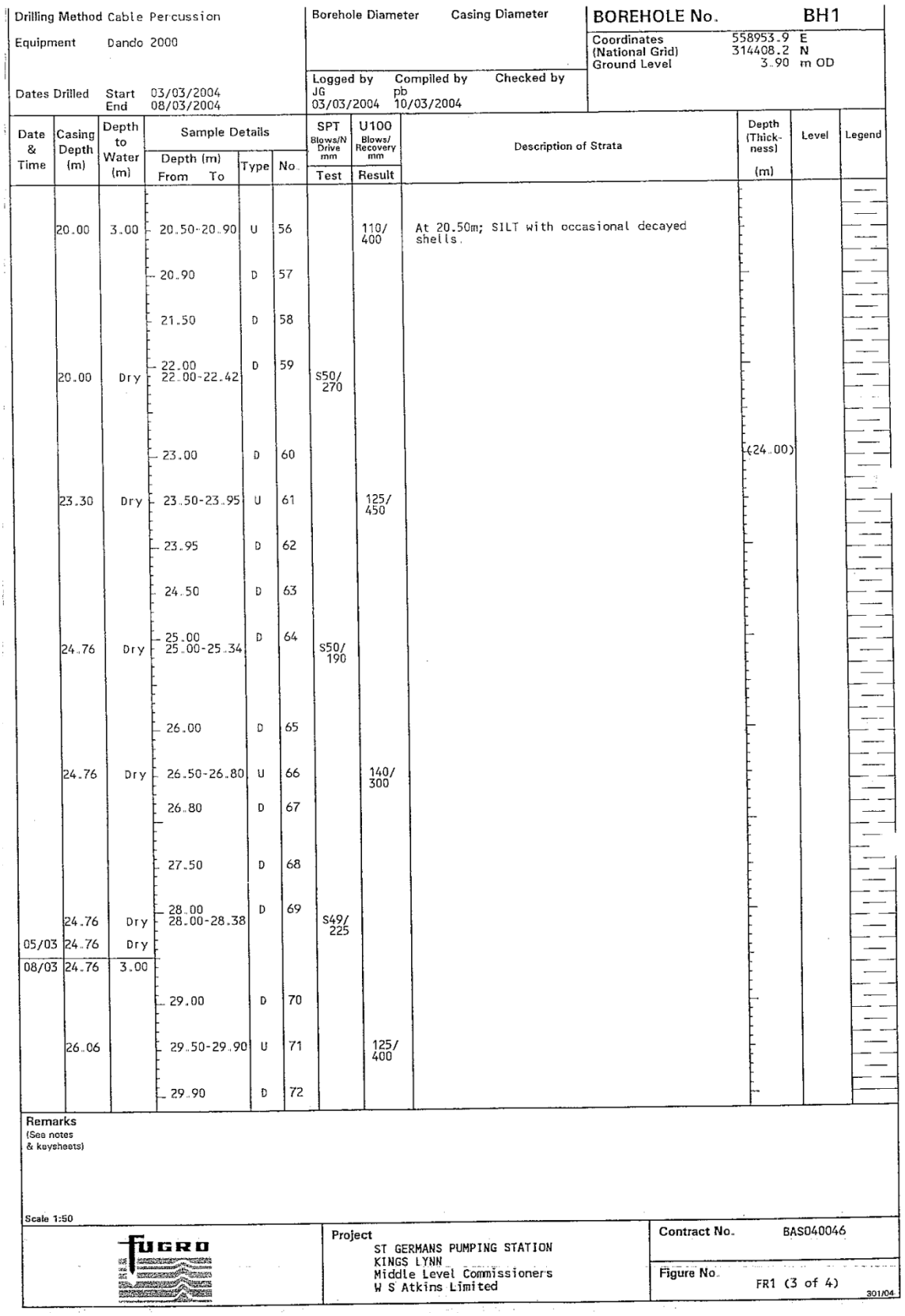

Figure A.3: Borehole 1 – page 3 of 4

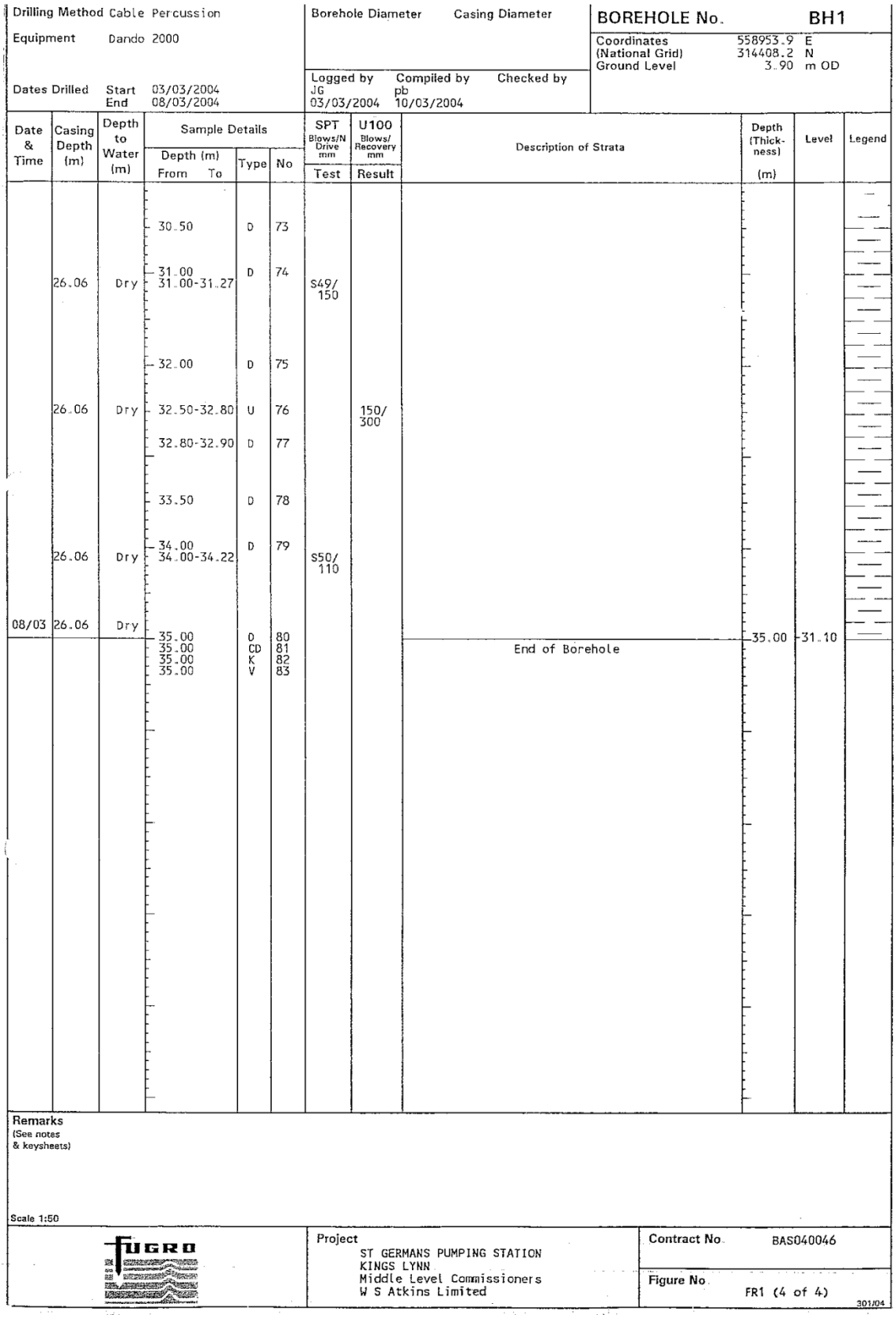

Figure A.4: Borehole 1 – page 4 of 4

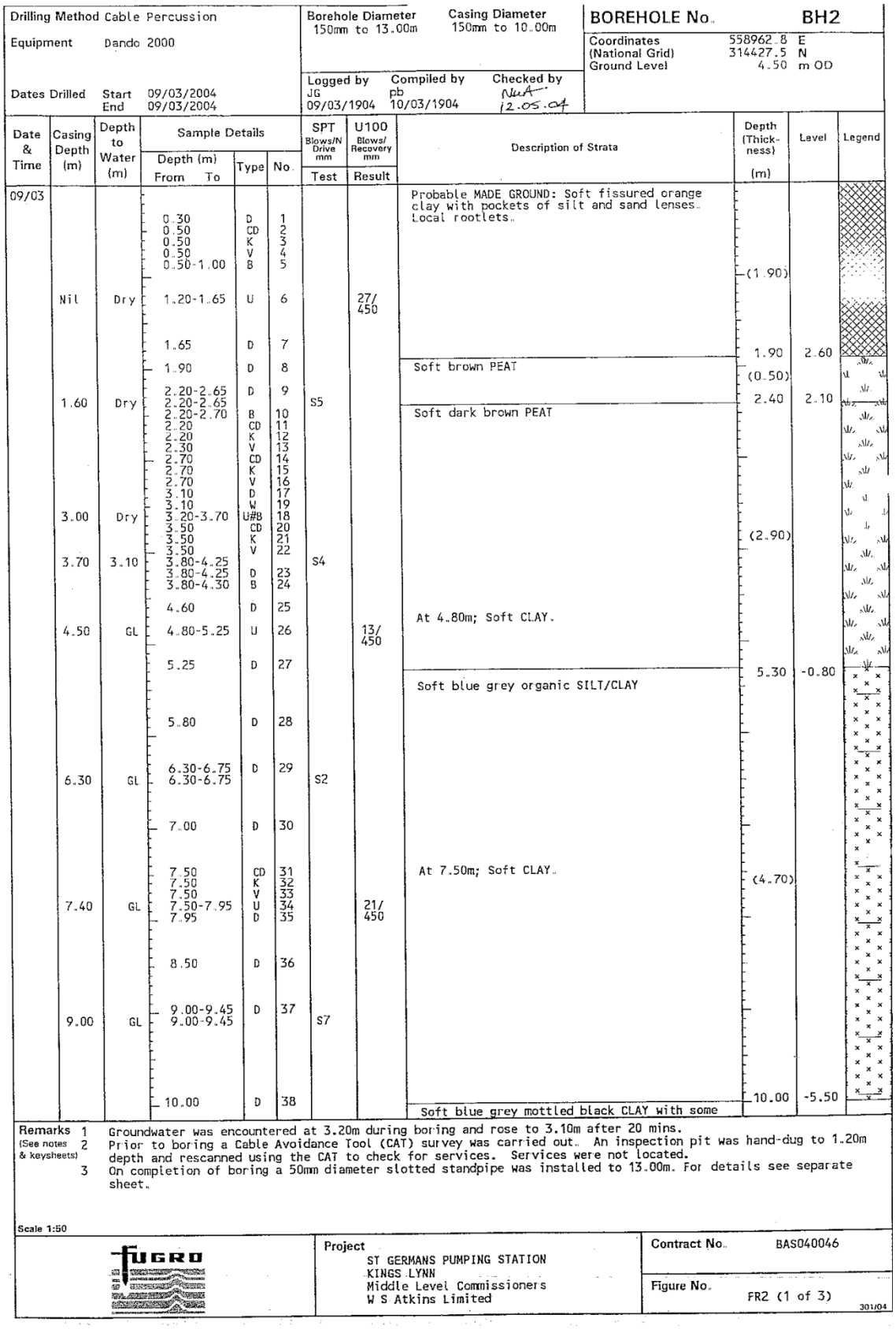

Figure A.5: Borehole 2 – page 1 of 3

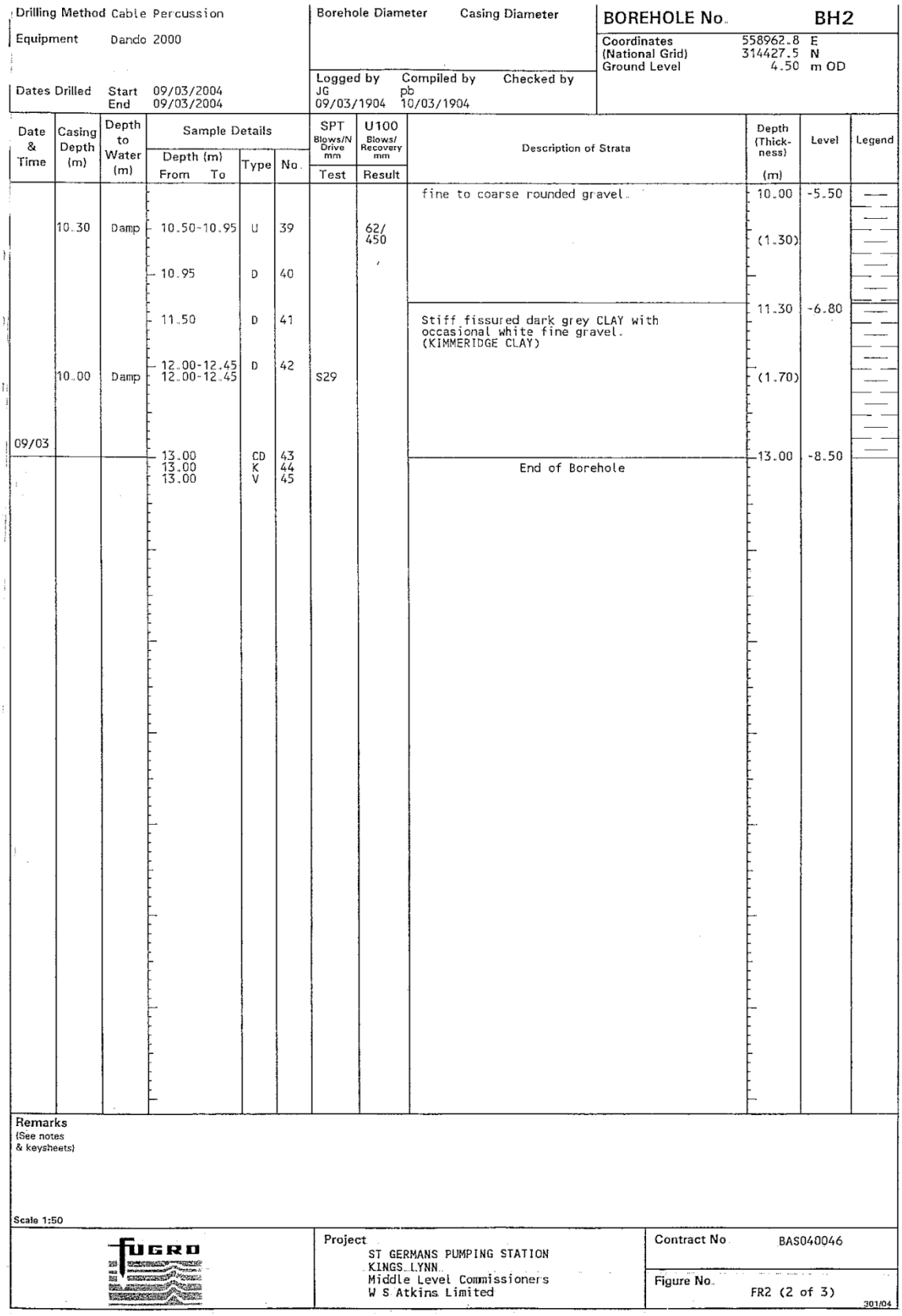

Drilling Method Cable Percussion
Equipment Dando 2000
Dates Drilled Start 09/03/2004 End 09/03/2004
Borehole Diameter Casing Diameter
Logged by JG 09/03/1904 Compiled by pb 10/03/1904 Checked by
BOREHOLE No. BH2
Coordinates 558962.8 E
(National Grid) 314427.5 N
Ground Level 4.50 m OD

Date & Time	Casing Depth (m)	Depth to Water (m)	Sample Details: Depth (m) From	To	Type	No.	SPT Blows/N Drive mm Test	U100 Blows/ Recovery mm Result	Description of Strata	Depth (Thick-ness) (m)	Level	Legend
									fine to coarse rounded gravel.	10.00	-5.50	
	10.30	Damp	10.50	10.95	U	39		62/ 450		(1.30)		
			10.95		D	40						
			11.50		D	41			Stiff fissured dark grey CLAY with occasional white fine gravel. (KIMMERIDGE CLAY)	11.30	-6.80	
	10.00	Damp	12.00	12.45	D	42				(1.70)		
09/03			12.00	12.45			S29					
			13.00		CD	43				13.00	-8.50	
			13.00		K	44			End of Borehole			
			13.00		V	45						

Remarks
(See notes & keysheets)

Scale 1:50

FUGRO

Project
ST GERMANS PUMPING STATION
KINGS LYNN
Middle Level Commissioners
W S Atkins Limited

Contract No. BAS040046

Figure No. FR2 (2 of 3)

301/04

Figure A.6: Borehole 2 – page 2 of 3

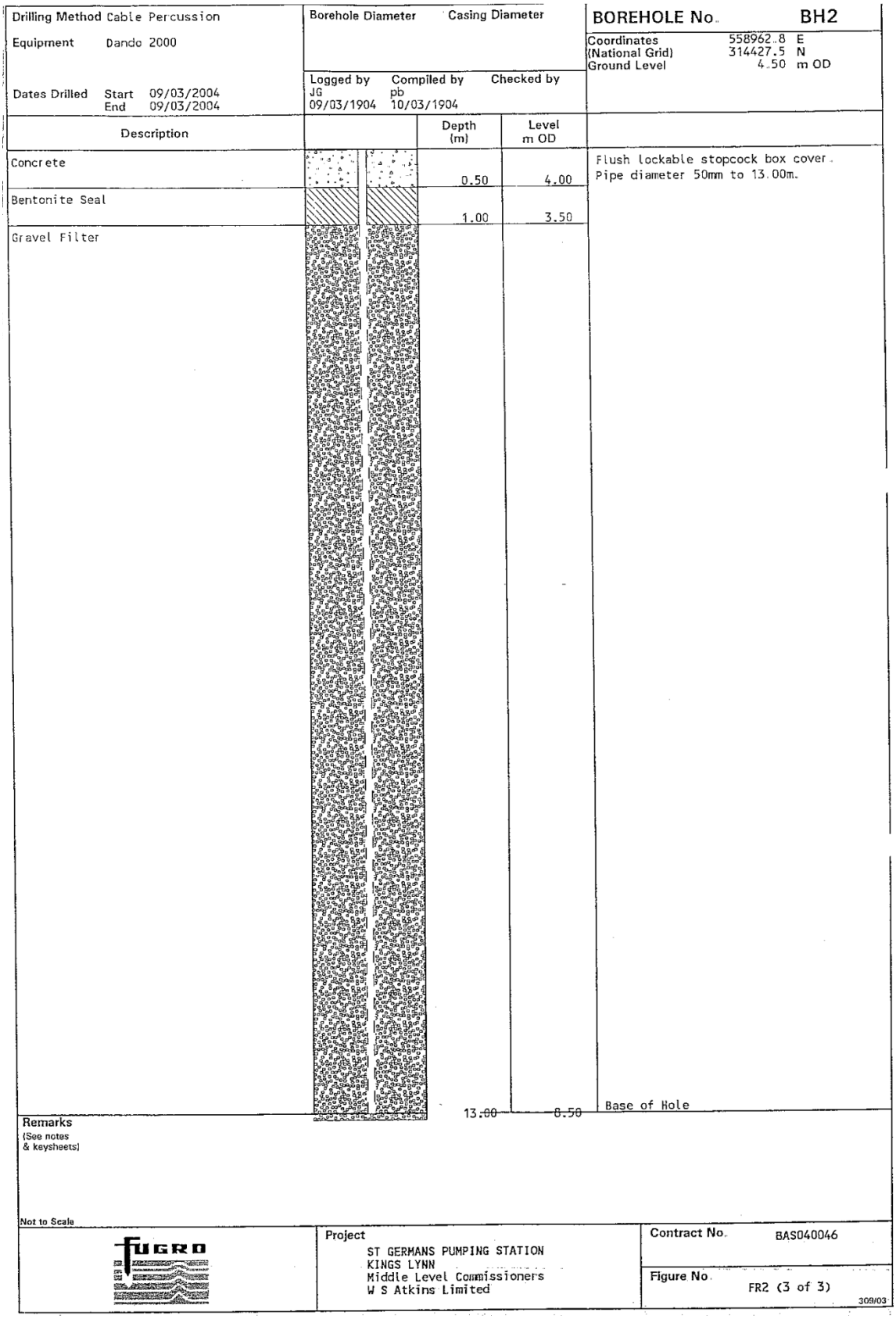

Figure A.7: Borehole 2 – page 3 of 3

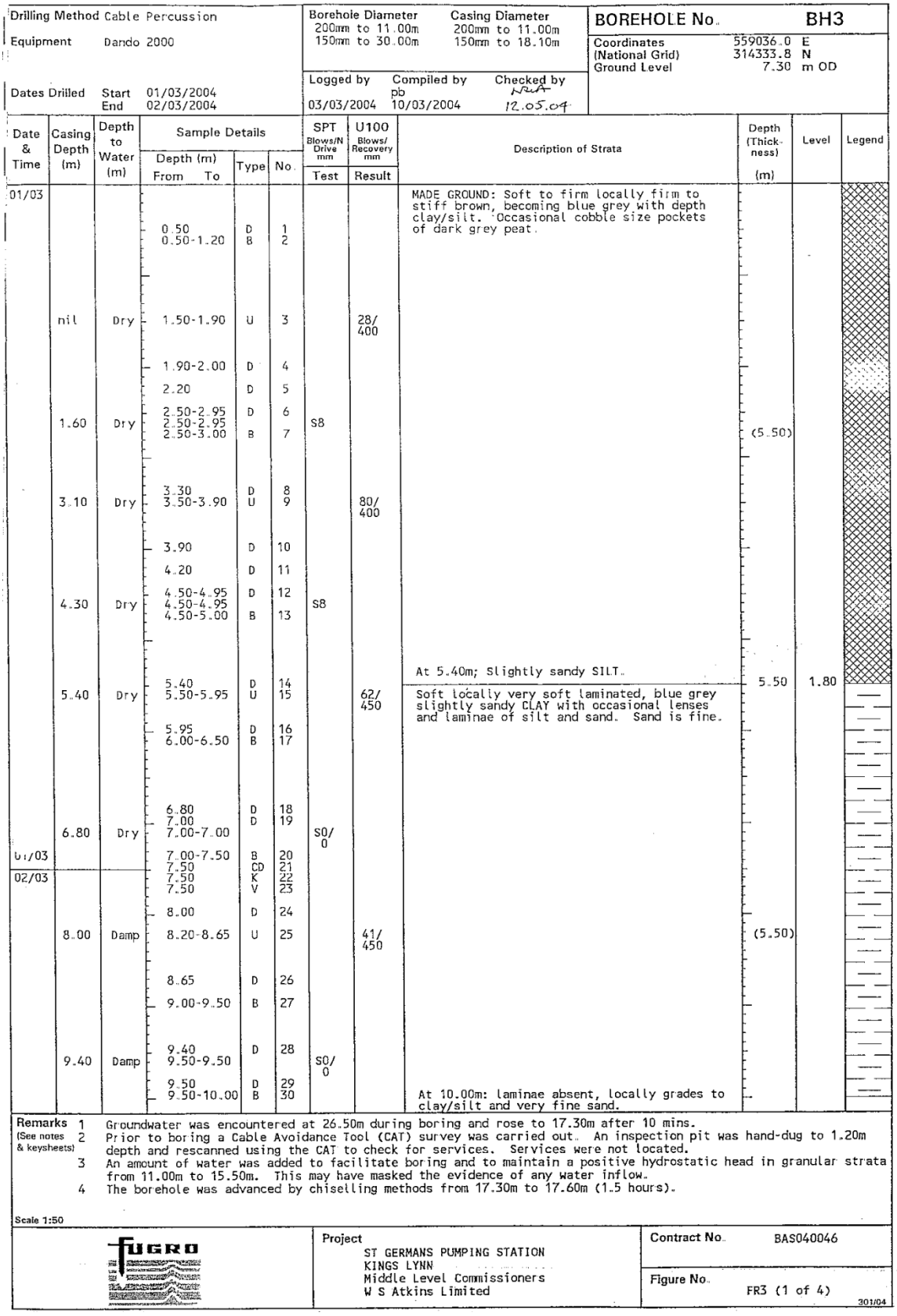

Figure A.8: Borehole 3 – page 1 of 4

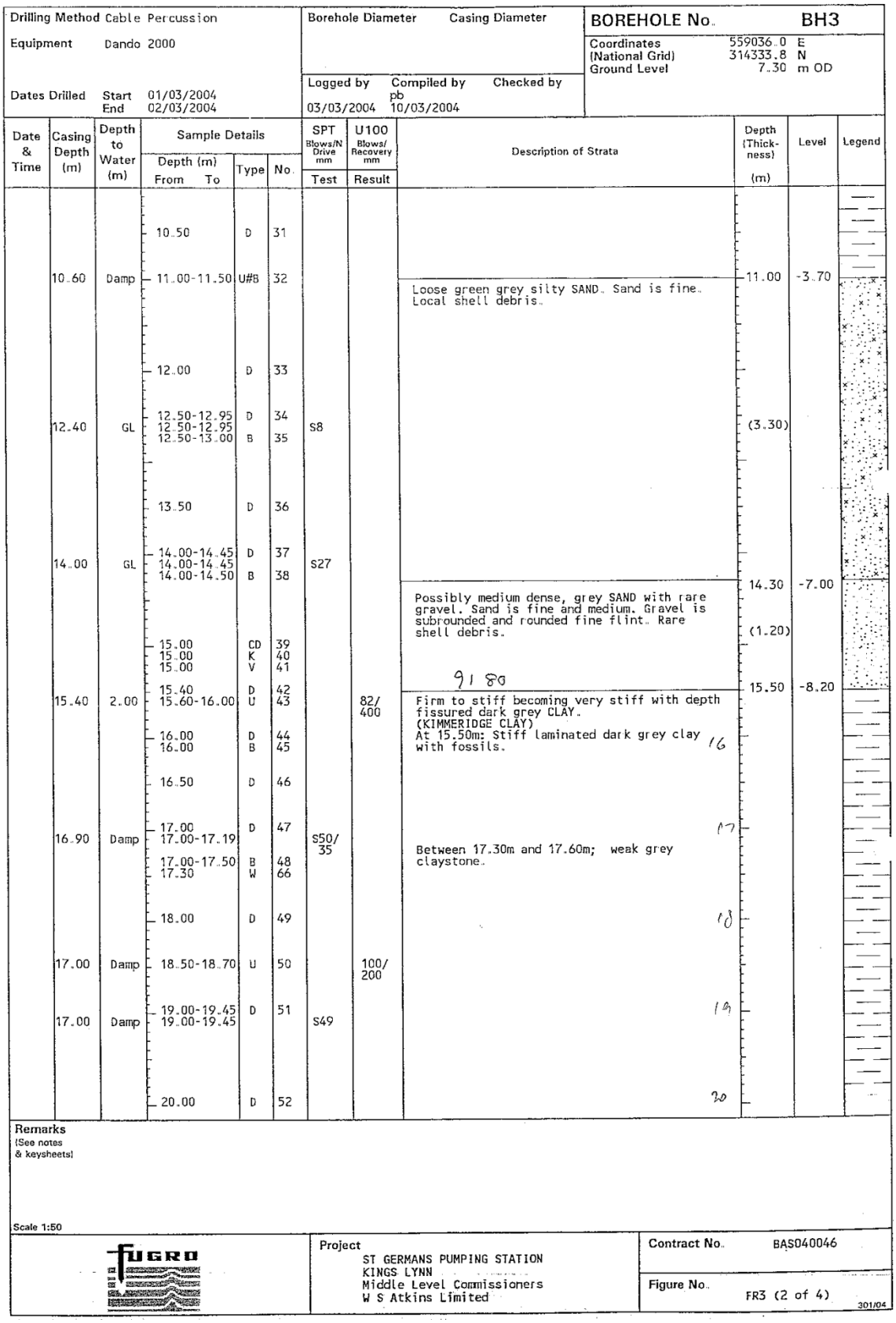

Figure A.9: Borehole 3 – page 2 of 4

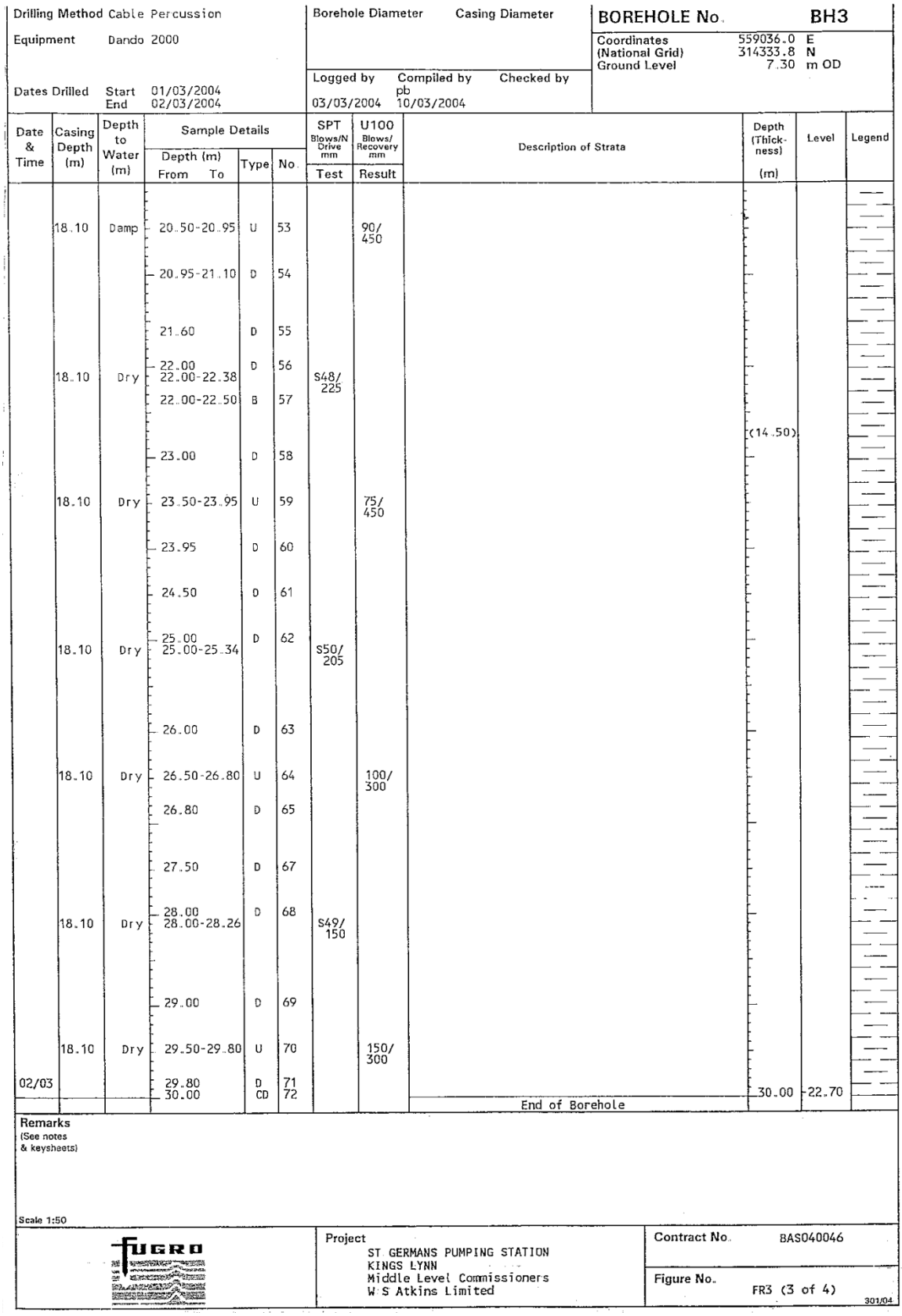

Figure A.10: Borehole 3 – page 3 of 4

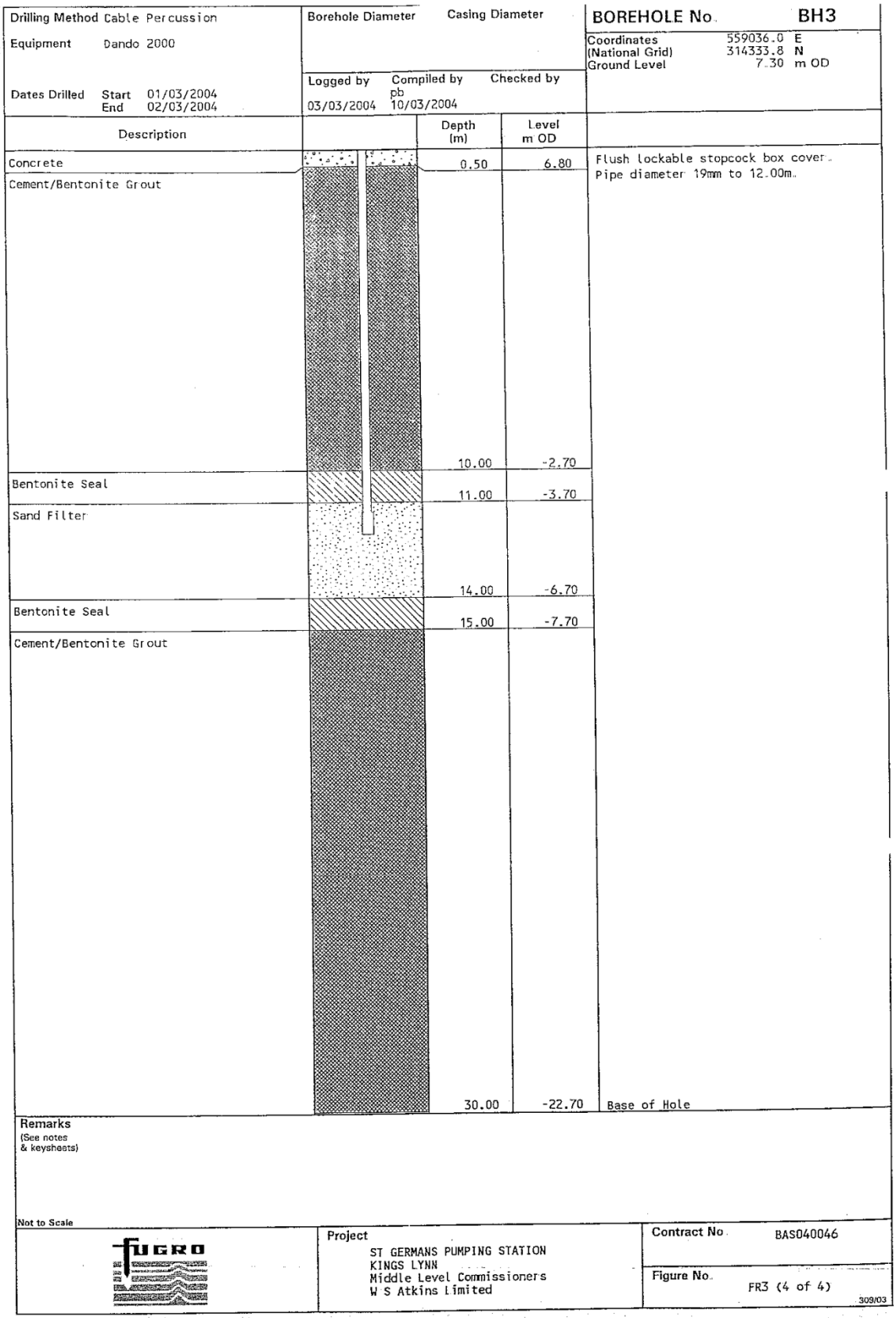

Figure A.11: Borehole 3 – page 4 of 4

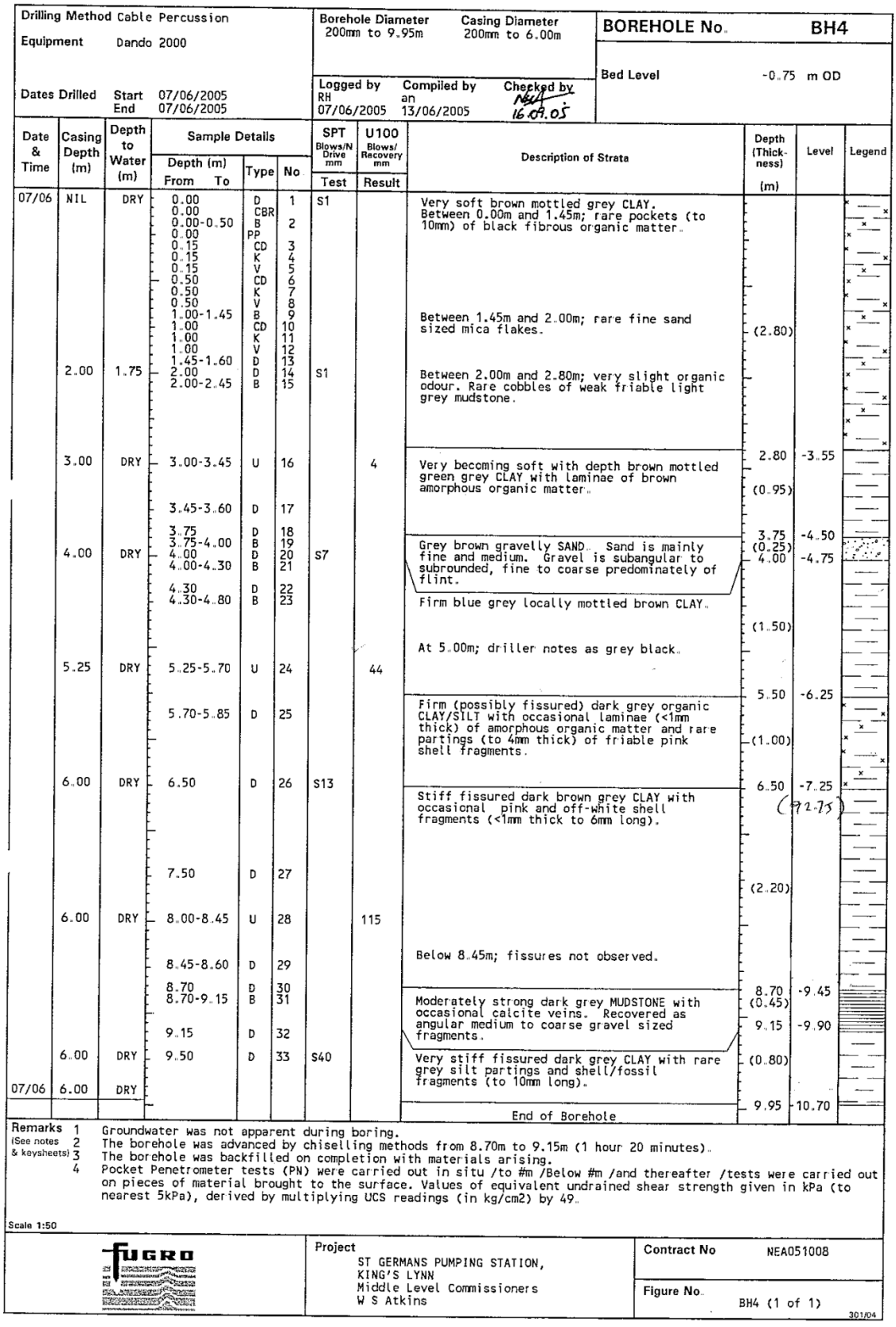

Figure A.12: Borehole 4 – page 1 of 1

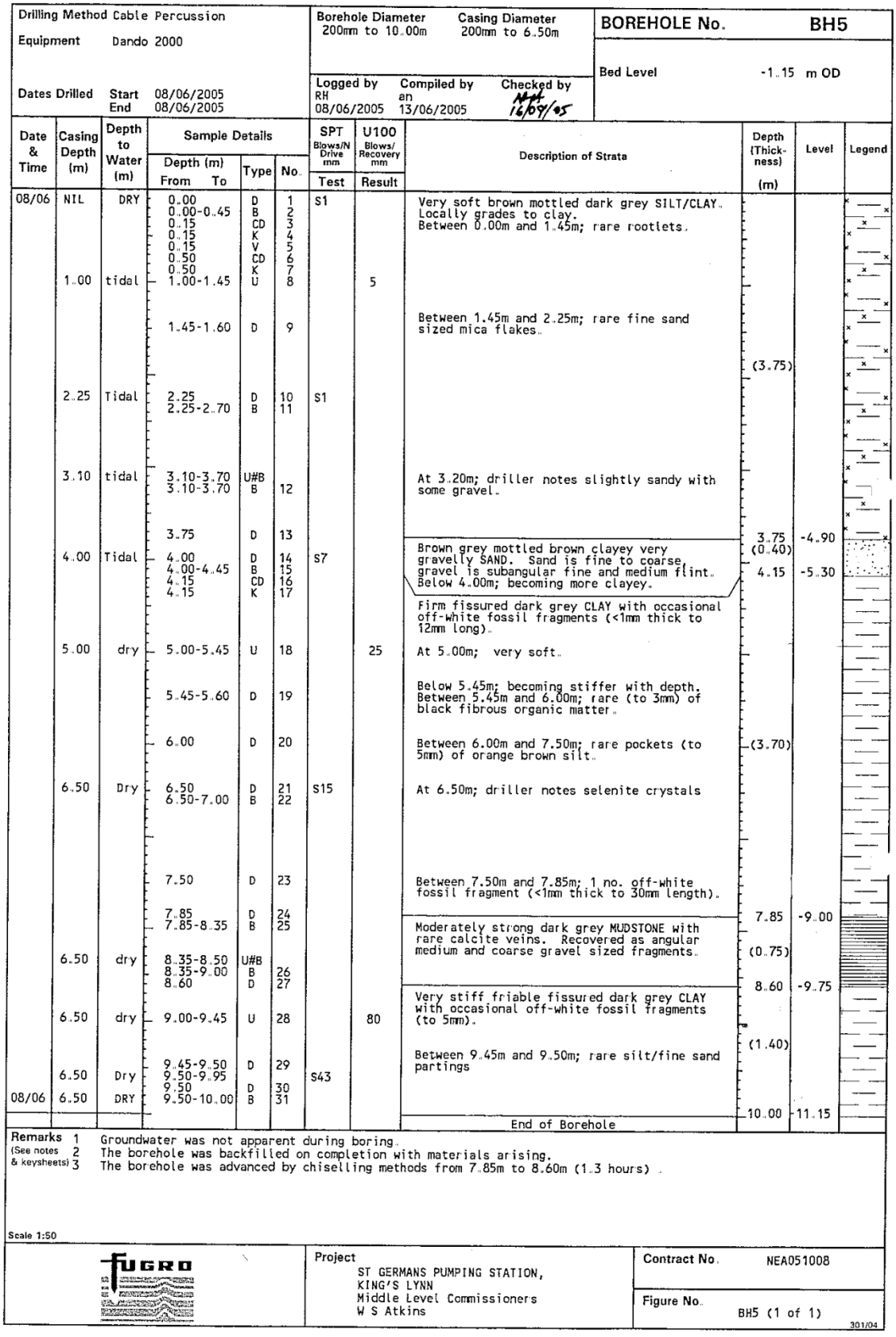

Drilling Method Cable Percussion
Equipment Dando 2000
Dates Drilled Start 08/06/2005 End 08/06/2005
Borehole Diameter 200mm to 10.00m
Casing Diameter 200mm to 6.50m
Logged by RH 08/06/2005
Compiled by an 13/06/2005
Checked by NH 16/09/05

BOREHOLE No. BH5

Bed Level -1.15 m OD

Date & Time	Casing Depth (m)	Depth to Water (m)	Sample Details: Depth (m) From	To	Type	No.	SPT Blows/N Drive mm Test	U100 Blows/ Recovery mm Result	Description of Strata	Depth (Thickness) (m)	Level	Legend
08/06	NIL	DRY	0.00		D	1	S1		Very soft brown mottled dark grey SILT/CLAY. Locally grades to clay. Between 0.00m and 1.45m; rare rootlets.			
			0.00-0.45		B	2						
			0.15		CD	3						
			0.15		K	4						
			0.15		V	5						
			0.50		CD	6						
			0.50		K	7						
	1.00	tidal	1.00-1.45		U	8		5				
			1.45-1.60		D	9			Between 1.45m and 2.25m; rare fine sand sized mica flakes.			
										(3.75)		
	2.25	Tidal	2.25		D	10	S1					
			2.25-2.70		B	11						
	3.10	tidal	3.10-3.70		U#B				At 3.20m; driller notes slightly sandy with some gravel.			
			3.10-3.70		B	12						
			3.75		D	13				3.75	-4.90	
	4.00	Tidal	4.00		D	14	S7		Brown grey mottled brown clayey very gravelly SAND. Sand is fine to coarse, gravel is subangular fine and medium flint. Below 4.00m; becoming more clayey.	(0.40)		
			4.00-4.45		B	15				4.15	-5.30	
			4.15		CD	16						
			4.15		K	17						
									Firm fissured dark grey CLAY with occasional off-white fossil fragments (<1mm thick to 12mm long).			
	5.00	dry	5.00-5.45		U	18		25	At 5.00m; very soft.			
			5.45-5.60		D	19			Below 5.45m; becoming stiffer with depth. Between 5.45m and 6.00m; rare (to 3mm) of black fibrous organic matter.			
			6.00		D	20			Between 6.00m and 7.50m; rare pockets (to 5mm) of orange brown silt.	(3.70)		
	6.50	Dry	6.50		D	21	S15		At 6.50m; driller notes selenite crystals			
			6.50-7.00		B	22						
			7.50		D	23			Between 7.50m and 7.85m; 1 no. off-white fossil fragment (<1mm thick to 30mm length).			
			7.85		D	24				7.85	-9.00	
			7.85-8.35		B	25			Moderately strong dark grey MUDSTONE with rare calcite veins. Recovered as angular medium and coarse gravel sized fragments.	(0.75)		
	6.50	dry	8.35-8.50		U#B							
			8.35-9.00		B	26						
			8.60		D	27				8.60	-9.75	
	6.50	dry	9.00-9.45		U	28		80	Very stiff friable fissured dark grey CLAY with occasional off-white fossil fragments (to 5mm).			
										(1.40)		
			9.45-9.50		D	29			Between 9.45m and 9.50m; rare silt/fine sand partings			
	6.50	Dry	9.50-9.95				S43					
			9.50		D	30						
08/06	6.50	DRY	9.50-10.00		B	31						
									End of Borehole	10.00	-11.15	

Remarks (See notes & keysheets)
1 Groundwater was not apparent during boring.
2 The borehole was backfilled on completion with materials arising.
3 The borehole was advanced by chiselling methods from 7.85m to 8.60m (1.3 hours).

Scale 1:50

FUGRO

Project
ST GERMANS PUMPING STATION,
KING'S LYNN
Middle Level Commissioners
W S Atkins

Contract No. NEA051008

Figure No. BH5 (1 of 1)

301/04

Figure A.13: Borehole 5 – page 1 of 1

Appendix B: Displacement vectors plot for river water level at highest flood level (107m MLD) for small strain effective stress analysis in FLAC^{2D}

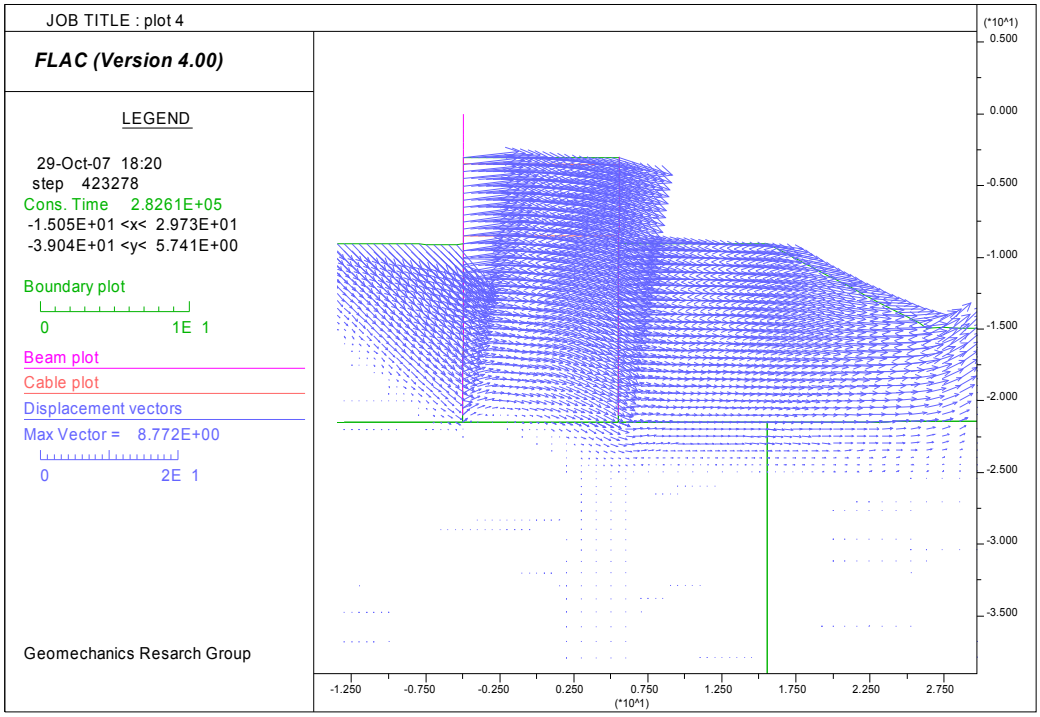

Figure B.1: Displacement vectors plot for ϕ' ' = 24.8° (FOS 1.25)

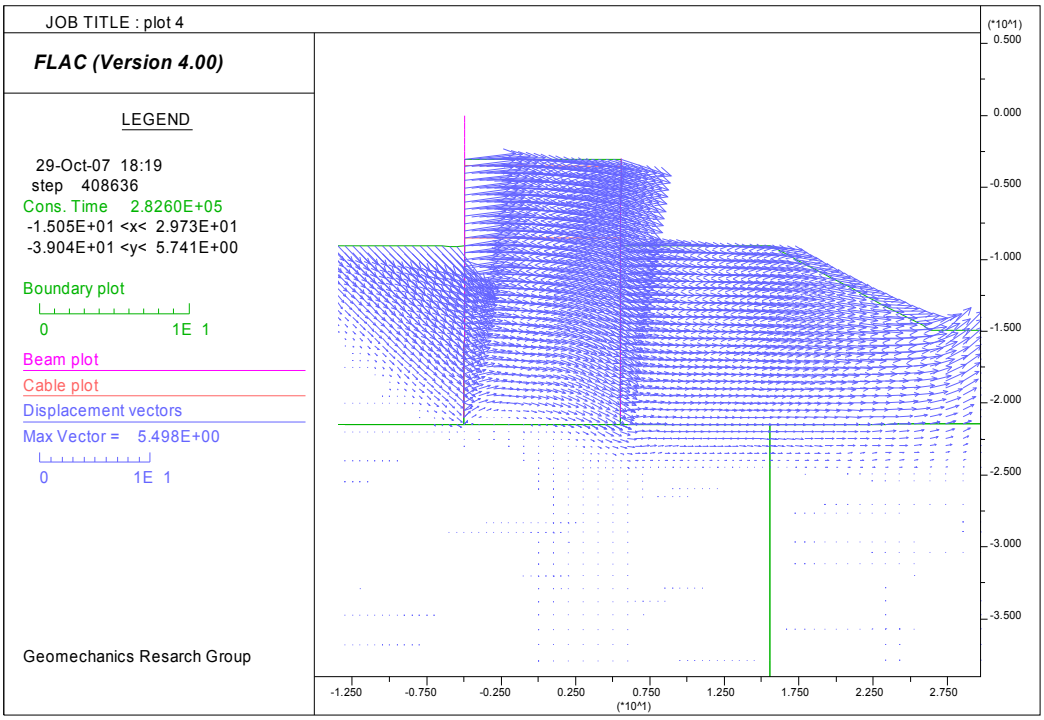

Figure B.2: Displacement vectors plot for $\phi' = 25.7°$ (FOS 1.20)

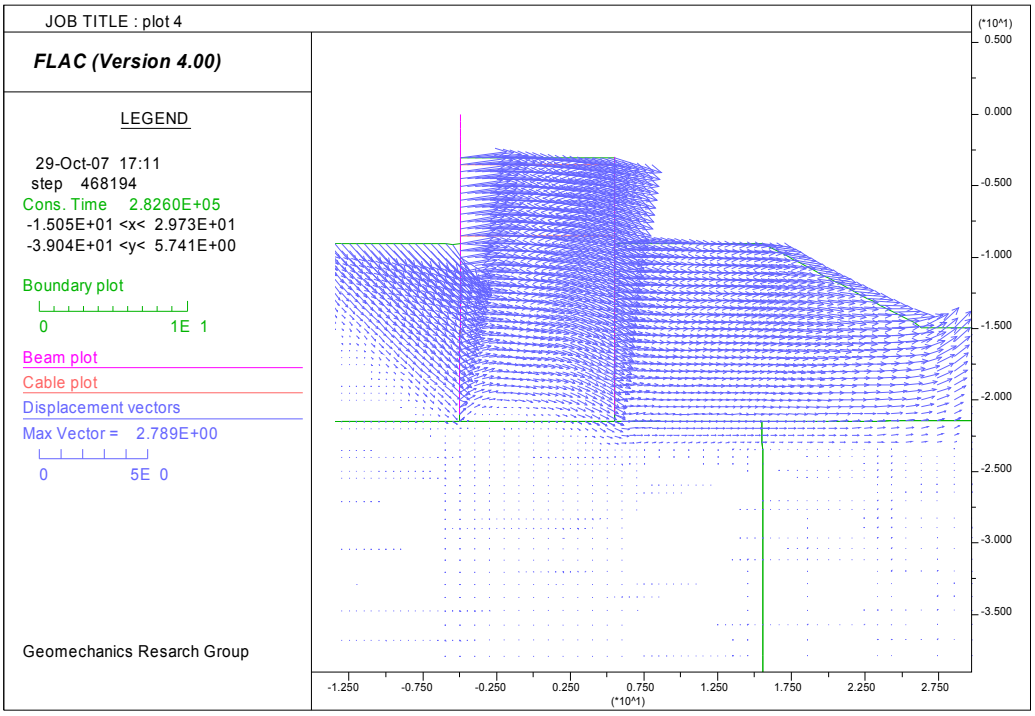

Figure B.3: Displacement vectors plot for $\phi' = 26.7°$ (FOS 1.15)

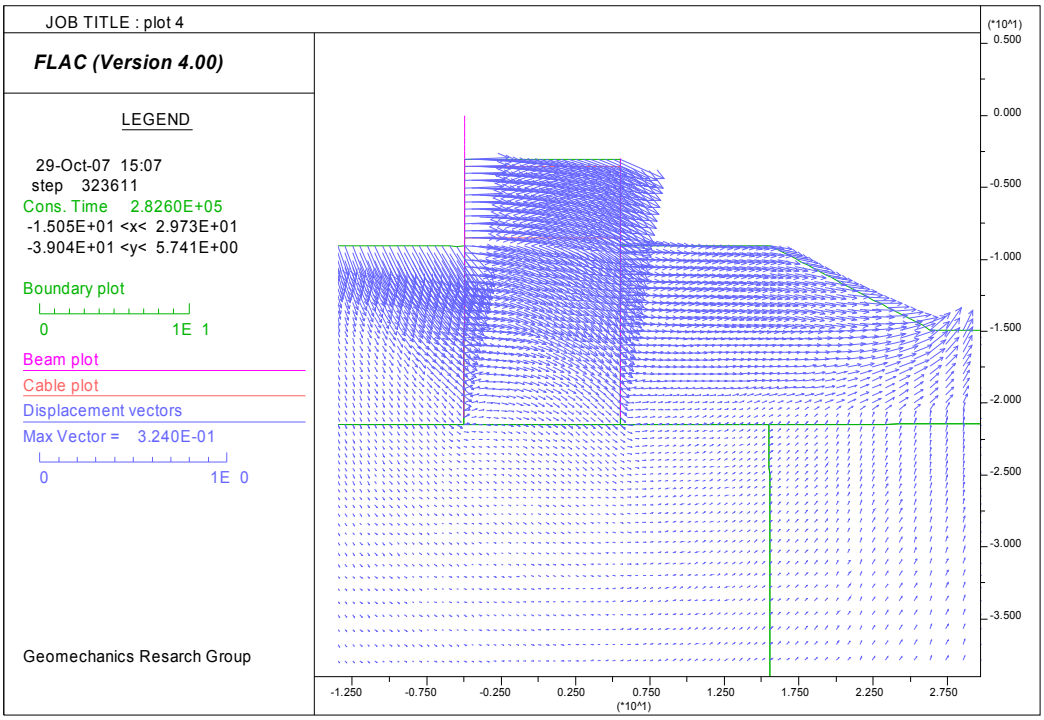

Figure B.4: Displacement vectors plot for $\phi' = 27.7°$ (FOS 1.10)

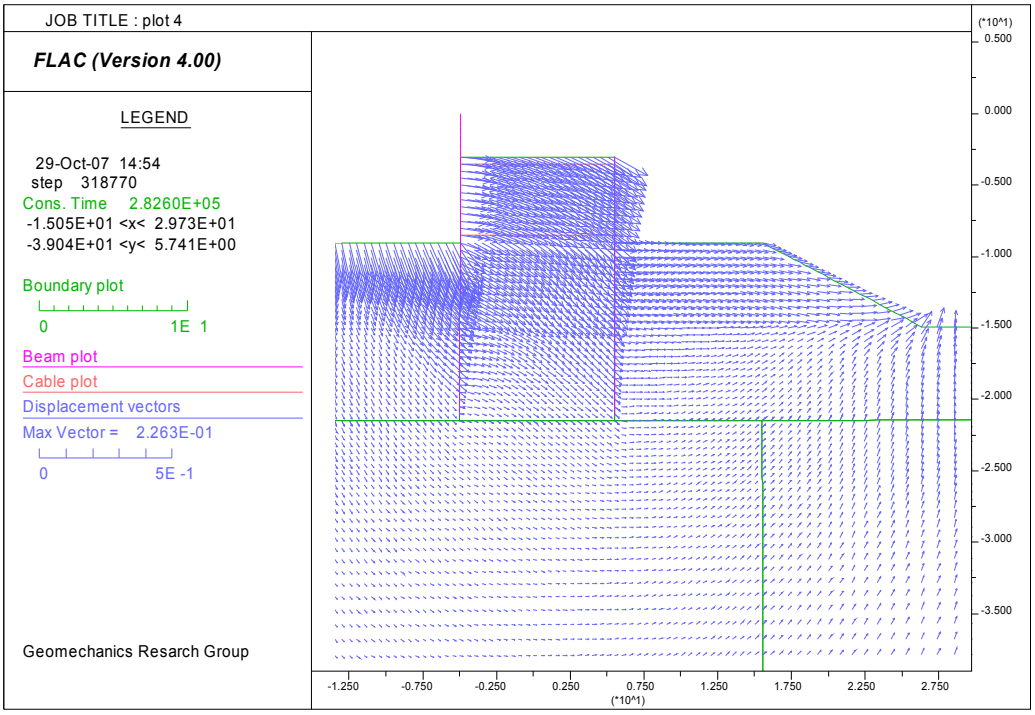

Figure B.5: Displacement vectors plot for $\phi' = 30°$ (FOS 1.0)

Appendix C: Velocity vectors plot for river water level at highest flood level for small strain effective stress analysis in FLAC^{2D}

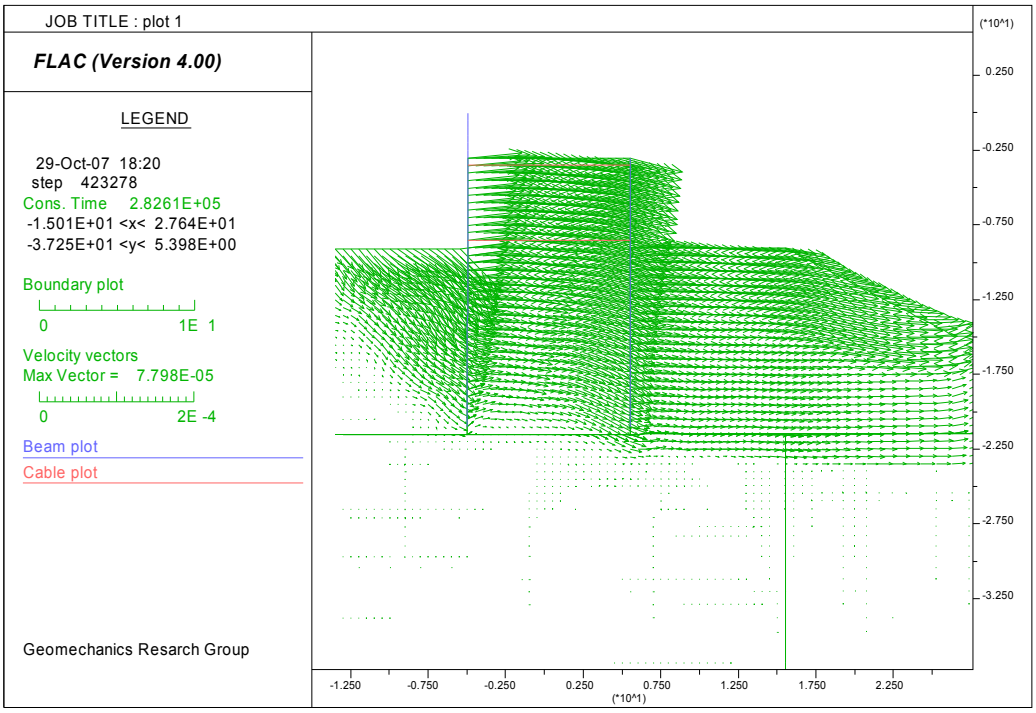

Figure C.1: Velocity vectors plot for ϕ' = 24.8° (FOS 1.25)

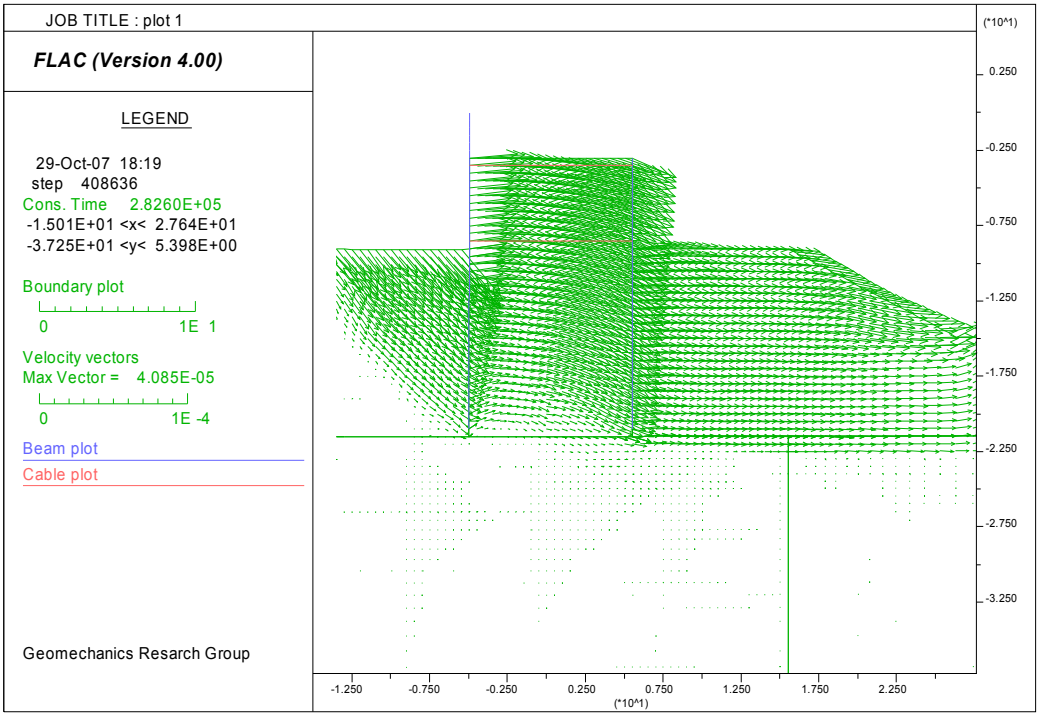

Figure C.2: Velocity vectors plot for ϕ' = 25.7° (FOS 1.20)

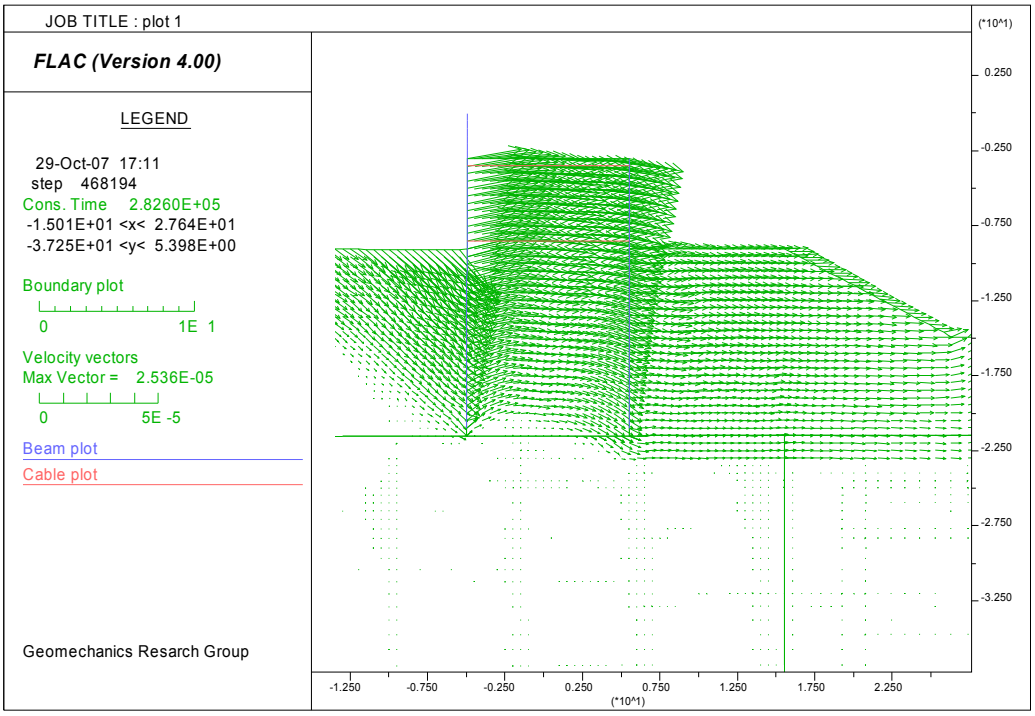

Figure C.3: Velocity vectors plot for ϕ' = 26.7° (FOS 1.15)

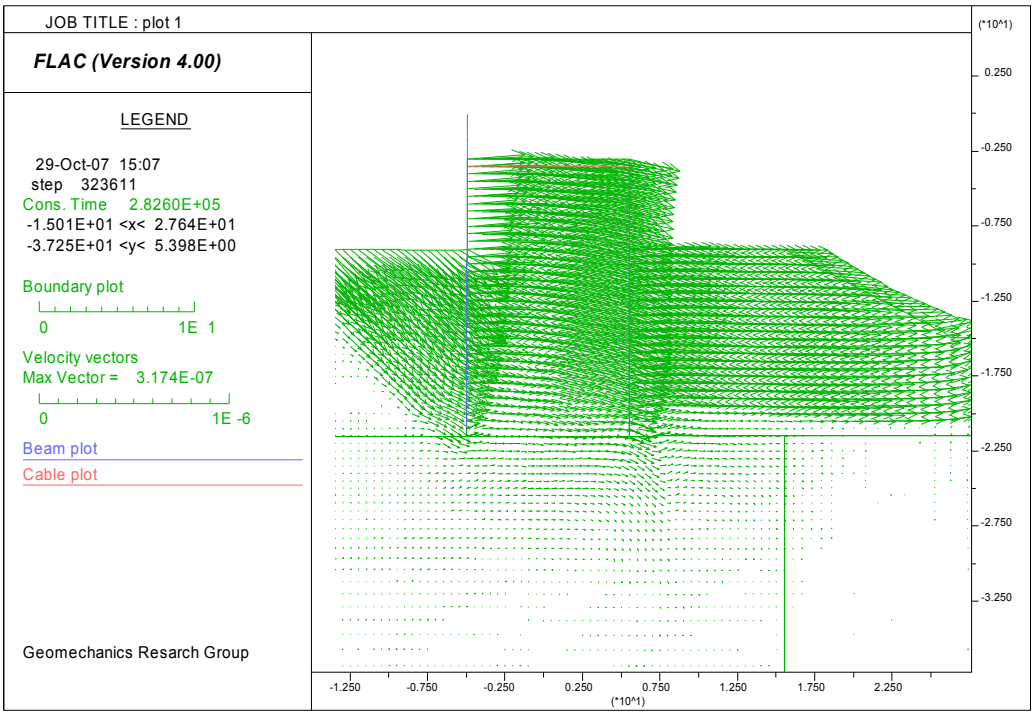

Figure C.4: Velocity vectors plot for ϕ' = 27.7° (FOS 1.10)

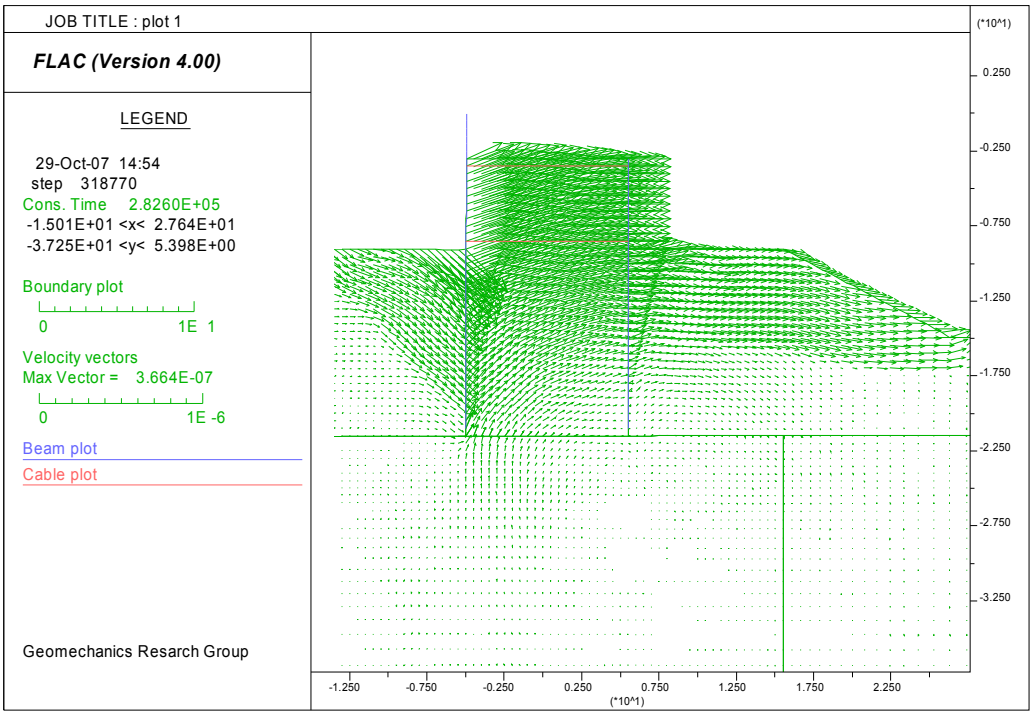

Figure C.5: Velocity vectors plot for ϕ' = 30° (FOS 1.0)

References

Atkins (2005). *St Germans Pumping Station: Geotechnical Interpretive Report*. Atkins UK.

Batten, M. and Powrie, W. (2000). Measurement and analysis of temporary prop loads at Canary Wharf underground station, east London. *Proc. Institution of Civil Engineers, Geotechnical Engineering*, 143(July): 151-163.

Batten, M., Powrie, W., Boorman, R., Yu, H.-T. and Leiper, Q. (1999). Use of vibrating wire strain gauges to measure loads in tubular steel props supporting deep retaining walls. *Proc. Institution of Civil Engineers*, 137(Jan): 3-13.

Blum, H. (1944). *Beitrag zur berechnung von spundwandfangedämmen mitteilungen aus dem gebiedes wasserbaues und der Baugrundforschung*, Heft 16 Berlin 1944.

Boardman, C.S., (1917). Discussion of: Coffer-dam for 1000 feet pier. *Transactions of the American society of civil engineers*, Volume 81, pp 553-569.

Bolton, M.D. and Powrie, W. (1987). Collapse of diaphragm walls retaining clay, *Geotechnique* volume 37, No. 3, pp 335-353.

British Geological Society, (1995). *Map sheet 159*. BGS, Murchison House, West Mains Road, Edinburgh.

British Standards Institution (2004). Eurocode 7: *Geotechnical design. Part 1: General rules*, EN1997-1:2004. BSI, London.

British Standards Institution BS 6349 (1988). *Code of practice for maritime structures*, British standards Institution, London.

British Standards Institution (2001). BS 8002:1994, *Code of practice for earth retaining structures*, (British standards Institution, 1994 amended 2001).

British Standards Institution (1981). BS5930 *Code of practice for site investigations*, British standards Institution, London.

Cattin, P. (1955). *Comparative analyses of double wall cofferdams design theories*. Princeton University, USA.

CIRIA (2002). *The AGS-M Format for the electronic transfer of monitoring data*. Construction Industry Research and Information Association PR082

Clark, J. (2005). *Performance of a propped retaining wall at the CTRL, Ashford*. Ph.D. thesis University of Southampton, UK.

Clough, G.W., and Hansen L.A. (1977) A Finite Element Study of the Behavior of the Willow Island Cofferdam. *Technical Report No. CE-218*, Department of Civil Engineering, Stanford University, Stanford, C.A.

Clough, G.W. and T. Kuppusamy, T. (1985). Finite Element Analyses of Lock and Dam 26 Cofferdam. *Journal of the Geotechnical Engineering Division*, ASCE, Vol 3, No. 4, pp 521-544.

Coetzee, M.J., Hart, R.D., Varona, P.M. and Cundall, P.A. (1998). *FLAC Basics*. Itasca Consulting Group Inc, Minneapolis Minnesota, United States of America.

Cornfield, G.M. (1968). Driven piles: Method and equipment. *Journal of the British Steel Piling Co Ltd*, No 15.

Corps of Engineers Department of Army (1974). An analysis of cellular cofferdam failures. *Technical report*, Ohio River Division, Cincinnati, P.A.

COSTAIN (2007). *St Germans pumping station: Design Philosophy.* document 1205/001 Revised 16th June 2007.

Cripps, J.C. and Taylor, R.K. (1987). Engineering characteristics of British over-consolidated clays and mudrocks. II Mesozoic deposits, *Engineering Geology*, No 23, pp 218-253.

Cummings, E. M., (1957). Cellular cofferdams and docks. *Proceedings of ASCE*, Volume 83, Number WW3.

Daly, M.P. and Powrie, W. (2001). Undrained analyses of earth berms as temporary supports for embedded retaining walls. *Proceedings of the Institution of Civil Engineers, Geotechnical Engineering*, No 149, issue 4, pp 237-248.

Department of Army Corps of Engineers (1970). *Design of pile structures and Foundations*. Engineering Manual 111-2-2906 (Draft), US Army, Washington DC.

Department of Army Corps of Engineers (1989). *Design of pile structures and Foundations*. Engineering Manual 1110-2-2503, US Army, Washington DC.

Descans, L. (1952-54). *Constructions cellulaires en palplanches plates*. L'Ossature Metallique, October 1952, Jan-Feb 1954.

Descans, L. (1958). Constructions cellulaires en palplanches plates, *Proc. Conf. Earth Pres. Problems*, Vol II, Brussels.

Dismuke, T.D. (1970). Stress analyses of sheet piling in cellular structures. *Proceedings of Conference on design and installation of pile foundations and cellular structures*, Envo publishing Co. Lehigh Valley, pp 339-365.

Dunnicliff, J. (1993). *Geotechnical instrumentation for monitoring field performance*. John Wiley & Sons, Inc., NY 10158-0012.

Fröhlich O.K. (1940). *Bodenmechanische Gesichtspunkte fur Berechnung von Fangedammen*. Die Bautechnik 1940, Heft 47/48, Berlin.

Fugro site investigation report (2004). *St. Germans pumping station Wiggenhall - Factual report on ground investigation*, BAS040046 .

Fugro site investigation report (2005). *St. Germans pumping station Wiggenhall - Factual report on ground investigation* NEA051008.

Gaba, A.R., Simpson, B., Powrie, W. and Beadman, D.R. (2003). *Embeded retaining walls: Guidance for economic design*. CIRIA report C580.

Godwin, H. (1940). Studies of the post-glacial history of British vegetation. *Phil. Trans. Roy. Soc., B.*, 230, pp 239-246.

Hansen, B. J. (1953). Earth pressure calculation. *The institution of Danish civil engineers*. The Danish technical press Copenhagen.

Hvorslev, M.J. (1951). Time lag and soil permeability in ground water observations, *Bulletin No. 36, Waterways Experimental station*, Vicksburg, USA.

Itasca (2009). *FLAC^{2D} and FLAC^{3D} online manuals*. Itasca publications, Minneapolis USA. Last accessed during May 2009.

Jacoby, H. S. and Davies, R. P. (1941). *Foundations of bridges and buildings*, New York, 1958.

Kenny, T. C. (1963). "Atterberg limits." *Correspondence Geotech*, No 13, pp 159–162.

Kenny, T.C. (1959). *Discussion. Proceedings of ASCE, Journal of soil mechanics and foundation engineering division*. 85, SM3, pp 67-79

Khan, M.R.A., Takemura, J. Fukushima, H. and Kusakabe, O. (2001). Behaviour of double sheet pile wall cofferdam on sand observed in centrifuge tests. *International journal of physical modeling in geotechnics.* Vol 1, 4, pp 1-16.

Khan, M.R.A., Takemura, J. and Kusakabe, O. (2006). Centrifuge model tests on behavior of double sheet pile wall cofferdam on clay. *International journal of physical modeling in geotechnics.* 3, pp 1-23.

Kittisatra, L. (1976). *Finite element analyses of circular cell bulkheads*. PhD thesis, Oregon State University, Corvallis, O.R.

Lee, D. H. (1945). *Sheet piling cofferdams and cassions*, Concrete publications limited London.

Macalloy Ltd (2007). *Macalloy 17MHS bars for use in tie bar applications: Design data*, Macalloy steel Ltd, Sheffield, UK.

Maitland J. K. and Schroeder, W. L. (1979). Model Study of Circular Sheetpile Cells. *Journal of the Geotechnical Engineering Division, ASCE*, Vol 105, No. GT7, pp 805-821.

Martin J. R. and Clough G. W. (1988). *A Sudy of the Effects of Differential Loadinq on Cofferdams.* Technical Report under Contract No. DACW39-86-0007, Virginia Polytechnic Institute and State University, Blacksburg, V.A.

Middle level commissioners (1999). *The Middle Level: The Area, The Problems and The Solutions*, http://www.waterwaysguides.co.uk, accessed on 27th June 2008.

Mosher, R.L. (1992). *Three dimensional finite element analyses of sheet-pile cellular cofferdams*, Department of the Army, US Army Corps of Engineers.

National instruments (2009). www.zone.ni.com, *Strain gauge configuration types*.

NAVFAC (1971). *Design manual DM-7.* Naval Facilities Engineering Command, Soil Mechanics and Foundations division, Department of Navy.

New Civil Engineer (2007). Flood defences: St Germans Pumping Station. *Institution of Civil Engineers*, October 2007, pp 28-29.

Ovesen N.K., (1962). Cellular cofferdams, calculation methods and model tests, *Bulletin No 14, The Danish geotechnical institute*, Copenhagen 1962.

Pennoyer, R. L. (1934). Gravity bulkheads and cellular cofferdams. *Civil Engineering*, volume 4, No. 6.

Powrie, W. (1996). Limit equiblirium analysis of embedded retaining walls. *Geotechnique*, 46, 4, pp 709-723.

Preene, M., Roberts, T.O.L., Powrie, W. and Dyer, M.R. (2000). *Groundwater control-design and practice*. CIRIA report C515.

Raymond B. S., Robert G. B. (2006). *Initial comments on interim (70%) IPET study report*. National Science Foundation-Sponsored Independent Levee Investigation Team (ILIT) University of California at Berkeley.

Richards, D.J., Chandler, R.J. and Lock, A.C. (2003). Electronic data transfer systems for field monitoring. *Proceedings of Institution of Civil Engineers. Geotechnical engineering*, 156(1), pp 47-55.

Richards, D.J., Clark, J. and Powrie, W. (2006). Installation effects of bored pile walls in overconsolidated clays. *Geotechnique* 56, No. 6, pp 411–425

Richards, D.J., Holmes, G. and Beadman, D.R. (1999). Measurement of temporary prop loads at Mayfair car park. *Proc. Inst. Civ. Engrs. Geotech. Engng* 137(July), pp 165-174.

Richards, D.J. and Powrie, W. (1998). Centrifuge model tests on doubly propped embedded retaining walls in overconsolidated kaolin clay. *Geotechnique*, 48, No. 6, pp 833-846.

Schlim, R. and Reuter, E. (2005). *British Sheet Piling Handbook*, Arcelor RPS, January 2005.

Shannon and Wilson, Inc. (1982). *Final Report Tasks 3.2, 3.3, and 3.4; Finite Element Models for Lock and Dam No. 26 (Replacement) First Stage Cofferdam*. Technical Report, prepared for US Army Engineer District, St. Louis.

Simm, K.F. and Busbridge, J.R. (1976). 31m deep excavation for construction of Barton anchorage for Humber bridge. *Proceedings of 6th European conference on soil mechanics and foundation engineering*, Vienna, 1, 2, pp 651-656.

Skempton, A.W. (1945). A slip in the west bank of the Eau brink cut. Discussion on civil engineering research and its future. *The Institution of Civil Engineers Journal*, London, pp 267-286.

Smethurst, J.A. and Powrie, W. (2008). Effective-stress analysis of berm-supported retaining walls. *Proceedings of the Institution of Civil Engineers, Geotechnical Engineering,* 161, February 2008, Issue GE1, pp 39–48

Stevens, R.F. (1980). *Study of the Behavior of a Cellular Cofferdam*. PhD thesis, Duke University, Durham, N.C.

Swatek E. P. Jr. (1970). Summary-cellular structure design and installation. *Proceedings, Conference on design and installation of pile foundations and cellular structures*, Envo publishing Co., Lehigh Valley, pp 413-423.

Tennessee Valley Authority (1957). *Steel sheet piling cellular cofferdams on Rocks*. TVA Technical Monograph No. 75, Vol 1.

Terzaghi, K. (1944). Stability and stiffness and cellular cofferdams. *Proceedings of ASCE*, September 1944.

Terzaghi, K. (1945). Stability and stiffness and cellular cofferdams. *Transactions, ASCE*, Volume 110, pp 1083-1202.

Terzaghi, K. and Peck, R.B. (1967). *Soil Mechanics in Engineering Practice*. John Wiley&Sons, 1967.

Thomas, H. E., Miller, E. J. and Speaker, J. J. (1975). Difficult Dam Problems - Cofferdam Failure. *Civil Engineering ASCE*, Vol. 45, No. 8, August 1975, pp 66-70.

Verdeyen, j. (1948). The use of flat sheet piling in cellular construction. *Proc. Sec. Int. Conf. Soil. Mech.* Vol. VII, Rotterdam 1948.

ASCE (2007). *What went wrong and why: The New Orleans hurricane protecting system*. A report by American Society of Civil Engineers.

Williams, B.P. and Waite, D. (1993). *The design and construction of sheet-piled cofferdams*. Special publication No 95, Construction industry research and information association (CIRIA).

Zaczek, S. (1952). *Etude Théorique et Expérimentale sur la stabilité des constructions cellularies en palplanches plates*. Université Libre de Bruxelles.